UNIVERSITY OF SOUTHAMPTON

FACULTY OF NATURAL and ENVIRONMENTAL SCIENCES

SCHOOL OF CHEMISTRY

The Modification of Carbon Electrodes for Biosensor Applications

by

IZZET KOCAK

Thesis for the degree of Doctor of Philosophy

June_2013

UNIVERSITY OF SOUTHAMPTON

ABSTRACT

FACULTY OF NATURAL and ENVIRONMENTAL SCIENCES

School of Chemistry

Thesis for the degree of Doctor of Philosophy

THE MODIFICATION OF CARBON ELECTRODES FOR BIOSENSOR APPLICATIONS

Izzet Kocak

This thesis reports upon the covalent attachment of 6 different types of linkers bearing the Boc protecting group to the surface of glassy carbon electrodes, highly ordered pyrolytic graphite with the edge and basal plane orientation and multi-walled carbon nanotube abrasively immobilised onto a glassy carbon substrate by electrochemical oxidation or reduction of the corresponding diazonium salt. Removal of the Boc group allows redox probes, such as anthraquinone-2-carboxyl acid, 4 nitrobenzoyl chloride and 3 and 4 dihydroxybenzoyl chloride, to be coupled to the surface using solid-phase coupling methods. The surface coverage, scan rate and pH effects, as well as the determination of the kinetic parameters, were evaluated using cyclic voltammetry. It was found that the type of carbon electrode and the choice of linkers had a significant influence on the surface coverage of redox probes and the electron transfer rate.

A 4-(N-Boc-aminomethyl) benzene diazonium tetrafluoroborate salt linker ($C_6H_4CH_2NH–$) was also spontaneously grafted onto the CNTs by refluxing in the $C_6H_4CH_2NHBoc$ diazonium salt at 60 ^oC in an acetonitrile solution. After the removal of the Boc protecting group, the anthraquinone (AQ) and nitrobenzene (NB) groups were attached to the benzyl amine linker by solid-phase amide coupling. The grafted CNTs were characterized using FTIR and cyclic voltammetry techniques; the surface coverage and the stability of the tethered functional groups were also investigated.

The oxygen reduction reaction was studied on bare and anthraquinone (AQ) modified edge planes, on a basal plane with highly oriented pyrolytic graphite, and on glassy carbon (GC) and multi-walled carbon nanotube electrodes. The anthraquinone-modified rotating disc GC electrode results show the two electron oxygen reduction reactions with hydrogen peroxide as the final product. The immobilization of laccase (*ThL*) onto GC electrodes modified with anthraquinone and

anthracene through EDA and $C_6H_4CH_2NH$– linkers was also achieved by employing high-throughput screening using a multichannel potentiostat for a library of 12 electrodes; the activity of these electrodes to oxygen reduction was examined. The experimental findings demonstrated a successful attachment of laccase to the modified glassy carbon, as well as successful electron transfer between substrate- and enzyme-active sites.

DFT calculations were used to investigate the structural properties of the functionalized basal plane of graphene after modification and to discover why the edge site shows higher reactivity to the attachment of linkers than the basal sites and whether the type of linker has an effect on the surface coverage of AQ. On the basis of considering the relationship between binding energy and charge transfer, the root of the effect of the type of linker on surface coverage was investigated to ensure whether it is steric, electronic, or both.

Contents

The List of Figures

ACRONYMS

A : Electrode Area

ACN : Acetonitrile

AFM : Atomic Force Microscopy

AQ : Anthraquinone

BDA N-Boc-1, 4 butanediamine

BPPG : Basal Plane Pyrolytic graphite

CNT : Carbon nanotube

CV : Cyclic Voltammetry

D : Diffusion Coefficient

DFT : Density Functional Theory

DMF **:** Dimethylformamide

DOS : Density of States

E : Experimental Potential vs Reference Electrode

EDA N-Boc-ethylenediamine

EDDA N-Boc-2,2`-(ethylenedioxy)diethylamine

E_{mp} : midpotential

EPPG : Edge Plane Pyrolytic graphite

F : Faraday constant

GC : Glassy carbon

GGA : Generalized Gradient Approximation

HBTU : 2-(1h-benzotriazol-1-yl)-1,1,3,3-tetramethyluronoium hexafluorphosphate

HDA N-Boc-1,6 hexanediamine

HOMO Highest occupied Molecular Orbital

HOPG : Highly Ordered Pyrolytic Graphite

I : Current

k_s: Standart Rate Constant

LDA : Local Density Approximation

LUMO: Lowest Unoccupied Molecular Orbital

n : number of electrons

PDOS : Partial Density of States

Q : Charge

RDE : Rotating Disc Electrode

SECM: Scanning Electrochemical Microscopy

SEM : Scanning Electron Microscopy

ThL : Trametes hirsuta laccase

XDA1-N-Boc-aminomethyl-4-(aminomethyl) benzene

α : Transfer Coefficient``

Γ = Surface Coverage

ΔE : Peak Separation

DECLARATION OF AUTHORSHIP

I, Izzet Kocak

declare that the thesis entitled

THE MODIFICATION OF CARBON ELECTRODES FOR BIOSENSOR APPLICATIONS

and the work presented in the thesis are both my own, and have been generated by me as the result of my own original research. I confirm that:

- this work was done wholly or mainly while in candidature for a research degree at this University;
- where any part of this thesis has previously been submitted for a degree or any other qualification at this University or any other institution, this has been clearly stated;
- where I have consulted the published work of others, this is always clearly attributed;
- where I have quoted from the work of others, the source is always given. With the exception of such quotations, this thesis is entirely my own work;
- I have acknowledged all main sources of help;
- where the thesis is based on work done by myself jointly with others, I have made clear exactly what was done by others and what I have contributed myself;
- Parts of this work have been published as:

  M. A. Ghanem; I. Kocak; A. Al-Mayouf; M. AlHoshan; P. N. Bartlett; Covalent modification of carbon nanotubes with anthraquinone by electrochemical grafting and solid phase synthesis**;** *Electrochim. Acta* **2012**, *68*, 74.

  M. A. Ghanem; I. Kocak; A. Al-Mayouf; M. AlHoshan; P. N. Bartlett; Solid phase modification of carbon nanotubes with anthraquinone and nitrobenzene functional groups; *Electrochem. Commun* **2013,** *34*, 258

  I. Kocak; M. A. Ghanem; A. Al-Mayouf; M. AlHoshan; P. N. Bartlett; Oxygen reduction at edge plane, basal plane and glassy carbon electrodes modified with anthraquinone immobilised by electrochemical and solid phase coupling; *J. Electroanal. Chem*. **2013,** *706*, 25

I. Kocak; C. K. Skylaris, M. A. Ghanem; P. N. Bartlett, J. Kilburn; Electrochemical Modification of Carbon Electrodes Using Solid Phase Synthesis and a DFT study; **Manuscript in preparation**.

Signed: .....

Date:.....

Acknowledgements

I can`t find right words to express my sincere gratitude and respect to **Professor Phil N. Bartlett** for his guidance throughout my PhD study and research and for his patience, enthusiasm, and deep knowledge. He inspired me to become an independent researcher and helped me realize the significance of critical thinking. Beside my supervisor, I also would like to thank my advisor, **Dr Guy Denuault** and **Dr. Chris Skylaris** for his guidance on understanding the basic principles of Density Functional theory.

There is no way to how to convey my deep thanks to **Dr. Mohamed Ghanem** for his massive contribution to my thesis and his assistance to understand electrochemistry in depth. Special thanks go to past and current member of **Bartlett research group: Dr. Maciej Sosna, Dr. Aleksandra Pinczewska, Emma Wright, Ahmet Celiktas, Dr. Rob Johnson, Dr. David Cook, and Mohammed Aziz**

I cannot forget friends who have helped me adapt to life in the UK , cheered me on, and celebrated each achievement: **Ali Demirok, Mahmut Gunaydin, Dr. Ugur Mart Naci Kalkan, Sinan Kalaz, Ahmet Alp, Omer Faruk Ucan, Erdogan Guk, Ali Karakas, Alp Yahya Mercan, Ruhican Akin, Mustafa Cagri Kutlu, Cagri Koc, Osman Necmettin Erbakan** and every single staff at **Portswood Poppins Restaurant**.

I also would like to thank **Turkey Ministry of National Education** for financial support during my language and PhD study.

Finally I must allocate a separate sheet to express my feelings about every single member of my Family. I profoundly thank **my parents**, **my sister`s family** and my beloved nephew, "**Elif Zehra Hatil**" for being generous with their love and spiritual assistance throughout my life.

Chapter 1

INTRODUCTION

1.1. Overview

The functionalization of conductive surfaces (e.g. carbon electrodes, such as glassy carbon (GC);[1-3] highly ordered pyrolytic graphite (HOPG)[4-6] electrodes with the orientation of edge and basal plane; carbon nanotube[7,8] and graphene[9]; metal surfaces, such as nickel[10] and gold;[11] and semiconductor electrodes with organic functionalities) has drawn considerable interest over the last two decades.[12] The modification of electrode surfaces is widely adopted by researchers due to the fact that it permits us to control the properties of the substrate being modified. This method is rather flexible, which implies that the corresponding electrode surface can be tailored in a desirable way for specific applications.[13] This approach therefore has led to a wide variety of applications for the relevant modified electrodes in the field of electrochemistry, such as sensors and bioelectronics.[14] It is well recognised that organic compounds can be covalently grafted to the surface of various carbon electrodes by the electrochemical oxidation of primary amines or the electrochemical reduction of diazonium salts.[15] Both of these methods were reviewed in detail in our work with a wide variety of functional groups.[16-22] In this chapter, we will attempt to describe some of the carbon microstructures as an electrode material by comparing the electron transfer kinetics at these carbon electrodes. Both approaches for surface functionalization with different types of substrates, adsorbates or chemical compounds and strategies will be discussed. In this thesis, density functional theory (DFT) is used as a tool to investigate the possible changes in the structural and electronic properties of carbon surfaces after functionalization. Thus, we include, to some extent, a discussion of the fundamentals and background of DFT. Finally, oxygen reduction on different types of plain, quinone and enzyme (for example laccase) modified electrode materials are introduced.

1.2. Carbon-Electrode Materials

As an electrode material, carbon and its allotropes have been one of the most extensively employed substances by researchers owing to the fact that they 1) are reasonably low-priced, 2) possess high electrical conductivity, 3) have relatively wide potential windows, and 4) can be used in a variety of areas, from laboratory to industrial

applications.[23-25] It is commonly known that, even though there is a similarity in the electronic properties of carbon and metal electrodes, carbon materials used for electrochemical applications are different from metals in terms of structure and electronic properties (such as band structures, the density of states, and the chemical properties of their surface chemistry). This difference is believed to stem not only from the surface bonds and functional groups on the corresponding carbon electrode but also from the microstructure of carbon electrodes which differs from the type of carbon material used.[21]

Carbon is available in a large variety of forms and microstructures, such as graphene, graphite, diamond, carbon nanotube, glassy carbon, carbon fiber, and boron doped diamond, and it is widely accepted that all of these carbon materials have different electrochemical properties. In this thesis, we will be examining electrochemical and chemical modification of these different forms and microstructures of carbon materials so as to see how they differ.

1.2.1. Graphene

The single layer of graphene sheet (which is a two dimensional sheet of sp^2 hybridized carbon atoms densely packed in a honeycomb crystal lattice such that each aromatic ring is surrounded by six adjoining ones) is regarded as the most primitive component of some carbon allotropes, e.g., graphite, carbon nanotubes and fullerenes.[21,25-30] Figures 1.1.a and 1.1.b show the lattice structure of graphene and the electronic band structure of graphene, respectively. There is a close relationship between these two dimensional characters, the honeycomb lattice symmetry, and the exceptional electronic and transport properties of graphene. One of the unique electronic properties of this structure is that the completely occupied valence band and the fully vacant conduction band are in contact with each other at points, as depicted in Figure 1.1.b. These points are named as K points, which are present at six angles of Brillouin zone hexagon. The Brillouin zone (BZ) can be envisaged as an unit cell in reciprocal space and can be visualized by continual set of points (k_x, k_y. k_z) across reciprocal space. This leads to graphene being a semiconductor without a band gap, indicating constant conversion from p-type to n-type by doping.[31] The innovative discovery by Geim and Novoselov from Manchester University regarding the identification of single layer graphene was recognized by the Nobel Prize committee in 2010.

Graphene has received an enormous amount of attention owing to its unique properties; for example, its large surface area, superb electrical and thermal conductivity, mechanical flexibility, good electrocatalytic activity, wide potential window, and optical transparency. Graphene and its allotropes can be utilized as substrates for modification by a wide range of species and this leads to many application areas, including memory devices, energy storage, catalysis, photocatalysis, solar cells, sensing platforms and molecular imaging.[32] Graphene modified electrodes are also expected to play a significant role in electrochemical sensors and biosensors.[26,33,34]

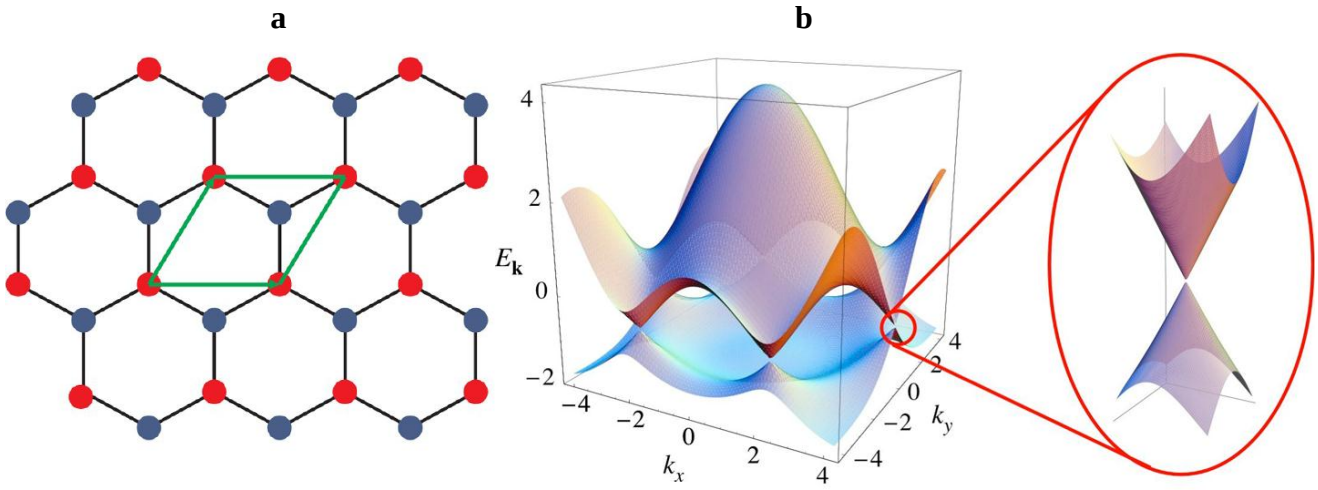

Figure 1.1. *(a) Lattice structure of graphene. (b) Electronic band structure of graphene. The zoom shows the dispersion relation in graphene near the Fermi level. Adapted from reference* [31].

1.2.2. Highly Ordered Pyrolytic Graphite

Unlike the graphene sheet, highly ordered pyrolytic graphite (HOPG) and natural crystalline graphite are three dimensional. HOPG is prepared by the disintegration of hydrocarbons (frequently acetylene) under high temperature and pressure. Since graphite contains many impurities, it is only occasionally used for electrochemical applications. HOPG is assumed to be made up of sp^2 hybridized carbon atoms with a bond length of 1.42 Å and an interlayer spacing of 13.35 Å.[21,25,35,36] As illustrated in figure 1.2, HOPG naturally possesses two distinctive surfaces depending on how the graphite material is cut. If it is cut parallel or perpendicular to the graphite layers, the resulting electrode could be abundantly

basal plane pyrolytic graphite (BPPG) or edge plane pyrolytic graphite (EPPG), respectively.[37,38]

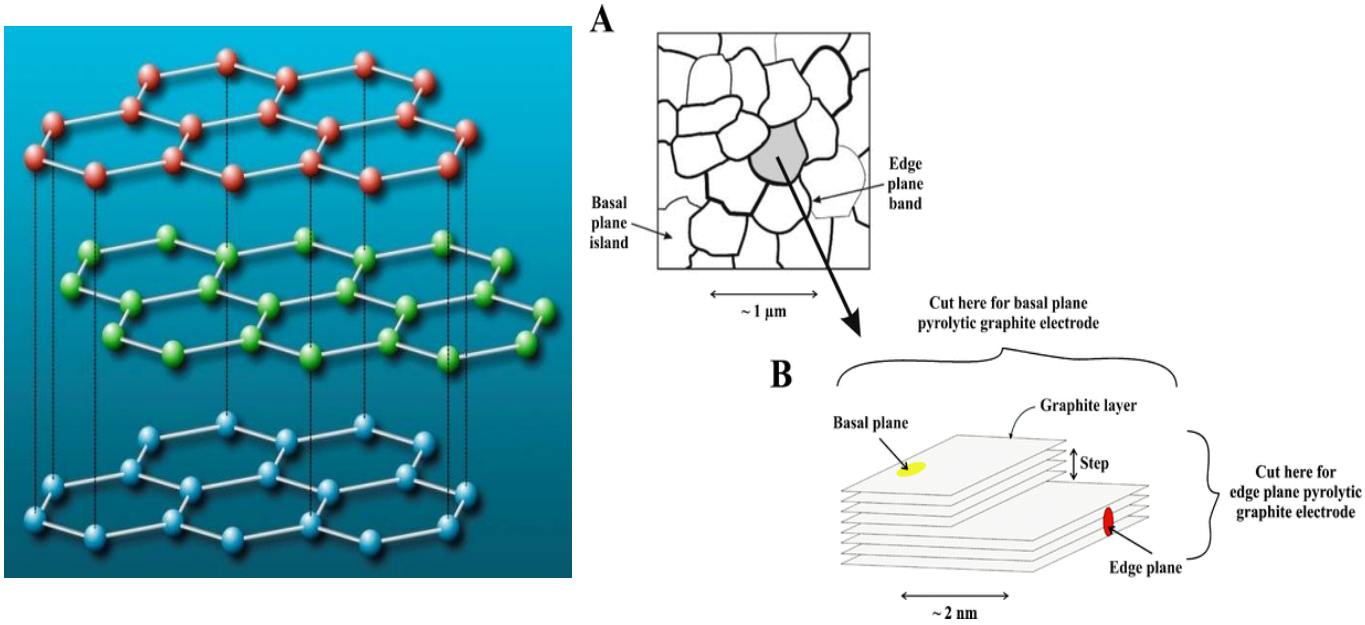

Figure 1.2. *(A) shows systematic representation of graphite (B) systematic representation of HOPG with orientation of edge and basal plane sites (adapted from references [39,40]).*

1.2.3. Glassy Carbon

Another type of carbon electrode, glassy carbon (GC), also referred to as vitreous carbon, is one of the most utilized carbon materials for electrochemical purposes. GC is made by the controlled degradation of polymers (generally polyacrylonitrile) under high pressure and temperature in an inert ambient. Treatment with heating continues until all atoms—apart from the carbon—are completely removed. The resulting carbon material has a conjugated carbon microstructure and commercially comes in shape of rods, plates or disks. The structure of GC is comprised of interwoven graphitic ribbons. As a consequence of this structure, GC is a harder material than graphite. Therefore, this material is believed to be water and gas resistant.[21,25,35,41] Due to the fact that GC electrodes are known to have a random combination of edge and basal sites (unlike HOPG electrodes which have predominantly edge and basal sites), this carbon microstructure has both a complex surface chemistry and organic functional groups containing oxygen with relatively low surface

coverage present at graphitic edge sites. Hence, the electrochemical response attained at this surface greatly depends on the preparation and pre-treatment of this carbon electrode.

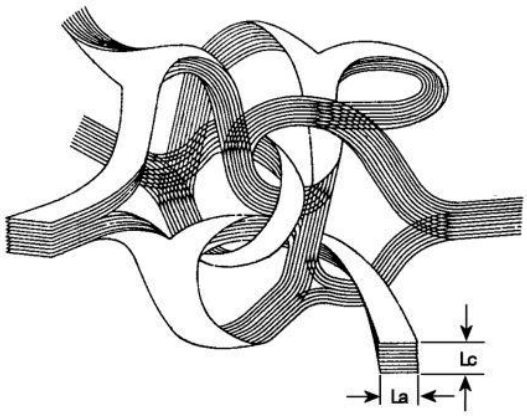

Figure 1.3. *The representation of the structure of glassy carbon (adapted from reference [42]). (La ~ 50Å: Intraplanar Microcrystaline Size, Lc ~ 31 Å: Interplanar Microcrystaline Size).*

1.2.4. Carbon Nanotubes

Carbon nanotubes (CNT) can be considered as a graphene sheet rolled up to form a tube. CNTs usually fall into two groups, single-walled carbon nanotubes (SWNT) and hollow multi-walled carbon nanotubes (H-MWCNT). SWNTs contain only one layer of graphene and multi-walled carbon nanotubes which, as the name suggests, contain several tubes that all share the same axis. If these tubes are situated one inside the other, the resulting structure is that of an H-MWCNT. If these are placed at a particular angle to the axis of the tube, this leads to a bamboo-like multi-walled carbon nanotube and, as a consequence of such an alignment, a high amount of edge sites exits at these CNTs.[37,43,44] When CNTs are compared to graphite, although the tube walls and the tube ends can be considered basal and edge plane like, sometimes this assumption causes a misunderstanding, which corresponds to the fact that the walls are identical to basal plane or graphene in terms of electronic structure. For instance, semiconducting CNT, which is believed to exhibit more structure with respect to graphite, does not have electronic states, whereas metallic SWNT exhibits rather good DOS distribution (refers to the number of electrons at particular energy level occupied by electrons) above and below the Fermi level. Hence, SWNT can be metallic or semiconducting carbon materials depending on the tube diameter.[21] In fact, one in a third of

SWNCT are metallic while the rest of them are semiconductive. Figure 1.3 shows the different types of CNTs mentioned above.

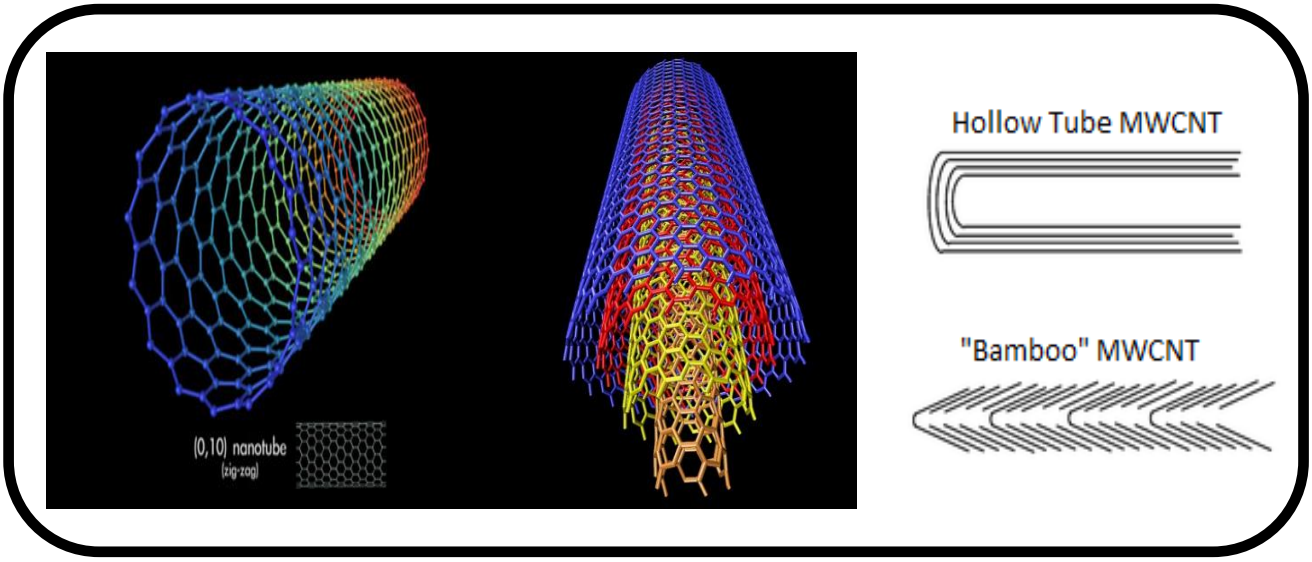

Figure 1.4. *Depicts the representation of SWCNT [45] and the various different MWCNT morphologies.* [37,46]

1.3. Electron Transfer Kinetics at Carbon Electrodes

It is well known that edge sites exhibit considerably faster electron transfer kinetics than basal sites for most redox couples. For example, according to theoretical work carried out using CNTs[47] and a review,[48] the tube ends, regarded as edge plane, were found to be more reactive than the tube walls, which are basal plane. Hence the edge plane frequently shows reversible behaviour whereas, in some cases, the basal plane might reveal irreversible voltammetry. As a consequence of this, there is a direct relationship between peak separation and rate constant, which means that a lower proportion of edge sites corresponds to higher peak separation and lower electrochemical rate constant.[36,37,49,50]

A work[51] carried out to compare electron transfer rates at HOPG and GC electrodes with the aid of redox probes found that GC had at least 3-5 times faster electron transfer kinetics than HOPG. As expected, such a difference is directly related to the lower density of states at HOPG as compared to GC. Banks *et al.*[37] compared the rate of electron transfer at

edge and basal sites and concluded that, since electrocatalysis predominantly occurs at edge plane sites, the electron transfer rate at edge sites is superior to basal sites. This finding was also supported by Edwards *et al.*[52] who investigated the electroactivity of different sites of HOPG electrodes by dropping a Nafion film containing redox systems such as tris(2-2′-bipyridyl)ruthenium(II), ($[Ru(bpy)_3]$)$^{2+}$ and hexaaminoruthenium(III) ($[Ru(NH_3)_6]^{3+}$) onto HOPG. It was then shown that the electron transfer rate at HOPG surfaces was diminished because of the fact that diffusion is considerably decreased due to the presence of the thin layer film and due to the fact that the electroactivity of the edge and basal plane of HOPG towards redox couples differs.

In the case of the electrochemical reduction of a redox probe, ferricyanide, at plain basal plane pyrolytic graphite (BPPG), BPPG modified with CNT film and edge plane pyrolytic graphite (EPPG), peak separations for those types of carbon electrodes were found to be 350 mV, 78 mV and 58 mV, respectively, indicating that CNTs exhibit the fastest electron transfer kinetics whereas the electron transfer rate for BBPG is rather sluggish,[37,49] considering that all electrodes have a similar surface area. When the voltammetry of ferricyanide at the EPPG is taken into account, the peak separation attained for EPPG is slightly higher than for CNT; this difference is attributed to impurities of basal site that exists in EPPG electrodes. Similar work[53] was also performed for electrochemical oxidation of epinephrine and NADH and, as for the electrochemical reduction of ferricyanide, identical results were obtained in terms of peak separation and electron transfer kinetics.

In order to show that faster electron transfer can be accounted for by the presence of the edge sites, BPPG surface can be roughened by polishing with alumina slurries, which undoubtedly introduces edge sites or defects in the electrode surface. It was then stated by the Compton group that electrochemical responses obtained at the BPPG electrode after polishing and the EPPG electrode are almost identical, which clearly indicates that faster electron transfer at edge plane of HOPG compared to basal plane electrodes is directly related to the proportion of edge sites at HOPG electrodes.[37] There are also a few published works supporting very slow electron transfer at basal sites of HOPG surface predominantly provided by step edges.[54-59]

If we wish to evaluate electron transfer rates observed at different sorts of carbon electrode, three factors, the redox mechanism, the surface density of electronic states and the

fraction of edge sites, always need to be considered.[60] In the case of the redox mechanism, the electron transfer rate is highly affected by the existence of functional groups containing oxygen[61,62] or hydrogen bonding sites.[63,64] It was shown that edge sites were found to be more reactive to metal deposition[65,66] and functionalization by diazonium salt.[67] Regarding the second factor, electron transfer depends on the density of electronic states. It is recognized that the basal plane of HOPG has a low DOS near the Fermi level.[68] As a consequence of this, conductive surfaces that possess low DOS are expected to have a low electron transfer rate. Finally, the proportion of edge defects is significant for electrochemical reactivity. For example, the modification of edge and basal plane electrodes with anthraquinone disulfonic acid was found to be more durable at the edge sites than at the basal sites because of differences in the interaction energy and hydrogen binding sites.[64] In addition, the surface coverage determined by electrochemical methods is 30 times higher than by STM. These high resolution STM images showed that these surface defects stimulate electronic disruption to the surface.[64]

As previously noted, it is broadly accepted that the basal plane of HOPG is recognised to possess relatively low reactivity to any electrochemical or chemical process. Therefore, electron transfer at the basal surface of HOPG electrodes for many redox systems is attributed to step edges that intersect the basal surface of HOPG. However, this general approach regarding the inactivity of basal sites, which is predominantly claimed by Compton`s research group, has been contradicted by Unwin *et al.* For instance, a recent article[69] by Unwin`s research group contradicts the fact that fast electron transfer at the basal plane of HOPG electrodes is due to step edges.[54,58] According to their experimental findings, CV measurements were carried out on 5 different grades of the highest quality, mechanically cleaved HOPG electrodes with different surface coverage of step-edge and height in the presence of $[Fe(CN)_6]^{-4/-3}$ and $[Ru(NH_3)_6]^{+3/+2}$. It was then found that slightly reversible voltammograms were obtained for freshly cleaved HOPG electrodes with the peak separation of 59 mV, which is close to the theoretical value. The peak separation for HOPG electrodes that have different proportions of edge defects and step spacings were also found to be quite similar to each other. By running CVs for the freshly cleaved basal plane of HOPG electrodes at different scan rates, a diffusion coefficient for $Fe(CN)_6^{-4/-3}$ of $7.3(\pm0.3) \times 10^{-6}$ cm^2 s^{-1} was obtained, which is consistent with reported values in the literature.[70] All these interpretations based on electrochemical results contradict previous works that claim that fast electron

transfer kinetics are only associated with edge sites. These results were also supported by using high spatial resolution electrochemical imaging in a scanning electrochemical cell microscopy.[71] It was then shown that the electron transfer kinetics for $[Fe(CN)_6]^{-4/-3}$ and $[Ru(NH_3)_6]$ were nearly reversible with $k_0 > 0.1$ cm s^{-1}. It is also noteworthy that the electrochemical response of $[Fe(CN)_6]^{-4/-3}$ at the basal surface decreases over time while the electrochemical imaging process is in operation. Similar studies were also performed on freshly cleaved HOPG with the aid of the scanning micropipette contact method; there, basal sites were found to show good reactivity towards $[Fe(CN)_6]^{-4/-3}$. Anne[72] and Frederix[73] also demonstrated that HOPG electrodes with basal plane orientation exhibited good reactivity to $[Ru(NH_3)_6]^{3+/2+}$ by using SECM-AFM. Furthermore, the effect of the continuous CV measurements and exposure of HOPG surfaces to the environment were also investigated; the peak separation was found to increase as the number of cycles increased and where electrodes were more exposed to air, which was confirmed by *in situ* AFM measurements. According to this, apparent electron transfer decreases as more species are physically adsorbed onto the HOPG electrode as a result of a blocking effect, while conducting AFM measurements illustrated that local surface conductivity declines over time after cleavage of the surface. Obviously, one must always remember that the electrochemical properties of any type of carbon electrode greatly depend on the history of the carbon material and the polishing procedures that were utilised. Moreover, the same research group also explored the active sites for catalysing many chemical reactions.[69] As mentioned above, in the case of NADH oxidation, the pristine basal plane of graphite was found to be inactive. Patel *et al.*[69] investigated dopamine and catechol oxidation on graphite electrodes. As with the study explained above, they found that the basal plane of HOPG exhibits the electro-oxidation of dopamine and catechol.

Luque *et al.*[74] also contradict a recent article by Nissim *et al.*[75] which claims that there was an inevitable relationship between the DOS of the electrode material at the Fermi level and the kinetics for electron transfer reactions of quinone adsorbed on graphite and gold. According to their work, it was found that the rate of electron transfer (outer-sphere reactions) is proportional to the DOS. However, Luque et al. reports that, since it is not certain whether adiabatic electron transfer takes place on graphite electrodes or not, on the basis of DFT results, they suggested that this reaction is adiabatic.

Very recently, Compton *et al.*[76] have published another paper in response to the comments made by Luque et al. and Unwin et al. who pointed out that, since there is a large

amount of literature that supports the idea of faster electron transfer at edge sites as compared to basal sites. Non-adiabatic electron transfer process occurs. In reply to Unwin *et al.*, they questioned how reliably the local microscopic findings correlated with the large scale electrochemical responses of HOPG electrodes; they also mentioned that there are many papers supporting the fact that step edges mainly account for this fast electron transfer. In addition, they also question whether their voltammograms are fully reversible and, if so, how likely others are to produce their pristine HOPG electrodes.

In conclusion, in terms of electron transfer kinetics at the basal surface of HOPG, there are few disagreements between results because electrochemical transfer is noted to be sluggish at basal sites with conventional electrochemical methods, while the basal surface of HOPG was found to be electrochemically active by using micro- and nano-scale measurements. Therefore, it is extremely crucial to review all of those articles critically for the purpose of understanding the electrochemical activity of different sites of HOPG electrode.

1.4. Modification of Electrodes

The covalent bonding of organic functionalities to conducting surfaces, carbon (glassy carbon, carbon nanotube), metal surfaces (nickel, gold) and semiconductor electrodes has drawn considerable interest over the last two decades.[12] This approach has led to a wide variety of applications of the relevant modified electrodes in the field of electrochemistry, such as sensors and bioelectronics.[77] It is well recognised that organic compounds can be covalently grafted to the surface of various carbon electrodes by the electrochemical oxidation of primary amines or the electrochemical reduction of diazonium salts, which were reviewed in depth for a wide range of organic functional groups and electrode materials, such as glassy carbon, carbon nanotube, gold, platinum, and iron surfaces by various researchers.[20-22] The electrochemical attachment of an organic layer to conductive surfaces is achieved through an electron transfer between the surface to be functionalized and an organic compound. These approaches for surface modification are regularly regarded as being appealing methods since they result in a covalent bond between the substrate and the organic layer.

1.4.1. The Modification of Electrode Surfaces by Reduction of Diazonium Salts

The functionalization of conductive surfaces by the electrochemical reduction of diazonium ions to form C-C covalent bonds was first introduced in 1990 by Pinson.[78] The method is rather easy. A diazonium salt is dissolved in an aprotic solvent (acetonitrile or DMF) in the presence of supporting electrolytes. A potential is applied to the electrode to be modified by means of a potentiostat; this results in a rather broad irreversible peak on the first scan at the potential of 0 V vs SCE, depending on the substituents on the phenyl ring; it then disappears on the successive scans, corresponding to the fact that the electrode surface is completely coated with an organic layer that hinders the access of diazonium radicals to the substrate. Following sonication of the modified electrode so as to remove any substance which could form a weak bond on the surface, the electrode is finally characterised by numerous methods. The redox potential of phenyl radical/phenyl anion can be determined by simulating the corresponding voltammogram (E^0 = 0.05 V vs SCE) and this value is also in good agreement with the value attained by density functional theory (DFT).[79] For both methods, electron transfer is attributed to breaking the bond of dinitrogen. This low reduction potential generally stems from the strong electron-withdrawing effect of the N_2^+ group. In addition, a reduction of the aryl diazonium salt can occur without an applied potential because the irreversible nature of the aryl diazonium salt reaction provides the driving force to generate radicals which couple to the surface.[80,81] Reducing reagents can also be used to derivatize the carbon surfaces in the presence of diazonium salts. In this case, reducing the reagents (such as ferrocenemethanol, iodide, and hypophosphorous acid) initiates the formation of aryl radicals that react with carbon surfaces, such as carbon powder[82-88] and polymers.[89] Sometimes, the surface itself acts as the reducing agent,[90](in most cases, when it is a metal,[91] such as copper, iron, zinc,[92,93] or titanium,[94]) which means that the surface reduces the diazonium salt to a radical; this spontaneously generated radical thereby couples to the corresponding surface. Spontaneous attachment of 4-nitrobenzenediaazonium salt to glassy carbon surfaces was observed in the presence of acetonitrile and tetrabutlyammonium tetrafluoroborate (NBu_4BF_4).[95]

The general reaction mechanism for the functionalization of surfaces with the reduction of aryl diazonium salts is depicted in Scheme 1. According to this scheme, a

radical is generated under the applied potential; then, this radical reacts at the carbon surface to form a covalent bond, which is durable and stable.[12]

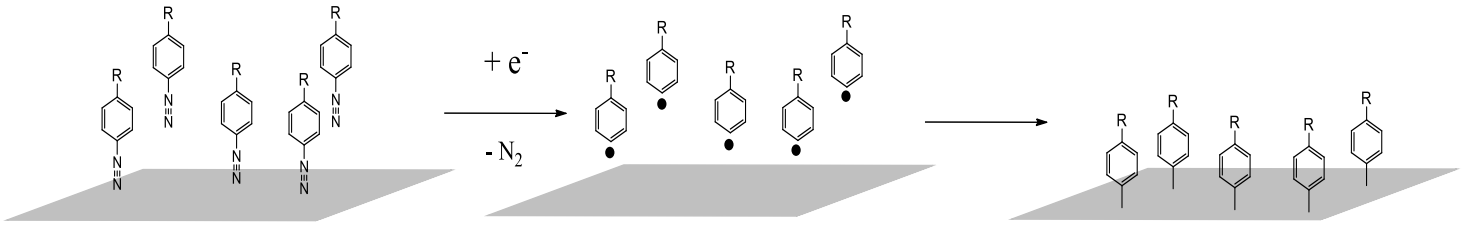

Scheme 1.1. *General description for modification of conductive surfaces by the reduction of diazonium salts.*

Electrografting of aryl diazonium salts has been achieved onto a wide variety of substrates, such as carbon electrodes, GC, highly ordered pyrolytic graphite with edge and basal plane sites,[96,97] graphene,[98-100] carbon fibers[101] and nanofibers,[102] carbon nanotubes,[103,104], mesoporous carbons[105-107] and diamond,[108-110] metals and nanoparticles,[111-114] TiO_2,[115] SiO_2, SiC[89] and teflon.[116]

Electrochemical reduction of aryl diazonium salts onto carbon electrodes exhibits a very different behaviour from other substrates such as metals, nanoparticles and inorganic substrates. For instance, it is well established that this reaction takes place faster at the edge plane sites than basal plane sites, which is also verified by applying DFT calculations to aryl modified single layer graphene sheets and carbon nanotubes.[19,117] According to this mechanism on HOPG electrodes, firstly, the electrografting of diazonium salt occurs at the edge sites; then, the coating grows over this already grafted layer.[117] Various types of phenyl groups bearing different functional groups (such as phosphonic acid,[118] N,N-diethylamine and diphenylamine,[119] maleimide,[120] boronic acid,[121,122] and quinone[123,124]) have been attached to conductive materials. 4-nitrobenzene is broadly regarded as the most examined organic compound since it can be easily determined with spectroscopic methods, infrared spectroscopy (antisymmetric and symmetric vibration at 1520 and 1340 cm^{-1}), and XPS (signal at 406 eV).[125]

The efficiency of the immobilisation of diazonium salts to electrode surfaces needs to be taken into account. The faradaic efficiency of this process is usually less than 100%. Work by Allongue[126] claimed that the efficiency of attachment of diazonium salts depends on the electrode material, showing that 84% and 56% of the generated radicals couple to the GC

surface and highly oriented pyrolytic graphite, respectively. The estimated surface coverage of a modified electrode obtained by the reduction of a diazonium salt is at maximum 1.2 nmol/cm^2, which is subject to the size of the corresponding diazonium salt to be coupled to the electrode surface and the minimum spacing between molecules on the surface. In reality, experimental coverages are lower than this value.[127,128]

It is also possible to perform further modification onto functionalized surfaces. For example, after electrochemical reduction of 4 nitrobenzenediazonium salt, further functionalization onto this modified surface is viable since amine groups obtained by either electrochemical or chemical reduction of the nitro group are rather reactive. Good examples of this methodology is given by Lyskawa and Nielsen *et al.* focusing on the coupling of anhydrite[129] and isocyanides[130] to amine modified electrodes obtained after the electrochemical reduction of nitro benzene. The covalent attachment of biotin terminated by an acetylene group to carbon surfaces modified by azido and ethyl groups via the electrochemical reduction of phenyl azide and phenylacetylene diazonium salts was achieved as shown in figure 1.5.[131] Reilsons and Zhong`s research groups also showed that dihidroxybenzene derivatives were able to be grafted onto GC electrodes by the electrochemical reduction of a benzene diazonium salt containing catechol groups, followed by a further covalent binding of ferrocene to the modified GC surface by employing a click chemistry strategy.[132,133] Gehan *et al.* investigated the grafting of gold nanoparticles to gold surfaces by the electrochemical reduction of a diazonium salt followed by the click chemistry approach.[134]

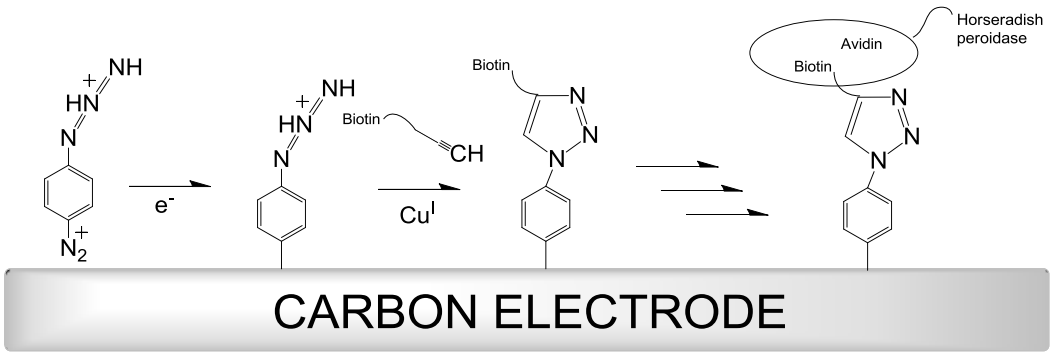

Scheme 1.2. *Covalent attachment of biotin to a GC surface using click chemistry methodology (adapted from reference [131]).*

A number of biosensors have been developed using methods based on the modification of conductive surfaces through the electrografting of diazonium salts. In this

approach, the organic layer can be considered as a platform for the further attachment of biomolecules, proteins, enzymes and DNA. Baker *et al.* carried out the attachment of DNA oligonucleotides terminated with ester group coupled to the amino phenyl modified surface obtained by the reduction of a nitro phenyl group in order to give rise to an amide bond.[135] Hansen[136] also showed the attachment of DNA to GC and gold electrode linkers bearing triazene, ferrocene, and activated ester functionalities. Once triazene is converted to a diazonium salt, electrochemical grafting of GC and gold is achieved; then, the attachment of DNA to these functionalized surfaces is conducted.

Carbon surfaces (such as GC,[137,138] HOPG,[139] carbon nanotubes[140] and gold[141]) are used as a platform for the attachment of a wide variety of enzymes (e.g. glucose oxidase,[142,143] horseradish peroxidase,[144,145] laccase[146] and cytochrome P4502B4.[147]

Even though the diazonium salt method for the derivatization of surfaces provides many advantages, there is still a drawback, which is multilayer formation. The mechanism of multilayer formation on the surfaces is depicted in Scheme 1.3. According to that Scheme, aryl radicals are a substantialy reactive species that can form a covalent bond on the electrode surface where they are generated. However, in Scheme 1.3. They also react with already-grafted aryl layers and the cyclohexadienyl radical as shown in reactions 1-3. Afterwards, the cyclohexadienyl radical anion can follow either route i or ii. In the case of route i., a polyphenyl layer is formed through the reaction mechanism involving the reoxidation of the radical and the reduction of the benzene diazonium cation. If the mechanism follows route ii, subsequent to the generation of the cyclohexadianyl radical, a polymeric chain is produced which is triggered by the coupling of a diazonium cation onto the cyclohexadienyl radical, followed by the prompt reduction of the radical cation to give structure 6. The last step involves the reoxidation of a cyclohexadiene, which is expected due to the aromatic stabilization of the product.[125]

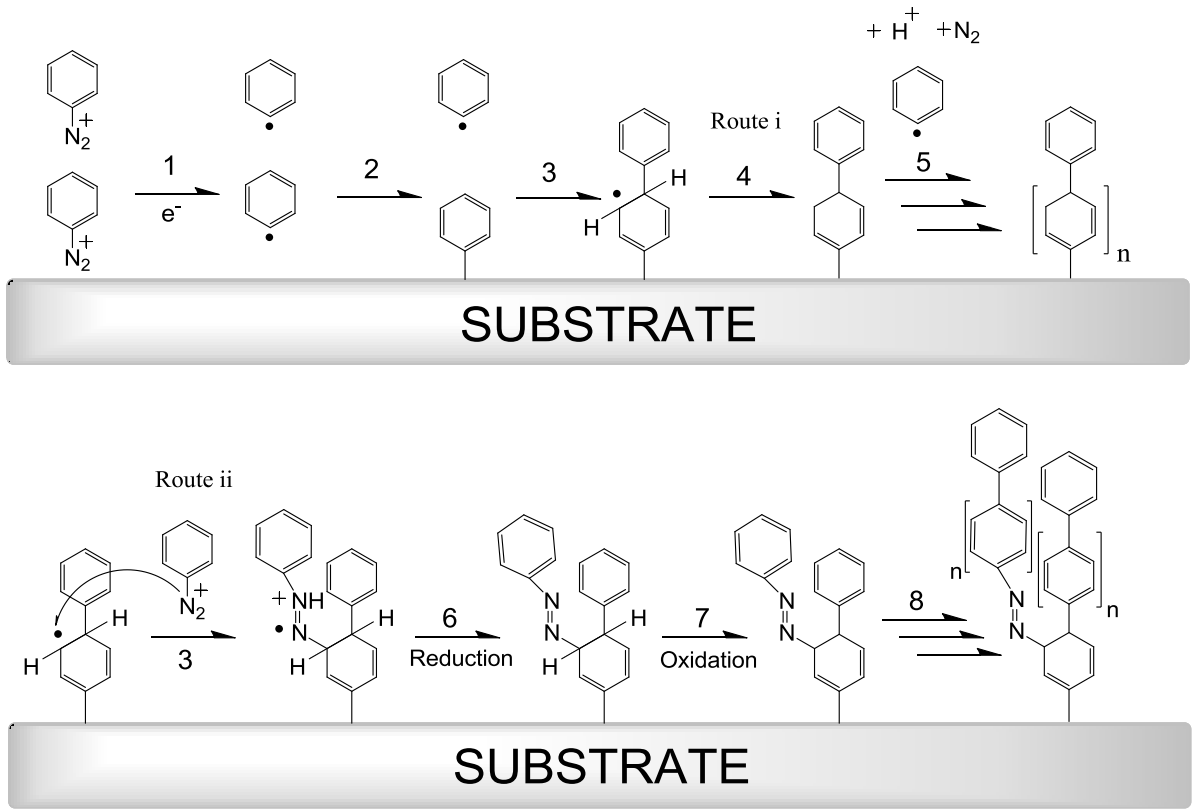

Scheme 1.3. *The formation of multilayers on an electrode surface by the reduction of diazonium salts.*

As previously mentioned, all linkers used for the functionalization of carbon electrodes in this work bear a Boc protecting group so as to supress the formation of multilayer and bridge structures. The *tert*-butyloxycarbonyl (Boc) group is commonly used to protect amines and amino acids.[148-150] It is believed to prevent the basic and nucleophilic attacks of a radical or negatively charged ion towards a target. Other protecting groups (Fmoc, CBz) are therefore optimal choices for the multistep synthesis of many organic compounds. In the case of the modification of surfaces by the electro-reduction of benzene diazonium tetrafluoroborate salt, the presence of the Boc-protecting group avoids the formation of multilayers, because the bulky Boc protecting group minimises multilayer formation by diminishing the grafting rate on the first layer formation, which means that the Boc protecting group prevents the attack of the generated radicals on the ortho positions of the aromatic rings already attached to the electrode.[151,152]

1.4.2. The Modification of Electrode Surfaces by the Oxidation of Amines

The electrochemical derivation of conductive surfaces by the oxidation of amines was first reported in 1990 for carbon fibre[78] and GC electrodes.[22] The functionalization of surfaces by employing this method was studied in detail with a variety of organic compounds and electrode materials, such as GC, CNT, gold, platinum, and iron surfaces. The mechanism of this technique is based on the electrochemical formation of amine radicals by the oxidation of the relevant amines, which can then couple to an unsatisfied valence or double bond on the carbon electrode surface.[153-156] Barbier *et al*[78] suggested that the electrochemically generated amine radical is attached to the corresponding surface, as illustrated in Scheme 1.4. According to this investigation—carried out by employing electrochemical techniques and IR—, initially a radical cation is formed. This radical cation leads to the formation of a carbon radical through the deprotonation of the amine group, followed by a hydrogen shift that gives rise to an aminyl radical that couples with the substrate.

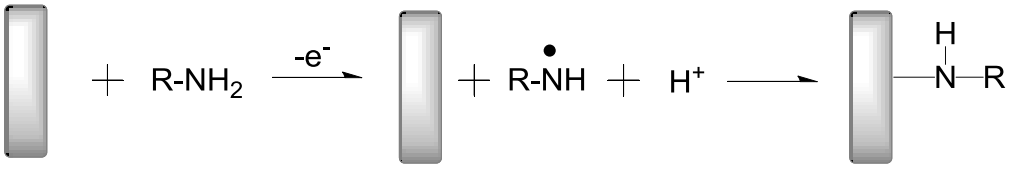

Scheme 1.4. *General description of the modification of conductive surfaces by the oxidation of amines.*

The electrochemical oxidation of aliphatic amines at the relevant substrate in organic solvents occurs at potentials beyond 1 V vs SCE by means of an irreversible one-electron process. The measured transfer coefficient α and the apparent rate constant k_{app} indicate the formation of a radical cation via a very slow electron transfer.[153] During the modification of the conductive surfaces by the electrochemical oxidation of amines both in aprotic or aqueous media, a rather broad irreversible anodic peak is observed and, on successive scans, the anodic peak disappears, indicating that the electrode surface has been completely blocked.

The degree of the substitution of the amine group is also quite crucial in carrying out immobilisation on the electrode surface. Thus, since the attachment of primary amines is considerably easier and the surface coverages are approximately three times larger than for secondary amines, the grafting of tertiary amines to electrodes is nearly impossible. This

difference might be attributed to steric effects and to the loss of a proton from the amine radical necessary for this mechanism (Scheme 1.4) which is impossible for tertiary amines.[153] The surface coverage obtained by CV ranges from 0.3 nmol cm^{-2} to 0.6 nmol cm^{-2}, which is close to the predicted coverage for a monolayer. The structure of the amines to be attached to the surface seems to have an impact on the surface coverage. For instance, this is the case for alkyl amines, as the length of the alkyl chain increases the surface coverage decreases. Also, amines bearing an aromatic ring appear to give lower coverage compared to alkyl amines. This difference is attributed to their steric effects.[157]

Not only aliphatic amines but also aliphatic amines bearing electrochemically active organic functionality (such as ferrocene[158], amino acids[159], nitro,[160] and aromatic amines, e.g. p-amino sulfonic, p-amino benzoic and p-aminobenzyl phosphate) are covalently attached to the surfaces by the electrochemical oxidation of the corresponding reagents.[161,162] Electrografting of hydrazine is also known to form a C-N bond. For example, aryl hydrazines that bear methoxy (-OCH_3), carboxylic and nitro groups were also electrochemically bonded to GC with the aid of SECM (Scanning Electrochemical Microscopy).[163-165] The functionalization of carbon electrodes via the electrochemical (EC) oxidation of amines can be utilized for the immobilization of DNA to previously modified substrates. For instance, Tang *et al.* accomplished the immobilization of DNA onto CNT that was modified with ethylenediamine by means of EC oxidation.[166]

Glucose oxidase was also coupled to carbon surfaces modified through jeffamine and 4-nitrobenzene diazonium salt with the help of SECM; it was shown that the amine functionalized carbon surface that was obtained subsequent to the electrochemical reduction of the already grafted nitrobenzene yielded more enzyme activity than its being coupled with jeffamine.[167]

Functionalized CNT by means of the electrochemical oxidation of amines was also applied for the deposition of nanoparticles. Downard and co-workers achieved the electrografting of tetraethyleneglycol diamine followed by the deposition of gold nanoparticles capped with citrate. The authors stated that the most important advantage of this procedure for the deposition of gold nanoparticles was that a robust attachment was attained even after ultrasonication.[168] [$Ag(NH_3)_2^+$] was also deposited on a CNT surface that was electrografted through 4-aminobenzoic acid. Subsequent to the functionalization of the

CNT, followed by the coupling of Ag nanoparticles, it is possible to acquire Ag nanoparticles after the electrochemical reduction of Ag^{+}[169].

Ghanem *et al.* modified GC surfaces with Boc-protected diamine and, following the removal of the BOC group using 4 M HCl in dioxane, a 25 member of library of dihydroxy benzene compounds were coupled with the grafted GC surfaces in order to investigate whether the position of the hydroxyl group on the aromatic ring has any effect on the surface coverage of dihydroxy benzene and NADH oxidation.[170] Carbon electrodes were also modified with amino acids for the purpose of detecting dopamine in the presence of ascorbic acid.[171] A screen-printed electrode was electrografted by the electrooxidation of thionine, followed by the coupling of horseradish peroxidase in the presence of glutaraldehyde as a coupling agent. The resulting electrode can be used for hydrogen peroxide detection.[159]

There are evidently various advantages to the modification of conductive surfaces by pursuing this method. For instance, a wide variety of amines can be grafted and a robust bond can be regularly obtained between the substrate and the organic layer. The only disadvantage to this method is that it can be applied to very few substrates, such as carbon, gold and platinum.[19] Furthermore, more effort should be devoted to shed light on the mechanism of determining whether multilayers can be formed during electrografting.

On the other hand, the method, based on the formation of primary or secondary amines' radical cations has the disadvantage of generating polymeric chains and bridge structures on the surface when organic molecules bearing two amino groups are used for the purpose of immobilisation.[172] Therefore, the modification of conductive surfaces by the oxidation of the corresponding diamines is not widely preferred. In order to overcome the formation of polymeric chains and bridge structures, a new approach has recently been introduced by Chretien and Ghanem[173] for the modification of carbon surfaces. By means of this new approach, a Boc-protecting group (tert-butyloxycarbonyl) bound to the amino group plays a crucial role in the modification of surfaces by multiple steps. The presence of tert-butyloxycarbonyl suppresses the nucleophilicity of the amino group. Therefore, it prevents the formation of polymeric chains and bridge structures. Another benefit of the Boc-protecting group is that it overcomes the issue related with synthesising diazonium salts with different functional groups. Once the protecting group is removed in order to give a free amino group, further modification with various redox probes, such as anthraquinone and

nitrobenzene, can be carried out at this reactive site by using solid-phase synthesis methodology, and the modified surfaces can subsequently be characterised by a wide variety of instrumental methods.

1.4.3. The Characterisation of Modified Surfaces

When the modification of the electrode surface is achieved by the reduction of diazonium salts or by the oxidation of amines and subsequent to the sonication of the electrode, we need to ensure that the desired organic layer is on the surface. There is a wide variety of instrumental methods, such as CV,[153] X-ray Photoelectron Spectroscopy (XPS),[80,174-177] Fourier Transform Infra-Red Reflection Absorption Spectroscopy (FTIRRAS), Raman,[178,179] AFM [180] and STM[181] which have been used by researchers for the characterisation of grafted surfaces.

Fourier Transform InfraRed Reflection Absorption Spectroscopy (FT IRRAS) has been frequently used to characterise organic layers on surfaces. For example, the nitrophenyl group exhibits two intense peaks at 1530 and 1350 cm^{-1}. This method can also be used as a confirmation of strong attachment between the substrate and the grafted layer of the benzylpheny and dimethylamino groups.[123,178] The coupling of diazonium salts with substrates can also be confirmed on the basis of the disappearance of the N_2 stretching band situated at between 2300 and 2130 cm^{-1} after the attachment of the diazonium salt.[81,179,182] Again, the covalent attachment of nitrophenyl and its derivatives to GC and HOPG electrodes with edge and basal plane sites was also evidenced with Raman spectroscopy through the assignment of spectra by the McCreery research group.[173] Raman spectroscopy also allows for one to determine the surface coverage by means of the integration of the baseline corrected peaks.[81,179] Raman spectroscopy is also quite a useful method for determining the initial, intermediate, and final products during the reduction of the nitro groups. X-ray Photoelectron Spectroscopy (XPS) is one of the most employed instrumental techniques for characterising organic layers after successful grafting. For example, it is well established that the N1 peak of the nitrophenyl group and amines are located at 406 and 400 eV, respectively.[126,174,179] Moreover, other functional groups (i.e. halogens, carboxylic groups, and quinone derivatives) have been observed by this technique. It is also possible to measure

the thickness of grafted layers. Atomic Force Microscopy (AFM)[178,183] and Scanning Tunneling Microscopy (STM)[181] are widely used to verify moieties with variable heights and roughnesses.

1.5. Solid Phase Synthesis Methodology on Modified Carbon Electrodes with Boc-protected Amines

In this work, the functionalization of carbon surfaces after both the electro-grafting of Boc-protected diamines and the de-protection of the Boc group is carried out by following the solid-phase synthesis methodology. This methodology is based on the formation of an amide bond between the amine terminated carbon surface after the removal of the Boc group and a carboxylic acid. This reaction is hence required for the activation of the carboxyl group, which can be transformed into a more reactive functional group, e.g. acyl halide, anhydride, and acyl azide. On the basis of this explanation, it can be concluded that this reaction proceeds against adverse thermodynamics. Because amide bond is formed between two functional groups, carboxylic acid and amine coupling of these both functional groups is not likely to spontaneously take place under the room temperature. Therefore it is essential to convert hydroxyl group into a better departing group before reacting with amine group. As a result of the difficulties of this reaction, including its low yield, racemization and initially activate the carboxylic group , some phosphonium and uronium salts have been widely used as coupling agents (e.g. HBTU, HATU, HOAt and TCTU). In this study, we used HBTU as it had been proven to be efficient and effective in forming amide bonds in earlier work conducted by the Bartlett group.[172-173] Scheme 1.5 presents a general description of the mechanism of solid phase synthesis.

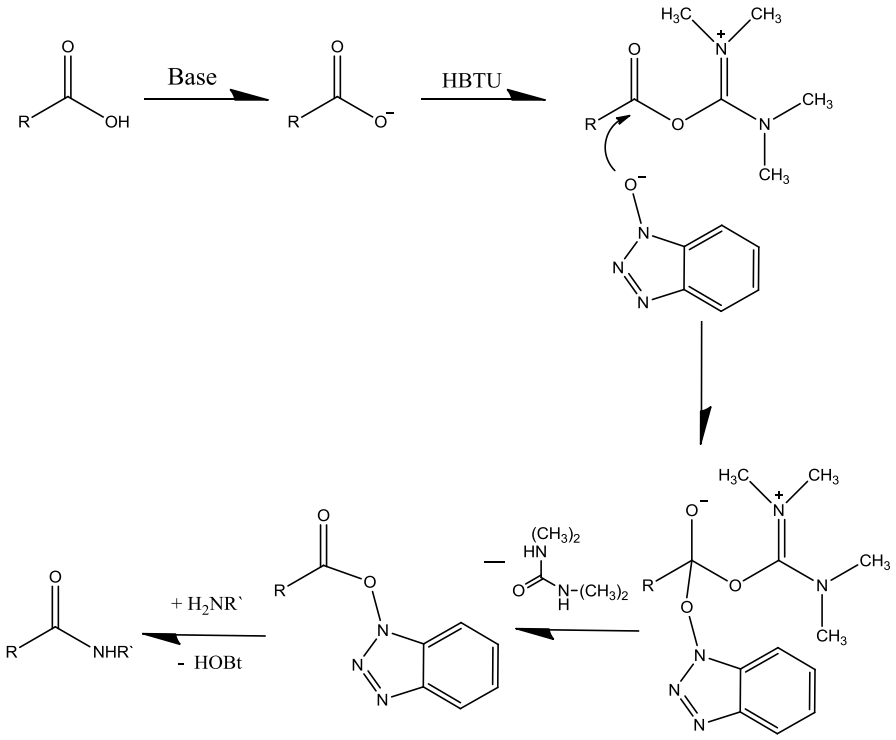

Scheme 1.5. *Mechanism of the Coupling Reaction of carboxylic acid in the presence of coupling agent, HBTU.*

In this study, GC and edge and basal plane graphite electrodes were electrochemically modified with different types of Boc-protected diamine linkers because we assumed that the different types of linkers have an impact on surface coverage and the kinetic of modified surfaces. After the removal of the protecting group by treatment, 4 M HCl in dioxane anthraquinone-2-carboxylic acid was coupled with the modified carbon electrodes by using solid phase synthesis methodology.

1.6. Oxygen Reduction

The electrochemical reduction of oxygen has been extensively studied by researchers because it is an essential reaction in fuel cells, metal-air batteries, gas sensors and in the electrosynthesis of H_2O_2.[184-187]

Unmodified carbon electrodes are regarded as very poor for the electrochemical reduction of O_2,[188] whereas carbon electrodes modified with appropriate quinone derivatives show excellent catalytic behaviour for O_2 reduction at neutral pH. The oxygen reduction

reaction takes place either via a two electron process which generates H_2O_2, or, depending on the pH and electrode material, four electron process with the final product of H_2O. Various types of carbon and metal electrodes have been used for oxygen reduction (e.g. HOPG,[189] PG (pyrolytic carbon),[190] graphite powder, porous graphite, natural graphite, GC,[191-193] CNT,[194] gold, gold nanoparticles, and nickel). It is widely known that the peak potential for O_2 reduction is more positive for GC and edge plane graphite compared to basal plane graphite. The reason for this behaviour is that the interaction of oxygen with functional groups on the surface is usually involved in the O_2 reaction. Moreover, edge plane graphite is more active to electron transfer and adsorption than basal plane graphite. The low reactivity of basal plane graphite is assigned to the low density of electronic states, the lack of functional groups and adsorption sites compared to edge plane and GC.[195-198] It is well established that carbon surfaces have many organic functionalities, such as carboxyl, phenolic hydroxyl, quinone derivatives. However, the question is which functional groups take part in the O_2 reduction. It was suggested that surface quinones are involved in O_2 reduction.[187] As the surface coverage of quinones on the surface is low, the attachment of quinone derivatives is commonly achieved by the reduction of the corresponding diazonium salts or the further modification of the grafted surface for the purpose of increasing the electrocatalytic activity in the O_2 reduction. A considerable amount of attention has been paid in order to determine the mechanism of the O_2 reduction on quinone modified carbon electrodes. It has been proposed that the reduction rate depends on the surface concentration of the semiquinone radical formed by the electrochemical reduction of quinones.[199] The radical anion then reacts with molecular O_2 to generate superoxide anion $O_2^{\cdot-}$, which follows an electrochemical mechanism.

$$Q + e^- \longrightarrow Q^{\cdot-} \qquad \text{I}$$

$$Q^{\cdot-} + O_2 \xrightarrow{k_c} O_2^{\cdot-} + Q \qquad \text{II}$$

$$2O_2^{\cdot-} + H_2O \longrightarrow O_2 + HO_2^- + OH^- \qquad \text{III}$$

Or, for the further reduction to H_2O_2

$$O_2^{\cdot-} + H_2O + e^- \longrightarrow HO_2^- + OH^- \qquad \text{IV}$$

Q represents the quinone species. Reaction (II) is regarded as the rate-determining step and, in this reaction model, the overall rate is determined by the concentration of $Q^{\bullet -}$. Reactions (III) and (IV) are considered to be fast and lead to the generation of H_2O_2.[200-202] Not only quinone derivatives, but also manganese oxide,[203] titanium silicates[204] and Au nanoparticles[205,206] were used for the O_2 reduction to H_2O_2 or H_2O.

In this study, the modified carbon electrodes with AQ that were attached through diamine linkers were evaluated for oxygen reduction by cyclic voltammetry and RDE. The reason that AQ is preferred for oxygen reduction is not only its variety of applications in electroanalytical chemistry and because of its reversible behavior but also because carbon electrodes modified by AQ through diamine linkers can be a good model for oxygen reduction reactions with Laccase, an enzyme commonly used for the construction of biosensors and biofuel cells.[207] Laccase is a multicopper oxidase, which drives four electron reduction of oxygen to water without any unwanted side and intermediate products, such as H_2O_2[208]. However, the major problem for enzyme-based biofuel cells is their short lifetime and their low power efficiency. It is also known that the direct electron transfer from electrode to enzyme is very difficult.[209] Therefore, the immobilization of the enzyme to a suitable electrode is a vital step. In order to overcome these difficulties, redox mediators—for instance, ABTS (2,2`-azinobis(3-ethylbenzothiazoline-6-sulfonate) and osmium-based polymers—have been used to shuttle electron transfer between laccase and electrode.[210] Furthermore, the electrode material can also be utilized as a platform after the attachment of an organic layer that facilities the immobilization of laccase. Naga et al.[211] accomplished the immobilization of laccase to MWCNT with 1-pyrenebutanoic acid succinimiyl ester as a tethering agent. After the determination of the kinetic parameters, such as the number of electrons transferred, the electrochemical rate constant and the electron transfer rate constant, using the rotating ring disk electrode technique, they concluded that a four electron reduction to water occurs at this electrode.[211] OH-functionalized MWCNT were also modified with anthracene groups followed by the immobilization of laccase that facilities the direct electron transfer between enzyme and electrode.[212] Similar work that concentrates on the coupling of anthraquinone and anthracene to GC electrodes already modified by the EC oxidation of Boc-protected diamines has been described in the literature, and AQ was found to be more reactive to the attachment of the enzyme[213]. Laccase was also immobilized onto gold

electrodes modified by anthracene-2-methanethiol[214] and aromatic diazonium salt[215] for the four electron reduction to H_2O, as illustrated in scheme 1.5.

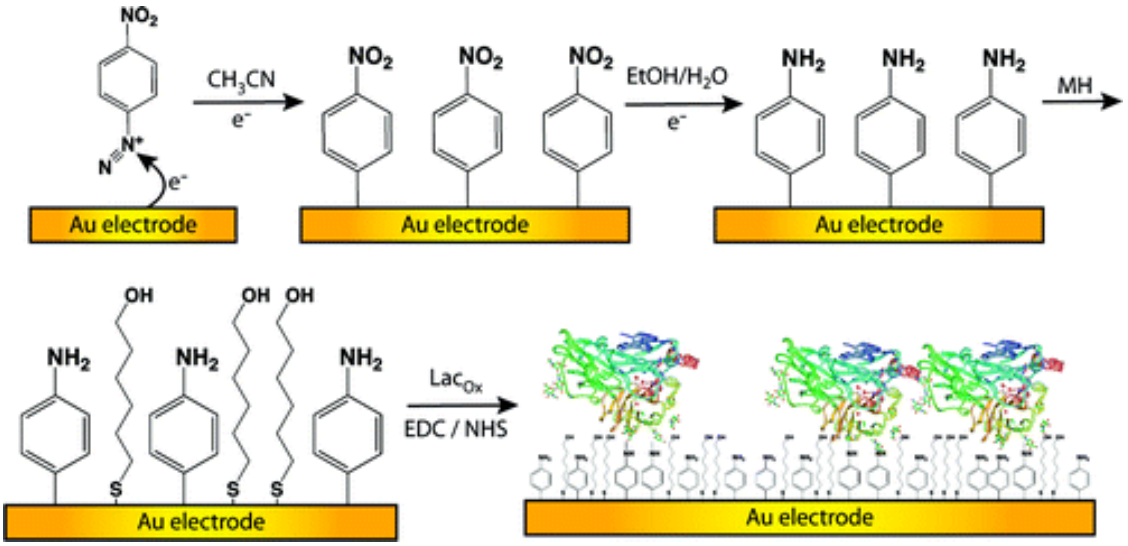

Scheme 1.6. *The modification of gold with an aryldiazonium salt and 6-mercapto-1-hexanol for laccase immobilization (adapted from reference [215]).*

In future work, laccase can be attached to the modified GC electrode by a wide variety of chemical compounds through different types of diamine linkers, and O_2 reduction reactions will be carried out at laccase immobilized electrodes with high-throughput screening using a multichannel potentiostat.

1.7. Density Functional Theory

As detailed in an earlier section, even though a great deal of practical effort has been expended to comprehend the mechanism of how organic molecules are attached to conductive surfaces, the details of the interfacial bonding between the substrate and layer are still vague. Since it is really complicated to understand this phenomenon with the aid of experimental findings, the first principals density functional theory (DFT) method has been used to shed light upon functionalized graphite, graphene, carbon nanotubes, metals and Si.[15]

DFT is a quantum mechanical theory considered as a theoretical approach to fulfil the calculation of the electronic structures of materials and molecules by following the Kohn-Sham or Hartree-Fock equations that contain electron exchange and that have a correlation

with the approximate functionals (which are generally local density approximation (LDA), generalized-gradient approximation (GGA), and hybrid functional (B3LYD)); and, after the development of GGA, there has been an increasing enhancement in the precision of DFT calculations.[15]

DFT is highly regarded as the most useful computational method for the estimation of the ground-state properties of electronic systems. Since there is a tremendous growing interest in DFT, it is broadly used in physics and chemistry to explore the electronic properties and structures of many complex bulk materials (such as solid surfaces, carbon nanotubes, polymers and proteins) due to its high accuracy and computational capability. DFT is based on finding ground state properties with electron density, which can be obtained by X-ray diffraction techniques. One of the advantages of using DFT is that, as no further assumption is required (i.e. the *ab initio* method), it is possible to perform DFT calculations for systems that consist of thousands of atoms by means of powerful computers. However, researches are continuing to improve some of the properties of DFT since it causes failure for the investigation of van der Waals forces when sparse material is used and underestimates the band gap and some of the electronic properties of corresponding systems. DFT employs electronic density *n(r)* instead of many-body wave function. DFT is based on the two theories introduced by Hohenberg and Kohn.[216]

First theorem;

The ground-state particle(electronic) density of many-body system uniquely determines the external potential, $V_{ext}(r)$. The energy functional of the corresponding system can be formulated in the sense of $V_{ext}(r)$ as follows,

$$E[n(r) = \int n(r)V_{ext}(r)dr + F[n(r)] \qquad \text{(Equation 1.1)}$$

Where $F[n(r)]$ is an unknown universal functional of $n(r)$, which can also be defined as Hamiltonian value. Ψ minimises this value and allows us to obtain ground state energy of the system.

$$E[n(\overrightarrow{r})] < \Psi\left|\hat{H}\right|\Psi > \qquad \text{(Equation 1.2)}$$

Where the Hamiltonian value is defined as follows,

$$|\widehat{H}| = |\widehat{F}| + |\hat{V}_{ext}| \qquad \text{(Equation 1.3)}$$

$|\widehat{F}|$ is the same for all system containing N electrons. Therefore, $|\widehat{H}|$ is determined by N and $\hat{V}_{ext}$.

Second Theorem;

This theorem is developed to obtain ground state energy and according to this theorem total energy of the corresponding system minimized by the density that corresponds to the exact ground state density.

In first theorem, it was demonstrated that $n(r)$ that can be used to define N and V_{ext} whereas V_{ext} describes $\hat{H}$ and Ψ. Therefore it is intrinsically noticed that Ψ is a functional of $n(r)$ and as a consequence of this F is a functional of $n(r)$.

$$F[n(r)] = <\Psi|\hat{F}|\Psi> \qquad \text{(Equation 1.4)}$$

Even though this theorem is widely recognised as competent, it is impossible to calculate ground state density, which is regarded as the one of the most significant drawback of this theory. This issue was sorted out by theory stated by Kohn-Sham[217]

Kohn-Sham Theory;

This equation is more useful for the calculation the energy of the electrons and forces of atoms. The main disadvantage of this theory is to comprehend the ground state kinetic energy of electrons. According to this theory, the DFT focuses on mapping the electrons of the interacting system onto fictitious non-interacting system that is in the motion within an effective Kohn-Sham single particle potential $V_{ext}(r)$

As it can easily be seen in Equation 1.1 the ground state energy of many-electron system can be acquired with the aid of energy functional. This situation can be expressed by Euler equation.

$$\mu = v_{ext}(\mathrm{r}) + \frac{\delta F[n(r)]}{\delta n(r)} \qquad \text{(Equation 1.5)}$$

Single particle orbitals can be used to determine the ground state wave function.

$$\Psi_{HF} = \frac{1}{\sqrt{N!}}|\Psi_1(\overrightarrow{r_1})\ \Psi_2(\overrightarrow{r_1})\ \ldots\ \Psi_N(\overrightarrow{r_1})|$$
$$|\Psi_1(\overrightarrow{r_2})\ \Psi_2(\overrightarrow{r_1})\ \ldots\ \Psi_N(\overrightarrow{r_2})|$$
$$\vdots\qquad \vdots\quad \ldots\quad \vdots$$
$$|\Psi_1(\overrightarrow{r_N})\ \Psi_2(\overrightarrow{r_1})\ \ldots\ \Psi_N(\overrightarrow{r_N})| \qquad \text{(Equation 1.6)}$$

The $F[n(r)]$ can be defined as follows,

$$F[n(\vec{r})] = T_s[n(\vec{r})] + E_H[n(\vec{r})]E_{xc}[n(\vec{r})] \quad \text{(Equation 1.7)}$$

Where $T_s[n(r)]$ and $E_H[n(r)$ represent the kinetic energy of non-interacting electrons and the electrons of the orbitals. $E_{xc}[n(r)]$ corresponds to the exchange correlation functional. On the basis of this explanation we can write Euler equation as follows.

$$\mu = v_{KS}(\mathrm{r}) + \frac{\delta T_s[n(r)]}{\delta n(r)} \qquad \text{(Equation 1.8)}$$

V_{KS} is made up of above stated equations.

$$V_{ks}(\vec{r}) = V_{ext}(\vec{r}) + V_H(\vec{r}) + V_{xc}(\vec{r}) \qquad \text{(Equation 1.9)}$$

$$V_H = \frac{\delta E_H[n(\vec{r})]}{\delta n(\vec{r})} = \int \frac{n(\vec{r})}{|r-r|} dr \qquad \text{(Equation 1.10)}$$

$$V_{xc} = \frac{\delta E_{xc}[n(\vec{r})]}{\delta n(\vec{r})} \qquad \text{(Equation 1.11)}$$

We could also define the ground state density by applying Schrödinger equations with external potential.

$$\left[-\frac{1}{2}\nabla^2 + V_{ks}(\vec{r})\right]\Psi_i(\vec{r}) = \varepsilon_i\Psi_i(\vec{r}) \qquad \text{(Equation 1.12)}$$

ε_i is Lagrange multipliers that is related to the orthonormality of N single particle states Ψ_s. The electron density is formulated as;

$$n(r) = \sum_i^N |\Psi_i(r)|^2 \qquad \text{(Equation 1.13)}$$

$T_s[n(r)]$ equals to

$$T_s[n(r)] = \sum_i^N < \Psi_i| -\frac{1}{2}\nabla^2 |\Psi_i > \qquad \text{(Equation 1.14)}$$

Equations, 1.9 and 1.12 and 1.13 are known as Kohn-Sham equations.

1.7.1. Spin polarised and unpolarised DFT

DFT is divided into 2 groups as, Spin polarised and unpolarised DFT. In the case of spin polarised DFT spin orbitals are able to possess same potential orbitals. This refers to the fact that up ↑ and down↓ spins indeed possess different spatial orbitals. Therefore we should anticipate that their energy also differ, $\Psi\uparrow(\vec{r})$, $\Psi\downarrow(\vec{r})$

$$X\uparrow(\vec{x}) = \Psi\uparrow(\vec{x})\alpha(\omega) \qquad \text{(Equation 1.15)}$$

$$X\downarrow(\vec{x}) = \Psi\downarrow(\vec{x})\beta(\omega) \qquad \text{(Equation 1.16)}$$

However for unpolarised DFT spin orbitals, up and down, possess same spatial orbitals $\varphi(\vec{r})$.

$$X\uparrow(\vec{x}) = \Psi(\vec{x})\alpha(\omega) \qquad \text{(Equation 1.17)}$$

$$X\downarrow(\vec{x}) = \Psi(\vec{x})\beta(\omega) \qquad \text{(Equation 1.18)}$$

$X\uparrow(\vec{x})$ and $X\downarrow(\vec{x})$ are Spin orbitals and $\Psi(\vec{x})$ is spatial orbital.

1.7.2. The Exchange Correlation Functional

As the unknown exchange correlation functional is involved in Kohn-Sham approach. It is hardly possible to solve Kohn-Sham equation unless there is no an additional information for this variable. Hence in order to overcome this issue and find a definitive few approximation methods have been developed for this term. The most broadly employed approximation method is LDA and GGA. By applying LDA we consider that exchange correlation energy per article of an electron can be expressed as;

$$E_{xc}^{LDA}[\mathrm{n}] = \int \mathrm{n}(\mathrm{r})\varepsilon_{xc}(n(r))dr \qquad \text{(Equation 1.19)}$$

However the main problem of LDA is that it is really hard to attain precise results as density of a particular system is not completely homogeneous. If we add gradient corrections to this approximation method

$$E_{xc}^{GGA}[\mathrm{n}] = \int \varepsilon_{xc}(\mathrm{n}(\mathrm{r}),|\nabla n(r)|,\ldots dr \qquad \text{(Equation 1.20)}$$

and GGA is obtained.

In our work, GGA was employed owing to the fact that it is superior to LDA in the case of the formation of a covalent bond between substrate and molecule.[218,219] GGA also has the advantage of overcoming the problem regarding the overbinding of LDA.[220] When a DFT calculation is carried out over a semiconductor and an insulator material, applying GGA is quite beneficial in terms of the enhancement of the band gap between the valence and the conduction band. Finally, if we wish to evaluate the efficiency of DFT calculations, the computational costs, numerical reliability and accuracy of the calculations have to be taken into account; moreover, GGA is known to provide satisfying results for all these requirements. Even though it is outstanding for the calculation of small molecules, it generally fails for delocalized systems.

1.7.3. The Plane Wave Cut-off Energy

Another parameter for the calculation to reveal the electronic and structural properties of a system is the energy cutoff that is used to fix the number of plane waves. As mentioned in Chapter 2, we tested energy cutoff for planewave systems by running single point energy calculations for similar systems. In practical, when a DFT calculation is carried out we only take into account a finite number of plane waves and the convergence of kinetic energy cut-off (E_{cut}) is attained as demonstrated in figure 1.5. Since cutoff energy is proportional to the number of planewaves, as cutoff energy increases, the accuracy of the calculation can evolve as a result of this (i.e. computational cost simulation becomes more expensive). The accuracy of solving the Kohn-Sham equation is essentially controlled by the size of basis set defined by energy cut-off value, referring to the fact that the larger E_{cut}, the more accurate results.

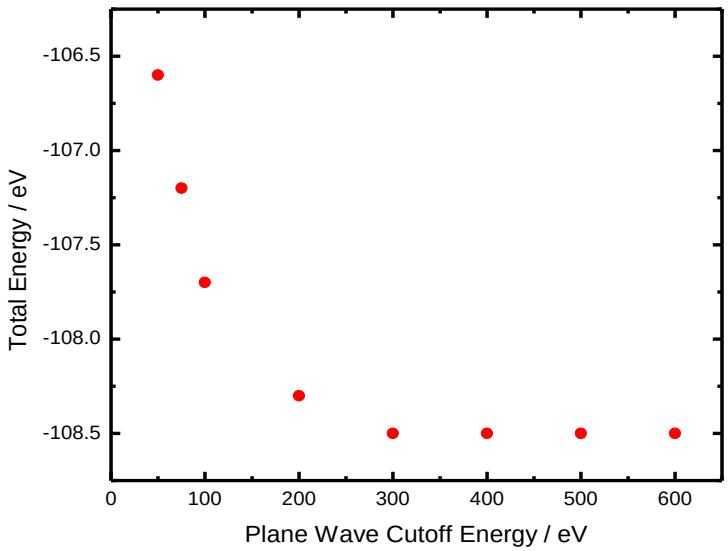

Figure 1.5. *illustrates relationship between convergence energy and cut off energy.*

As mentioned above, there are two types of approximations to the exchange correlation mostly used in DFT calculations by researchers (i.e. local density approximation and generalised gradient approximation). In our work, in order to study the electronic and structural properties of modified and unmodified graphene, CASTEP, which is made up of three types of calculations, such as single point energy, geometry optimization and molecular dynamic simulation (not employed in our work), was used. Single point energy is only carried out for the calculation of the corresponding structure without altering initial geometry of entire system. However, single point energy is regularly used to obtain some of the electronic properties of a structure, such as the density of states and the band structure after relaxing it. In this thesis, this type of calculation was performed to test the plane wave cut-off convergence as it converges immediately. Since the geometry optimization calculation is run in a conventional cell, it refers to relaxing the cell—as its name suggests. This calculation can also be applied with or without cell constraints. This calculation proceeds as follows: it relaxes the position of atoms until the residual forces between the atoms become smaller than the convergence. In first principal DFT implementation, in order to simplify the calculation of more complex systems, pseudopotential is employed as an approximation to replace external potential. Hence, it reduces computational duration by means of using simple numerical forms instead of basis functions. This approximation is based on the fact that ion cores are tightly bound to core electrons. Therefore, core electrons can be considered negligible and chemically inactive. As a consequence of this, only valance electrons are included for the calculation. Throughout this work, we utilized CASTEP code using first

principal density functional theory with a spin-polarized calculation. This code allows us to calculate some electronic properties such as DOS, band structures, and charge transfer, and allows us to visualize some interesting properties (for instance, the total and spin electron density, HOMO and LUMO and the electron localization function).

Considering carbon materials, such as graphene and carbon nanotube, it is really significant to explore which sites of carbon surfaces and aromatic rings are more likely to exhibit more reactivity towards the addition of a radical. Jiang et al.[117] investigated why the edge plane is more reactive than the basal plane for the attachment of phenyl groups on a single layer of graphene sheet; it was concluded that more energy is gained at the edge plane with regards of the basal plane, indicating that the attachment of a phenyl radical to the edge sites is energetically more favourable than HOPG with the orientation of basal sites. In this case, the basal site of HOPG was considered to have a perfectly smooth surface, even though this assumption could cause incorrect outcomes at the end of the simulation of such a system since the real surface area of HOPG is expected to be higher than that of pristine graphene and since, the interaction between the layers of HOPG is omitted. After the attachment of a phenyl radical, there is a significant alteration in the structural and electronic properties of the graphene sheet; for instance, the C-C bond lengths and angles, the displacement of carbon atoms where the phenyl group is anchored, the conversion from sp^2 and sp^3, and the conductivity and optical properties. It is also well established that the addition of the second linker predominantly takes place at para positions, as unpaired electrons mainly exist at this position of the aromatic ring and more energy is obtained. The reason why weaker binding is found at the ortho position probably stems from steric repulsion and, not surprisingly, the meta position is the least favourable one. Zhao et al.[221] also investigated the covalent attachment of phenyl groups to the single-walled carbon nanotubes; the para sites of the aromatic ring were found to be more reactive towards the addition of the phenyl radical. Similarly, the meta position is thermodynamically and energetically the least favourable site for the phenyl group. Since there is a growing attraction in density functional theory and it is also rather useful to understand the interaction between the substrate and adsorbate such as whether a particular molecule covalently attaches or physically adsorbs to the corresponding substrate. The robustness of the chemical bond between the substrate and adsorbate can be evaluated by considering the binding energy. DFT also allows us to observe the changes in the electronic properties of the substrate after the functionalization with the density and

partial density of the states and band structure. The various types of substrate modified by a wide variety of organic compounds have been evaluated using DFT; these are shown in Table 1.1.

Table 1.1. *Shows the carbon microstructure as a substrate modified by various types of organic compounds when applied with DFT methods.*

Substrate	Adsorbed molecule	Applied DFT method	Reference
Boron-nitride nanotube	Benzene, furan, pyridine, pyrrole	Gaussian 09 dispersion corrected wB97x-D	222
CNT	Benzene, alcohol and thiol terminated groups	Vienna ab inito LDA and GGA	223
CNT	OH groups	Gaussian 09, B3LYP	224
Graphene	Aryl groups	Vienna *ab inito* GGA	117
Graphene and CNT	Amide	Vienna *ab inito* LSDA	225
CNT	Aryl groups	Dmol3, GGA	221
Graphene	Methyl	Vienna *ab inito* NASP	226
CNT	Metalloporphyrin	Dmol3, GGA	227
Boron-nitride nanotube	NH_3 and NH_2 terminated molecules	Dmol3, GGA	228
CNT	Aryl diazonium	CPMD, PBE	229

Graphene	Nitrene	Gaussian 98, B3LYP	230
Graphene	Alkylic groups	Gaussian 98 B3LYP	231
CNT	AQ	Dmol3, GGA	232
CNT	NO_2	VASP, Perdew-Wang exchange correlation	233
Graphene	Alkyl groups	SIESTA, GGA	234
CNT	Alkyl groups	SIESTA, PBE, B97-D and MOG-L	235
Carbon nanotube	Carboxyl groups	Vienna *ab inito*, LDA	236
Graphene	1,3-dipolar cycloadditions	Gaussian 03, B3LYP	237

1.8. Research Aims and Thesis Overview

The research described in this thesis mainly focuses on the electrochemical and chemical functionalization of graphite electrodes, HOPG with edge and basal plane sites, glassy carbon and nanotubes with Boc (tert-butyloxycarbonyl) protected diamine linkers; this involves solid phase synthesis modification for the coupling of redox probes, such as, anthraquinone (AQ), nitrobenzene (NB) and dihidroxybenzene (di-HB) subsequent to the de-protection of the diamine linkers for biosensor applications. The overall goal of this research project is to comprehend the influence of the type of carbon materials and linkers on electrocatalysis and electrochemical modification and the further functionalization of carbon electrodes with redox centres that are named above with the aid of experimental and theoretical findings.

Chapter 2 gives details of the equipment, chemicals and methods for the electrografting and chemical modification of carbon electrodes, oxygen reduction study and how the parameters of the computational work with density functional theory implemented in CASTEP were optimized.

Chapter 3 is mainly focused on the modification of edge and basal planes and GC electrodes by electrochemical oxidation or the reduction of the corresponding Boc-protected diamines and diazonium linkers, followed by coupling with AQ, NB and di-HB. We attempted to discover why the surface morphology of graphite electrodes and the type of linkers have an influence on the surface coverage of redox probes and electron transfer kinetics. The effect of pH on AQ-modified electrodes was also investigated.

Chapter 4 describes the electrochemical modification of multi-walled CNTs abrasively immobilised onto the basal plane of HOPG by the electrochemical oxidation of Boc-protected ethylenediamine and diazonium linkers for the coupling of AQ. The effect of pH, scan rate and buffer capacity are also explained. Moreover, the chemical modification of multi-walled CNTs with anthraquinone and nitrobenzene subsequent to the spontaneous attachment of a diazonium tetrafluoroborate salt linker was carried out.

Chapter 5 concentrates on the oxygen reduction of AQ-modified graphite and CNT electrodes using the cycling voltammetry and rotating disk electrode (RDE) techniques. The number of electrons transferred during the oxygen reduction was also determined with RDE in different media.

Chapter 6 explores why the edge sites of graphene sheets are more reactive than basal sites and why, as the length of the linker increases and becomes bulkier, surface coverage decreases using first principal spin polarized density functional theory. We also tried to exhibit the changes in the electronic and structural properties of a single layer of graphene sheet after the electrografting of Boc-protected diamines.

Chapter 7 presents suggestions for future works.

1.9. References

(1) A. Mattiuzzi; I. Jabin; C. Mangeney; C. Roux; O. Reinaud; L. Santos; J-F. Bergamini; P. Hapiot; C. Lagrost, *Nat. Commun.* **2012**, *3*, 1130.

(2) P. Actis; G. Caulliez; G. Shul; M. Opallo; M. Mermoux; B. Marcus; R. Boukherroub; S. Szunerits, *Langmuir* **2008**, *24*, 6327.

(3) T. Breton; D. Bélanger, *Langmuir* **2008**, *24*, 8711.

(4) M. Tanaka; T. Sawaguchi; Y. Sato; K. Yoshioka; O. Niwa, *Langmuir* **2011**, *27*, 170.

(5) Q. Li; C. Batchelor-McAuley; N. S. Lawrence; R. S. Hartshorneb; R. G. Compton, *New J. Chem.* **2011**, *35*, 2462.

(6) P. Allongue; M. Delamar; B. Desbat; O. Fagebaume; R. Hitmi; J. Pinson; J. M. Saveant, *J. Am. Chem. Soc.* **1997.**, *119*, 201.

(7) M. Raicopol; L. Necula; M. Ionita; L. Pilan, *Surf. Interface Anal.* **2012**, *44*, 1081.

(8) A. Celiktas; M. A. Ghanem; P. N. Bartlett, *J. Electroanal. Chem.* **2012**, *670*, 42.

(9) E. Bekyarova; M. E. Itkis; P. Ramesh; C. Berger; M. Sprinkle; W. A. de Heer; R. C. Haddon, *J. Am. Chem. Soc* **2009**, *131*, 1336.

(10) M. Kullapere; K. Tammeveski, *Electrochem. Commun.* **2007**, *9* 1196.

(11) A. L. Gui; G. Liu; M. Chockalingam; G. Le Saux; J. B. Harper; J. J. Gooding, *Electroanalysis* **2010**, *22*, 1283

(12) J. J. Gooding, *Electroanalysis* **2007**, *20*, 573.

(13) A. Pinczewska; M. Sosna; S. Bloodworth; J. D. Kilburn; P. N. Bartlett, *J. Am. Chem. Soc.* **2012**, *134*, 18022.

(14) A. J. Downard; M. J. Prince, *Langmuir* **2001**, *17*, 5581.

(15) M. M. Chehimi, *Aryl Diazonium Salts : New Coupling Agents in Polymer and Surface Science*; Wiley-VCH: New York, 2012.

(16) S. Mahouche-Chergui; S. Gam-Derouich; C. Mangeney; M. M. Chehimi, *Chem. Soc. Rev.* **2011**, *40*, 4143.

(17) P. Abimana; G. G. Wildgoosea; R. G. Compton, *J. Phys. Org. Chem.* **2008**, *21*, 433.

(18) J-M. Zen; A. S. Kumar; D-M. Tsai, *Electroanalysis* **2003**, *15*, 1073.

(19) D. Bélanger; J. Pinson, *Chem. Soc. Rev*. **2011**, *40*, 3995.

(20) J. Pinson, F. Pedvorica. *Chem. Soc. Rev*. **2005**, *34*, 429.

(21) R. L. McCreery, *Chem. Rev*. **2008**, *108*, 2646.

(22) R. S. Deinhammer, M. Ho; J. W. Anderegg; M. D. Porter, *Langmuir* **1994**, *10*, 1306.

(23) Q. Li; C. B. McAuley; N. S. Lawrence; R. S. Hartshorne; R. G. Compton, *New J. Chem*. **2011**, *35*, 2462.

(24) C. C. M.Neumann; C. B. McAuley; C. Downing; R. G. Compton, *Chem. Eur. J*. **2011**, 7320.

(25) A. Wieckowski, *Interfacial Electrochemistry: Theory, Experiment, and Applications*; Marcel Dekker, Inc.: New York, 1999.

(26) Y. Liu; X. Dong; P. Chen, *Chem. Soc. Rev*. **2012**, *41*, 2283.

(27) T. Kuila; S. Bose; A. K. Mishra; P. Khanra; N. H. Kim; J. H. Lee, *Prog. Mater. Sci* **2012**, *57*, 1061.

(28) V. Georgakilas,; M. Otyepka,; A. B. Bourlinos; V.Chandra; N. Kim; K. C. Kemp; P. Hobza; R. Zboril; K. S. Kim, *Chem.Rev*. **2012**, *112*, 6156.

(29) J. Park; M. Yan, *Acc. Chem. Res.* **2013**, *46*, 181.

(30) G. L. C. Paulus; Q. H. Wang; M. S. Strano, *Acc. Chem. Res.* **2012**, *46*, 160.

(31) P. Huang; L. Jing; H. Zhu; X. Gao, *Acc. Chem. Res.* **2012**, *46*, 43.

(32) B. F. Machado; P. Serp, *Catal. Sci. Technol.* **2012**, *2*, 54.

(33) K. R. Ratinac; W. Yang,; J. J. Gooding; P. Thordarson; F. Braeta, *Electroanalysis* **2011** *23*, 803.

(34) T. Kuila; S. Bose; P. Khanra; A. K. Mishra; N. H. Kim; J. H. Lee, *Biosens. Bioelectron.* **2011**, *26*, 4637.

(35) C. G. Zoski, *Handbook of Electrochemistry*; Elsevier: Amsterdam, 2007.

(36) K. R. Ward; N. S. Lawrence; R. S. Hartshorne; R. G. Compton, *Phys. Chem. Chem. Phys.* **2012**, *14*, 7264.

(37) C. E. Banks; R. G. Compton, *Analyst* **2006**, *131*, 15.

(38) M. Gara; R. G. Compton, *New. J. Chem*. **2011**, *35*, 2647.

(39) J. Jaszczak, http://www.scifun.ed.ac.uk/card/flakes.html

(40) D. A. C. Brownson; D. K. Kampouris; C. E. Banks, *Chem. Soc. Rev*. **2012**, *41*, 6944.

(41) G. G. Wildgoose; P. Abiman; R. G. Compton, *J. Mater. Chem*. **2009**, *19*, 4875.

(42) http://www.als-japan.com/1037.html

(43) C. A. Thorogood; G. G. Wildgoose; J. H. Jones; R. G. Compton, *New. J. Chem*. **2007**, *31*, 958.

(44) A. T. Masheter; L. Xiao; G. G. Wildgoose; A. Crossley; J. H. Jones; R. G. Compton, *J. Mater. Chem*. **2007**, *17*, 3515.

(45) M. Strockhttp; http://www.nsf.gov/news/newsletter/jan_09/index.js,

(46) A. Rochefort, http://www.nanotech-now.com/nanotube-buckyball-sites.htm

(47) R. Scipioni; M. Pumera; M. Boero; Y. Miyahara; Ohnoz, T. |*J. Phys. Chem. Lett*. **2009**, *1*, 122.

(48) T. Lin; V. Bajpai; T. Ji; L. Dai *Aust. J. Chem*. **2003**, *56*, 635.

(49) C. E.Banks; R. R. Moore, T. J. Davies; R. G. Compton, *Chem. Commun.* **2005**, *16*, 1804.

(50) C. E. Banks; T. J. Davies; G. G. Wildgoose; R. G. Compton, *Chem. Commun.* **2005**, 829.

(51) K. K. Cline; M. T. McDermott, R. L. McCreery, *J. Phys. Chem*. **1994**, *98*, 5314.

(52) M. A. Edwards; P. Bertoncello; P. R. Unwin, *J. Phys. Chem. C* **2009**, *113*, 9218.

(53) R. R. Moore; Banks, C. E.; Compton, R. G. **2004**, *76*, Anal. Chem.

(54) C. E. Banks; T. J. Davies; G. G. Wildgoose; R. G. Compton *Chem. Commun.* **2005**, 829.

(55) C.-Y. Lee; A. M. Bond *Anal. Chem*. **2009**, *81*, 584.

(56) C.-Y. Lee; S.-X. Guo; A. M. Bond; K. B. Oldham *J. Electroanal. Chem*. **2008**, *615*, 1.

(57) I. Dumitrescu; P. R. Unwin; J. V. Macpherson *Chem. Commun.* **2009**, *7345*, 6886.

(58) M. Pumera, *Chem. Soc. Rev*. **2010**, *39*, 4146.

(59) R. J. Bowling; R. T. Packard; R. L. McCreery *J. Am. Chem. Soc.* **1989**, *111*, 1217.

(60) R. L. McCreery; M.T. McDermott *2012* **Anal. Chem.**, *84*, 2602.

(61) C. A. McDermott; K. Kneten; R. L. McCreery *J. Electrochem. Soc.* **1993** *140*, 2593.

(62) P. Chen; M. Fryling; R. L. McCreery *Anal. Chem.* **1995**, *67*, 3115.

(63) S. DuVall; R. L. McCreery *Anal. Chem.* **1999**, *71*, 4594.

(64) S. DuVall; R. L. McCreery *J. Am. Chem. Soc.* **2000**, *122*, 6759.

(65) E. C. Walter; B. J. Murray; F. Favier; G. Kaltenpoth; M. Grunze; R. M. Penner *J. Phys. Chem. B* **2002**, *106*, 11407.

(66) H.-B. Ram Lee; S. H. Baeck; T. F. Jaramillo; S. F. Bent *Nano Lett.* **2013**, *13*, 457.

(67) J. K. Kariuki; M. T. McDermott *Langmuir* **1999**, *15*, 6534.

(68) H. Gerischer; R. McIntyre; D. Scherson; W. Storck *J. Phys. Chem. B* **1987**, *91*, 1930.

(69) A. N. Patel; M. G. Collignon; M. A. O'Connell; W. O. Y. Hung; K. McKelvey; J. V. Macpherson; P. R. Unwin *J. Am. Chem. Soc.* **2012**, *134*, 20117.

(70) K. Aoki; K. Akimoto; K. Tokuda; H. Matsuda; J. Osteryoung *J. Electroanal. Chem.* **1984**, *171*,, 219.

(71) S. C. S. Lai; A. N. Patel; K. McKelvey; P. R. Unwin *Angew. Chem. Int. Ed.* **2012**, *51*, 5405

(72) Anne, A.; E.Cambril; Chovin, A.; Demaille, C.; C.Goyer *ACS Nano* **2009**, *3*, 2927−2940.

(73) Frederix, P. L.; Bosshart, P. D.; Akiyama, T.; Chami, M.; Gullo, M. R.; Blackstock, J. J.; Dooleweerdt, K.; Rooij, N. F. d.; Staufer, U.; Engel, A. *Nanotechnology* **2008**, *19*, 384004.

(74) N. B. Luque; W. Schmickler *Electrochim. Acta* **2013**, *88*, 892.

(75) R. Nissim; C. Batchelor-McAuley; M. C. Henstridge; R. G. Compton *Chem. Comm.* **2012**, *48*, 3294.

(76) C. Batchelor-McAuley; E. Laborda; M. C. Henstridge; R. Nissim; R. G. Compton *Electrochim. Acta* **2013**, *88* 895.

(77) A. J. Downard; M. J. Prince, *Langmuir* **2001**, *17*, 5581.

(78) B. Barbier, J. Pinson, G. Desarmot, M. Sanchez *J. Electrochem. Soc.* **1990**, *137*, 1757.

(79) Y. Fu; H.-Z. Yu; Y.-M. Wang; Q.-X. Guo, *J. Am. Chem. Soc* **2005**, *127*, 7227.

(80) M. P. Stewart, F. Maya, D. V. Kosynkin, S. M. Dirk, J. J. Stapleton, C. L. McGuiness, D. L. Allara, J. M. Tour *J. Am. Chem. Soc.* **2004**, *126*, 370.

(81) T. Itoh, R. L. McCreery *J. Am. Chem. Soc.* **2002**, *124*, 10894.

(82) D. Kosynkin; T. M. Bockman; J. K. Kochi, *J. Am. Chem. Soc.* **1997**, *119*, 4846.

(83) Pandurangappa, M.; Ramakrishnappa, T.; Compton, R. G. *J. Solid State Electrochem.* **2008**, *12*, 1411.

(84) H. C. Leventis; I. Streeter; G. G. Wildgoose; N. S. Lawrence; L. Jiang; T. G. J. Jones; R. G. Compton, *Talanta* **2004**, *63*, 1039.

(85) G. G. Wildgoose; H. C. Leventis; J. Davies; A. Crossley; N. S. Lawrence; L. Jiang; T. G. J. Jones; R. G. Compton, *J. Mater. Chem.* **2005**, *15*, 2375.

(86) A. T. Masheter; G. G. Wildgoose; A. Crossley; T. G. J. Jones; R. G. Compton, *Mater. Chem.* **2007**, *17*, 3008.

(87) C. G. R. Heald; G. G. Wildgoose; L. Jiang; T. G. J. Jones; R. G. Compton, *ChemPhysChem* **2004**, *5*, 1794.

(88) N. S. Lawrence; R. G. Compton, *Analyst* **2002**, *127*, 1568.

(89) C. Bureau; J. Pinson; FR2892325, F. P., EP1948720, E. p., Eds.

(90) F. Barriére; A. J. Downard, *J. Solid State Electrochem.* **2008**, *12*, 1231.

(91) A. Adenier; E. Cabet-Deliry; A. Chausse; S. Griveau; F. Mercier; J. Pinson; C.Vautrin-Ul, *Chem. Mater.* **2005**, *17*, 491.

(92) B. L. Hurley; R. L. McCreery, *J. Electrochem. Soc.* **2004**, *151*, B252.

(93) G. Chamoulaud; D. Bélanger, *J. Phys. Chem. C* **2007**, *111*, 7501.

(94) A. M. Mahmoud; A. J. Bergen; R. L. McCreery, *Anal. Chem.* **2009**, *81*, 6972.

(95) F. L. Floch; J.-P. Simonato; G. Bidan, *Electrochim. Acta* **2009**, *54*, 3078.

(96) M. Delamar; R. Hitmi; J. Pinson; J.-M. Savéant, *J. Am. Chem. Soc.* **1992**, *114*, 5883.

(97) K. Ray; R. L. McCreery, *Anal. Chem.* **1997**, *69*, 4680.

(98) R. J. Lomeda; C. D. Doyle; D. V. Kosynkin; W.-F. Hwang; J. M. Tour, *J. Am. Chem. Soc.* **2008**, *130*, 16201.

(99) A. Sinitskii; A. Dimiev; D. A. Corley; A. A. Fursina; D. V. Kosynkin; J. M. Tour, *ACS Nano* **2010**, *4*, 1949.

(100) R. Sharma; J. H. Baik; C. J. Perera; M. S.Strano, *Nano Lett.* **2010**, *10*, 398.

(101) M. Delamar; G. Désarmot; O. Fagebaume; R. Hitmi; J. Pinson; J.-M Savéant, *Carbon* **1997**, *35*, 801.

(102) F.Barroso-Bujans; J. L. G. Fierro; S. Rojas; S. Sanchez-Cortes; M. Arroyo; M. A. Lopez-Manchado, *Carbon* **2007**, *45*, 1669.

(103) J. L. Bahr; J. Yang; D. V. Kosynkin; M. J. Bronikowski; R. E. Smalley; J. M. Tour, *J. Am. Chem. Soc.* **2001**, *123*, 6536.

(104) P. R. Marcoux; P. Hapiot; P. Batail; J. Pinson, *New J. Chem.*. **2004** *28*, 302.

(105) Z. Li; S. Dai, *Chem. Mater.* **2005**, *17*, 1717.

(106) Z. Li; W.Yan; S. Dai, *Langmuir* **2005**, *21*, 11999.

(107) X. Wang; R. Liu; M. M. Waje; Z. Chen,; Y. Yan; K. N. Bozhilov; P. Feng, *Chem. Mater.* **2007**, *19*, 2395.

(108) J. Wang; M. A. Firestone; O. Auciello; J. A.Carlisle, *Langmuir* **2004**, *20*, 11450.

(109) S. Q. Lud; M. Steenackers; R. Jordan; P. Bruno; D. M. Gruen; P. Feulner; J. A. Garrido; M. J. Stutzmann, *Am. Chem. Soc.* **2006**, *128*, 16884.

(110) C. Mangeney; Z. Qin; S. A. Dahoumane; A. Adenier; F. Herbst; J.-P. Boudou; J. Pinson; M. M. Chehimi, *Diamond Relat. Mater.* **2008**, *17*, 1881.

(111) F. Mirkhalaf; J. Paprotny; D. J. Schiffrin, *J. Am. Chem. Soc.*, **2006**, *128*, 7400.

(112) D. Ghosh; S. Pradhan; W. Chen; S. Che, *Chem. Mater.* **2008**, *20*, 1248.

(113) D. Ghosh; W. S. Chen, *J. Mater. Chem.* **2008**, *18*, 755.

(114) V. K. R. Kumar; K. R. Gopidas, *Chem.–Asian J.* **2010**, *5*, 887.

(115) A. Merson; T. Dittrich; Y. Zidon; J. Rappich; Y. Shapira, *Appl. Phys. Lett.* **2004**, *85*, 1075.

(116) C. Combellas; F. Kanoufi; D. Mazouzi; A. Thiébault; P. Bertrand; N. Médard, *Polymer* **2003**, *44*, 19.

(117) D. Jiang; B. G.Sumpter; S. Dai, *J. Phys. Chem. B* **2006**, *110*, 23628.

(118) S. Han; Y. Yuan; L. Hu; G. Xu, *Electrochem. Commun.* **2010**, *12*, 1746.

(119) F. L. Floch; G. Bidan; L. Pilan; E.-M. Ungureanu; J.-P. Simonato, *Mol. Cryst. Liq. Cryst.* **2008**, *486*, 271.

(120) J. C. Harper; R. Polsky; D. R. Wheeler; S. M. Brozik, *Langmuir* **2008**, *24*, 2206.

(121) Z. Y. Lin; L. K. Ping; M. Anupa; C. Zhi-Kuan, *Chem. Mater.* **2008**, *20*, 3137.

(122) R. Polsky; J. C. Harper; D. R. Wheeler; D. C. Arango; S. M. Broznik, *Angew. Chem., Int. Ed.* **2008**, *47*, 2631.

(123) A. Adenier; M.-C. Bernard; M. M. Chehimi; E. Cabet-Deliry; B. Desbat; O. Fagebaume; J. Pinson; F. Podvorica, *J. Am. Chem. Soc.* **2001**, *123*, 4541.

(124) M. Kullapere; M. Marandi; V. Sammelselg; H. A. Menezes; G. Maia; K. Tammeveski, *Electrochem. Commun.* **2009**, *11*, 405.

(125) D. Bélanger; J. Pinson, *Chem. Soc. Rev*. **2011**, *40*, 3995.

(126) P. Allongue; M. D. B. Desbat; O. Fagebaume, R. Hitmi, J. Pinson, J. M. Saveant *J. Am. Chem. Soc.* **1997**, *119*, 201.

(127) A. C. Cruickshank, E. S. Q. T., P. A. Brooksby, A. J. Downard *Electrochem. Commun.* **2007**, *9*, 1456.

(128) P. A. Brooksby, A. J. D., S. S. C. Yu *Langmuir* **2005**, *21*, 11304.

(129) J. Lyskawa; A. Grondein; D. Be´langer, *Carbon* **2010**, *48*, 1271.

(130) Nielsen, L. T.; Ceccato, M.; Holm, A. H.; Kristensen, M. V.; Pedersen, S. U.; Daasbjerg, K. *Langmuir* **2009**, *25*, 12160.

(131) D. Evrard; F. Lambert; C. Policar; V. Balland; B. Limoges, *Chem.–Eur. J.* **2008**, *14*, 9286.

(132) R. Reilson; M. Kullapere; K. Tammeveski, *Electroanalysis* **2010**, *22*, 513.

(133) Y. L. Zhong; K. P. Loh; A. Midya; Z.-K. Chen, *Chem.Mater.*, **2008**, *20*, 3137.

(134) H. Gehan; L. Fillaud; N. Felidj; J. Aubard; P. Lang; M. M. Chehimi; C. Mangeney, *Langmuir* **2010**, *26*, 3975.

(135) S. E. Baker; K.-Y. Tse; E. Hindin; B. M.Nichols; T. L. Clare; R. J. Hamers, *Chem. Mater.* **2005**, *17*, 4971.

(136) M. N. Hansen; E. Farjami; M. Kristiansen; L. Clima; S. U. Pedersen; K. Daasbjerg; E. E. Ferapontova; K. V. Gothelf, *J. Org. Chem.*, **2010**, *75*, 2474.

(137) M. Pellissier; D. Zigah; F. Barriére; P. Hapiot, *Langmuir* **2008**, *24*, 9089.

(138) A. LeGoff; F. Moggia; N. Debou; P. Jegou; V. Artero; M. Fontecave; B. Jousselme; S. Palacin, *J. Electroanal. Chem.* **2010**, *641*, 57.

(139) O. Ruediger; J. M. Abad; E. C. Hatchikian; V. M. Fernandez; A. L. D. Lacey, *J. Am. Chem. Soc.* **2005**, *127*, 16008.

(140) J. Wang; J. A. Carlisle, *Diamond Relat. Mater.* **2006**, *15*, 279.

(141) A.-E. Radi; X. Munoz-Berbel; M. Cortina-Puig,; J.-L. Marty, *Electroanalysis* **2009**, *21*, 696.

(142) G. Liu; M. N. Paddon-Row; J. Gooding, *Electrochem. Commun.* **2007**, *9*, 2218.

(143) N. Ferreyra; L. Coche-Guerente; P. Labbe, *Electrochim. Acta* **2004**, *49*, 477.

(144) R. Polsky; J. C.Harper; S. M. Dirk; D. C. Arango; D. R. Wheeler; S. M. Brozik, *Langmuir* **2007**, *23*, 364.

(145) M. A. Alonso-Lomillo; O. Dominguez-Renedo; P. Matos; M. J. Arcos-Martinez, *Anal. Chim. Acta* **2010**, *665*, 26.

(146) C. F. Blanford; R. S. Heath; F. A. Armstrong, *Chem. Commun.* **2007**, 1710.

(147) M. A. Alonso-Lomillo; C. Yardimci; O. Dominguez-Renedo; M. J. Arcos-Martinez, *Anal. Chim. Acta* **2009**, *633*, 51.

(148) N. Ravindranath; C. Ramesh; M. Ravinder Reddy; Biswanath Das *Adv. Synth. Catal.* **2003**, *345*, 1207.

(149) T. W. Greene; P. G. M. Wut *in Protecting Groups in Organic Synthesis*; John Wiley & Sons, Inc.: New York, 1991; .

(150) M. Bodanszky, *Principles of peptide chemistry*; Springer Verlag: New York, 1984.

(151) C. Combellas; D. Jiang; F. Kanoufi; J. Pinson; Podvorica, F. *Langmuir* **2009**, *25*, 286.

(152) K. Malmos; M. Dong; S. Pillai; P. Kingshott; F. Besenbacher; S. U. Pedersen; Daasbjerg, K. *J. Am. Chem. Soc* **2009**, *131*, 4928.

(153) A. Adenier, M. M. C., I. Gallardo, J. Pinson, N. Vila *Langmuir* **2004**, *20*, 8243.

(154) A. J. Downard, D. J. G., E. S. Q. Tan *Langmuir* **2006**, *22*, 10739.

(155) A. J. Downard, E. S. Q. T., S. S. C. Yu *New J. Chem.* **2006**, *30*, 1283.

(156) I. Gallardo, J. P., N. Vila *J. Phys. Chem. B* **2006**, *110*, 19521.

(157) J. M. Chrétien, M. A. G., P. N. Bartlett, J. D. Kilburn *Chem. A. Eur. J.* **2009**, *15*, 11928.

(158) O. Buriez; E. Labbe ; P. Pigeon; G. Jaouen; C. Amatore, *J. Electroanal. Chem.* **2008**, *619–620*, 169.

(159) L. Zhang, *Microchim. Acta* **2007**, *161*, 191.

(160) G. C. Wildgoose; S. J. Wilkin; G. R. Williams; R. R. France; D. L. Carnahan; L. Jiang; T. G. J. Jones; R. G. Compton, *ChemPhysChem* **2005**, *6*, 352.

(161) G. Yang; Y. Shen; M. Wang; H. Chen; B. Liu; S. Dong, *Talanta* **2006**, *68*, 741.

(162) G. Yang; B. Liu; S. Dong, *J. Electroanal. Chem*. **2005**, *585*, 301.

(163) W. B. Nowall; D. O. Wipf; W. G. Kuhr, *Anal. Chem*. **1998**, *70*, 2601.

(164) M. A. Hayes; W. G. Kuhr, *Anal. Chem*. **1999**, *71*, 1720.

(165) K. Malmos; J. Iruthayaraj; S. U. Pedersen; K. Daasbjerg, *J. Am. Chem. Soc.* **2009**, *131*, 13927.

(166) H. Tang; J. Chen; K. Cui; L. Nie,; Y.Kuang; S. Yao, *J. Electroanal. Chem*. **2006**, *587*, 269.

(167) F. Ge; R. C. Tenent; D. O. Wipf *Anal. Sci.* **2001**, *17*, 27.

(168) A. J. Downard; E. S. Q. Tan; S. S. C. Yu, *New J. Chem*. **2006**, *30*, 1283.

(169) G. Gao; D. Guo; C. Wang; H. Li, *Electrochem. Commun*. **2007**, *9*, 1582.

(170) M. A. Ghanem; J. M. Chrétien; J. D. Kilburn,; P. N. Bartlett, *Bioelectrochemistry* **2009**, *76*, 115.

(171) L. Zhang; J. Zhang; C.Zhang, *Biosens. Bioelectron.* **2009**, *24*, 2085.

(172) M. A. Ghanem; J. M. Chrétien; P. N. Bartlett; J. D. Kilburn, *Chem. Eur. J.* **2008**, *14*, 2548.

(173) M. A. Ghanem; J. M. Chrétien; A. Pinczewska; J. D. Kilburn, P. N. Bartlett, *J. Mater. Chem*. **2008**, *18*, 4917.

(174) B. L. Hurley; R. L. McCreery, *J. Electrochem. Soc.* **2004**, *151*, B252.

(175) C. P. Andrieux; J. Pinson. *J. Am. Chem. Soc.* **2003**, *125*, 14801.

(176) C. Saby; B. Ortiz; G. Y. Champagne; D. Belanger, *Langmuir* **1997**, *13*, 6805.

(177) M. C. Bernard; A. Chausse; E. Cabet-Deliry; M. M. Chehimi; J. Pinson; F. Podvorica; C. Vautrin-Ul; *Chem. Mater.* **2003**, 3450.

(178) J. K. Kariuki; M. T. McDermott, *Langmuir* **2001**, *17*, 5947.

(179) Y. C. Liu; R. L. McCreery, *J. Am. Chem. Soc.* **1995**, *117*, 11254.

(180) F. Anariba; S. H. DuVall; R. L. McCreery, *Anal. Chem*. **2003**, *75*, 3837.

(181) P. Allongue; C. Henry de Villeneuve; G. Cherouvrier; R. Cortes; M. C. Bernard, *J. Electroanal. Chem*. **2003**, *2003*, 550.

(182) M.-C. Bernard; A. Chausse; E. Cabet-Deliry; M. M. Chehimi; J. Pinson; F. Podvorica; C. Vautrin-Ul, *Chem. Mater.* **2003**, *15*, 3450.

(183) P. A. Brooksby; A. J. Downard, *Langmuir* **2004**, *20*, 5038.

(184) A. Salimi; H. Eshghi; H. Sharghi; S. M. Golabi; M. Shamsipur, *Electroanalysis* **1999**, *11*, 114.

(185) P. Manisankar; A. Gomathi *Electroanalysis* **2005**, *17*, 1051.

(186) P. Manisankar; A. Gomathi; D.Velayutham *J. Solid State Electrochem.* **2005**, *9*, 601.

(187) B. Slijukic; C. E. Banks; R. G. Compton, *J. Iran. Chem. Soc.* **2004**, *2*, 1.

(188) N. M. Pontikos; R. L. McCreery *J. Electroanal. Chem.* **1992**, *324*, 229.

(189) M. S. Hossain; D. E. Y.Tryk *Electrochim. Acta* **1989**, *34*, 1733.

(190) R. E. Davis; G. L. Horvath; C. W. Tobias *Electrochim. Acta* **1967**, *12*, 287.

(191) K. Tammeveski; K. Kontturi; R. J. Nichols; R. J. Potter; D. J. Schiffrin, *J. Electroanal. Chem.* **2001**, *515*, 101.

(192) K. Vaik; D. J. Schiffrin; K. Tammeveski *Electrochem. Commun.* **2004**, *6*, 1.

(193) K. Vaik; A. Sarapuu; K. Tammeveski; F. Mirkhalaf; D. J. Schiffrin; *J. Electroanal. Chem.* **2004**, *564*, 159.

(194) G. Jürmann; K. Tammeveski, *J. Electroanal. Chem.* **2006**, *597*, 119.

(195) R. McIntyre; D. Scherson; W. Storek; H. Gerischer, *Electrochim. Acta* **1987**, *32*, 51.

(196) M. T. McDermott; K. Kneten; R. L. McCreery *J. Phys. Chem.* **1992**, *96*, 3124.

(197) M. T. McDermott; R. L. McCreery *Langmuir* **1994**, *10*, 4307.

(198) K. K. Cline; M. T. McDermott; R. L. McCreery, *J. Phys. Chem.* **1994**, *94*, 5314.

(199) A. Sarapuu; K. Vaik; D. J. Schiffrin; K. Tammeveski *J. Electroanal. Chem.* **2003**, *541*, 23.

(200) J-M Seinberg; M. Kullapere; U. Mäeorg; F. C. Maschion; G. Maia; D. J. Schiffrin; K. Tammeveski *J. Electroanal. Chem.* **2008**, *624*, 151.

(201) M. Kullapere; J.-M. S., U. Maeorga; G. Maia; D. J. Schiffrin; K. Tammeveski *Electrochim. Acta* **2009**, *54*, 1961.

(202) M. Kullapere; K. Tammeveski *Electrochem. Commun.* **2007**, *9*, 1196.

(203) K. H. Mancy; D. A. Okun; C. N. Reilley; *J. Electroanal. Chem.* **1962**, 65.

(204) D. T. Sawyer; L. V. Interrnate *J. Electroanal. Chem.* **1961**, *2*, 310.

(205) N. Alexeyeva; J. Kozlova; V. Sammelselg; P. Ritslaid; H. Mandar; K. Tammeveski *Applied Surface Science* **2010**, *256*, 3040.

(206) F. Mirkhalaf; K. Tammeveski; D. J. Schiffrin *Phys. Chem. Chem. Phys.* **2009**, *11*, 3463.

(207) K. Karnicka; K. Miecznikowski; B. Kowalewska; M. Skunik; M. Opallo; J. Rogaski; W. Schuhmann; P. J. Kulesza *Anal. Chem* **2008**, 7643.

(208) H. L. Pang; J. Liu; D. Hu; X. H. Zhang; J. H. Chen, *Electrochim. Acta* **2010**, *55*, 6611.

(209) L. Amir; T. K. Tam; M. Pita,; M. M. Meijler; L. Alfonta; E. Katz *J. Am. Chem. Soc.* **2008**, *131*, 826.

(210) W. Zheng; H. M. Zhou; Y. F. Zheng; N.Wang *Chemical Physics Letters* **2008**, *457*, 381.

(211) N. S. Parimi; Y. Umasankar; P.Atanassov; R. P. Ramasamy *ACS Catal.* **2012**, *2*, 38.

(212) Meredith, M. T.; Minson, M.; Hickey, D.; Artyushkova, K.; Glatzhofer, D. T.; Minteer, S. D. *ACS Catal.* **2011**, *1*, 1683.

(213) M. Sosna; J.-M Chretien; J. D.Kilburn; P. N.Bartlett, *Phys.Chem.Chem.Phys.* **2010**, *12*, 10018.

(214) M. S. Thorum; C. A. Anderson; J. J. Hatch; A. S. Campbell; N. M. Marshall; S. C. Zimmerman; Y. Lu; A. A. Gewirth, *J. Phys. Chem. Lett.* **2010**, *1*, 2251.

(215) M. Pita; C. G.-Sanchez; D. Olea; M. Velez; C. G.-Diego; S. Shleev; V. M. Fernandez; A. L. D. Lacey, *J. Phys. Chem. C* **2011**, *115*, 13420.

(216) P. Hohenberg; W. Kohn, *Phys. Rev. B* **1964**, *136*, B864.

(217) W. Kohn; L. Sham, J. *Phys. Rev. B* **1965**, A1133.

(218) D. W. Boukhvalov; M. I. Katsnelson *J. Phys.: Condens. Matter.* **2009**, *21* 3 44205.

(219) M. C. Schabel; J. L. Martins *Phys. Rev. B* **1992** *46*, 7185.

(220) S. Ciraci; S. Dag; T. Yildirim; O. Gulseren; R. T. Senger *J. Phys.: Condens. Matter.* **2004**, *16* R901.

(221) J.-X. Zhao; Y.-H. Ding, *J. Phys. Chem. C.* **2008**, *112*, 13141.

(222) Y. Zhao; X. Wu; J. Yang; X. C. Zeng, *Phys. Chem. Chem. Phys.* **2011**, *13*, 11766.

(223) S. Lim; N. Park, *Appl. Phys. Lett.* **2009**, *95*, 243110.

(224) E. Chelmecka; K. Pasterny; T. Kupka; L. Stobinski, *Phys. Status Solidi A* **2011**, *208*, 1774.

(225) P. Lu; R. Zhou; W. Guo; X. C. Zeng, *J. Phys. Chem. C* **2012**, *116*, 13722.

(226) L. Mandelort; P. Choudhury; J. K. Johnson; J. T. Yates, *J. Phys. Chem. Lett.* **2012**, *3*, 1680.

(227) J.-X. Zhao; Y.-H. Ding, *J. Phys. Chem. C* **2008**, *112*, 11130.

(228) X. Wu; W. An; X. C. Zeng, *J. Am. Chem. Soc* **2006**, *128*, 12001.

(229) A. J. Du,; S. C. Smith, *Molecular Simulation* **2006**, *32*, 1213.

(230) K. Suggs; D. Reuven; X.-Q. Wang, *J. Phys. Chem. C* **2011**, *115*, 3313.

(231) P. D. Astudillo; A. Galano; F. J. Gonzalez, *J. Electroanal. Chem.* **2007**, *610*, 137.

(232) T. Nongnual; S. Nokbin; P. Khongpracha; P. A. Bopp; J. Limtrakul, *Carbon* **2010**, *48*, 1524.

(233) Y. Zhang; C. Suc; Z. Liu; J. Li, *J. Phys. Chem. B* **2006**, *110*, 22462.

(234) P. A. Dennis; F. Iribarne, *Chem. Eur. J.* **2012**, *18*, 7568.

(235) P. A. Dennis, *Journal of Computational Chemistry* **2012**, *33*, 1511.

(236) N. Al-Aqtash; I. Vasiliev, *J. Phys. Chem. C* **2011**, *115*, 18500.

(237) Y. Cao; K. N. Houk, *J. Mater. Chem,* **2011**, *21*, 1503.

Chapter 2

MATERIALS AND METHODS

2.1. Reagents

All chemicals were used as received and without any further purification. All aqueous solutions used throughout this study were made with reagent-grade water (18 MΩ cm) from a Whatman RO80 system coupled to a Whatman "Still Plus". All glassware was immersed in a solution of 5% Decon 90 (Aldrich) for at least 5 days before using and then rinsed with deionized water followed by drying in an oven at 50 °C. Argon (Pureshield Argon, 99.998 %) and oxygen were supplied by BOC gases. All chemicals used during the period of this thesis are reported in Table 2.1.

Table 2.1. *List of Chemicals used.*

Chemical	CAS Number	Purity / Grade	Supplier
1-(*N*-Boc-aminomethyl)-4-(aminomethyl)benzene (XDA)	108468-00-4	≥98.0% (NT)	Sigma Aldrich
1,4-Dioxane	123-91-1	Certified ACS	Fisher Scientific
Acetic acid, glacial	64-19-7	HPLC	Fisher Scientific
Acetonitrile	75-05-8	HPLC	Rathburn Chemicals
Ag (wire, Φ 500μm)	7440-22-4	99.9 %	GoodFellow
Anthraquinone-2- carboxylic acid	117-78-2	>99.0%(T)	TCI Chemicals
Dichloromethane	75-09-2	% 99	Fisher Scientific
Dimethylformamide	68-12-2	HPLC	Fisher Scientific
Ethanol	64-17-5	HPLC	Rathburn Chemicals
Hexammineruthenium (III) chloride	123334-23-6	98 %	Sigma Aldrich
Hydrochloric acid	7647-01-0	37 % Aristar	BDH

N-Boc-1,4-butanediamine (BDA)	68076-36-8	≥97.0%	Sigma Aldrich
N-Boc-2,2`-(ethylenedioxy) diethylamine (EDDA)	153086-78-3	≥95.0% (NT)	Sigma Aldrich
N-Boc-1,6 hexanediamine (HDA)	51857-17-1	≥98.0% (NT)	Sigma Aldrich
N-Boc-ethylenediamine (EDA)	57260-73-8	≥98.0% (NT)	Sigma Aldrich
N,N-diisopropylethylamine (DIEA)	7087-68-5	99 %	Sigma Aldrich
O-(benzotriazol-1-yl)-N,N,N0,N tetramethyluronium hexafluorophosphate (HBTU)	94790-37-1	<= 99 %	Merck
o-Phosphoric acid	7664-38-2	85 %	Fisher Scientific
Platinum (mesh) %	7440-06-4	99.9	Goodfellow
Potassium chloride	7447-40-7	99.9 %	Fluka
Potassium ferricyanide	13746-66-2	> 99	Fisons Sci. Equipment
Pyridine	110-86-1	> 99	Fisons Sci. Equipment
Sodium acetate trihydrate	6131-90-4	99 % AnalaR	BDH
Sodium hydroxide	1310-58-3	98 % AnalaR	BDH
Sodium dihydrogen orthophospate (Sodium phosphate monobasic)	7558-80-7	98 % anhydrous	Sigma Aldrich
Tetrabutylammonium tetrafluoroborate	429-42-5	99 %	Sigma Aldrich

2.2. Reference and Counter Electrodes

Throughout all electrochemical measurements described in this thesis, for aqueous solutions home-made saturated calomel electrode (SCE) and for organic solvents, predominantly for modification of carbon electrodes, silver / silver chloride (Ag / AgCl) were used. These electrodes were fabricated as reported by Bartlett[1] and kept in saturated potassium chloride solution when not being used. As the counter electrode, a 1.0 cm^2 platinum gauze was used.

2.3. Construction of Glassy Carbon and Basal and Edge Plane of HOPG Electrodes

Working carbon electrodes used in this study are glassy carbon (GC) and edge and basal plane graphite. 3 mm diameter GC electrodes rods (HTW, Germany) were sealed in glass and connected to copper wires using melted indium (Aldrich). The edge and basal plane graphite electrodes were embedded into epoxy resin (Struers) and connected to a rod using silver epoxy(Agar). Figure 2.1 shows the GC, edge and basal plane of HOPG electrodes constructed by procedures detailed above. Finally the conductivity of each electrode was checked with an ohm meter to ensure good electrical connection before performing electrochemical experiments.

Figure 2.1. *Examples of the GC, basal and edge plane electrodes employed during of this work*

2.4. Electrode Pre-treatment

Prior to modification, the GC and edge plane graphite electrodes were polished with silicon carbide polishing paper (grade 1200) then with 1 μm and 0.3 μm alumina (Buehler) on polishing cloth (Buehler) and rinsed thoroughly with deionized water and eventually dried under an argon stream. The prepared basal plane graphite electrodes were generated by cleaving with adhesive tape before each experiment. However, polishing the basal plane electrodes by applying a piece of sellotape undoubtedly introduces adhesive impurities. Therefore subsequent to polishing basal plane electrodes with tape, electrodes were thoroughly washed with acetone in order to remove any adhesive materials on the surface. Before performing electrochemical modification of HOPG electrodes with the orientation of edge and basal plane and GC, it is necessary to ensure that all the electrodes have more a less similar surface area after polishing. Hence background currents were obtained for each type of carbon electrode by running CVs in phosphate buffer, pH 7. The resulting background currents were compared and they consistently seemed to be quite similar to each other for each type of carbon electrode.

2.5. Electrochemical Measurements

All electrochemical measurements were performed with an Autolab PGSTAT30 Potentiostat/Galvanostat and controlled using General Purpose Electrochemical System (GPES), conventional three-electrode system which consist of a GC or edge or basal plane HOPG as working electrode electrode, 1 cm^2 platinum gauze as the counter electrode and a home-made saturated calomel electrode (SCE) was used as the reference electrode, figure 2.2. All potentials are reported versus the SCE in aqueous solution and Ag/AgCl in the case of aprotic medium at room temperature. Apart from oxygen reduction studies on bare and anthraquinone-modified carbon electrodes, Ar was purged through the cell for 10 minutes before electrochemical measurement was started. Excluding investigation of pH influence on modified carbon electrodes with anthraquinone and oxygen reduction, all CV measurements reported in this work for AQ-modified carbon electrodes were conducted in pH 4.8 acetate buffer.

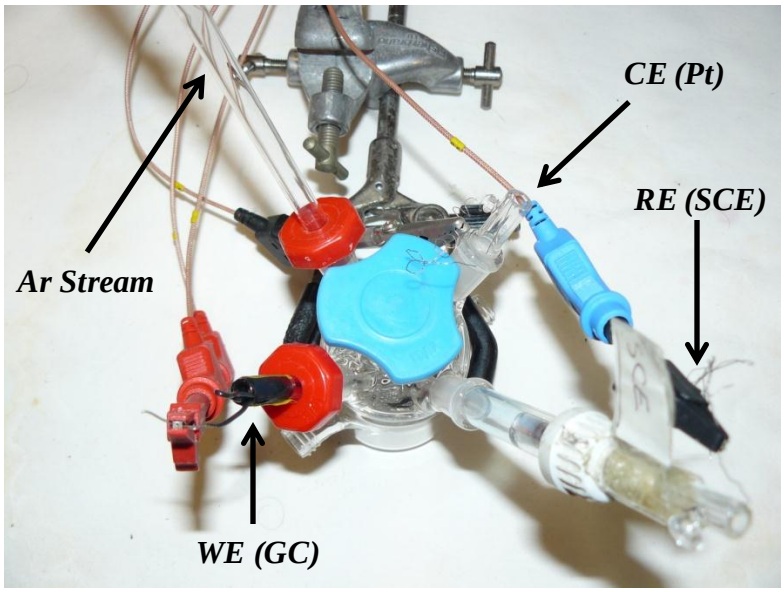

Figure 2.2. *A conventional three-electrode system which consist of a GC or edge or basal plane HOPG as working electrode electrode, 1 cm^2 platinum gauze as the counter electrode and a home-made saturated calomel electrode (SCE) as reference electrode.*

2.6. The Synthesis of 4-(N-Boc-aminomethyl) Benzene Diazonium Tetrafluoroborate Salt

This is based on a procedure detailed in published work by Lee *et al.*[2] and *Chrétien et al.*[3] According to this procedure, initially, tert-butyl N-(4-aminobenzyl)carbamate (1.67 g, 7.5 mmol) was dissolved in a solution of HBF_4 (40%, 1.65 mL, 7.5 mmol) and water (10 mL). The resulting suspension was cooled down on a block of ice followed by dropwise addition of 2 mL of dissolved $NaNO_2$ (0.55 g, 8.0 mmol) in water while the solution is being stirred and argon gas is being purged through the reaction vessel. The resulting solution was then warmed up until it lost half its volume. The residue was cooled down on ice again and an orange diazonium salt was obtained followed by washing with dietyl ether and drying under vacuum.

2.7. Electrochemical Modifications of GC and HOPG and Multiwalled Carbon Nanotube Electrodes

Electrografting of mono-Boc-protected amine linkers, Boc-EDA, Boc-BDA, Boc-EDDA, Boc-HDA, Boc-XDA, and $BocNHCH_2C_6H_4$ to GC and HOPG electrodes with edge

and basal plane orientations were carried out by electrochemical oxidation or reduction from the corresponding solutions containing 10 mM Boc-EDA, Boc-BDA, Boc-HDA, Boc-EDDA, Boc-XDA, 5 mM $BocNHCH_2C_6H_4$ and 0.1 M TBATFB in acetonitrile. The modification of electrodes was performed by cycling the electrode potential from 0.7 to 2.2 V versus Ag/AgCl for Boc-protected diamine linkers, from 1 to -1.5 V versus Ag/AgCl for $BocNHCH_2C_6H_4$ linker, this is similar to published works by the Bartlett research group.[4-6] Following the removal of the Boc group (to be explained below), a carbon electrode with the free amine terminated is obtained, which allows us to achieve further modification using solid phase synthesis methodology as shown in Figure 2.3.

The covalent attachment of $C_6H_4CH_2NHBoc$ to the dry abrasive or wet casted immobilized CNTs and GC surface was performed by electrochemical reduction from solution containing 5 mM $C_6H_4CH_2NHBoc$ diazonium salt and 0.1 M TBATFB in acetonitrile. Modification of three electrodes in parallel was carried out by cycling the electrode potential from 0.55 to −0.95 V vs. SCE for three cycles at a scan rate of 50 mV s^{-1} . The grafting of the Boc-EDA spacer was achieved from a solution containing 10 mM Boc-EDA and 0.1 M TBATFB in acetonitrile by electrochemical cycling (3 cycles) in the potential range from 0.45 to 1.75 V vs. SCE at a scan rate of 50 mV s^{-1}. In order to ensure that the related carbon surfaces were completely passivated by electrografting of these linkers the electrode was held at around 1.8 V for 10 minutes.

2.8. General Procedure for Boc Deprotection of Modified GC and HOPG and MWCNT Electrodes

All GC, edge plane and basal plane and MWCNT electrodes were suspended in a solution of 4 M HCl in dioxane at room temperature for 1 h. The electrode was then washed by DMF, deionised water and absolute ethanol prior to electrochemical characterisation.

2.9. Coupling Reaction of Anthraquinone-2-carboxylic Acid at the Grafted GC, and HOPG and MWCNT Electrodes

Anthraquinone-2-carboxylic acid (252 mg, 1.0 mmol), HBTU (450 mg, 1.2 mmol) and DIEA (4.2 mmol) were dissolved in DMF. The mixture was heated at 60 °C for 15 min with magnetic stirring to obtain a homogeneous dark brown solution. All modified carbon electrodes with the above-mentioned linkers were then suspended in this solution, which was allowed to cool down to room temperature and stirred for 16 h. The electrode was then washed with DMF and absolute EtOH before electrochemical characterisation. Figure 2.3 shows the experimantal set up for coupling of AQ-2-carboxylic acid to modified graphite electrodes.

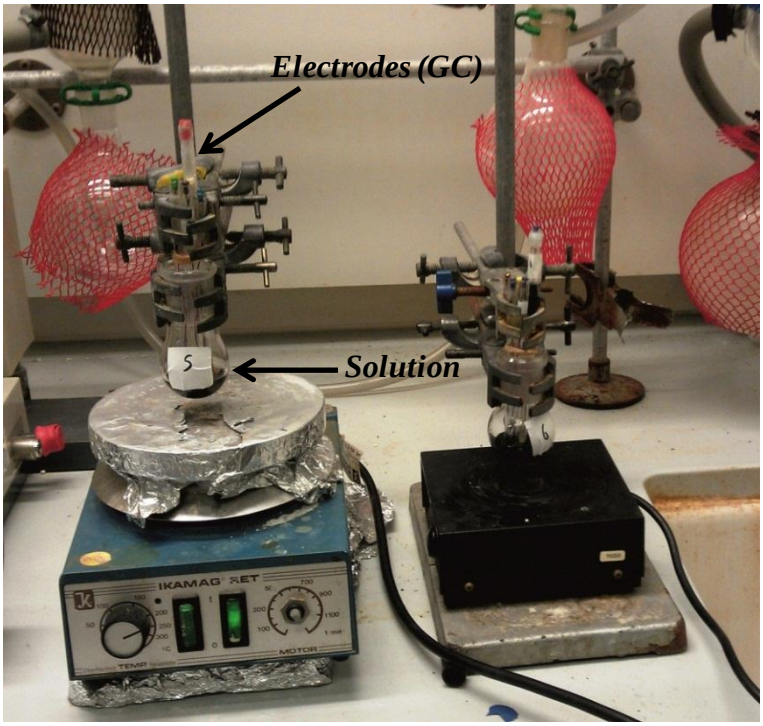

Figure 2.3. *Experimantal setup for coupling of AQ-2-carboxylic acid to amine terminated graphite electrodes through linkers shown in figure 2.3 after deprotection of Boc group.*

2.10. Coupling Reaction of Acetyl Chloride at the Modified GC, HOPG and MWCNT Electrodes

4-Nitrobenzoyl chloride (186 mg, 1 mmol) or (3, 4-dimethoxyphenyl)-acetyl chloride (1 mmol) was dissolved in a mixture of dichloromethane-pyridine 1:1. Modified electrodes were allowed to react with this solution for 16 hours at room temperature. The resulting electrodes were finally washed with DMF and ethanol. Deprotection of the methoxy groups

was carried out with 1 M of BBr_3 for 1 hour. The resulting electrode was washed with DMF and ethanol before characterization.

Figure 2.4 shows a general representation of the electrochemical modification of carbon electrodes followed by removal of the Boc group with 4 M HCl and coupling of redox centres in the presence of coupling agent, HBTU, and N,N-diisopropylethylamine in dimethylformamide for anthraquinone and for nitrobenzene and dihidroxybenzene in the presence of dichloromethane and pyridine.

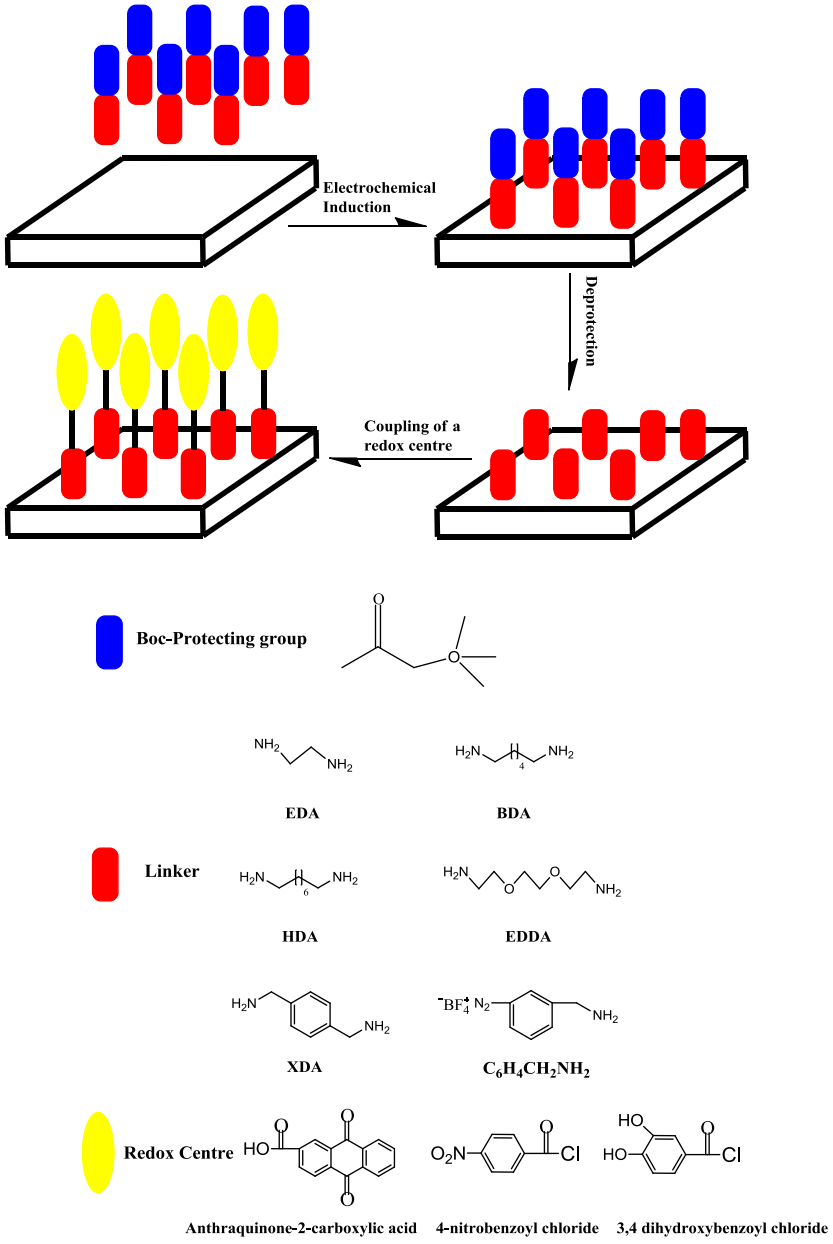

Figure 2.4. *General procedure used in this work for the modification of carbon electrodes.*

2.11. Bifunctionalization of AQ Modified HOPG Electrodes with Nitrobenzene and Dihidroxybenzene

AQ-modified edge and basal plane electrodes were suspended in a solution consisting of 4-nitrobenzene chloride or (3,4 dimethoxyphenyl) acetyl chloride, dichloromethane and pyridine for 16 hours. The resulting electrodes were washed with DMF and ethanol prior to electrochemical measurements. For deprotection of the methoxy groups, the resulting electrodes were then treated with 1 M of BBr_3 for 1 hour followed by washing with DMF and ethanol before differential pulse voltammetry (DPV) analysis. Differential pulse voltammetry was recorded using pulse amplitude of 5 mV, pulse time of 50 ms, and scan rate of 10 mV s^{-1}

2.12. Abrasive and Wet Casting Immobilisation of MWCNT and to GC surface

CNTs were physically immobilized by dry abrasion and wet casting methods. For dry immobilization, the CNTs were gently rubbed into the GC disk electrodes (geometric surface area = 0.071 cm^2) for 5 minutes. In order to characterize abrasively immobilised MWCNT to GC, high resolution images were taken with a Jeol 6500F Field Emission Gun Scanning Electron Microscope (FEGSEM) with the electron beam energized at 15 kV. It was possible to reach nanometre resolution easily with this electron microscope.

The wet attachment of CNTs was carried out by placing 2 mg of CNTs in 1 mL of DMF followed by ultrasonic agitation. The obtained suspension of CNTs was then deposited onto the surface of a mirror like polished GC electrode (geometric surface area = 0.196 cm^2) by dropping 15 or 30 µL aliquots (about 30 or 60 mg of CNTs) of this suspension on the GC surface. The solvent was evaporated by mild hot air flow, 70–80 °C for 5 minutes. For comparison the control experiments were conducted on mirror like polished GC electrodes using the same chemical modification procedures and the current was normalized to the geometric area of the glassy carbon electrodes.

Even though carbon nanotubes are known to possess many beneficial properties, there has been arising concern about their safety because there is structural resemblance between carbon nanotube and asbestos, which is regarded as a toxic material. It is believed that carbon nanotubes might be carcinogenic and remain in the body for a long time in the case of exposure to this material. However a recent paper by Kostarelos group revealed that the toxic

and hazardous effect of carbon nanotubes can be entirely lessened by functionalising their surface and reducing their length via chemical modification.[7] Due to uncertainty about handling and disposing this material we treated this material cautiously for example, safety glasses, lab coat, gloves and mask were worn at all the times when using it. All experiments were carried out in a fume cupboard. We attempted to maintain MWCNT wet to reduce the risk of it becoming airborne. All used carbon nanotube samples were stored in a separate plastic container before disposal.

2.13. Spontaneous Attachment of $C_6H_5CH_2NH$ and Coupling of AQ, NB and di-HB to MWCNT

Spontaneous attachment of 4-(N-Boc-aminomethyl)benzene diazonium tetrafluoroborate salt was accomplished by mixing 0.1 g of MWCNT with 10 mM of diazonium salt containing 0.1 M TBATFB in ACN. The solution was constantly stirred for 1 hour at the room temperature. Subsequent to the spontaneous attachment of linker, the solution was filtrated and the modified MWCNT were then washed with acetone, ethanol and water, respectively. Finally the sample was dried in the oven at 40 °C.

The coupling of AQ, NB and di-HB to modified MWCNT through $C_6H_5CH_2NH$- was achieved by, for AQ coupling, placing modified CNTs into the suspension containing anthraquinone-2-carboxylic acid (252 mg, 1.0 mmol) in the presence of HBTU (450 mg, 1.2 mmol), DIEA (4.2 mmol) and DMF, and for acetyl chloride by immersing the modified CNTs in a solution of 4-nitrobenzoyl chloride (1 mmol) or (3,4-dimethoxyphenyl)-acetyl chloride (1 mmol) containing a mixture of dichloromethane-pyridine 1:1. These suspensions were stirred for 16 hours with magnetic stirring. After the coupling of these corresponding organic redox probes, suspensions were filtrated and the resulting MWCNT were then washed with acetone, ethanol and water, respectively until the filtrate ran colorless. Samples were dried in the oven at 40 °C followed by sonication of AQ, NB and di-HB modified MWCNT in DMF.

Infra-red spectra for modified MWCNT with $C_6H_5CH_2NH$ and AQ-modified MWCNT through $C_6H_5CH_2NH$ were recorded directly from solid samples on a BIORAD Golden Gate FTS 135 spectrometer equipped with a Single Reflection Diamond ATR.

2.14. Determination of Surface Coverage and Effect of Scan Rate

The associated surface coverages, Γ, are calculated from Faraday`s law,[8]

$$\Gamma = Q / nFA\rho \qquad \text{(Equation 2.1.)}$$

where Q is the charge obtained from integration of the baseline-corrected area under the oxidation or reduction peak, F the Faraday constant, A the geometric area of the electrode (0.071 cm^2), n = 2 the number of electrons transferred in the case of cyclic voltammetry taken for AQ modified carbon electrodes, and ρ is the roughness of the electrode. However for graphite electrodes, Jaegfeldt *et al.* found that the roughness factor was between 2 and 5 by employing electron microscopy when 600 grit emery paper was used for polishing.[9] On the other hand, we obtain mirror like graphite electrodes subsequent to our polishing procedure detailed in section 2.3 that ends with 0.3 μm alumina treatment. Therefore roughness factor are considered as below 2 throughout this work as stated in literature.[10]

The scan rate effect on the voltammetry of AQ modified graphite electrodes was investigated by fitting peak positions of voltammograms as a function of log(scan rate) derived by Laviron.[11]

2.15. Oxygen Reduction Studies on the Unmodified and AQ-Modified Carbon Electrodes

For oxygen reduction on the AQ modified and bare GC and HOPG electrodes with the edge and basal plane orientation, oxygen was purged through the cell containing 20 ml of buffer solution for 10 minutes. This was optimized by bubbling oxygen with a flow rate of 1 m / s for different durations such as 1, 2, 5, 10 and 20 minutes. As no substantial increase was observed in the peak current between 10 and 20 minutes, 10 minutes was adopted. To investigate the effect of dissolved oxygen concentration the solutions were sparged with mixtures of oxygen and argon prepared using a Smart-Trak mass flow controller connected to portable potentiostat controlled using PSTrace software, Figure 2.5.

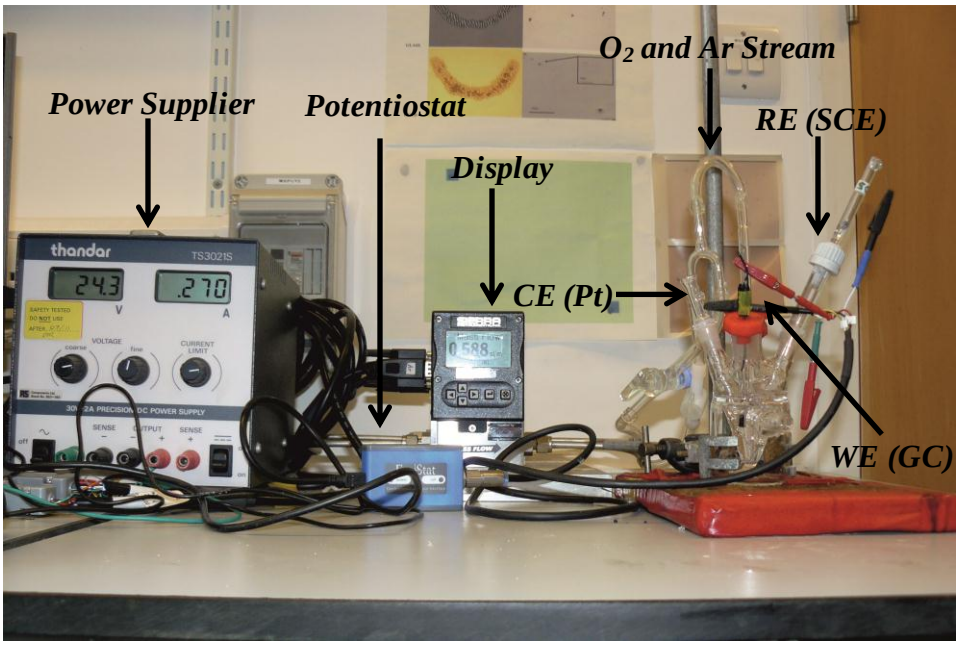

Figure 2.5. *Smart-Trak mass flow controller used to purged Ar and oxygen simultaneously.*

In order to determine the kinetic parameters for O_2 reduction RDE experiments were carried out at different rotation rates and pH values. The rotator and glassy carbon disc electrode were supplied by Pine. Figure 2.6 shows the experimantal setup for oxygen reduction studies on bare and modified GC rotating disc electrodes modified with AQ through the EDA linker in different solutions.

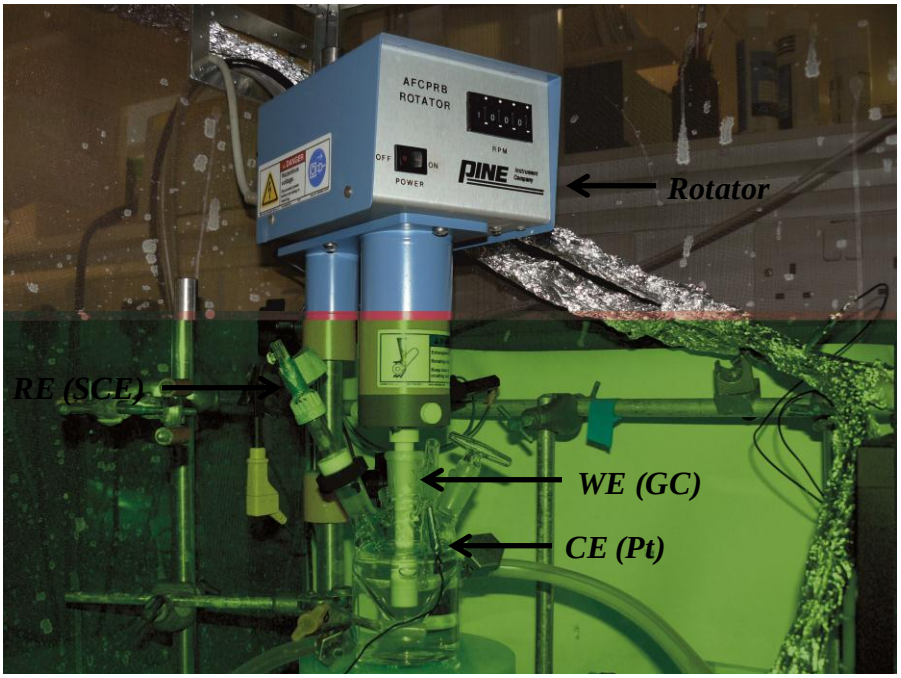

Figure 2.6. *Experimantal design for oxygen reduction on the rotating disk clean and AQ-modified GC electrodes.*

2.16. Enzyme Immobilisation onto AQ modified GC electrodes

The imobilization of *Trametes hirsuta* laccase (ThL) onto GC modified with anthraquinone and anthracene through six different linkers shown in section 2.7 is based on the method descriped by Sosna *et al.*[10] *ThL* was provided by VTT Technology (Finland). The concentration of enzyme was found to be approximately 2.1 mg / ml by Bradford assay. When not in use, the enzym was stored in citrate buffer at -18 ^{0}C. The immobilization of enzyme to the AQ-modified GC electrode surfaces was carried out as follows, first 10 µL of 2.1 mg ml^{-1} laccase in 20 mM citrate buffer was deposited onto the modified GC electrodes and incubated overnight at 4 °C. After immobilization was achieved the electrodes were rinsed with water and washed with 100 mM citrate buffer. Immobilized GC electrodes with ThL through AQ were always kept in 100 mM citrate buffer, pH 5 when not in use.

2.17. Oxygen Reduction on Laccase Immobilzed GC Electrodes Using High-Throughput Screening

Oxygen reduction on AQ-modified and laccase immobilized GC electrodes was carried out with a high-throughput electrochemistry analyser HTEA Mark II Potentiostat (Ilika) in 0.1 M citrate buffer pH. High-throughput electrochemical (HTP) experiments were carried out in a conventional three-electrode cell with a homemade saturated calomel electrode (SCE) and about 25 cm^{-2} platinum mesh as reference electrode and counter electrode, respectively. Employing high-throughput electrochemical measurement has the advantage of performing the experiment under the same circumstances at the same time. Experimental set up for high-throughput cyclic voltammetry measurements for AQ modified and laccase immobilised GC electrodes was adopted from the work from Pinczewska *et al.*[6] In order to ensure oxygen was uniformly distributed across the cell, two experiments were designed using 8 modified GC electrodes with AQ. In this case these electrodes are placed at the edge and middle of across the holder. In terms of peak shape and current it was noticed that there were no indistinguishable differences between both experiments. The experimental set up of the high-throughput screening of the library of 18 electrodes using the Ilika multichannel potentiostat controlled using HT-DAVE software is shown in Figure 2.7.

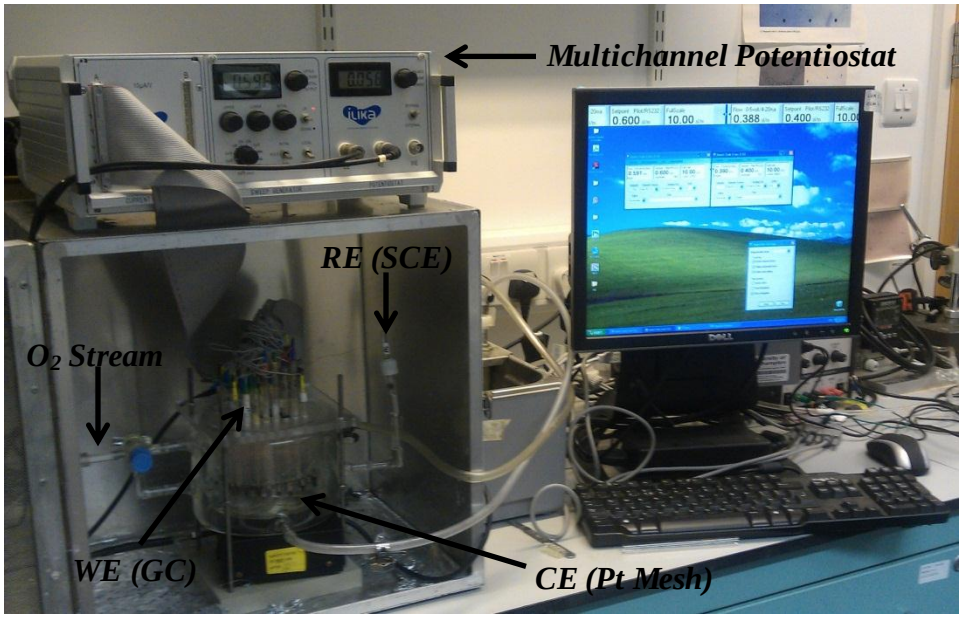

Figure 2.7. *High-throughput screening of library of 18 GC electrodes modified with AQ through diamine linkers for O2 reduction.*

In order to make sure that all 12 GC electrodes used for high throughput screening of oxygen reduction at laccase electrodes had relatively the same surface area, a CV measurement was carried out using the multichannel potentiostat in the presence of 3 mM potassium ferricyanide solution containing 0.1 M of KCl. As clearly seen in the Figure 2.8 it is hard to distinguish each voltammogram of the individual electrodes from the average one. Hence all electrodes can be assumed to possess similar surface area.

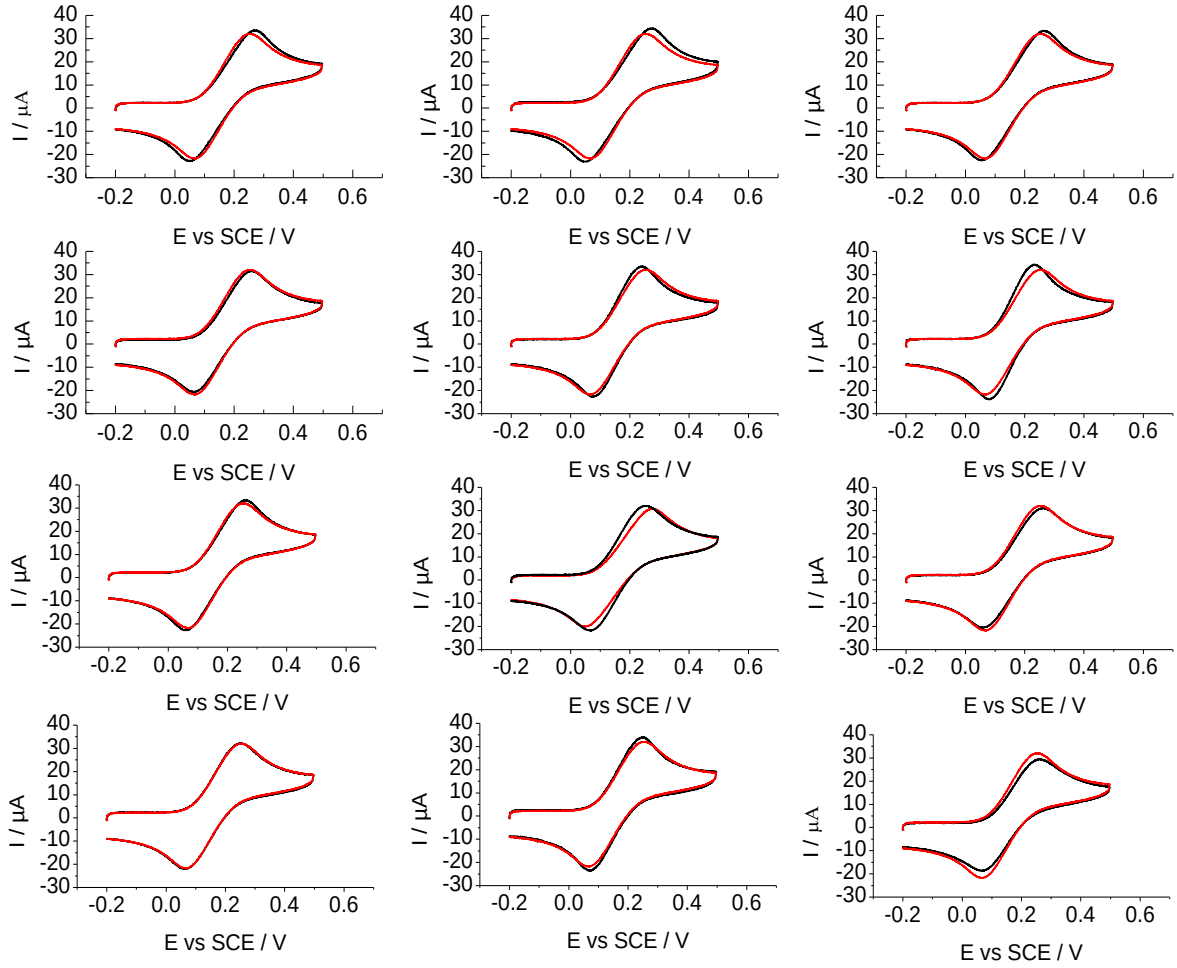

Figure 2.8. *Cyclic voltammetry of each electrode in 3 mM + 0.1 M HCl at 50 mV s-1. Black line is voltammogram of each electrode, red line is the average voltammogram*

2.18. Computational Details

The geometry optimization and electronic properties of plain and modified graphene sheet were performed by spin polarized density of functional theory (DFT) using the ultrasoft pseudopotentials plane-wave method with CASTEP[12] implemented in the Materials Studio 5.5, which are commercially available software packages. Generalized-gradient approximation (GGA) with the Perdew-Burke-Ernzerhof (PBE) is employed for the exchange correlation. All parameters for calculation are chosen after testing and ensure a good enough convergence of total energies. In order to evaluate the nature of the bond between the carbon atom of the aromatic ring on the graphene and the linker and electronic properties of the pristine and modified single layer of graphene sheet such as total and partial spin density of

states and charge transfer, Highest Occupied Molecular Orbital and Lowest Unoccupied Molecular Orbital and binding energy were computed. To shed light on the reason why edge sites exhibits more reactivity towards electrochemical grafting of diamines linkers in accordance to basal sites and in order to find out why type of linkage has impact on the surface coverage of AQ, DFT was performed.

2.19. References

(1) P. N. Bartlett, *Biosensors : A Practical Approach*; Oxford University Press: Oxford, 1990.

(2) J. Lee; M. Kang; M.Shin; J. M. Kim; S. U.Kang; J. O. Lim; H. K. Choi; Y. G. Suh; H. G. Park; U. Oh; H. D. Kim; Y. H. Park; H. J. Ha; Y. H. Kim; A.Toth; Y. Wang; R. Tran; L. V. Pearce; J. D. Lundberg; P. M. Blumberg, *J. Med. Chem.* **2003**, *46*, 3116

(3) J.-M. Chrétien; M. A. Ghanem; P. N. Bartlett; J. D. Kilburn, *Chem. Eur. J.* **2008** *14*, 2548

(4) M. A. Ghanem; J.-M. Chrétien; A. Pinczewska; J. D. Kilburn; P. N.Bartlett, *J. Mater. Chem.* **2008**, *18*, 4917.

(5) M. A. Ghanem; I. Kocak; A. Al-Mayouf; M. AlHoshan; P. N. Bartlett, *Electrochim. Acta* **2012**, *68*, 74.

(6) A. Pinczewska; M. Sosna; S. Bloodworth; J. D. Kilburn; P. N. Bartlett, *J. Am. Chem. Soc.* **2012**, *134*, 18022−18033.

(7) A. H.-Boucetta; A. Nunes; R. Sainz; M. A. Herrero; B.Tian; M. Prato; A. Bianco; K. Kostarelos, *Angewandte Chemie* **2013**, *125*, 2330.

(8) A. J. Bard; L. R. Faulkner, *Electrochemical Methods : Fundamentals and Applications*; Wiley: New York, 2001.

(9) H. Jaegfeldt; T. Kuwana; G. Johansson, *J. Am. Chem. Soc.*, **1983**, *105*, 1805.

(10) M. Sosna; J.-M.Chrétien; J. D. Kilburn; P. N. Bartlett, *Phys. Chem. Chem. Phys.* **2010**, *12*, 10018.

(11) E. Laviron, *J. Electroanal. Chem.* **1979**, *101*, 19.

(12) M. Kibalchenko; M. C. Payne; J. R. Yates, *ACS Nano* **2011**, *5*, 537.

Chapter 3

THE MODIFICATION OF GRAPHITE ELECTRODES

3.1. Overview

As described in the introduction, the functionalization of carbon surfaces by the electrochemical oxidation of amines and the reduction of diazonium salts has been frequently used for electrochemical applications such as biosensors. The modification of electrode surfaces is widely adopted by researchers due to the fact that it permits control of the properties of the substrate to be modified and because this method is rather flexible, which implies that the corresponding electrode surface can be tailored in any desirable way for the specific application.[1] The mechanism of this technique is based on the electrochemical formation of a radical by either the electro-oxidation of the relevant amines or the reduction of the corresponding diazonium salt linker, which can then couple to an unsatisfied valence or double bond on the carbon electrode surface.[2-5]

In this study, glassy carbon and HOPG electrodes with edge and basal plane orientation were modified with Boc-protected diamine and diazonium salt linkers with a phenyl ring and different length of alkyl chain by either electrochemical oxidation or the reduction of the related linkages. It is assumed that the different types of linkers have an impact on the surface coverage and the kinetics of modified surfaces. After the removal of the protecting group by treatment with 4 M HCl in dioxane anthraquinone (AQ)-2-carboxylic acid, 4-nitrobenzoyl (NB) chloride and (3.4-dihymethoxyphenyl) (di-HB) acetyl chloride were coupled to the modified carbon electrodes using solid phase synthesis methodology.[6] The presence of the Boc-protecting group prevents the formation of multilayers and bridge structures as detailed in Chapter 1. The blocking properties of the electrografted layer towards redox couples, such as potassium ferricyanide and hexaammine ruthenium III chloride, and the effect of scan rate and pH were also investigated. Finally, the bifunctionalization of graphite electrodes with AQ, NB, and di-HB were carried out.

3.2. The Modification of Graphite Electrodes

Five different types of mono-Boc-protected diamine linkers, N-Boc-ethylenediamine (EDA), N-Boc-1, 4 butanediamine (BDA), N-Boc-2,2`-(ethylenedioxy)diethylamine (EDDA), 1-N-Boc-aminomethyl-4-(aminomethyl) benzene (XDA), N-Boc-1,6 hexanediamine (HDA) and 4-(N-Boc-aminomethyl) benzene diazonium tetrafluoroborate

salt were grafted by electrochemical oxidation and the reduction of the corresponding Boc-protected-diamines and diazonium salt, respectively, onto both glassy carbon (GC) and edge and basal plane graphite electrodes. The modification procedures for each linker were carried out from the appropriate solutions in ACN and 0.1 M TBATFB. Following the removal of the Boc group, anthraquinone-2-carboxylic acid was coupled onto the different electrode surfaces modified with the different linkers by employing solid-phase synthesis methodology.

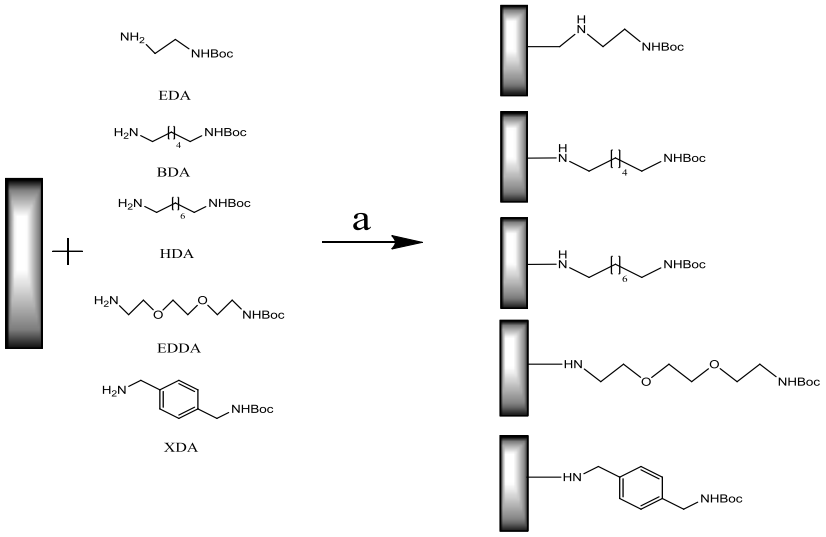

Scheme 3.1. *Electrochemical immobilisation of mono-Boc-protected diamines on the edge and basal planes and GC surfaces. Conditions: (a) 5 to 10 cycles from 0.6 to 2.2 V vs. Ag/AgCl, in CH_3CN.*

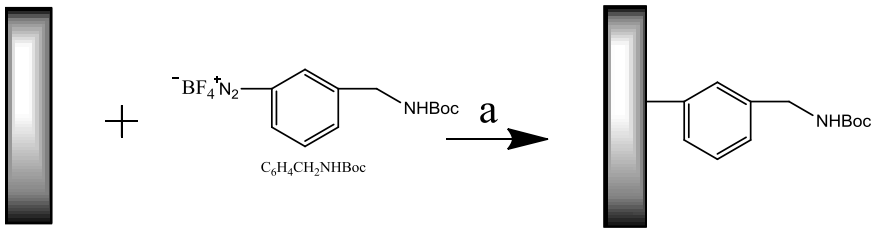

Scheme 3.2. *Electrochemical immobilisation of $C_6H_4CH_2NHBoc$ on the edge and basal planes and GC surfaces. Conditions: (a) 5 to 10 cycles from 0.6 to -1.5 V for $C_6H_4CH_2NHBoc$ vs. Ag/AgCl, in CH_3CN.*

3.3. Grafting of GC and HOPG electrodes by the Oxidation of Boc-protected-Diamines

The attachment of the mono-Boc-protected diamine linkers onto the GC, edge and basal plane electrodes was carried out by the electrochemical oxidation of the corresponding protected diamine linkers in ACN and TBATFB. Figure 3.1 shows the first and third cyclic voltammograms obtained after holding the electrode in the second scan at the potential of 1.8

V for 15 minutes for 10 mM XDA in 0.1 M TBATFB for each electrode material, recorded at the scan rate of 50 mV s^{-1}.

As seen in Figure 1, on the first scan, there is a broad irreversible peak, which can be assigned to the formation of the amine radical that couples to the electrode surface. However, on the third scan, this peak is absent, indicating the blocking of the electrode surface. This is consistent with results in the literature.[7] Similar voltammograms and results were also obtained for other linkers.

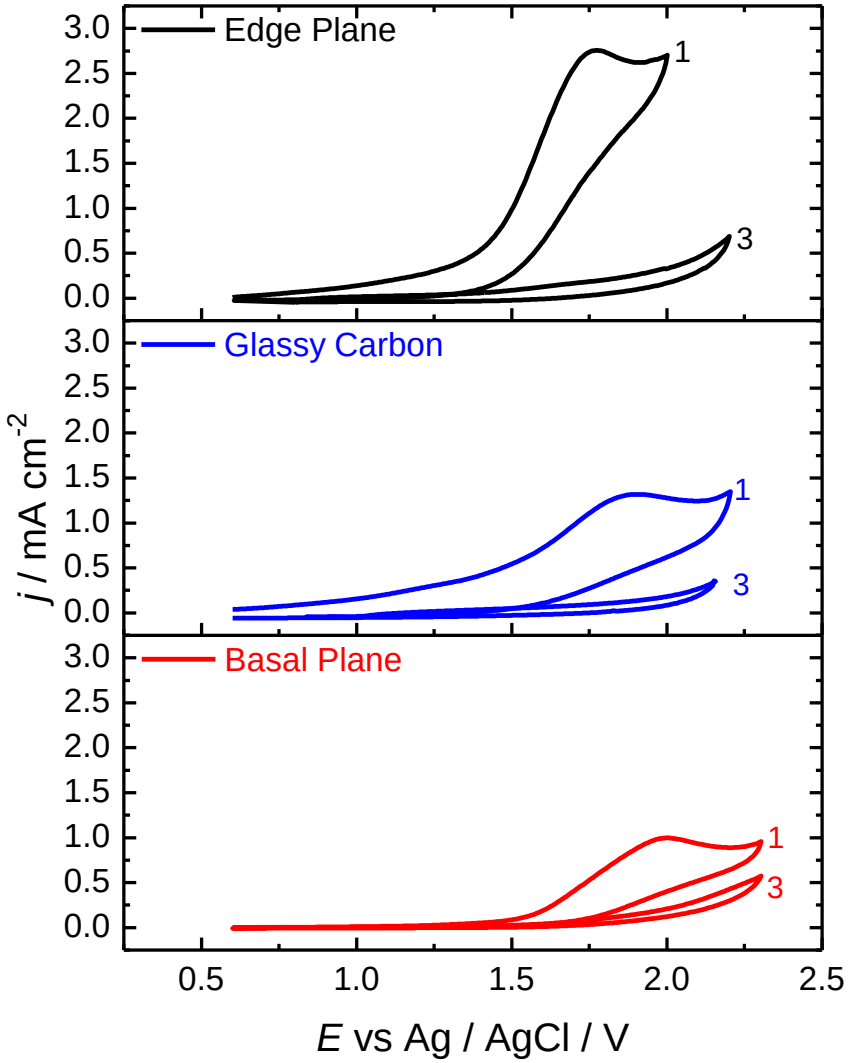

Figure 3.1. *Cyclic voltammograms recorded at the scan rate of 50 mV s^{-1} for edge and basal plane and GC electrodes versus Ag/AgCl for 10 mM of mono-Boc-XDA linker in ACN with 0.1 M of TBATFB. First two voltammograms obtained for edge plane, GC and basal plane indicate 1st and 3rd cycles.*

However, the charge calculated by integrating the area under the first peak is 9.70, 5.44 and 3.12 mC cm^{-2} for the edge plane, GC and basal plane, respectively—much larger than that required to form a monolayer. (0.009 mC cm^{-2} calculated for close packing based on

the geometric size of the linker and the minimum spacing between molecules on a flat surface). This suggests that the faradaic coupling efficiency at the electrode surface is low in all cases. The reason that more charge is passed for the edge sites can be attributed to three phenomena. First, depending on the electrode's history, the roughnesses of the edge and basal plane electrodes are likely to be different since the edge plane is prepared by polishing. We could therefore expect that the surface roughness can possibly make a contribution to the overall current. Secondly, the charge at basal sites is considerably lower because of the fact the coupling of diamine linkers predominantly takes place on the cleavage defects or atomic defects. Finally, it is possible that the reactivity of the two surfaces towards the radical is different, which can be proven theoretically by using DFT (which will be discussed in Chapter 6). Moreover, during the electrografting process, there might be side reactions, such as the binary coupling of radicals that leads to a higher charge.

Table 3.1. *First scan peak potential and peak current at the edge, GC and basal plane electrodes for 10 mM of diamine and 5 mM of diazonium salt linkers in ACN at the scan rate of 50 mV s^{-1}.*

Linker	Electrode	Peak Potential (V vs SCE)	Peak Current (± 5 µA cm^{-2})
Boc-EDA	Edge	1.66	3475
	GC	1.75	2860
	Basal	2.05	945
Boc-BDA	Edge	1.69	3204
	GC	1.81	2655
	Basal	2.1	875
Boc-HDA	Edge	1.69	2910
	GC	1.80	2613
	Basal	2.08	753
Boc-EDDA	Edge	1.69	2750
	GC	1.81	2427
	Basal	2.1	792
Boc-XDA	Edge	1.70	2780
	GC	1.75	2545
	Basal	2.04	840
Boc-Diazo	Edge	-0.43	775
	GC	-0.49	614
	Basal	-0.59	208

On the other hand, when the peak potentials and the magnitude of the peak currents for the oxidation of the XDA linker at the GC, edge and basal are taken into account, it can be seen that the oxidation of the Boc-protected-diamine linkers onto the edge plane graphite occurs much faster than on the GC and basal plane. As a consequence of this interpretation, the electrode kinetics of the oxidation of the Boc-protected diamine linkers are fast at the edge sites and much slower at the basal sites because the peak potential of the oxidation of the corresponding linker at the edge plane graphite occurs at less positive potentials. In contrast, at the basal plane, the peak potential is more positive and, consequently, the passivation competes more strongly so that the electrode surface is blocked before the mass transport limited current can be attained. The results for the GC electrode are consistently intermediate between the edge and basal plane graphite electrodes, which supports the idea that the edge and basal planes are present in approximately equal proportion at the glassy carbon surface.

These two findings concerned with peak potential and peak current for the oxidation of the diamines could be attributed to the surface properties of the different carbon electrodes, which means that the edge plane electrodes possess more organic functional groups containing oxygen (such as phenols, quinones and carboxylic acid and unsatisfied valences as well) than the GC and basal plane electrodes. It is thus assumed that a strong interaction takes place between the electrode surface and the reactant, which means that the tendency to react with the linker for the edge plane electrode is higher than that for the GC or basal plane.

3.4. Grafting of GC and HOPG Electrodes by the Reduction of Boc-protected-Diazonium Salt

The grafting of the $BocNHCH_2C_6H_4$ linker to GC and HOPG electrodes was carried out by the electrochemical reduction of the corresponding diazonium salt, at 50 mV s^{-1}. A 5 mM solution of $BocNHCH_2C_6H_4$ in ACN containing 0.1M TBATFB was used for the modification procedures. As mentioned in Section 3.3, the modification of GC, edge and basal plane electrodes by the electrochemical oxidation of the Boc-protected-diamine linkers, rather broad irreversible peaks were observed, referring to one electron reduction of $BocNHCH_2C_6H_4$ and the formation of the radical that couples to electrode surfaces. Complete peak disappearance on the following scans shows that the electrode surface has

been passivated.[6,8] which was previously observed, for the modification of carbon surfaces by means of the electrochemical oxidation of the diamine linkers. The area under the first peak is larger than that required for monolayer formation. The total charge passed obtained by the integration of the areas under the first scan is 10.40, 6.40 and 2.70 mC cm^{-2}, for the edge, GC and basal plane respectively, and significantly exceeds the charge required to form a monolayer (0.009 mC cm^{-2}) of the $BocNHCH_2C_6H_4$-. While in terms of the peak position and the magnitude of the peak current for the reduction of $BocNHCH_2C_6H_4$ at all relevant electrodes, similar results were obtained as previously mentioned in the oxidation of protected diamine linkers (Section 3.3).

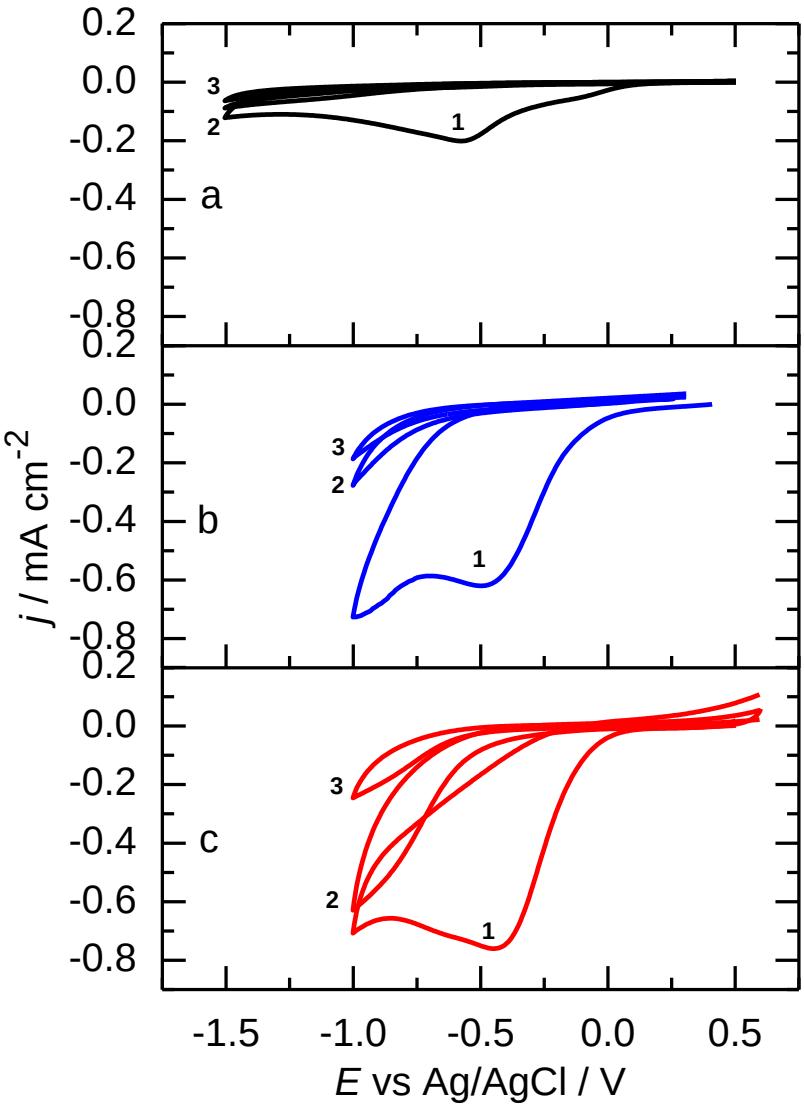

Figure 3.2. *Cyclic voltammetry recorded at 50 mV s^{-1} for a) basal plane, b) glassy carbon and c) edge plane electrodes in 5.0 mM 4-(N-Boc-aminomethyl) benzene diazonium tetrafluoroborate and 0.1 M TBATFB in ACN. The black, blue and red lines represent basal, GC and edge plane, respectively.*

3.5. Blocking Properties of Modified Carbon Electrodes

By employing CV and redox probes, the existence of the grafted layer can be determined. The barrier properties of the grafted layer are greatly affected by the charge and hydrophobicity of the redox probes used and the type of solvent utilized.[9-11] The voltammogram of $[\mathrm{Fe(CN)_6}]^{-3}$ exhibits reversible behavior at the bare electrode with a redox potential of 187 mV. It is clearly apparent that after the modification of the electrode by means of the oxidation of Boc-protected EDA, no peak was detected within the scanned potential window, which could be attributed to the blocking behaviour of the modified surface. After the removal of the Boc group, the electrochemical response of the modified surface becomes almost indistinguishable from that of the bare electrode. This blocking behaviour stems from the electrostatic interaction between the layer and redox probe, indicating that ammonium ions (NH_4^+) created under the neutral pH are likely to interact with the redox probe. In this case, $[Fe(CN)_6]^{-3}$ ions are capable of accessing the electrode surface as there is no significant difference in the peak current compared to that for the bare

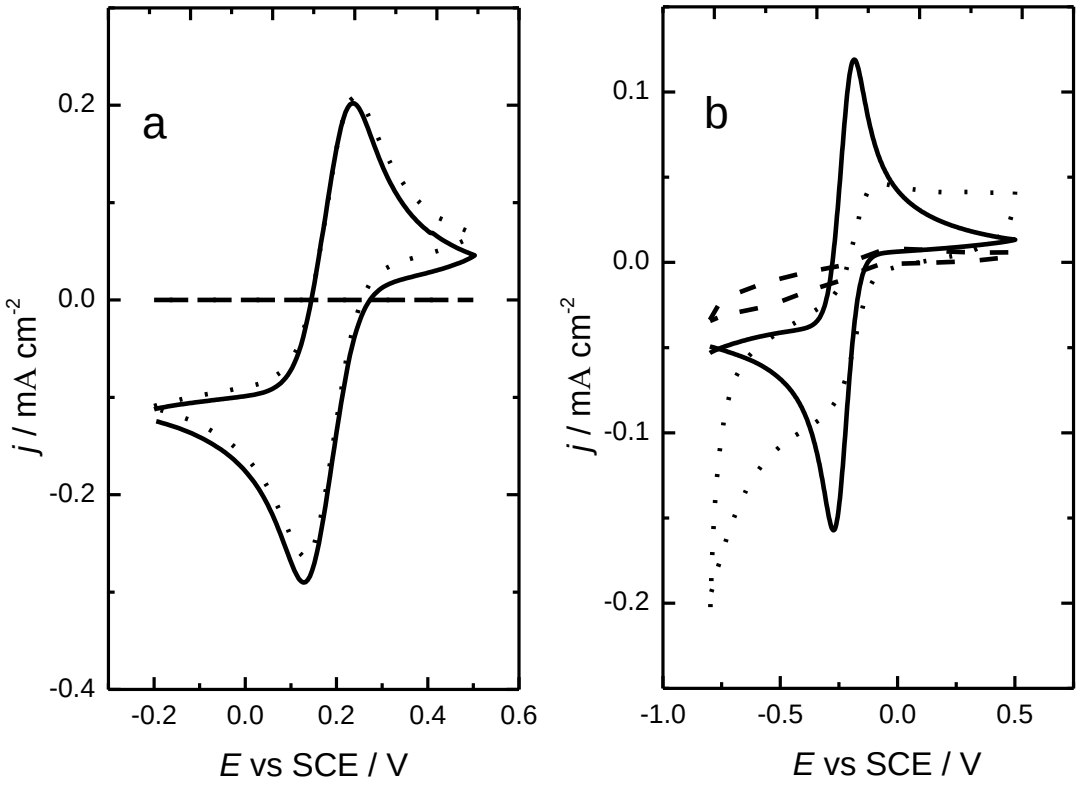

Figure 3.3. *Electrochemical response of edge plane electrode towards a) $K_3Fe(CN)_6$ and b) $Ru(NH_3)_6Cl_3$ at the scan rate of 50 mV s^{-1}. Solid line is freshly polished edge plane electrode, dashed line is after the grafting of the Boc-protected-EDA linker, and the dott line is after the removal of the Boc group.*

electrode; this indicates that, after the removal of the Boc group, the grafted layer exhibits a very low blocking effect for charge transfer between the layer and the redox probe.[12] In order to verify this explanation, a similar study was performed in the presence of a positively charged $[Ru(NH_3)_6]^{3+}$ redox system in an acidic medium. The CV was recorded in pH 3 in order to increase the electrostatic repulsion as much as possible between $[Ru(NH_3)_6]^{2+}$ and the grafted layer.[13] When the positively charged redox probe, $[Ru(NH_3)_6]^{3+}$, was used, as shown on Figure 3.b, the CV recorded at the bare edge plane electrode shows a quasi-reversible behaviour with a peak separation of 85 mV. As for the $[Fe(CN)_6]^{3-}$, after the modification of the surface by means of the electrochemical oxidation of the EDA linker, no peak is observed at all, indicating that the carbon surface is completely passivated. However, subsequent to the removal of the Boc protecting group, and contrary to the $[Fe(CN)_6]^{3-}$ case, the peak separation dramatically increases to 256 mV and the CV of the $[Ru(NH_3)_6]^{3+}$ at the amine terminated edge plane surface is greatly affected and the cathodic and anodic peak height is largely suppressed, which can be attributed to a coulombic repulsion between the positively charged $[Ru(NH_3)_6]^{3+}$ and the grafted layer.

3.6. Coupling of Anthraquinone-2-carboxylic Acid to Modified GC and HOPG Electrodes

After the modification of the different electrodes by electrochemical oxidation or the reduction of the linkers used in this study, the electrodes were sonicated for 5 minutes. The Boc protecting groups were then removed in a 4 M solution of HCl in dioxane. Following the removal of the Boc group, the electrodes were washed with water and ethanol. The de-protected modified electrodes were suspended in a solution of 1 mM of AQ-2-carboxylic acid, 1.2 mM of HBTU and 4.2 mM of DIEA in DMF for 16 hours at room temperature. After the chemical modification the electrodes, they were sonicated in DMF for 5 minutes, and then rinsed with de-ionized water prior to the electrochemical characterization.

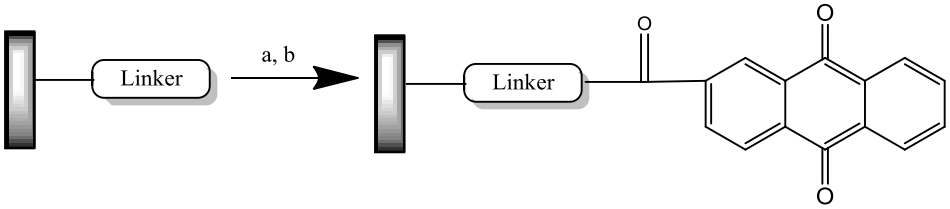

Scheme 3.3. *General procedure for obtaining AQ-modified edge plane, GC and basal plane electrodes. a) 4.0 M HCl in dioxane, RT, 1 h. b) Anthraquinone-2-carboxylic acid, HBTU, DIEA, DMF, RT, 16 h.*

Figure 3.4 shows the cyclic voltammograms of the AQ-modified GC, edge and basal plane electrodes through EDA, BDA, EDDA, HDA, XDA and $BocNHCH_2C_6H_4$ linkers in 0.1M acetate buffer (pH 4.8), recorded at the scan rate of 50 mV s^{-1}.

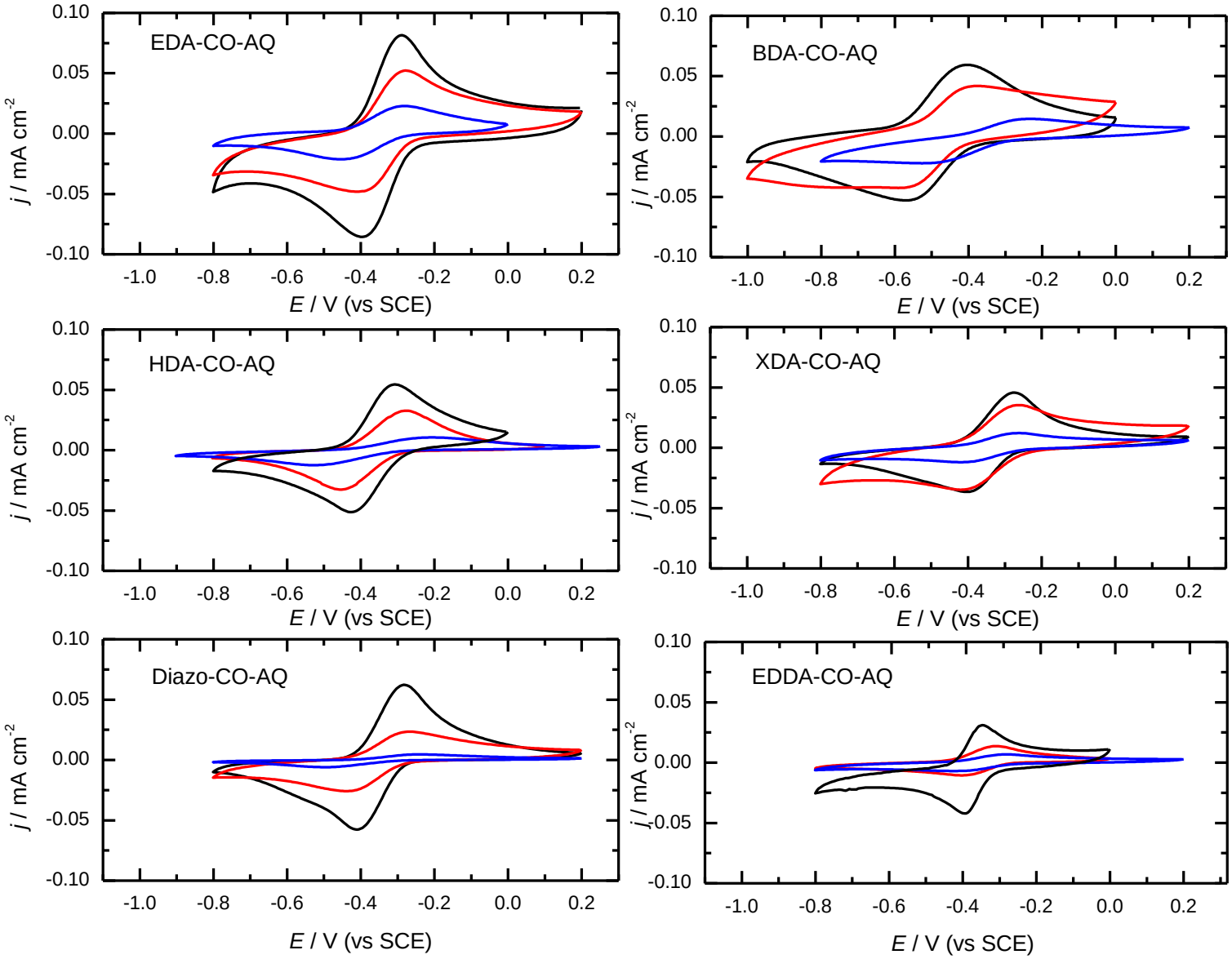

Figure 3.4. *Cyclic voltammograms recorded at a scan rate of 50 mV s^{-1} in 0.1 M of acetate buffer, pH 5, for edge, GC and basal plane electrodes modified by AQ through various linkers. Black, red and blue lines represent edge plane, GC and basal plane, respectively.*

All voltammograms show characteristic AQ peaks, depending on the type of linker and electrode. Table 2 reports peak separation ΔE, the midpoint potential E_{mp} and the surface coverage Γ AQ-modified GC, edge and basal plane electrodes. Since the mid-potential of

AQ-modified GC and edge plane electrodes attained through six diamine linkers vary only slightly, the type of linkage and electrode materials do not seem to have a substantial effect on the thermodynamics of the AQ. Any small differences could be assigned to local solvation around the linker.

Table 3.2. *AQ peak separation ΔE, midpoint potential E_{mp} and surface coverage Γ for edge, GC and basal plane electrodes in 0.1 M acetate buffer at the scan rate of 50 mV s^{-1}.*

Linker	Electrode material	Γ [nmol cm^{-2}]	ΔE (±5 mV)	E_{mp} (±5 mV) vs SCE
EDA	Edge	1.71 (±0.18)	110	-340
	GC	1.21 (±0.08)	165	-365
	Basal	0.42 (±0.02)	180	-370
BDA	Edge	1.32 (±0.07)	169	-483
	GC	0.84 (±0.10)	225	-498
	Basal	0.35 (±0.04)	282	-375
HDA	Edge	1.10 (±0.21)	123	-353
	GC	0.77 (±0.06)	160	-365
	Basal	0.32 (±0.04)	320	-360
XDA	Edge	0.91 (±0.11)	126	-343
	GC	0.71 (±0.04)	160	-340
	Basal	0.24 (±0.02)	232	-360
Diazo	Edge	1.18 (±0.20)	160	-345
	GC	0.62 (±0.09)	185	-354
	Basal	0.15 (±0.01)	210	-360
EDDA	Edge	0.57 (±0.17)	80	-371
	GC	0.31 (±0.06)	95	-353
	Basal	0.17 (±0.03)	145	-350

It is interesting to note that, for AQ, at the modified edge and basal plane and GC electrodes attained through the diamine linkers, there is a significant difference in the peak separation; especially for the basal plane electrodes, the observed peak separation is considerably larger with respect to the GC and edge plane electrodes. This indicates that the electron transfer kinetics of AQ-modified GC and edge plane electrodes are faster than that of the basal plane electrode. It is also noteworthy that the AQ-modified electrodes obtained throught the reduction of the $BocNHCH_2C_6H_4$ linker seem to possess slower electron transfer

kinetics as the value of the peak separation for the electrodes modified by these corresponding linkers are rather larger than that of the Boc-protected-diamine linkers.

The surface coverages of each AQ-modified electrode by each linker were calculated from Faraday`s law:[14]

$$\Gamma = Q/nFA \qquad \text{(Equation 3.1.)}$$

where Q is the charge obtained from the integration of the baseline-corrected area under the oxidation or reduction peak, F is the Faraday constant, A is the geometric area of the electrode, and n = 2 (i.e. the number of electrons transferred). The results for the surface coverage can be divided into two groups. First, as previously observed, for the modification of those linkers to the GC, edge and basal plane electrodes, the chemically modified edge plane electrodes with AQ through all the different linkers mentioned in this study consistently have the largest, and the basal plane electrodes have the smallest, surface coverage in all cases. These coverages are calculated based on the geometric areas of the electrodes and do not take account of any differences in roughness. Comparing these coverages to the total charges passed in Figure 3.1 for the diazonium and XDA linkers coupling and passivation of the surface, we see that the ratio of charges between the edge and basal plane electrodes agrees with the ratio of surface coverages. Since we have no reason to expect the efficiency of the coupling of anthraquinone to differ at the two electrodes, this suggests that the predominant difference here reflects the difference in the true surface areas of the two electrodes due to the differences in surface roughness and to possible differences in the initial surface coverage of the linker. The estimated coverage for a close packed monolayer of the Boc protected linker (based on a close packed array of the Boc groups estimated using the known density of t-butanol) is 0.43 nmol cm^{-2}. This is a little higher than the estimated coverage of 0.345 nmol cm^{-2}.[15] In this context, it is worth considering the fact that the reaction of a highly reactive species at the surface will not, in general, lead to a close packed monolayer because the species are unable to move around once they are attached at the surface. Considerations of two-dimensional random sequential adsorption suggest that the maximum coverage would be 0.547 of a monolayer[16] which is in reasonable agreement with the surface coverage of AQ through all linkers for the basal plane found here. This suggests that the coverage of the basal plane is complete and, in the case of diamine linkers, the higher coverages of AQ for the edge plane and glassy carbon surfaces reflect about ~ 3.7 and ~ 2.2

times higher surface roughness, respectively, than the basal plane electrode. For the diazonium linker, however, the edge plane and glassy carbon surfaces are ~9 and 4.7 times rougher than that of the basal plane surface. On the other hand, for the aliphatic linkers, as the length of the chain increases and becomes more flexible (EDDA), the surface coverages of the AQ-modified GC, edge and basal plane electrodes through all linkers decreases.

3.7. Effect of Scan Rate

The effect of scan rate on the electrochemical behavior of AQ-modified GC, edge and basal plane electrodes was investigated using cyclic voltammetry at various scan rates in an acetate buffer (pH 4.8). Figure 3.5 shows a series of cyclic voltammograms recorded at different scan rates ranging from 5 to 600 mV s^{-1} for the basal plane electrodes modified with AQ attached through the $NHCH_2C_6H_4$ linker.

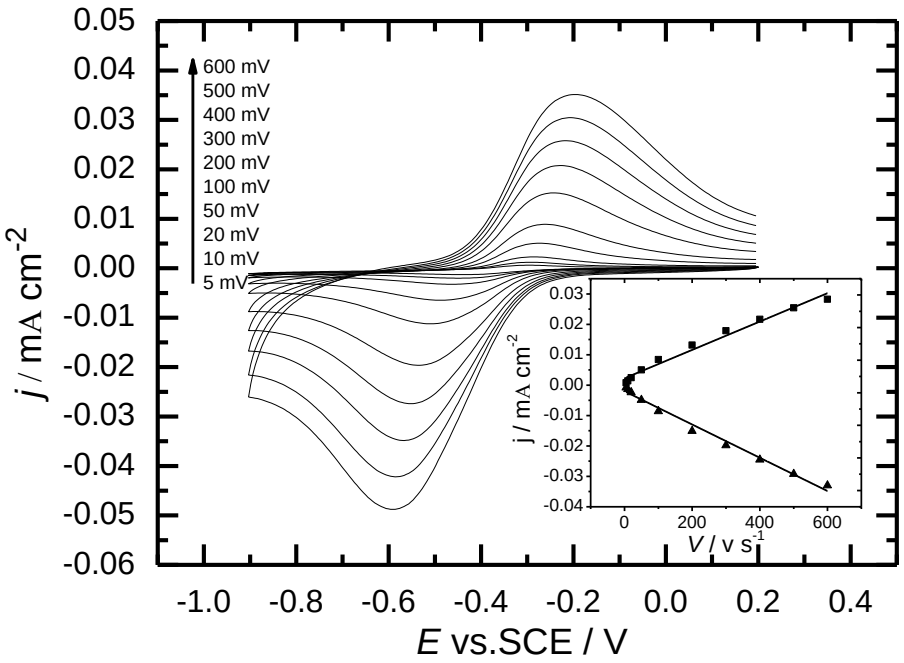

Figure 3.5. *Effect of scan rate on $C_6H_4CH_2NH$-CO-AQ-modified basal plane electrode in 0.1 M of acetate buffer, pH 5. Inset shows plot of AQ anodic and cathodic peak currents as a function of the scan rate.*

As can be seen, the anodic and cathodic peak currents increase as a function of the scan rate for each of the modified electrodes. On the basis of this finding, it can be interpreted that the film that formed on the corresponding electrode surface by AQ is not under the diffusion control[17] and that this linear relationship between peak current and scan rate is in good agreement with the surface immobilization of AQ,[18] regarded as one of the most

significant characteristics of the redox species on the surface. Laviron derived a general formula for the linear potential sweep voltammetric response for surface-confined electrodes by electroactive species.[19] This method was evaluated to determine the apparent rate constant k_{app} and transfer coefficient α. The Laviron plot can be obtained by measuring the variation of peak potential separation ΔE (E_p-E_{mp}) as a function of the logarithm of the scan rate.

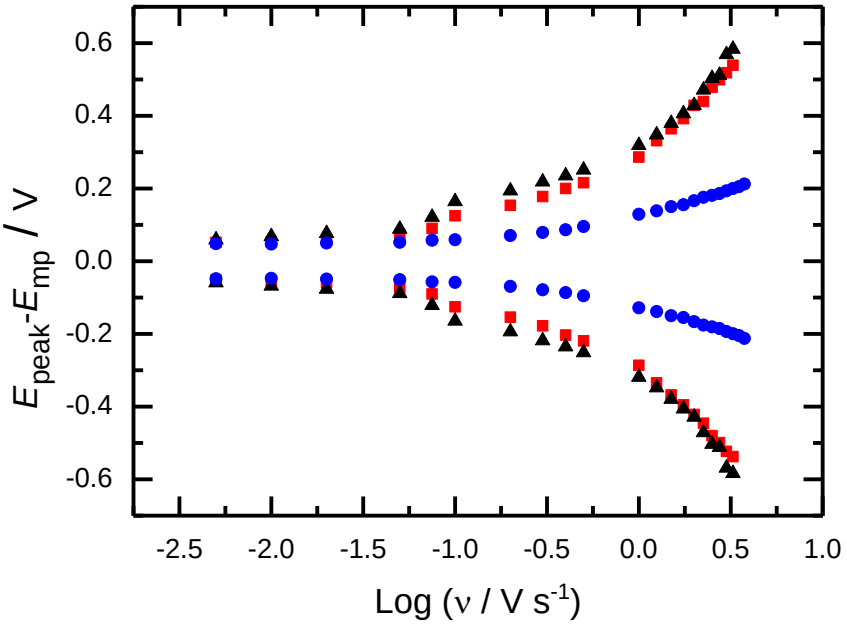

Figure 3.6. *Plot of E_{peak}-E_{mp} vs the logarithm of the scan rate for a) edge plane (▲), basal plane (●) and GC (■) modified electrodes by AQ through EDA linker, 0.1 M of acetate buffer, pH 5.*

Figure 3.6 shows the plots of the E_{peak}-E_{mp} versus the log scan rate for the AQ-modified GC, edge and basal plane electrodes by the electrochemical oxidation of the EDA linker. As shown in Figures 3.6, the anodic and cathodic peak separation ΔE_p remains almost unchanged at the lower scan rates and has a value between 50 and 110 mV for the modified electrodes with different linkers. Even though this behaviour is not well understood, it has been encountered by other researchers focusing on surface confined redox probes. At the higher scan rates, ΔE_p increases. The slopes of the linear portion of the anodic and cathodic branch equal to $2.3RT/(1-\alpha)nF$ and $2.3RT/\alpha nF$, respectively, which can be used to determine the transfer coefficient α from the slope of the straight lines based on the equation

$$\log\frac{v_a}{v_c} = \left[\log\left(\frac{\alpha}{1-\alpha}\right)\right] \quad \text{or} \quad \frac{v_a}{v_b} = \left(\frac{\alpha}{1-\alpha}\right) \qquad \text{(Equation 3.2.)}$$

where α and $(1-\alpha)$ represent electron transfer coefficient for anodic and cathodic process and υ_a and υ_c are critical scan rate for anodic and cathodic process. It is also noticeable that the

anodic and cathodic branches of the plots in Figure 3.6 are symmetric, which clearly indicates that the value of the transfer coefficient α is around 0.5.[20] When the difference of ΔE_p is also larger than 200 mV/*n*, the value of k_s can be determined by solving equation 3.3 below.

$$\log(k_s) = \alpha \log(1-\alpha) + (1-\alpha)\log\alpha - \log\left(\frac{RT}{nFv}\right) - \alpha(1-\alpha)\frac{nF\Delta E_p}{2.3RT} \quad \text{(Equation 3.3.)}$$

Where *R*, *T*, *F* and *n* have their usual meanings, *v* is the critical scan rate obtained by explorating the linear portion of the anodic and cathodic branches. However, it has been constantly neglected in the publications focusing on AQ-modified electrodes that Laviron`s model was derived for *n* = 1, but herein, the number of electrons equals 2. In this case, the electron transfer coefficient for the anodic and cathodic branches does not have to add to 1 as they might refer to different transition states.

The results in Table 3 can be divided into two groups. The first tendency which comes to our attention is that the rate constants of the AQ-modified edge plane electrodes by all linkers mentioned in this chapter are relatively higher than that of the basal plane and GC electrodes. This behaviour was already expected because of the surface formation of the edge plane as described in the previous chapter. When the rate constant belonging to the AQ-modified electrodes by each linker is compared, we encounter a quite surprising result in that, as the length of the linker increases, the rate constant also increases. Similar results were also obtained by Hong and Park[21] for hydroquinone attached to gold electrodes through alkene thiols. A work from Holm *et al.*,[22] which is related to hydroquinone-modified carbon electrodes, is also consistent with our results. This phenomenon was attributed to the predisposition of the longer chains to fold back onto the surface.

Table 3.3. *Electron transfer coefficient and rate constant for AQ-modified edge plane, GC and basal plane electrodes by various linkers in 0.1 M of acetate buffer, at pH 5.*

Linker	Electrode material	α	k_s / s^{-1}
EDA	Edge	0.49	11.82 (±0.9)
	GC	0.5	10.11 (±0.8)
	Basal	0.5	6.77 (±1.2)
BDA	Edge	0.5	12.84 (±1.1)
	GC	0.5	8.22 (±0.7)
	Basal	0.49	5.70 (±1.1)
HDA	Edge	0.5	16.22 (±1.6)
	GC	0.5	13.64(±1.1)
	Basal	0.5	12.04(±1.3)
XDA	Edge	0.5	10.22 (±0.8)
	GC	0.45	5.25 (±1.2)
	Basal	0.47	2.50 (±0.7)
Diazo	Edge	0.5	9.20 (±0.5)
	GC	0.5	3.15(±0.7)
	Basal	0.5	1.20 (±0.3)
EDDA	Edge	0.5	12.11 (±1.0)
	GC	0.5	7.25 (±0.8)
	Basal	0.49	7.85 (±0.7)

3.8. Stability of AQ-Modified Carbon Electrodes

The stability of the AQ-modified electrodes was evaluated by performing CVs in acetate buffer at pH 5 at different times in air at room temperature. Table 2 shows the change in ΔE, E_{mp} and Γ for the electrodes modified with AQ through the diazonium linker over a period of one month. There is a negligible change in the ΔE, E_{mp} and surface coverage of AQ, which gradually decreased by 20% and 21% and 23% for EP, GC and BP, respectively, at the end of one month. On the basis of this outcome, it can be said that modified graphite and GC electrodes exhibit noticeable stability as only a 20% decrease is observed in the surface coverage of AQ and peak separation.

Table 3.4. *The stability of AQ-modified carbon electrodes through EDA linker over time at pH 5*

AQ-modified Electrode	Time (days)	ΔE / mV	E_{mp} / mV vs SCE	Γ / nmol cm^{-2}
Edge	0	110	-340	1.71 (±0.18)
GC		165	-365	1.21 (±0.08)
Basal		180	-370	0.42 (±0.02)
Edge	5	112	-347	1.65 (±0.12)
GC		168	-364	1.15 (±0.07)
Basal		182	-371	0.39 (±0.01)
Edge	10	115	-345	1.58 (±0.06)
GC		172	-365	1.04 (±0.04)
Basal		187	-374	0.37 (±0.04)
Edge	20	119	-347	1.45 (±0.08)
GC		175	-363	0.95 (±0.04)
Basal		188	-378	0.35 (±0.02)
Edge	30	122	-346	1.37 (±0.03)
GC		179	-366	0.91 (±0.04)
Basal		192	-379	0.31 (±0.01)

3.9. Effect of pH

Since the electrochemical properties of anthraquinone are pH dependent, owing to the fact that it undergoes two-proton/two-electron reduction to form the corresponding hydroquinone derivative, it was assumed that the redox behaviour of modified electrodes would be pH dependent.[18] In order to test this, voltammograms of each modified electrode were obtained in an acetate buffer solutions whose pH ranged from 1 to 5 and a phosphate buffer whose pH ranged from 7 to 13. Figure 8 shows voltammograms for an AQ-modified GC electrode modified by the EDA linker in pH levels of 2.8, 3.6, 5, 8 and 10.2.

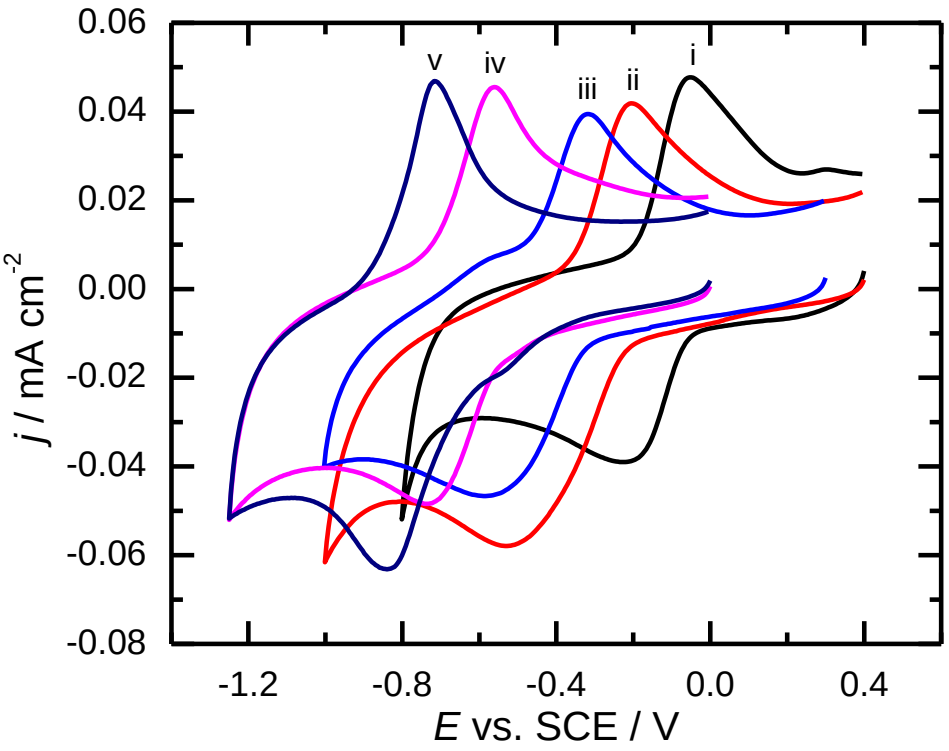

Figure 3.7. *Cyclic voltammograms at a scan rate of 50 mV s^{-1} for the GC electrode modified by AQ through an EDA linker in different pH solutions. i) pH 2.8, ii) pH 3.6, iii) pH 5, iv) pH 8 and v) pH 10.2.*

Each voltammogram shows the AQ redox peaks for all studied pH values. In acidic solutions, E_{mp} shifts to more positive potentials, whereas in relatively alkaline solutions, E_{mp} is about -720 mV vs SCE. In alkaline solutions, a considerable decrease in the peak currents occurs, which could be assigned to the hydrolysis of the immobilised anthraquinone at higher pH levels.[23,24] This hydroquinone hydrolysis is not recovered by cycling in acid, as confirmed with our own experiments by recording a voltammogram at a scan rate of 50 mV s^{-1} for the same electrode in acidic solutions. Figure 3.8 shows the relationship between E_{mp} for anthraquinone-modified GC, edge and basal plane electrodes for the diazo linker. In the pH range from 1 to 8, E_{mp} shifts linearly to more negative potentials with a slope of 57, 58 and 63 mV per pH unit for edge and basal plane and GC electrodes, respectively, which is nearly equal to the expected Nernstian value for a two-electron/two-proton process. It is noteworthy that the slope of the plot decreases for pH > 8. Probably a two-electron one-proton reduction occurs above pH 8 to form the hydroquinone anion. This makes it difficult to investigate the redox behaviour of anthraquinones at high pH. On the basis of this information, it can be concluded that the pK_a of anthraquinone is not changed by immobilisation.[7]

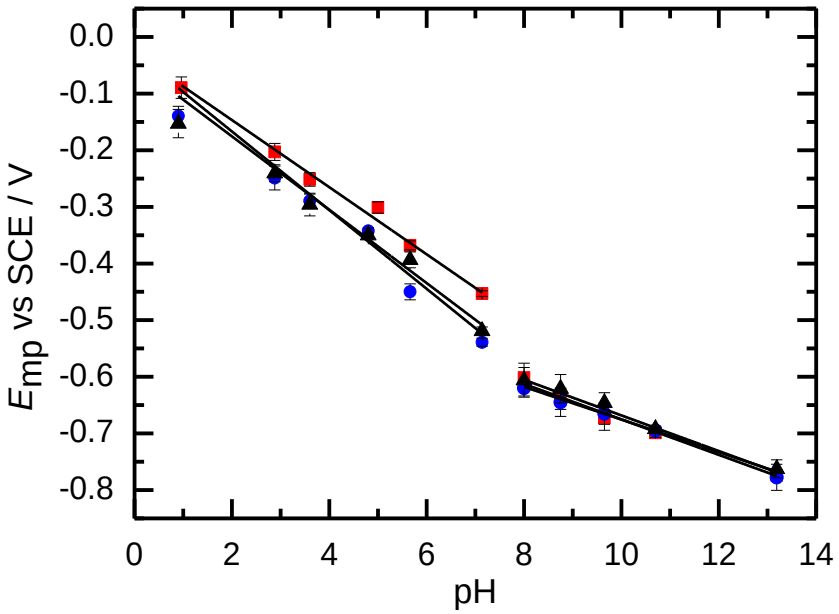

Figure 3.8. *The dependence of AQ midpoint potential Emp on pH for AQ-modified electrodes by diazonium salt. Edge plane (▲), basal pane (●) and GC (■)*

3.10. The Coupling of Nitrobenzene (NB) and Dihydroxybenzene (di-HB) to Graphite Electrodes

Using the same methodology applied for the coupling of anthraquinone-2-carboxylic acid, the coupling of NB and di-HB to modified graphite electrodes with an EDA linker were carried out in the presence of dichloromethane and pyridine as shown in Scheme 3.4. In this reaction, pyridine is used to activate the acyl chloride and to act as a solvent along with dichloromethane. Subsequent to the removal of the Boc-protecting group and several washings with absolute ethanol and water, the electrodes were reacted with a suspension made up of NB or di-HB acyl chlorides and the mixture of pyridine and dichloromethane (1:1). Figure 3.9 shows the successive CV of basal, edge plane, and GC electrodes modified with NB through an EDA linker. There are quite large peaks at around -1, -0.7 and -0.6 V for the basal plane, GC and edge plane, respectively. Such an outcome had already been anticipated because we have already shown in this chapter that, as the edge ratio at the carbon surfaces increases, the corresponding anodic and cathodic peaks are more likely to appear at less negative potentials and more current is attained. However, as we continue to cycle, this peak disappears, indicating the complete reduction of the nitrobenzene to phenyl amine or phenylhydroxyl amine. On the other hand, on the second and third scans it can clearly be seen that there is a reversible behaviour with the redox potential of -275, -110 and -53 mV for the basal plane, GC, and edge plane electrodes, respectively, which is in good agreement with our results acquired for AQ regarding electron transfer kinetics. These reversible peaks also

indicate that nitrobenzene is not totally converted into phenyl amine. The electrochemical behaviour of nitrobenzene grafted to different types of surfaces is well described in the literature,[25-28] and herein, our results are consistent with them. In order to calculate the surface coverage of NB, we definitely need to know the number of electrons transferred during this process. It is well established in the literature that NB undergoes a two electron, two proton oxidation to phenylnitrosoamine.

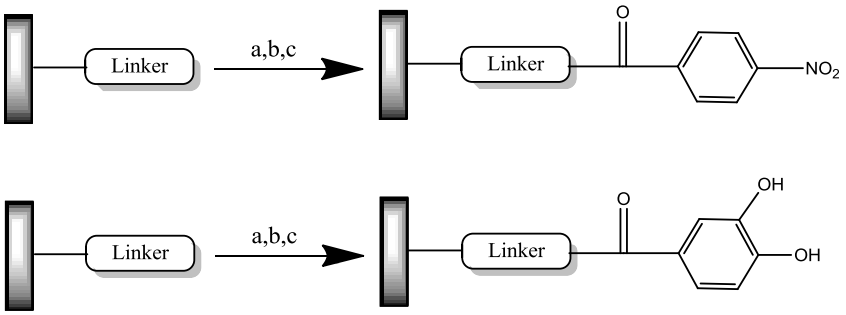

Scheme 3.4. *General procedure for the functionalization of modified electrode surfaces by NB and di-HB. a) 4.0 M HCl in dioxane, RT. 1 b) 3.4 nitrobenzoyl chloride or (3.4-dihimethoxyphenyl)acetyl chloride, Py, dichloromethane, RT, 16 h, BBr_3 for 1 hour.*

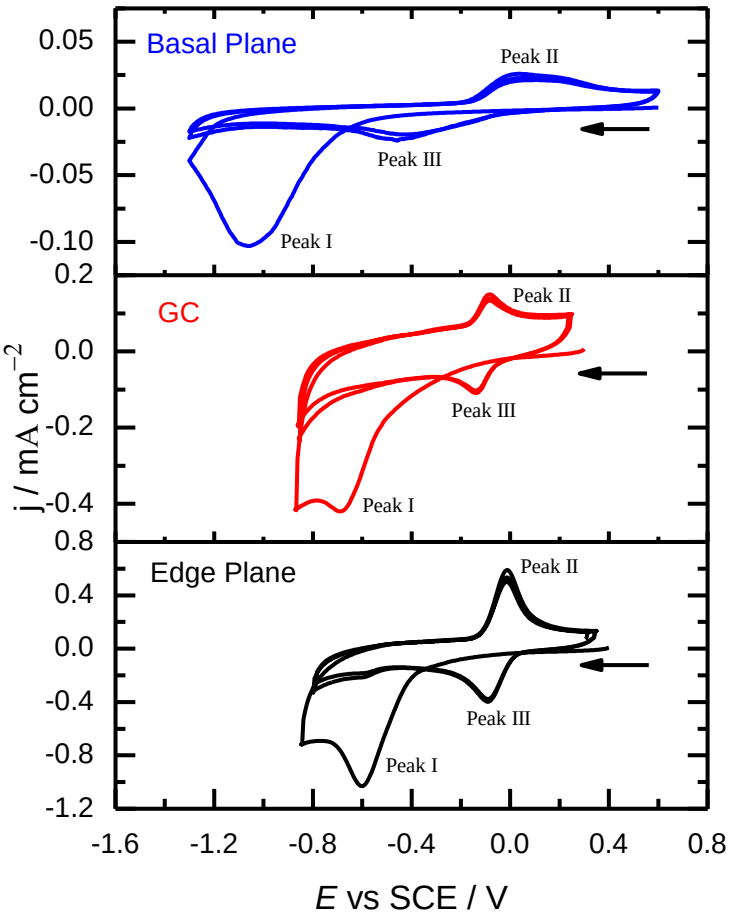

Figure 3.9. *CV for NB-modified edge plane, basal plane, and GC electrodes through an EDA linker at 50 mV s^{-1} in phosphate buffer, pH 7.*

The first irreversible peak corresponds to a six electron, six proton electrochemical reduction of nitrobenzene to phenyl amine through the phenylhydroxyl amine.[18,29] Chretien *et al.*[18] describe the calculation of the surface coverage of NB using equation 3.4:

$$\Gamma = \frac{(Q1+Q2)}{6\,FA} \qquad \text{(Equation 3.4.)}$$

where Γ is the surface coverage of NB, Q_1 and Q_2 represent the charge obtained from the integration of the baseline corrected area under the first peak and the average charge under the second and third peaks, F is the Faraday constant and A is the electrode area. Table 3.5 reports the surface coverage, peak separation, and mid-potential of NB-modified carbon electrodes. As expected from the results related to the surface coverage of AQ obtained for edge plane, basal plane, and GC electrodes, the edge plane has the highest surface coverage while the basal plane has the lowest, with GC having an intermediate surface coverage, which is exactly the same tendency with surface coverage of AQ. Moreover, in terms of the peak separation obtained for the reversible peaks at the NB-modified graphite electrodes, the same trend occurs again for the AQ-modified graphite electrodes, i.e., the edge plane electrode exhibits the fastest electron transfer kinetics, whereas the basal plane electrode has the most sluggish electron transfer kinetics.

Table 3.5. *Surface coverages and peak separations for edge plane, basal plane, and GC modified electrodes with NB by an EDA linker. Cyclic voltammetry experiments were carried out in 0.1 M of phosphate buffer (pH 7) at 50 mV* s^{-1}.

Electrode	Γ_{NB} [nmol cm^{-2}]	ΔE [±5 mV]
Edge	1.80 (±0.92)	53
GC	1.12 (±0.14)	110
Basal	0.52 (±0.12)	275

The coupling of di-HB is also achieved by following the same methodology. The tethering of dihydroxybenzene derivatives to conductive surfaces has attracted substantial interest because of their electrocatalytic activity for NADH oxidation, which is widely regarded as a very significant coenzyme due to its potential application in the field of biosensors. However, we will not discuss about the NADH oxidation of unmodified edge plane, basal plane, and GC electrodes modified with di-HB as it is outside the scope of this

study. As shown in the scheme, once we achieved the coupling of (3.4-dihimethoxyphenyl) acetyl chloride to carbon electrodes, the removal of the methoxy group is carried out with BBr_3 (1 M in dichloromethane). As seen in figure 3.10, well-defined voltammograms are obtained for all carbon electrodes. The surface coverage of di-HB is calculated based on a two electron process. The results are illustrated in table 3.6. Not surprisingly, a similar trend was obtained in terms of the surface coverage of di-HB and peak separation.

Table 3.6. *Surface coverages and peak separations for edge plane, basal plane, and GC modified electrodes with di-HB by an EDA linker. Cyclic voltammetry experiments were carried out in 0.1 M of phosphate buffer (pH 7) at 50 mV* s^{-1}.

Electrode	$\Gamma_{di\text{-}HB}$ [nmol cm^{-2}]	ΔE [±5 mV]
Edge	0.89 (±0.11)	30
GC	0.28 (±0.04)	101
Basal	0.16 (±0.01)	125

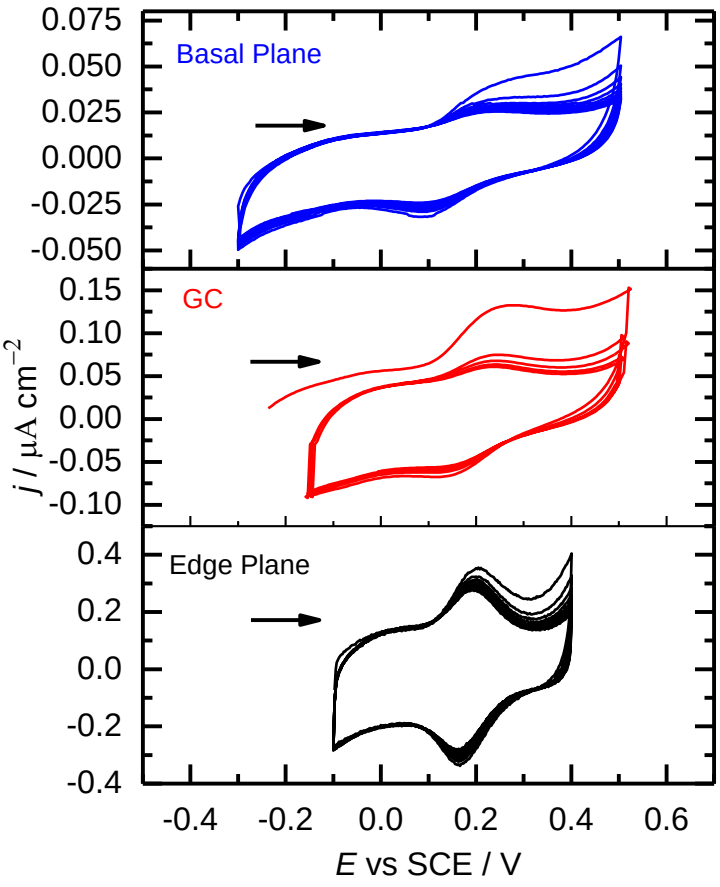

Figure 3.10. *CV for di-HB modified edge plane, basal plane, and GC electrodes through an EDA linker at 50 mV* s^{-1} *in phosphate buffer, pH 7.*

3.11. Bi-functionalization of Edge and Basal Plane Electrodes

Chretien *et al.*[6] have recently demonstrated the possibility of the bi-functionalization of modified GC electrode surfaces with redox probes such as nitrobenzene (NB) and dihidroxybenzene (di-HB). In this study, subsequent coupling of nitrobenzene and dihidroxybenzene to modified edge and basal plane electrodes through an EDA linker was performed. AQ-modified edge and basal plane electrodes were suspended in a solution consisting of 4-nitrobenzene chloride, dichloromethane and pyridine for sixteen hours. The resulting electrodes were washed with DMF and ethanol prior to the CV measurements.

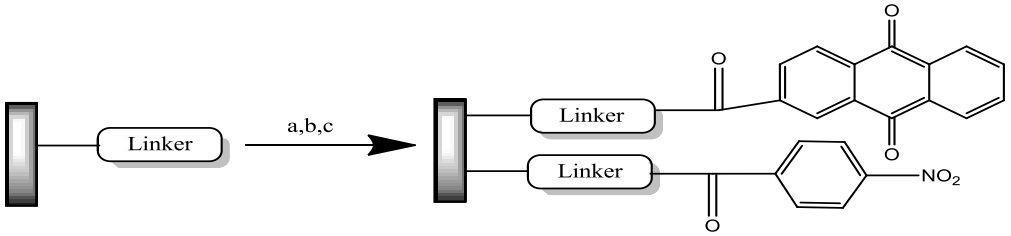

Scheme 3.5. *General procedure for the bi-functionalization of modified electrode surfaces by AQ and NB. a) 4.0 M HCl in dioxane, RT. 1, b) Anthraquinone-2-carboxylic acid, HBTU, DIEA, DMF, RT, 16 h. c) nitrobenzoyl chloride, Py, dichloromethane, RT, 16 h.*

Figure 3.11 shows an edge plane electrode sequentially modified by AQ and NB. On the second scan, there is an unsymmetrical peak with a redox potential of -379 (peak II and IV) mV and 32 mV (peak III and V), which is certainly assigned to AQ and NB. Figure 3.11 b presents sequentially modified basal plane electrodes by AQ and NB by an EDA linker. As for the edge plane electrode, there is a reversible peak at 38 mV (peak II and peak III), which is assigned to NB. Although there is an oxidation peak at -0.7 V on the second cycle, on the reverse scan, no peak was detected. Therefore, this peak might indicate that the sequential coupling of AQ is not achieved or all attached NB is not totally converted to amine. The first peak on the initial scan might be associated with the reduction of both AQ and NB, both because they are overlapped and because the peak at the reverse scan could be assigned to an oxidation of AQ.

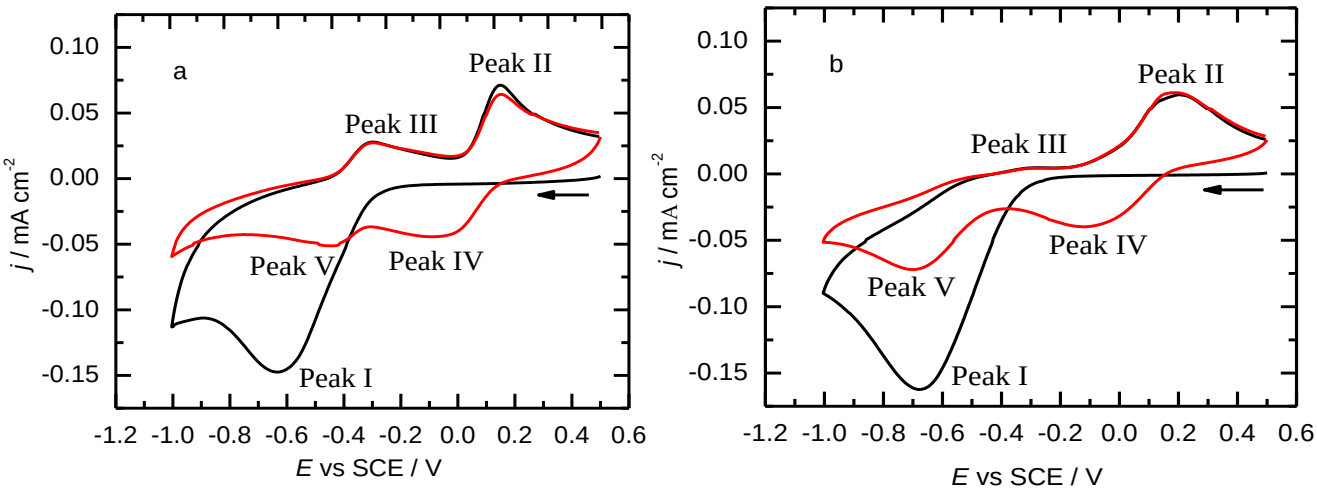

Figure 3.11. *Cyclic voltammetry for subsequentially bi-functionalized edge and basal plane electrodes by AQ through an EDA linker in 0.1 M of acetate buffer (pH 5) and at the scan rate of 50 mV s^{-1}. a) edge plane, b) basal plane.*

We can interpret these voltammograms as previously described in Section 3.9. Peak I is attributed to the six electron, six proton irreversible reduction of immobilised nitrobenzene to phenyl amine through the phenylhydroxyl amine intermediate. However, the phenylhydroxyl amine is not completely reduced to phenyl amine and can undergo a quasi-reversible two electron, two proton oxidation (peak II) to phenylnitrosoamine (peak III). As we carry on cycling, the complete peak disappearance of peak I occurs, indicating the accomplishment of the reduction of nitrobenzene to phenyl amine or phenylhydroxyl amine.

Table 3.7. *AQ and NB surface coverages for edge and basal plane modified electrodes by an EDA linker. Cyclic voltammetry experiments were carried out in 0.1 M of acetate buffer (pH 5) at 50 mV s^{-1}.*

Electrode	Γ_{AQ} [nmol cm^{-2}]	Γ_{NB} [nmol cm^{-2}]
Edge	0.74 (±0.06)	0.62 (±0.05)
Basal	-	0.22 (±0.07)

Table 3.7 reports the surface coverage of AQ calculated by integrating the area under the corresponding oxidation peak based on a two electron reduction. However, for NB, the surface coverage was estimated from the charge under the first reduction peak on the first scan and the oxidation peak on the second scan based on a six electron reduction. As expected from the results in Section 3.6, the surface coverage of NB on the edge plane electrode is higher than that on the basal plane electrode. Interestingly, on the reverse scan, no peak was detected belonging to AQ for the basal plane electrode. As a result of this, it can

be concluded that the coupling of AQ to the basal plane electrode modified with an EDA linker in the presence of NB does not seem to work. Hence, differential pulse voltammetry (DPV) was used in order to more sensitively characterize the sequentially modified surfaces with AQ and NB. DPV is considered as a more sensitive electrochemical method for the characterization of the surface-confined electroactive layer when the surface concentration is small so that the capacitance current is high. Figure 3.12 shows the DPV at a scan rate of 10 mV s^{-1}, with a pulse amplitude of 5 mV and a pulse time of 50 ms, for edge and basal plane electrodes subsequently modified by AQ and NB through the EDA linker. DPV shows two distinct peaks, which correspond to the oxidation of AQ and NB, respectively.

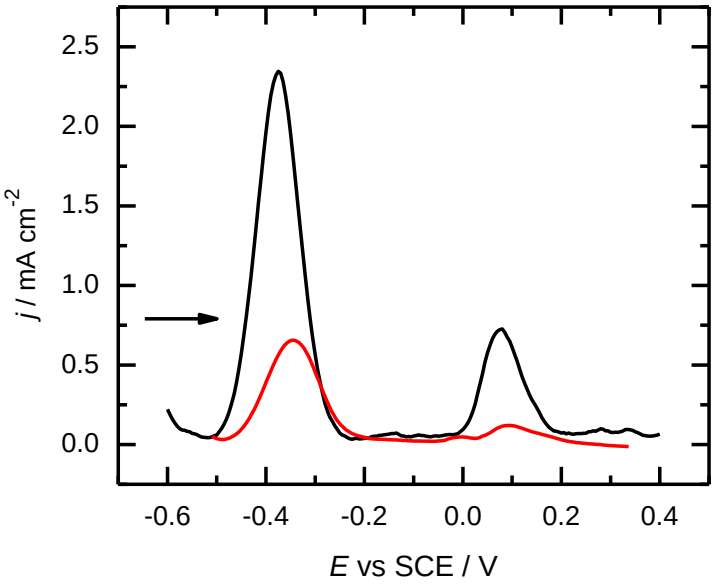

Figure 3.12. *Differential pulse voltammetry for edge and basal plane electrodes subsequentially modified with AQ and NB through the EDA linker in 0.1 M of acetate buffer (pH 5). DPV parameters were set at pulse amplitude 5 mV, scan rate at 10 mV s^{-1}, and pulse time 50 ms. Black and red lines represent edge and basal plane electrodes, respectively.*

The bi-functionalization of the modified edge and basal plane electrodes by means of the oxidation of the EDA linker was carried out with AQ and di-HB. AQ-modified electrodes were suspended in (3,4 dimethoxyphenyl) acetyl chloride in dichloromethane in the presence of pyridine at room temperature for sixteen hours. The resulting electrodes were then treated with 1 M of BBr_3 for the de-protection of the methoxy groups. The resulting electrode was washed with DMF and ethanol and then characterized by DPV. The DPV shows a characteristic oxidation peak for AQ at about -380 mV, and a second oxidation peak for di-HB at 300 mV, which is very consistent with the electrochemistry of separately immobilised AQ or di-HB.

Table 3.8. *AQ and di-HB surface coverages for edge and basal plane modified electrodes by the EDA linker. Cyclic voltammetry experiments were carried out in 0.1 M of acetate buffer (pH 5) at 50 mV s^{-1}.*

Electrode	Γ_{AQ} [nmol cm^{-2}]	$\Gamma_{di\text{-}HB}$ [nmol cm^{-2}]
Edge	0.68 (±0.08)	0.41 (±0.06)
Basal	0.36 (±0.05)	0.12 (±0.02)

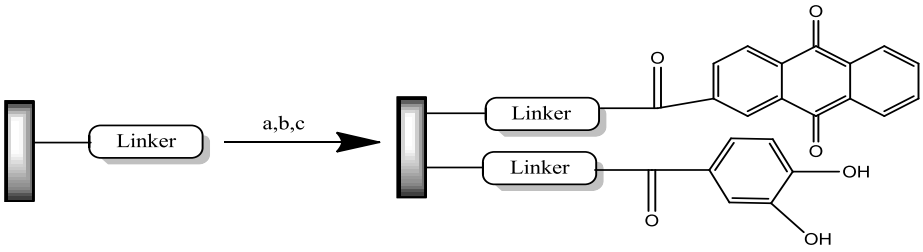

Scheme 3.6. *General procedure for bi-functionalization of modified electrode surfaces by AQ and di-HB. a) 4.0 M HCl in dioxane, RT. b) Anthraquinone-2-carboxylic acid, HBTU, DIEA, DMF, RT, 16 h. c) (3,4-dimethoxy-phenyl)acetyl chloride, Py, dichloromethane, RT, 16 h. d) 1.0 M BBr_3 in dichloromethane, RT, 1 h.*

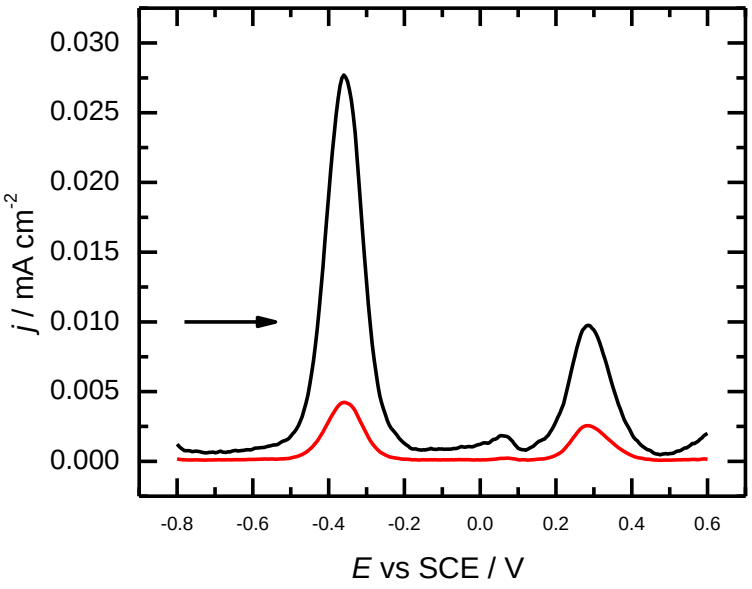

Figure 3.13. *Differential pulse voltammetry for edge and basal plane electrodes subsequentially modified with AQ and di-HB through the EDA linker in 0.1 M of acetate buffer (pH 5). DPV parameters were set at pulse amplitude 5 mV, scan rate at 10 mV s^{-1}, and pulse at 50 ms. Black and red lines represent edge and basal plane electrodes, respectively.*

3.12. Conclusion

Glassy Carbon and HOPG with the orientation of edge and basal plane electrodes were grafted by Boc-protected-diamine linkers and diazonium tetrafluoroborate salt by either the electrochemical oxidation or the electrochemical reduction of the corresponding diazonium salts. As the edge density on the carbon materials increases, the electrochemical attachment of the linker used in this work seems to become more facile since the corresponding peak appears at more positive potentials and the peak currents obtained at the edge sites are greater than at the basal sites. Once the Boc-protecting group was removed, further modification onto the grafted surface was carried out with AQ, NB and di-HB by using solid phase synthesis methodology. The surface coverage of AQ-modified surfaces through each linker was evaluated with cyclic voltammetry (CV). It was found that the obtained surface coverage of AQ, NB and di-HB on edge plane electrodes is much higher than GC and basal plane electrodes; furthermore, GC electrodes always lie between the edge and basal planes of HOPG. Such an outcome was already anticipated owing to the fact that the GC electrode is believed to be made up of a random combination of edge and basal sites and the proportion of edge sites is relatively higher than that of basal sites. Therefore, its electrochemical properties resemble edge plane rather than basal plane.[30] Moreover, it must be stressed that the relative roughness of the edge and basal plane of HOPG and GC surfaces have to be taken into account if the surface coverage of AQ differs at the carbon electrodes modified by the same linker. Moreover as there is no direct relationship between the coupling efficiency of AQ and modified carbon surfaces by de-protected amine linkers, it can hence be concluded that the difference in the surface coverage for the different types of carbon electrodes is primarily originated from surface roughness or a possible difference in the surface coverage of the linker obtained during the electrochemical grafting process. It is also noteworthy that the modified electrodes with AQ obtained using solid phase synthesis methodology show rather good stability as there is no significant change in the surface coverage and peak separation over the period of one month.

Furthermore, the type of linker and carbon material does influence surface coverage and electron transfer kinetics. As the length of the alkyl chain increases, the surface coverage decreases and the electron transfer coefficient increases. Besides linkers bearing an aromatic ring, they also appear to give lower surface coverage than the linker which have a relatively

short chain. The effect of scan rate was also evaluated with the Laviron procedure in order to find out how the type of AQ-modified graphite electrode affects the electron transfer kinetics. The edge plane modified electrodes with AQ through all six linkers was found to have the largest electron transfer rate. It is also noteworthy that, as the length of the linker increases, the electron transfer rate increases. In contrast, bulky linkers have a relatively low electron transfer rate. The subsequent bi-functionalization of edge and basal plane electrodes with AQ & NB and AQ & di-HB were also achieved. A similar trend was found for edge and basal plane electrodes in terms of surface coverage and peak separation.

3.13. References

(1) A. Pinczewska; M. Sosna; S. Bloodworth; J. D. Kilburn; P. N. Bartlett, *J. Am. Chem. Soc.* **2012**, *134*, 18022.

(2) A. Adenier; M. M. Chehimi; I. Gallardo; J. Pinson; N.Vila, *Langmuir* **2004**, *20*, 8243.

(3) A. J. Downard, D. J. G., E. S. Q. Tan *Langmuir* **2006**, *22*, 10739.

(4) A. J. Downard; E. S. Q. Tan; S. S. C. Yu, *New J. Chem.* **2006**, *30*, 1283.

(5) I. Gallardo; J. Pinson; Vila, N. *J. Phys. Chem. B* **2006**, *110*, 19521.

(6) J. M. Chrétien; M. A. Ghanem; P. N. Barlett; J. D. Kilburn, *Chem. Eur. J.* **2008**, *14*, 2548.

(7) J. M. Chrétien; M. A. Ghanem; P. N. Barlett; J. D. Kilburn, *Chem. A. Eur. J.* **2009**, *15*, 11928.

(8) M. A. Ghanem; J. M. Chrétien; J. D. Kilburn; P. N. Bartlett, *J. Mater. Chem.* **2008**, *18* 4917.

(9) S. Schauff; M. Ciorca; A. Laforgue; D. Be´langer, *Electroanalysis* **2009**, *21*, 1499

(10) R. Reilson; M. Kullapere; K. Tammeveski, *Electroanalysis* **2010**, *22*, 513

(11) A. J. Downard; M. J. Prince, *Langmuir* **2001**, *17*, 5581.

(12) Y. R. Leroux, J-M. Noel, C. Roux, P. Hapiot, *J. Am. Chem. Soc.* **2010**, *132*, 14039.

(13) S. Kesavan; S. B. Revin; S. A. John, *J. Mater. Chem.* **2012**, *22*, 17560.

(14) A. J. Bard; L. R. Faulkner, *Electrochemical Methods: Fundamentals and Applications*, New York : John Wiley&Sons **2001**.

(15) A. P. Brown; F. C. Anson, *Anal. Chem.* **1977**, *49*, 1589.

(16) E. L.Hinrichsen; J. Feder; T.Jøssang, *J. Stat. Phys.* **1986**, *44* 793.

(17) S. Y. Rhieu; D. R. Ludwig; V. S. Siu; G. T. R. Palmore, *Electrochem. Commun.* **2009**, *11*, 1857.

(18) M. A. Ghanem; J. M. Chrétien; A. Pinczewska; J. D. Kilburn; P. N. Bartlett, *J. Mater. Chem.* **2008**, *18*, 4917.

(19) E. Laviron, *J. Electroanal. Chem.* **1979**, *101*, 19.

(20) H.-G. Hong, *Bull. Korean Chem. Soc.* **1995**, *16*, 886.

(21) H-G. Hong; W. Park, *Langmuir* **2001**, *17*, 2485.

(22) A. H. Holm; K. H. Vase; B. Winther-Jensen; S. U. Pedersen; K. Daasbjerg, *Electrochim. Acta* **2007**, *53*, 1680.

(23) M. Shamsipur; J. Ghasemi; F. Tamaddon; H. Sharghi,*Talanta* **1993**, *40*, 697

(24) D. Almasifar; A. Forghaniha; Z. Khojasteh; J. Ghasemi; H. Sharghi; M. Shamsipur, *J. Chem. Eng. Data* **1997**, *42*, 1212

(25) I. Rubinstein, *J. Electroanal. Chem.* **1985**, *183*, 379.

(26) B. Ortiz; C. Saby; G. Y. Champagne; D. Be´langer, *J. Electroanal. Chem.* **1998**, *455*, 75.

(27) P. A. Brooksby; A. Downard, *Langmuir* **2004**, *20*, 5038.

(28) M. Pandurangappa; N. S. Lawrene; R. G. Compton, *Analyst* **2002**, *127*, 1568.

(29) V. K. Sarin; S. B. H. Kent; R. B. Merrifield, *Anal. Biochem.* **1981**, *117*, 147.

(30) K. R. Kneten; R. L. McCreery *Anal. Chem.* **1992**, *64*, 2518.

Chapter 4

THE FUNCTIONALIZATION OF CARBON NANOTUBES

4.1. Overview

The characteristic electronic properties of carbon nanotubes (CNTs)[1-3] make them very attractive for many scientific and nanotechnology applications. Carbon nanotubes in their native state are water insoluble and are inappropriate for water-based environments but can be used as film on the electrode surface. To overcome this problem the surface of carbon nanotubes needs to be modified by surface functional groups chosen to make them compatible for the particular application. Two main approaches have been extensively used to modify the surfaces of carbon nanotubes. One is the non-covalent adsorption, or wrapping of functional molecules around the nanotubes.[4-6] This approach has disadvantages of limited control over the amount of attached material and suffers from poor stability. The second approach is to use covalent bonding of functional molecules to the CNTs surface using chemical oxidation under harsh conditions with concentrated acids[6-10] or by chemical and electrochemical reduction of aromatic diazonium salts.[4,8,11-14] In the chemical oxidation process the CNTs are treated by heating in a mixture of concentrated nitric and sulphuric acid in an ultrasonic bath. Although this aggressive treatment leads to the formation of oxygen functional groups (COOH, COH, CO) at the CNTs surface it lacks control over the surface coverage and type of functional group, and damages the CNTs.[6] The covalent modification of CNTs based on the reduction of substituted diazonium salts has the advantages of not damaging the CNTs combined with the ability to control surface coverage and functionality. A limitation of direct modification by the diazonium method is the availability of diazonium salts bearing suitable functional groups and their limited stability. In addition, under some circumstances multilayers of substituted aromatic compounds can be formed by grafting with diazonium salts.[15,16] Nevertheless, in both cases the robust linkage between the carbon surface and the modifier makes the covalently attached monolayer very suitable for further chemical modification and the functional groups at the CNTs surface can be used in further reactions to attach various target molecules to the CNT surface.

In the present work we use anthraquinone (AQ) as a model system because it shows reversible electrochemistry and it has been widely investigated as a mediator for oxygen reduction, which will be discussed in Chapter 5 and in pH sensing.[17,18] Very recently Marken *et al.*[19] reported the attachments of AQ to the surface of carbon nanoparticles chemically modified by amine functional groups. The electrochemical attachment of EDA and (*N*-Boc-

aminomethyl)phenyl linkers to abrasively immobilized GC electrodes and spontaneous attachment of (*N*-Boc-aminomethyl)phenyl linker to the surface of CNTs followed by Boc-deprotection and coupling of AQ and NB functional groups by amide solid-phase coupling were carried out. The surface modifications, coverage and stability of the attached AQ and NB groups have been characterized by FTIR and cyclic voltammetry.

4.1.1. Electrochemical Immobilization of $C_6H_4CH_2NHBoc$ and Boc-EDA Spacers to CNT Surfaces

The dry abrasive immobilized CNTs showed very stable electrochemical performance and have been used to explore the electrocatalytic activity of CNTs toward many electrochemical reactions.[20-22] Here we used dry abrasive CNT immobilization because it produces robust modified electrodes and CNTs sustain multistep modification process without detaching from the substrate. However the dry CNT abrasive immobilization can causes roughening to the substrate as well as changes to the CNT surfaces which could alter the chemical and electrochemical behaviour. Therefore in this work we carried out a parallel control experiment using wet casting immobilization of CNTs which avoids the above roughening effects. The abrasive immobilization of CNTs was monitored by measuring the capacitance current using cyclic voltammetry in 0.1 M PBS. The maximum CNT loading was achieved after 5 min abrasion. The background current for the immobilized CNTs was compared with that for the polished glassy carbon electrode using cyclic voltammetry in 0.1 M PBS and was about two to three times bigger than that for the bare glassy carbon electrode. Figure 4.1 shows a surface scanning electron microscope image for CNTs immobilized by dry abrasion on to GC. Clearly the SEM image shows that the immobilized CNTs are very compacted together and distributed uniformly over the GC surface. The thickness of the CNT film, as estimated from a side image view varies, between 1.0 and 1.5 μm. This gave an estimate of between 10 and 15 μg of CNTs loaded on the GC electrode with a geometric area of 0.071 cm^2 (the density of CNTs on the surface varied between 1.3 and 1.4 g/cm^3). However this is only a rough estimate and it could vary somewhat from one electrode to another.

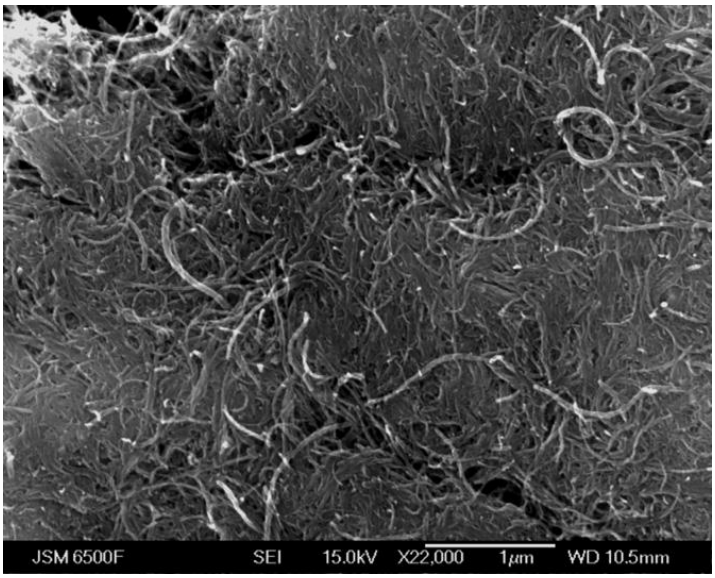

Figure 4.1. *SEM image of CNTs immobilized by dry abrasion on to a GC substrate.*

The immobilization of the $C_6H_4CH_2NHBoc$ linker onto dry and wet immobilized CNTs was performed by electrochemical reduction of the corresponding diazonium tetrafluoroborate salt as shown in Scheme 4.1. Figure 4.2 shows the consecutive cyclic voltammograms for the dry abrasive immobilized CNTs at 50 mV s^{-1} in 5.0 mM $C_6H_4CH_2NHBoc$ diazonium salt in acetonitrile containing 0.1 M TBATFB. The cyclic voltammetry for polished glassy carbon is shown for comparison.

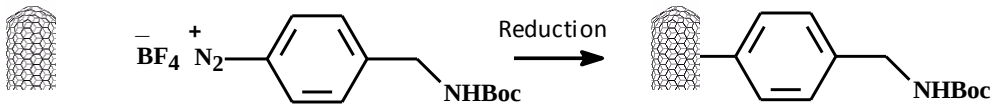

Scheme 4.1. *Electrochemical immobilization of $C_6H_4CH_2NHBoc$ on to CNT modified electrodes.*

On the first scan we observe two broad irreversible peaks at potentials about 120 and -450 mV vs. SCE attributed to the reduction of the $C_6H_4CH_2NHBoc$ diazonium salt and formation of the aromatic radical which reacts with the CNTs surface. The presence of two peaks for the reduction of $C_6H_4CH_2NHBoc$ can be linked to the differences in surface reactivity of the CNTs. The CNTs used in this work have the bamboo like structure where the edge plane carbon is predominant and coexists with basal plane carbon and it is known that the edge planes are more reactive than the basal plane for many electrochemical reactions[21,23].

We therefore suggest that the peaks at 120 and −450 mV can be related to reduction of the diazonium salt at the edge and basal plane sites respectively[21,23] with the input of the underlying GC surface as well. On the subsequent scans these peaks are diminished and the voltammogram eventually becomes featureless consistent with blocking of the electrode by the organic layer bonded to the CNTs during the first cycle.

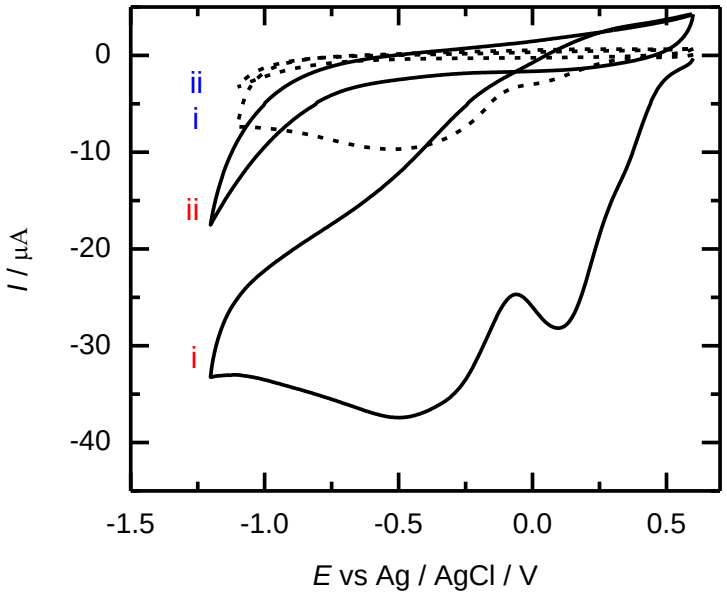

Figure 4.2. *Cyclic voltammetry at 50 mV s^{-1} for (red) abrasive immobilized CNTs and (blue) glassy carbon electrodes in 5 mM 4-(N-Boc-aminomethyl) benzene diazonium tetrafluoroborate salt in acetonitrile containing 0.1 M TBATFB. In each case the first two cycles are shown.*

.

The attachment of the EDA-Boc linker to abrasive immobilized CNTs was performed by electrochemical oxidation of Boc-EDA at the CNT modified electrodes as shown in Scheme 4.2. Figure 3.3 shows the cyclic voltammetry at 50 mV s^{-1} for the electrochemical oxidation of 10 mM EDA-Boc at abrasive immobilized CNTs in acetonitrile with 0.1 M TBATFB. The first cycle shows a single oxidation peak located at about +1.55 V vs. SCE. This peak is irreversible and no cathodic peak can be observed on the reverse scan indicating that the amine cation radical generated after the first electron transfer undergoes a chemical reaction by binding to the CNTs surface (as shown in Scheme 4.2) or diffuses away from the surface forming dimers or polymeric species in the solution.[16] On the second scan the oxidation peak current is significantly reduced which is consistent with passivation of the electrode by the grafting of the EDA-Boc layer to the CNTs.

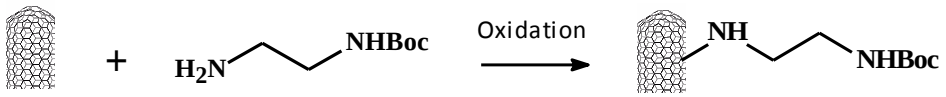

Scheme 4.2. *Electrochemical immobilization of Boc-EDA on to CNTs modified electrodes.*

Similar voltammetry was observed at plane glassy carbon electrodes for both linkers but with significantly smaller currents than in the case of the CNT modified electrodes. This difference in current correlates with the increase in real surface area after abrasive immobilization of CNTs on to glassy carbon and is very similar to the difference seen in the background currents for voltammetry in buffer solution for the electrodes.

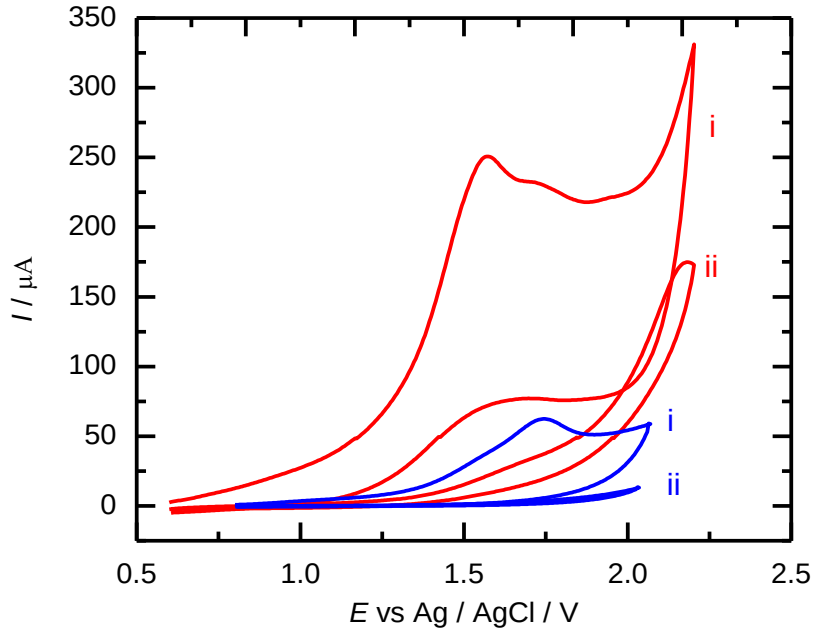

Figure 4.3. *Cyclic voltammetry at 50 mV s^{-1} for (red) abrasive immobilized CNTs and (blue) glassy carbon electrodes in 10 mM of Boc-EDA in acetonitrile containing 0.1 M TBATFB.*

4.1.2. Chemical Coupling and Characterization of Anthraquinone (AQ) Modified CNTs.

After the attachment of $C_6H_4CH_2NHBoc$ and EDA-Boc spacers on to the CNT surface the Boc group was removed by reaction with 4.0 M HCl in dioxane for 1 h. This gives a CNT surface modified with amine groups which can then be reacted with other functional molecules using amide coupling. To attach AQ to the surface, Scheme 4.3, the amine modified CNTs were reacted with anthraquinone 2-carboxylic acid in the presence of HBTU as the coupling reagent in DMF at room temperature for 16 h. The AQ modified CNT

electrodes were then washed several times in DMF and EtOH and characterized using cyclic voltammetry in PBS. Figure 4.4 shows the cyclic voltammetry at 50 mV s^{-1} in 0.1 M phosphate buffer solution at pH 7 for dry abrasive immobilized CNT electrodes modified with AQ through (a) $C_6H_4CH_2NH$ and (b) EDA linkers. For both linkers the coupling experiments were replicated 3 times and the cyclic voltammetry for plane glassy carbon electrode, treated under the same conditions, is shown for comparison.

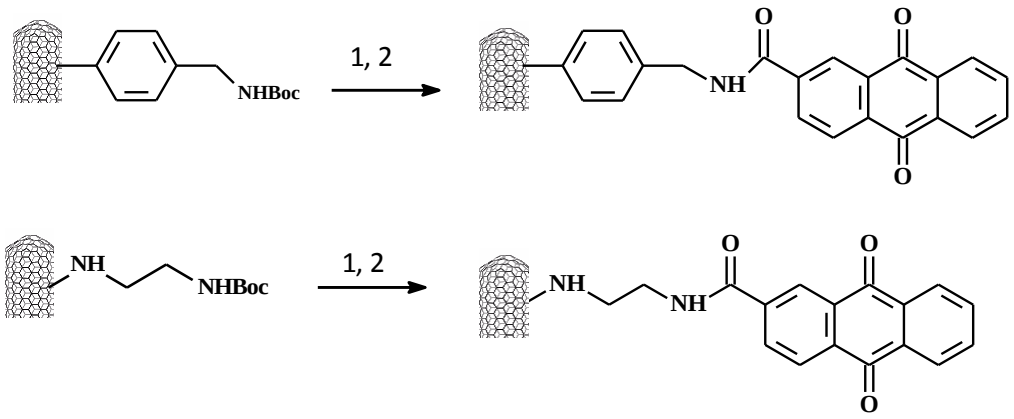

Scheme 4.3. *Preparation of anthraquinone modified CNTs electrodes: (1) 4.0 M HCl in dioxane for 4 h, (2) anthraquinone-2-carboxylic acid, HBTU, DIEA, DMF, rt, 16 h.*

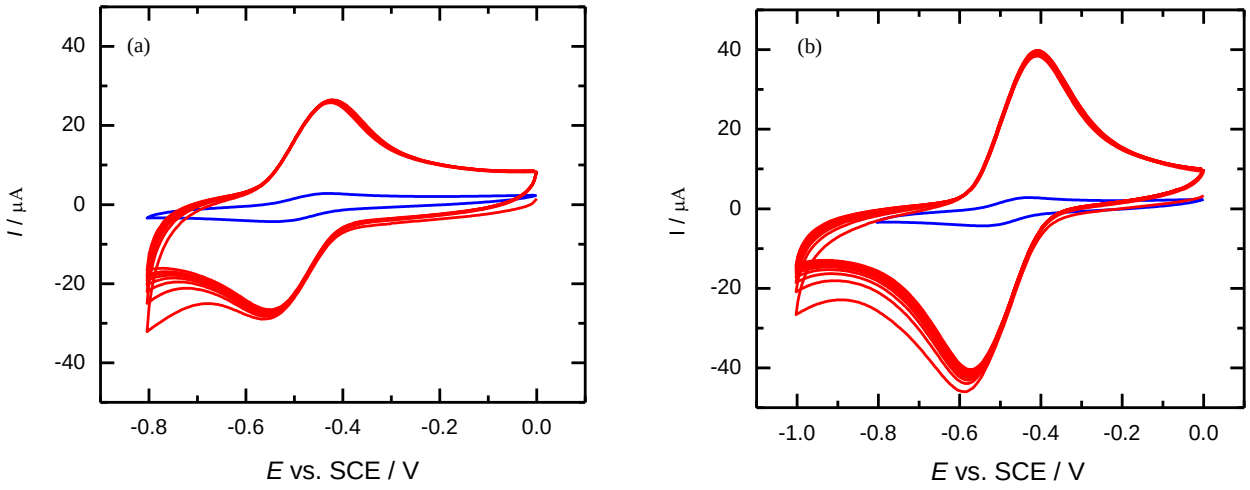

Figure 4.4. *Cyclic voltammograms at 50 mV s^{-1} in 0.1 M of PBS at pH 7 for (solid line) CNTs and (dashed line) GC modified electrodes by AQ through (a) EDA and (b) $C_6H_4CH_2NH$ linkers.*

The voltammograms for the CNTs modified electrodes show the characteristic, sharp redox peaks for AQ in all cases. In comparison with plain GC modified using the same conditions the AQ redox peak currents for the dry abrasive immobilized CNTs modified with

$C_6H_4CH_2NH$ and EDA linkers are about ten and seven times higher respectively. It is possible the abrasive immobilization of CNTs can roughen the GC electrode which could contribute to the observed AQ current enhancement. Therefore we performed a control experiment by immobilizing the CNTs using wet casting which eliminates any possible roughening effect. For wet immobilized CNTs, Figure 4.5 shows the cyclic voltammetry for different loadings (60 and 30 μg) of CNTs modified with AQ through the $C_6H_4CH_2NH$ linker recorded at 50 mV s^{-1} in 0.1 M phosphate buffer solution at pH 7.

In the case of the wet immobilized CNTs modified using the same conditions we observe a massive enhancement for the AQ redox peak currents. The peak current, depending on the CNTs loading, is up to 60 times higher in comparison with that for the polished GC electrode. In addition the AQ peak current doubles as the loading of modified CNTs increases from 30 to 60 μg. This clearly confirms that the linker and AQ modification process occurs at the CNT surface because the current is directly proportional to the amount of immobilized CNTs. In addition there is no contribution from substrate roughness because of wet casting CNTs immobilization. Table 1 reports the peak separation ($\Delta E = E_{pa} - E_{pc}$), the midpoint potential ($E_{mp} = ((E_{pa} - E_{pc})/2)$), and the surface coverage for AQ attached to CNT surfaces through $C_6H_4CH_2NH$ and EDA linkers using dry abrasive and wet casting immobilization. From the table we can see that there is a no change in the AQ redox potential, E_{mp}, with an average value of −490 ± 5 mV in 0.1 M PBS for the two linkers. On the other hand, the type of immobilization of linker does have a minor effect on the peak separation, ΔE. The EDA linker shows a smaller ΔE which suggests that the electron transfer kinetics is faster through the EDA than the $C_6H_4CH_2NH$ spacer. This result is consistent with that obtained for GC and graphite electrodes modified by AQ using the same methodology in Chapter 3.

The AQ coverage was calculated using the charge by integrating the area under the baseline corrected peaks, with a value of n equals 2 and normalized to the mass of CNTs in grams. The data in Table 4.1 show that the abrasive immobilized CNTs modified with the EDA linker gave a lower AQ surface coverage than for the $C_6H_4CH_2NH$ linker.

Table 4.1 : *AQ separation peak, midpoint potential and surface coverage for CNTs modified electrodes in 0.1 M PBS at the scan rate of 50 mV s^{-1}. Surface coverage is calculated using the estimated mass of immobilized CNTs.*

Linker	Type of immobilization	$\Delta E \pm 5$/ mV	$E_{mp} \pm 5$/ mV vs SCE	$\Gamma \pm 0.05$ (mmol / g)
–EDA–	Dry abrasive	130	-490	0.085
–$C_6H_4CH_2NH$–	Dry abrasive	165	-492	0.115
–$C_6H_4CH_2NH$–	Wet casting	115	-485	0.190

Interestingly this is the opposite of the case for the plain GC electrode where the AQ surface coverage in the case of the EDA-linker was higher than that in the case of the $C_6H_4CH_2NH$ linker. However for abrasive immobilization care should be taken as the mass of CNTs was estimated from the SEM images (about 15 μg) and could vary from one experiment to another. In the case of wet immobilized CNTs, the AQ surface coverage for the $C_6H_4CH_2NH$ linker was 0.190 mmol/g which is higher than that obtained for abrasive immobilized CNTs. This can attributed to the high packing density of the abrasive immobilized CNTs, as shown by SEM characterization, leading to lower porosity than for the wet immobilized CNTs which in turn can account for less surface modification and lower surface coverage. The stability of the AQ modified CNTs was monitored by recording the voltammograms in pH 7 buffer solution on repeated cycling. We find that after 50 cycles there is a slight decrease (3–5%) in the surface coverage as measured from the charge, demonstrating the good stability for this type of CNT modification. In addition there is a small decrease in ΔE (10–15 mV) but no change in the mid-peak potential, E_{mp}.

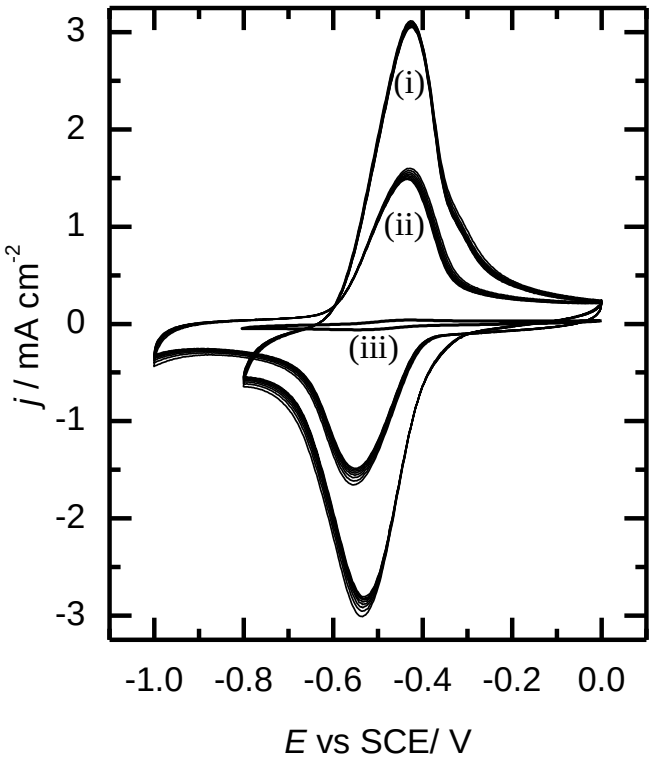

Figure 4.5. *Cyclic voltammograms at 50 mV s^{-1} in 0.1M of PBS at pH 7 for CNTs modified by AQ through $C_6H_4CH_2NH$- linker and immobilized by wet casting (i) 60 g, (ii) 30 µg CNTs and (iii) plane modified GC electrode.*

4.1.3. Effect of pH and Buffer Capacity

The voltammetry of AQ is pH dependent and in acidic solution we observe that E_{mp} is shifted to more positive potential at about −130 mV, while in basic solution E_{mp} is about −775 mV. In addition the value of ΔE is significantly decreased from 310 mV in acidic to 70 mV in basic solution. This demonstrates that the redox reaction of attached anthraquinone becomes more reversible in basic solution. Figure 4.7 show the variation in E_{mp} for the anthraquinone modified CNTs over the pH in range from 1 to 13. Between pH 1 and 10, the mid-peak potential, E_{mp}, shifts linearly to more negative potential with a slope of 59 mV/pH which is equal to the anticipated Nernstian value for a two electron two proton process. Above pH 10 the slope of the midpoint potential vs. pH plot slightly decreases because it becomes a two electron one proton process and this is consistent with the known pK_a of hydroquinone of 9.85.[24] An interesting effect observed for AQ modified CNTs is the change in the redox peak current and ΔE with increasing PBS buffer capacity. Figure 4.6 shows cyclic voltammograms for EDA AQ for abrasive modified CNTs in phosphate buffer solutions at different concentrations and pH 7. On increasing the PBS concentration from

0.01 to 1.0 M we note that the redox peak currents are doubled for the EDA AQ modified CNTs and ΔE decreases from 310 to 140 mV. This effect can be related to the fact that increasing the buffer capacity greatly reduces local pH changes for the porous and high surface area of carbon nanotube. To confirm this effect is due to the increase in buffer capacity and not due to the associated increase in the ionic strength of the solution or IR compensation, we performed a control experiment using the same EDA AQ modified CNTs at a constant buffer capacity of 0.1 M PBS (pH 7) and increased the concentration of KCl in the supporting electrolyte. The resulting cyclic voltammograms (not shown here) showed that the ionic strength of the solution has a significantly smaller effect on ΔE and the faradaic current than the effect observed for changing the buffer capacity. A similar buffer capacity effect has been observed for carbon nanoparticles chemically modified with AQ through a tosylate linker.[19]

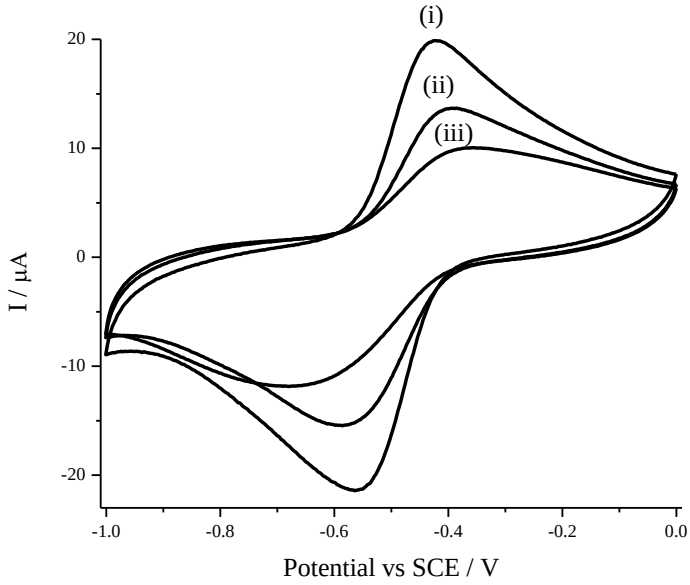

Figure 4.6. *Cyclic voltammograms of AQ-modified MWCNT attached through EDA linker at the different concentration of phosphate buffer (i) 1.0 M, (ii) 0.1 M, (iii) 0.01 M; pH 7 scan rate 50 mV* s^{-1}

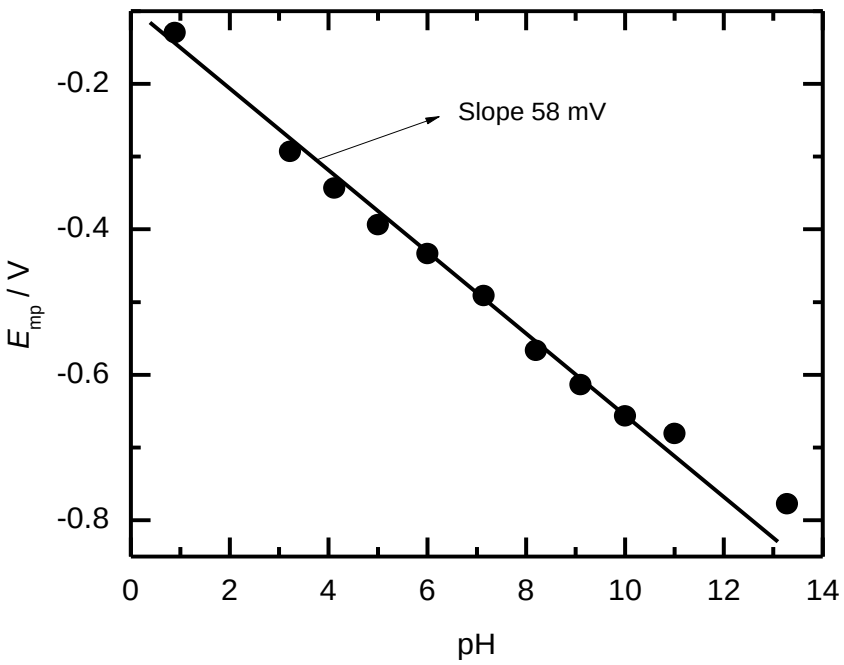

Figure 4.7. *Dependence of the mid-peak potential, E_{mp}, on pH for CNTs modified with $C_6H_4CH_2NH$ AQ.*

4.1.4. Effect of Scan Rate

The effect of scan rate on the electrochemical behavior of AQ modified CNTs is shown in Figure 4.8a As an example of a series of cyclic voltammograms recorded at scan rates from 5 to 600 mV s^{-1} in 0.1 M PBS at pH 7 for CNTs modified with $C_6H_4CH_2NH$ AQ. Fig. 4.8b clearly shows that the anodic and cathodic peak currents increase linearly with scan rate as expected for the surface immobilized AQ redox species.

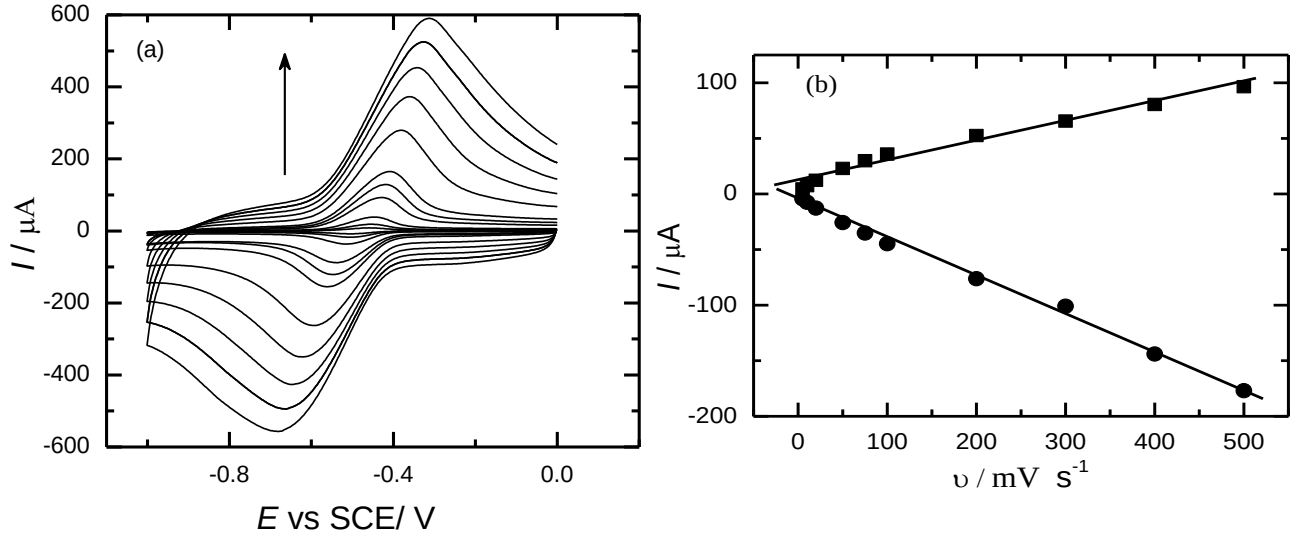

Figure 4.8. *Cyclic voltammograms of CNTs modified with –$C_6H_4CH_2NH$–AQ in 0.1 M pH 7 PBS buffer at scan rates from 5 to 600 mV s^{-1}.*

4.2. Chemical Immobilization of $C_6H_4CH_2NHBoc$ Spacer to CNTs Surface and Blocking Effect

As shown in scheme 4.4, the grafting of $C_6H_4CH_2NHBoc$ to CNT surface was achieved by spontaneous chemical reduction using reflux of the corresponding diazonium salt in acetonitrile at 25 and 60 ^oC overnight.

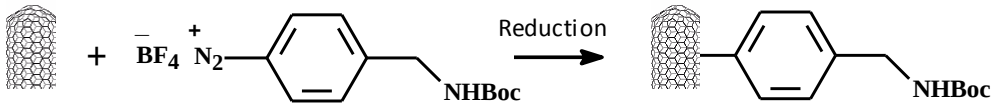

Scheme 4.4. *Spontaneous coupling of $C_6H_4CH_2NHBoc$ linker to CNTs modified electrodes.*

The grafting of the $C_6H_4CH_2NHBoc$ layer to the surface of the CNTs was confirmed by studying the electron transfer blocking effect in aqueous solution containing ferrocyanide $[Fe(CN)_6]^{3-}$. Figure 4.9 shows the cyclic voltammetry for bare CNTs and after the chemical grafting of $C_6H_4CH_2NHBoc$ linker in the presence of 5.0 mM $[Fe(CN)_6]^{3-}$ and 0.1 M KCl.

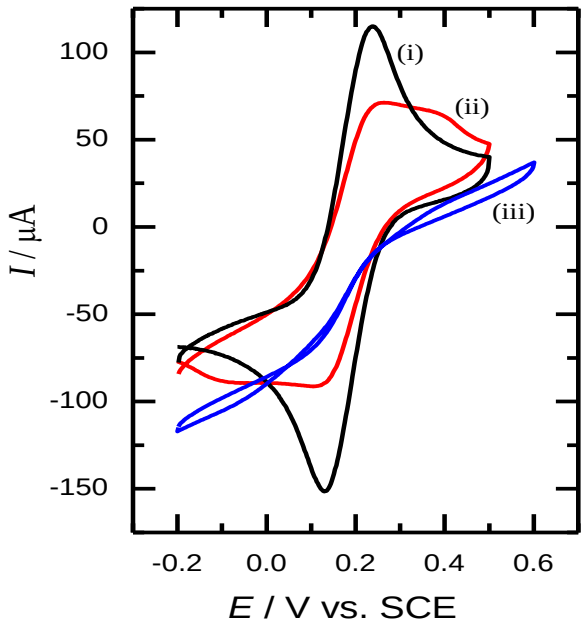

Figure 4.9. *Cyclic voltammetry at 50 mV s^{-1} and in 5.0 mM $[Fe(CN)_6]^{4-}$ and 0.1 M KCl for (i) bare CNTs, (ii) CNTs modified with C6H4CH2NHBoc linker at 25 ^{o}C and (iii) CNTs modified with $C_6H_4CH_2NHBoc$ linker at 60 ^{o}C overnight.*

At bare CNTs, a well-developed cyclic voltammogram is recorded with anodic and cathodic waves at 0.240 and 0.135 V vs. SCE, respectively and the apparent redox potential taken as the average of the anodic and cathodic peaks is 0.185 V. In case of CNTs modified with -$C_6H_4CH_2NHBoc$ linker at 25 ^{o}C, the peak current is partially decreased while in the case of modification at 60 °C (curve iii) the redox peaks are completely disappeared and the voltammogram shows sigmoidal current flow more like microelectrode response. This can be attributed to the reaction of $[Fe(CN)6]^{3-/4-}$ through pinholes at CNT surface or at the underneath GC electrode The inhibition of the $[Fe(CN)_6]^{4-}$/ $[Fe(CN)_6]^{3-}$ redox current indicates that the spontaneous coupling of linker at 60 ^{o}C is more efficient and compact than at 25 ^{o}C. A similar blocking behaviour was observed for glassy carbon electrodes modified by a nitrobenzene layer.[25]

After chemical attachment of the $C_6H_4CH_2NHBoc$ spacer to the CNTs surface, the Boc group was removed by reaction with 4.0 M HCl in dioxane for 4 h. This leaves the CNT surface modified with amine groups which can then be reacted with other functional molecules using solid phase amide coupling. One advantage of this chemical coupling method is the ability to produce large quantities of CNTs modified with $C_6H_4CH_2NH–$ linker for further surface characterization and applications.

The attachment of the $C_6H_4CH_2NH$–Boc linker was also confirmed by FTIR spectroscopy. Figure 4.10 shows the FTIR spectra for 4-(N-Boc-aminomethyl) benzene diazonium tetrafluoroborate salt, CNTs modified with the $C_6H_4CH_2NH$– linker after removal of the Boc group and for AQ attached to the CNT surface through the $C_6H_5CH_2NH$– linker. For CNTs modified with the $C_6H_4CH_2NH$– linker; two peaks located at 3120 and 3070 cm^{-1} are assigned to the N–H stretching mode of primary amines.[26] Strong peaks obtained at 1680 cm^{-1} and 1290 cm^{-1} are assigned to N–H bending and C–N stretching vibrations of the primary amine. Benzene ring C–C stretching at 1600 cm^{-1}, and benzene ring C–H out-of-plane bending at 761 cm^{-1} were also observed.[27] In addition the most significant indication of grafting the $C_6H_4CH_2NH$– linker to the CNTs is the disappearance of the stretching frequency of the (N≡N) group at 2280 cm^{-1} as presented in the FTIR of 4-(N-Boc-aminomethyl) benzene diazonium tetrafluoroborate salt.[28-31]

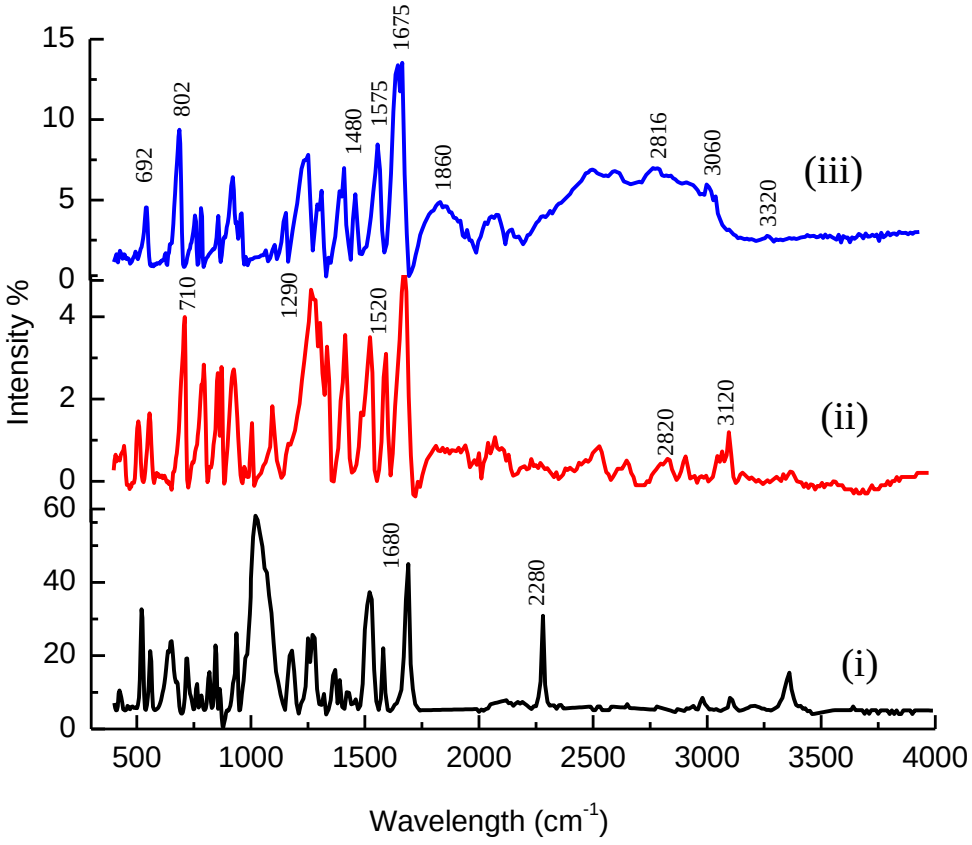

Figure 4.10. *FTIR spectra for (i) 4-(N-Boc-aminomethyl) benzene diazonium tetrafluoroborate salt, (ii) modified CNTs through $C_6H_4CH_2NH$– linker after deprotection and (iii) AQ-modified CNTs through $C_6H_4CH_2NH$– linker.*

The strong peak at 1670 cm^{-1} was assigned to the C=O stretching mode of the quinonyl groups whereas the weaker peaks at 2810 and 3050 cm^{-1} were assigned to the stretching mode of the aromatic ring.[32] Two other distinct bands at 1580 and 1470 cm^{-1} were also observed, related to the (–CONH–), corresponding to the (C=O) stretching band and to the (N-H) bending vibration bands[33], respectively, indicating that an amide bond was formed between AQ-2-carboxylic acid and $C_6H_4CH_2NH$– linker. Characteristic N-H stretching band is located at 3320 cm^{-1}. Out of plane N-H wagging corresponds to 690 and 800 cm^{-1}. On the other peak located at the 1860 cm^{-1} might be assigned to residual carboxylic acid stretch.

4.2.1. Chemical Coupling and Characterization of Anthraquinone (AQ) Modified CNTs

After removal of the Boc group the attachment of AQ to the CNTs surface through the linker was achieved as previously reported in Chapter 3 by reacting amine modified CNTs with anthraquinone 2-carboxylic acid in the presence of HBTU as the coupling reagent. Subsequently, 10 mg of the resulting sample was placed into 5.0 ml of DMF and sonicated for 5 minutes. Figure 4.11 shows photographs for CNTs after grafting the AQ function group through $C_6H_4CH_2NH$– linker in DMF solvent. After modification with AQ we can see that the CNTs are well dispersed in DMF and the resulting suspension seems quite homogenous and stable as no precipitation was observed after 30 days. A similar experiment was also carried out in DMF and ethanol after spontaneous attachment of diazonium linker and after removal of the Boc group; there was no precipitation at all for both solvents.

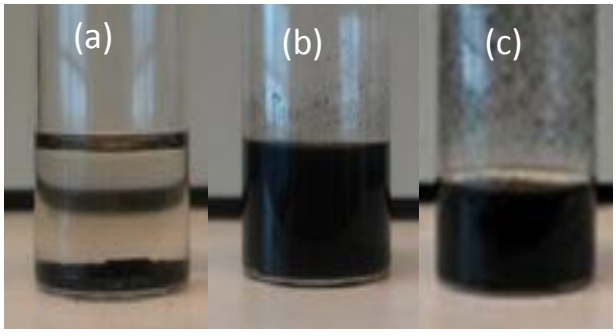

Figure 4.11. *Photographs for CNTs in DMF solvent (a) bare CNTs after 1 day, (b) AQ modified CNTs after 1 day and (c) after 30 days*

For cyclic voltammetry (CV) characterizations, different loadings of the AQ modified CNT dispersion was drop coated on the GC electrode and dried in the air at 25 ^{o}C. Figure 4.12a shows the cyclic voltammetry (20 cycles) at 50 mV s^{-1} in 0.1 M phosphate buffer solution at pH = 7 for a 2 µL deposit of CNTs (equivalent to 4 µg) chemically modified with AQ probe through $C_6H_4CH_2NH$– spacer. The CV clearly shows the presence of AQ reversible redox peaks located at a formal potential of 480 mV (±10 mV) vs SCE and with a peak separation of 70 mV (±5 mV). The CV is reproducible and is stable for more than 100 cycles which indicates high stability of the covalent bond between the CNTs and the AQ.

The effect of scan rate on the electrochemical behavior of CNTs chemically modified with AQ was studied to investigate the heterogeneous electron-transfer kinetics. Figure 4.12b clearly shows that the anodic and cathodic peak currents increase linearly with scan rate which is consistent with the surface immobilization of the AQ redox probe as shown in Chapter 3. The Laviron analysis was applied to find rate constant as previously described in Chapter 3. It was then found to be 10.25 s^{-1} (±0.04), which is higher than edge plane, GC and basal plane modified AQ through same linker, already expected because CNT is known to exhibit faster electron transfer kinetics.

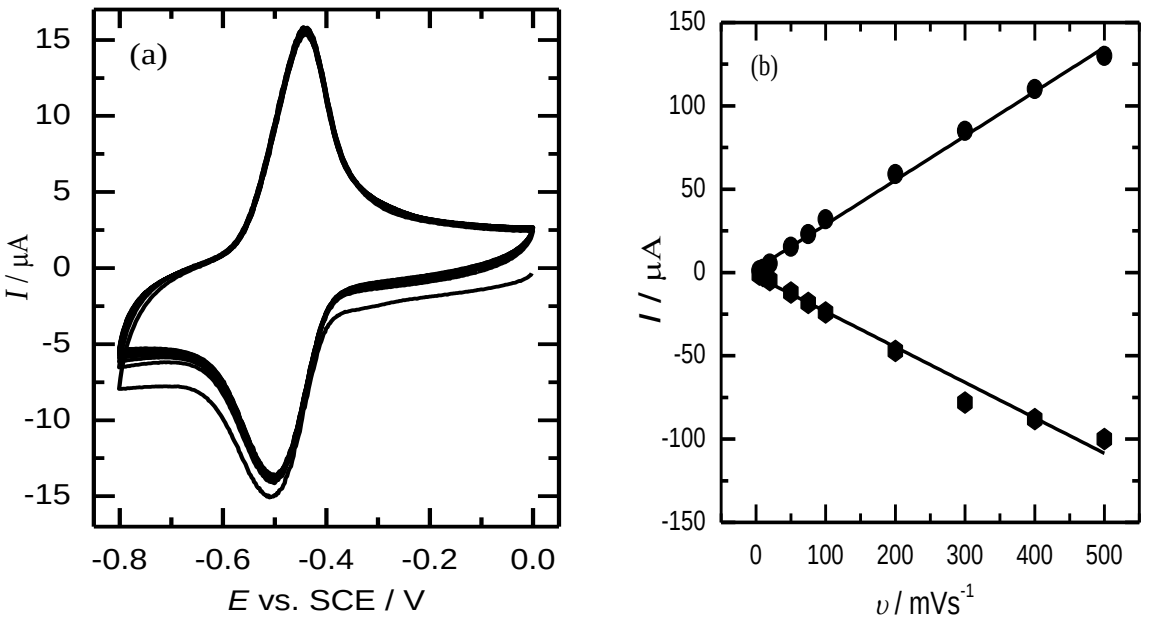

Figure 4.12. *(a) Cyclic voltammograms at 50 mV s^{-1} in 0.1 M of PBS at pH = 7 for CNTs chemically modified with AQ through $C_6H_4CH_2NH$- linker (deposit of 2 µL dispersion equivalent to 4 µg modified CNTs on 5 mm diameter GC electrode), (b) Relation between peaks current scan rate for 2 µL deposit of CNTs modified by $C_6H_4CH_2NH$–AQ.*

Figure 4.13 shows the cyclic voltammetry at 50 mV s^{-1} in 0.1 M phosphate buffer solution at pH = 7 for different loadings of AQ modified CNTs. The results shows that the redox peak current for oxidation of reduction for immobilized AQ are linearly increased by increasing loading of modified CNTs on the GC surface which confirms the attachments of AQ probe. In addition the redox peaks current is linearly increased with increasing the loading of modified CNTs as shown in Figure 4.13b. It is also apparent that the redox peak separation ΔE increases as the loading of modified CNTs increases. This effect was previously described for high surface area CNTs and carbon nanoparticles modified with AQ[19,34] and it arises because of local pH changes at the electrode surface when the buffer capacity of the solution is insufficient to compensate for the protons released/consumed in the redox reaction. Therefore it is worth investigating the effect of the ionic strength. As demonstrated in the figure 4.14 as the concentration of KCl an increase there is a decrease in the peak separation. The AQ surface coverage normalized to CNTs weight was estimated using the charge obtained by integrating the area under the baseline corrected peaks and was found to be around 0.210 (±0.01) mmol / g.

The AQ surface coverage achieved is slightly higher than that previously obtained (0.190 mmol / g) when the $C_6H_4CH_2NH–$ spacer was immobilized onto the CNT surface by electrochemical reduction of the linker diazonium salt. This indicates that spontenous chemical coupling of the $C_6H_4CH_2NH–$Boc linker achieved here is even more efficient than the electrochemical attachment.

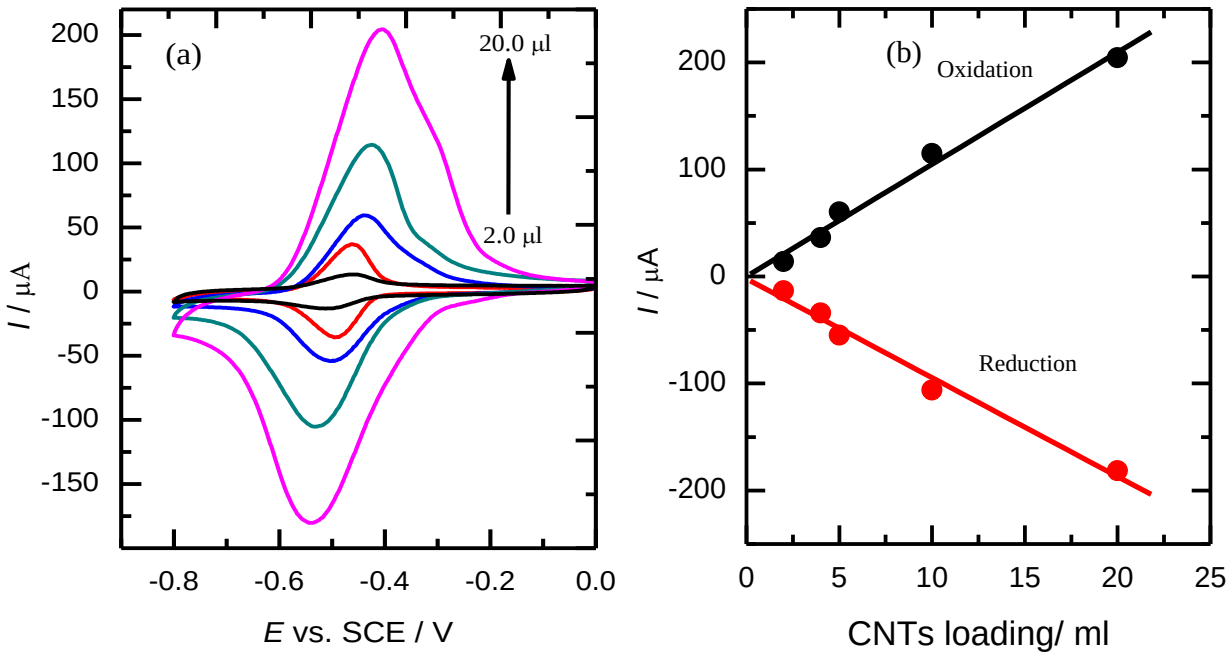

Figure 4.13. *(a) Cyclic voltammograms for the reduction of AQ modified CNTs through –$C_6H_4CH_2NH$– linker in 0.1 M phosphate buffer pH = 7, deposits of 2, 4, 5, 10 and 20 µL dispersion, (b) plot for AQ modified CNTs loading and peaks current.*

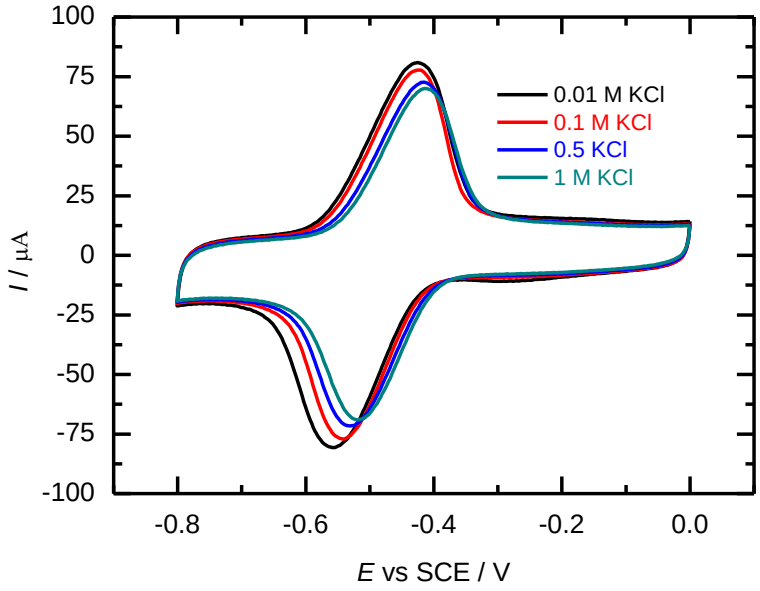

Figure 4.14. *The effect of ionic strength using different concentration of KCl for the 10 µL of dispersion in 0.1 M phosphate buffer pH =7 at the scan rate of 50 mV s^{-1}.*

4.2.2. Chemical Coupling and Characterization of Nitrobenzene (NB)

The coupling of NB to CNTs through the chemically immobilized $C_6H_4CH_2NH$- linker was achieved as reported earlier in Chapter 3 by treating the linker modified CNTs in 4-nitrobenzoyl chloride in a pyridine/dichloromethane mixture. Figure 4.15 illustrates the cyclic voltammograms recorded at 50 mV s^{-1} in PBS, pH 7, for 20 µl loading of the modified CNTs. For the cathodic scan, the voltammogram show a large irreversible reduction peak I at about -600 mV. On the reverse scan, a redox process peak II/III is observed at about -48 mV. This electrochemical behaviour of immobilized nitrobenzene is quite similar to the behaviour obtained previously at carbon electrodes and fully discussed in Chapter 3. Moreover, the redox peaks current is linearly increased with increasing the amount of NB modified CNTs as shown in Figure 4.15b, which clearly confirms the attachment of the NB to the CNTs through the $-NHCH_2C_6H_4$ linker. The surface coverage of NB at CNTs calculated by combining the charge at peak I and peak II/III as previously described[35] is equal to 0.20 (±0.01) mmol/g which is consistent with the AQ surface coverage obtained above.

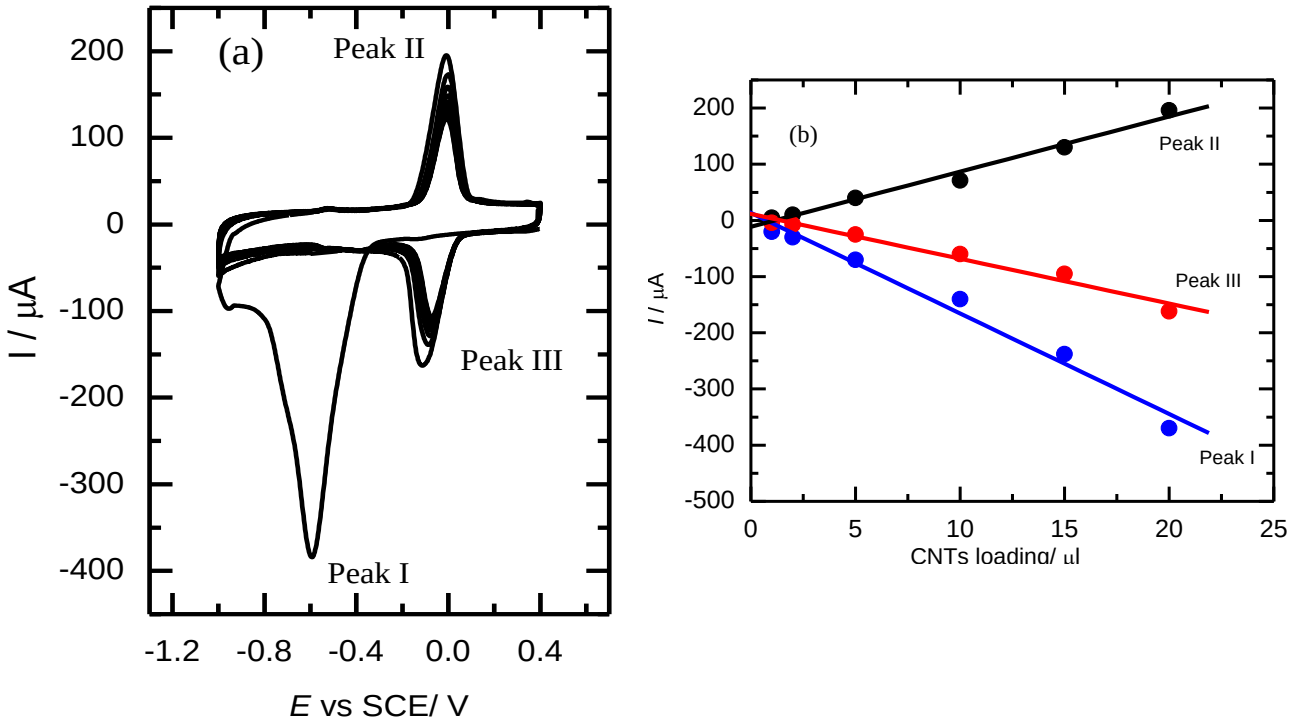

Figure 4.15. *(a) Cyclic voltammograms recorded at 50 mV s^{-1} in 0.1 M PBS, pH 7, for 30 µl CNTs chemically modified by nitrobenzene through $C_6H_5CH_2NH$- linker, (b) plot for NB modified CNTs loading and peaks current.*

4.3. Conclusion

This work has shown that the previously reported electrochemical and solid-phase modification methodologies[36-38] developed on glassy carbon electrodes can be applied to multiwall carbon nanotubes immobilized by dry abrasive or wetcasting processes on GC substrates. We have shown that anthraquinone can be attached to the CNTs by either a benzyl amine ($C_6H_4CH_2NH$) or ethylenediamine (EDA) linker using either the diazonium reduction or amine oxidation routes followed by deprotection of the amine and subsequent amide bond formation using conventional solid phase coupling chemistry. The AQ modified CNTs were fully characterized using cyclic voltammetry. We find that for wet casting immobilization the AQ surface coverage is directly proportional to the amount of immobilized CNTs and up to 0.190 mmol/g AQ surface coverage has been achieved. Our modification procedure, combining electrochemical grafting of a Boc protected amine, deprotection and then amide coupling, constitutes a robust and versatile method for the modification of multiwall CNTs with a wider range of molecular structures.

We also demonstrate that Boc-aminomethyl benzene ($-C_6H_4CH_2NHBoc$) linker can be spontaneously grafted to the CNTs surface by refluxing its diazonium salt at 60 ^oC in acetonitrile solution. Subsequent to the Boc-deprotection, anthraquinone and nitrobenzene groups were attached to the CNTs through benzyl amine linker by solid-phase amide coupling. The AQ and NB modified CNTs were fully characterized using cyclic voltammetry and FTIR. The surface coverage of AQ and NB functional groups reaches up to 0.20 mmol/ g and the redox current is directly proportional to the loading of modified CNTs. This spontaneous Boc-aminomethyl benzene grafting and solid phase functional groups coupling constitute a robust and versatile method for the modification and mass production of carbon based materials with a wide range of molecular architectures for catalysis, drug delivery, water purification, biosensors and combinatorial chemistry applications.

4.4. References

(1) D. S. Bethune; C. H. Klang; M. S. De Vries; G. Gorman; R. Savoy; J. Vazquez; R. Beyers, *Nature* **1993**, *363*, 605.

(2) S. Lijima, *Nature* **1991**, *354*, 56.

(3) S. Lijima; T. Ichihashi, *Nature* **1993**, *363*, 603.

(4) B. I. Kharisov; O. V. Kharissov; H. L. Gutierrez; U. O. Mèndez, Ind *Eng. Chem. Res.* **2009**, *48* 572.

(5) H. Paloniemi; T. Ääritalo; T. Laiho; H. Liuke; N. Kocharova; K. Haapakka; F. Terzi; J. Lukkari, *J. Phys. Chem. B* **2005**, *109*, 8634.

(6) N. Karousis; N. Tagmatarchis, *Chem. Rev*. **2010**, *110*, 5366.

(7) J. Chen; M. A. Hamon; H. Hu; Y. Chen; A. M. Rao; P. C. Eklund; R. C. Haddon, *Science* **1998**, *282* 95.

(8) J. L. Bahr; J. M. Tour, *J. Mater. Chem*. **2002**, *12*, 1952.

(9) S. Banerjee; T. H. Benny; S. S. Wong, *Adv. Mater.* **2005**, *17* 17.

(10) W. Xia; C. Jin; S. Kundu; M. Muhler, *Carbon* **2009**, *47*, 919.

(11) J. L. Bahr; J. Yang; D.V. Kosynkin; M. J. Bronikowski; R. E. Smalley; J. M. Tour, *J. Am. Chem. Soc.* **2001**, *123* 6536.

(12) K. Sadowska; K. P. Roberts; R. Wiser; J. F. Biernat; E. Jabłonowska; R. Bilewicz, *Carbon* **2009**, *47*, 1501.

(13) P. Abiman; G. G. Wildgoose; R. G. Compton, *Int. J. Electrochem. Sci.* **2008**, *3*, 104.

(14) P. R. Marcoux; P. Hapiot; P. Batail; J. Pinson, *N. J. Chem*. **2004**, *28*, 302.

(15) A. J. Downard *Electroanalysis,* **2000**, *12* 1085.

(16) B. Barbier; J. Pinson; G. Desarmot; M. Sanchez, *J. Electrochem. Soc.* **1990**, *137*, 1757.

(17) G. G. Wildgoose; M. Pandurangappa; N. S. Lawrence; L. Jiang; T. G. J. Jones; R. G. Compton, *Talanta* **2003**, *60*, 887.

(18) V. G. H. Lafitte; W. X. Wang; A. S. Yashina; N. S. Lawrence, *Electrochem. Commun.* **2008**, *10*, 1831.

(19) J. D. Watkins; K. Lawrence; J. E. Taylor; T. D. James; S. D. Bull; F. Marken, *Electroanalysis* **2010**, *23*, 1320.

(20) A. Salimi; C. E. Banks; R. G. Compton, *Analyst* **2004**, *129* 225.

(21) C. E. Banks; R. G. Compton, *Analyst* **2006**, *131*, 15.

(22) R. R. Moore; C. E. Banks; R. G. Compton, *Anal. Chem*. **2004**, *76* 2677.

(23) C. E. Banks; T. J. Davies; G. G. Wildgoose; R. G. Compton, *Chem*. *Commun*. **2005**, 829.

(24) A. H. Holm; K. H. Vase; B. W. Jensen; S. U. Pedersen; K. Daasbjerg, *Electrochim*. *Acta* **2007**, *53*, 1680.

(25) B. Ortiz; C. Saby; G. Y. Champagne; D. Be´langer, *J. Electroanal. Chem*. **1998**, *455*, 75.

(26) R. M. Silverstein; F. X. Webster; D. J. Kiemle, *The Spectrometric Identification of Organic Compounds*; John Wiley & Sons: New York, 2005.

(27) G. Giambastini; S. Cichi; A. Giannncsi; L. Lucani; A. Rossin; F. Mercuri; C. Bianchini; Brandi, A.; M. Melucci; G. Ghini; P. Stagnara; L. Conzatti; E. Passaglia; M. Zappi; T. Mantini; Farnasiera, P. *Chemistry of Materials* **2011**, *23*, 1923.

(28) C. Saby; Ortiz;, B.; G. Y. Champagne; D. Belanger, *Langmuir* **1997**, *13*, 6805.

(29) M. Pandurangappa; T. Ramakrishnappa, *Mater. Chem. Phys.* **2010**, *122*, 567.

(30) M. Pandurangappa; T. Ramakrishnappa; R. G. Compton, *Int. J. Electrochem. Sci.* **2008** 1218.

(31) M. Pandurangappa; T. Ramakrishnappa; R. G. Compton, *Carbon* **2009**, *47*, 2186.

(32) A. S. Kumar; P. Swetha, *Colloids and Surface A: Physicochem. Eng. Aspects* **2011**, *384*, 597.

(33) N. Follain; S. Montanari; I. Jeacomine; S. Gambarelli; M. R. Vignon, *Carbohydrate Polymers* **2008**, *74*, 333.

(34) M. A. Ghanem; I. Kocak; A. Al-Mayouf; M. AlHoshan; P. N. Bartlett, *Electrochim*. *Acta* **2012**, *68*, 74.

(35) M. A. Ghanem; J. M. Chrétien; J. D. Kilburn; P. N. Bartlett, *J. Mater. Chem*. **2008**, *18* 4917.

(36) J. M. Chrétien; M. A. Ghanem; P. N. Bartlett; J. D. Kilburn, *Chem.Eur. J*. **2008**, *14*, 2548.

(37) M. A. Ghanem; J-M. Chrétien; J. D. Kilburn; P. N. Bartlett, *Bioelectrochemistry* **2009**, *76*, 115.

(38) J. M. Chrétien; M. A. Ghanem; P. N. Bartlett; J. D. Kilburn, *Chem. Eur. J*. **2009**, *15*, 11928.

Chapter 5

OXYGEN REDUCTION STUDIES ON CARBON ELECTRODES

5.1. Overview

It is well known that carbon electrode surfaces can possess a range of functional groups; for instance, carboxyl, phenolic, hydroxyl and quinone derivatives,[1] depending on the pre-treatment and history of the electrode. However, the precise nature of the functional groups that actually participate in the oxygen reduction reaction is unclear. It has been suggested that surface quinone functional groups are involved[2] because the electrocatalytic activity is enhanced by increasing the quinone surface coverage.[3] Considerable experimental[4] and theoretical effort[5,6] has been expended to examine the mediation of oxygen reduction by anthraquinone and to identify the rate-determining step on unmodified and quinone-modified carbon electrodes.[2] In this chapter, a linker, -$C_6H_4CH_2NH$–Boc, bearing a protected amine group was electrochemically immobilised to glassy carbon (GC) and edge plane (EP) and basal plane (BP) HOPG electrodes by means of the electrochemical reduction of the corresponding diazonium salt. Following de-protection, anthraquinone-2-carboxylic acid was coupled to the linker using solid-phase chemistry. The surface coverage and stability of the immobilised anthraquinone redox centres was investigated by using cyclic voltammetry together with the effect of pH. The electrocatalytic activity of the different anthraquinone-modified electrodestowards O_2 reduction was studied by cyclic voltammetry at stationary and rotating disc electrodes. Oxygen reduction was also evaluated for laccase-modified electrodes. Laccase is a multicopper oxidase that drives a four electron reduction of O_2 to H_2O, immobilized onto anthraquinone and anthracene, and attached to a GC electrode's surface through EDA and -$C_6H_4CH_2NH$– linkers. O_2 reduction reactions are carried out at laccase immobilized electrodes with high-throughput screening using a multichannel potentiostat for twelve electrodes. In this work, *Trametes hirsuta* laccase (*ThL*) was used.

5.2. Modification of Graphite Electrodes

In this chapter, we will not discuss the details of the electrografting of -$C_6H_4CH_2NH$- , the coupling of AQ to the modified graphite electrodes, and reasons behind why the ratio of edge sites on the graphite electrodes increases, the diazonium coupling at these electrodes takes place more efficiently, and why the surface coverage and electron transfer kinetics are affected, since this subject was discussed in Chapter 3 in depth. Hence, we will commence this chapter by presenting Figure 5.1 which demonstrates CVs for the AQ-modified edge

plane, basal plane, and GC electrodes. Table 5.1 reports the peak separation, mid-peak potential and surface coverage for modified edge plane, glassy carbon and basal plane electrodes in 0.1 M acetate buffer, with pH 5, at 50 mV s^{-1}.

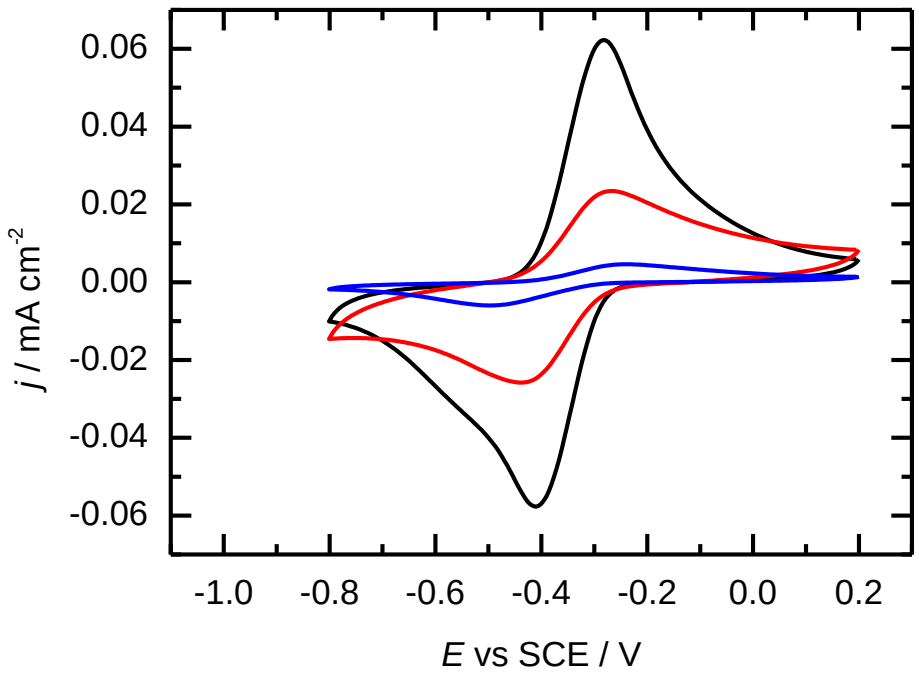

Figure 5.1. *Cyclic voltammograms recorded at 50 mV s^{-1} in 0.1 M of acetate buffer, pH 5, for edge plane (black), basal plane (blue) and glassy carbon (red) electrodes modified by anthraquinone through the $C_6H_4CH_2NH$- linker.*

All three voltammograms show redox peaks for the immobilized anthraquinone. The surface coverage was obtained by the integration of the charge under the redox peaks as reported in our previous work.[7] In order to test its reproducibility, the surface modification was repeated three times for each electrode type. As seen in the Table, the results are quite reproducible. In all cases, the mid-peak potentials, E_{mp}, are almost identical within experimental error, indicating that the nature of the carbon electrode material does not have a significant effect on the redox potential of the attached anthraquinone group.

Table 5.1. Peak separation, ΔE, mid-peak potential, E_{mp}, surface coverage, Γ, and charge, Q, for modified edge plain, glassy carbon and basal plane electrodes in 0.1 M acetate buffer pH 5 at 50 mV s^{-1}.

Carbon Electrode	ΔE / mV (±5 mV)	E_{mp} *vs.* SCE / mV (±5 mV)	Γ_{AQ} / nmol cm^{-2}	Q / mC
EP	157	353	1.180 (±0.21)	0.23
GC	173	340	0.620 (±0.09)	0.12
BP	320	350	0.145 (±0.01)	0.028

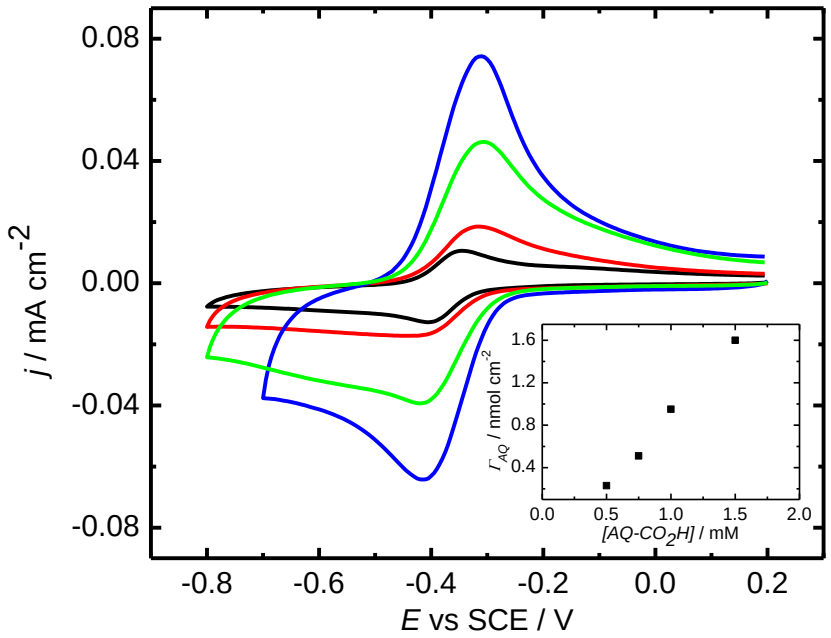

Figure 5.2. *Cyclic voltammograms for anthraquinone-modified edge plane electrodes recorded at 50 mV s^{-1} in 0.1 M of acetate buffer, pH 5. Blue, green, red and black lines represent voltammograms of anthraquinone-modified edge plane electrodes prepared using 1.5, 1.0, 0.75 and 0.5 M AQ-COOH in the reaction solution, respectively. The inset shows a plot of the surface coverage of anthraquinone as a function of the AQ-COOH concentration.*

An advantage of our modification methodology is the ability to control the surface coverage of the anthraquinone attached to the electrode surface through the linker by using solid phase synthesis methodology.[8] Below, we use this to investigate the effect of anthraquinone coverage on the O_2 reduction reaction. Figure 5.2 shows voltammograms for a set of edge plane electrodes modified with anthraquinone using different concentrations of anthraquinone-2-carboxylic acid in the reaction solution with 1.2 mM HBTU and 4.2 mM DIEA. From this Figure, we can see that changing the concentration of anthraquinone-2-carboxylic acid in the coupling reaction allows us to vary the surface coverage of

anthraquinone. In addition, it is clear from Figure 5.2 that the peak position and peak separation for the anthraquinone redox couple at the modified edge plane electrode does not change significantly with coverage, indicating that the differences in peak separation between the three types of carbon electrode seen in Figure 5.1 do not arise because of the differences in surface coverage and, therefore, this presumably reflects the differences in the electron transfer kinetics of the different carbon surfaces consistent with McCreery's results for solution redox couples.[9]

5.2.1. Oxygen Reduction at Anthraquinone-Modified Carbon Electrodes

It is well established that electrocatalytic reduction of O_2 can take place at anthraquinone-modified carbon electrodes.[10] Figure. 5.3 shows cyclic voltammograms at 50 mV s^{-1} for the reduction of O_2 at bare and AQ-$NHCH_2C_6H_4$- modified basal plane, glassy carbon and edge plane electrodes in pH 5 acetate buffer. In the presence of O_2, the voltammograms show an irreversible oxygen reduction peak at the bare electrodes whereas for the anthraquinone-modified electrodes the oxygen reduction peak currents are significantly larger and peak potentials are shifted to more positive values in each case. In addition the corresponding anodic peak for anthraquinone oxidation at around -0.35 V is either small (in the case of the edge plane) or absent (in the case of glassy carbon and basal plane) consistent with the catalytic reduction of O_2 by reduced anthraquinone at the modified electrode. Comparing the three bare electrodes it is clear that that the edge plane and glassy carbon electrodes behave rather similarly and that they are significantly better than the basal plane electrode for oxygen reduction. In all cases attachment of anthraquinone significantly improves in oxygen reduction kinetics, with the best results (lowest overpotential and largest peak current) being obtained for the modified edge plane electrode. For the anthraquinone-modified edge plane electrode there is evidence for the anodic peak for anthraquinone reduction on the reverse scan. This is probably because the coverage of anthraquinone is highest for this electrode (Table 5.1). For the anthraquinone-modified basal plane electrode, which has the lowest coverage, there is a slight shoulder on the cathodic scan at around -0.45 V before the peak at -0.6 V. We return to this point below.

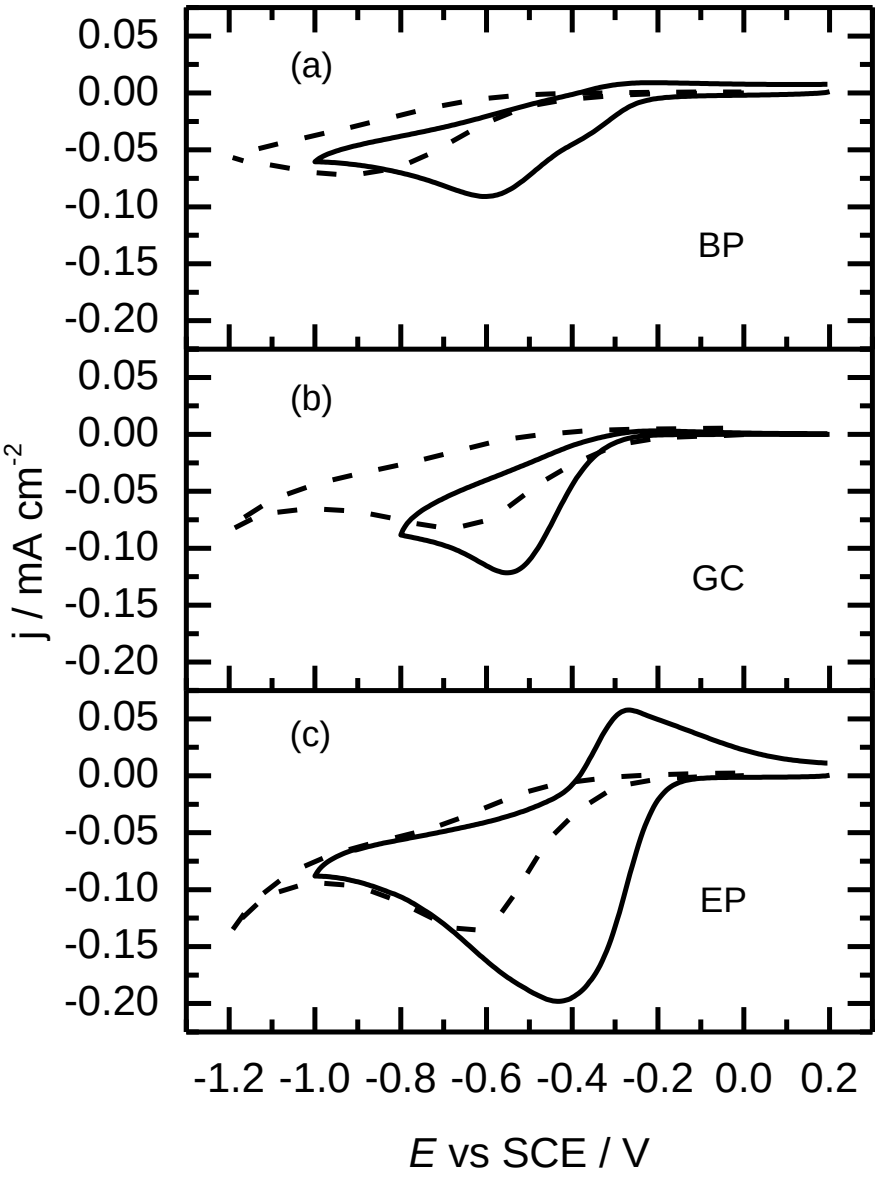

Figure 5.3. *Cyclic voltammograms recorded at 50 mV s^{-1} for O_2 reduction in oxygen saturated 0.1 M pH 5 acetate buffer at (a) basal plane (0.2 cm^2), (b) glassy carbon (0.196 cm^2) and (c) edge plane (0.25 cm^2) (dashed line) unmodified and (solid line) anthraquinone.*

The reduction of O_2 at anthraquinone-modified carbon electrodes has been shown to proceed through the reaction of the oxygen with the anthrasemiquinone radical anion[11]

$$Q + e^- \rightarrow Q^{\bullet -} \quad (1)$$

$$Q^{\bullet -} + O_2 \rightarrow O_2^{\bullet -} + Q \quad (2)$$

where Q represents the anthraquinone species. The superoxide anion then disproportionates

$$2O_2^{\bullet-} + H_2O \rightarrow O_2 + HO_2^- + OH^- \quad (3)$$

or undergoes further reduction to H_2O_2

$$O_2^{\bullet-} + H_2O + e^- \rightarrow HO_2^- + OH^- \quad (4).$$

Reaction (2) is regarded as the rate-determining step and, the overall rate is determined by the concentration of $Q^{\bullet-}$. Reactions (3) and (4) are considered to be fast and to lead to the generation of H_2O_2.

5.2.2. The Effect of Oxygen Concentration and Surface Coverage of AQ on Oxygen Reduction

The effect of oxygen concentration on the reduction at the anthraquinone-modified edge plane electrode was further investigated by cyclic voltammetry. The experiments were performed by sparging the solution with mixtures of argon and oxygen prepared using a mass flow controller. Figure 5.4.a shows a set of voltammograms at different O_2 concentrations for an anthraquinone-modified edge plane electrode in 0.1 M pH 5 acetate buffer. As seen in the figure, the cathodic peak current clearly increases as the concentration of O_2 increases and there is a slight, corresponding decrease in the anodic peak current. The variation of the peak current with oxygen concentration, Figure 5.4.b, is close to linear, with some slight falling away at high oxygen concentrations.

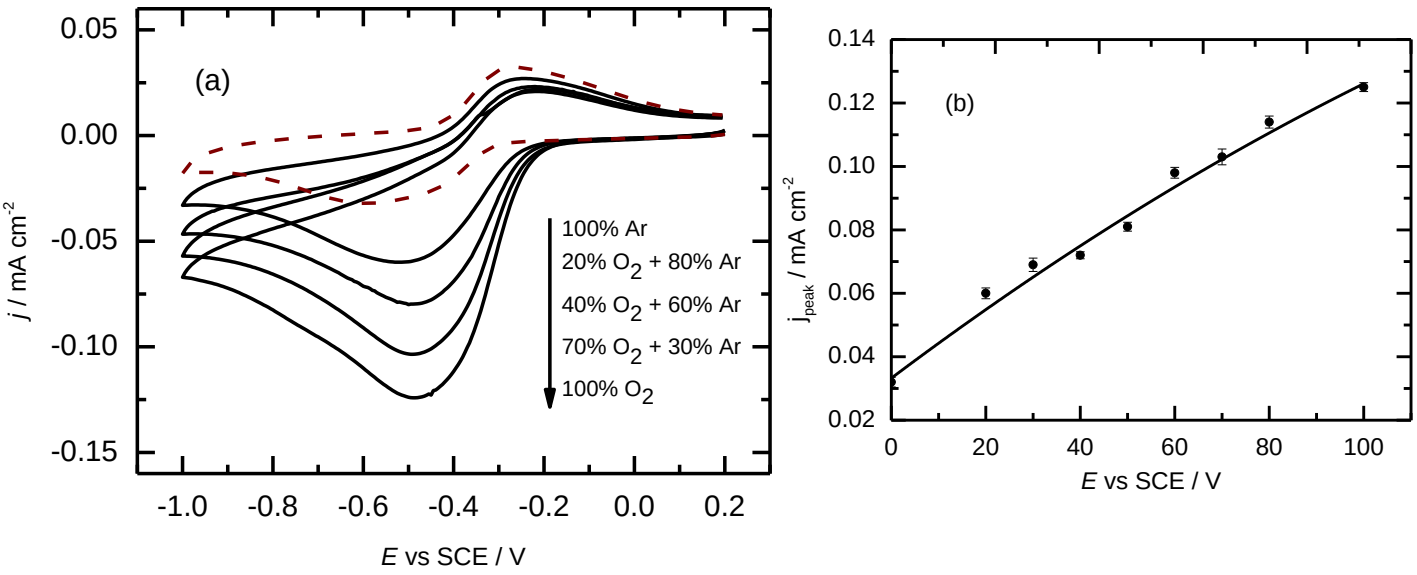

Figure 5.4. *(a) Voltammograms recorded at 50 mV s^{-1} for an anthraquinone-modified edge plane electrode (Γ = 0.980 nmol cm^{-2}) at different O_2 concentrations in 0.1 M pH 5 acetate buffer. (b) Plot of the peak current density against the O_2 saturation.*

We have also investigated the effect of surface coverage. Figure 5.5 shows the influence of the anthraquinone surface coverage at the edge plane electrode surface during the O_2 reduction reaction. As the surface coverage increases, the oxygen reduction peak shifts to more positive potentials and the peak current increases. In addition, for the highest coverages, Fig. 5.4.c and d, there is a clear anodic peak for the oxidation of anthraquinone on the reverse scan. This is because, as the anthraquinone coverage increases, there are more sites at the surface to catalyse an oxygen reduction and the peak potential approaches the anthraquinone redox potential. If we look at the voltammogram for the lowest surface coverage, Figure 5.5.a, we can see that, in the presence of oxygen, there is a shoulder at about -0.4 V, corresponding to the reduction of oxygen catalysed by anthraquinone, before the peak at -0.6 V, corresponding to the reduction of oxygen on the carbon surface itself, and that there is no corresponding anodic peak. Comparing this voltammogram to that for the modified basal plane electrode in Figure 5.3, which has a comparable surface coverage (i.e. 0.145, as compared to 0.230 nmol cm^{-2}), we see that the two are in fact very similar, indicating that the differences between the three electrode types of modified electrode, basal plane, glassy carbon and edge plane, for oxygen reduction in Figure 5.5 are primarily accounted for by differences in the anthraquinone surface coverage rather than differences in the underlying carbon surface.

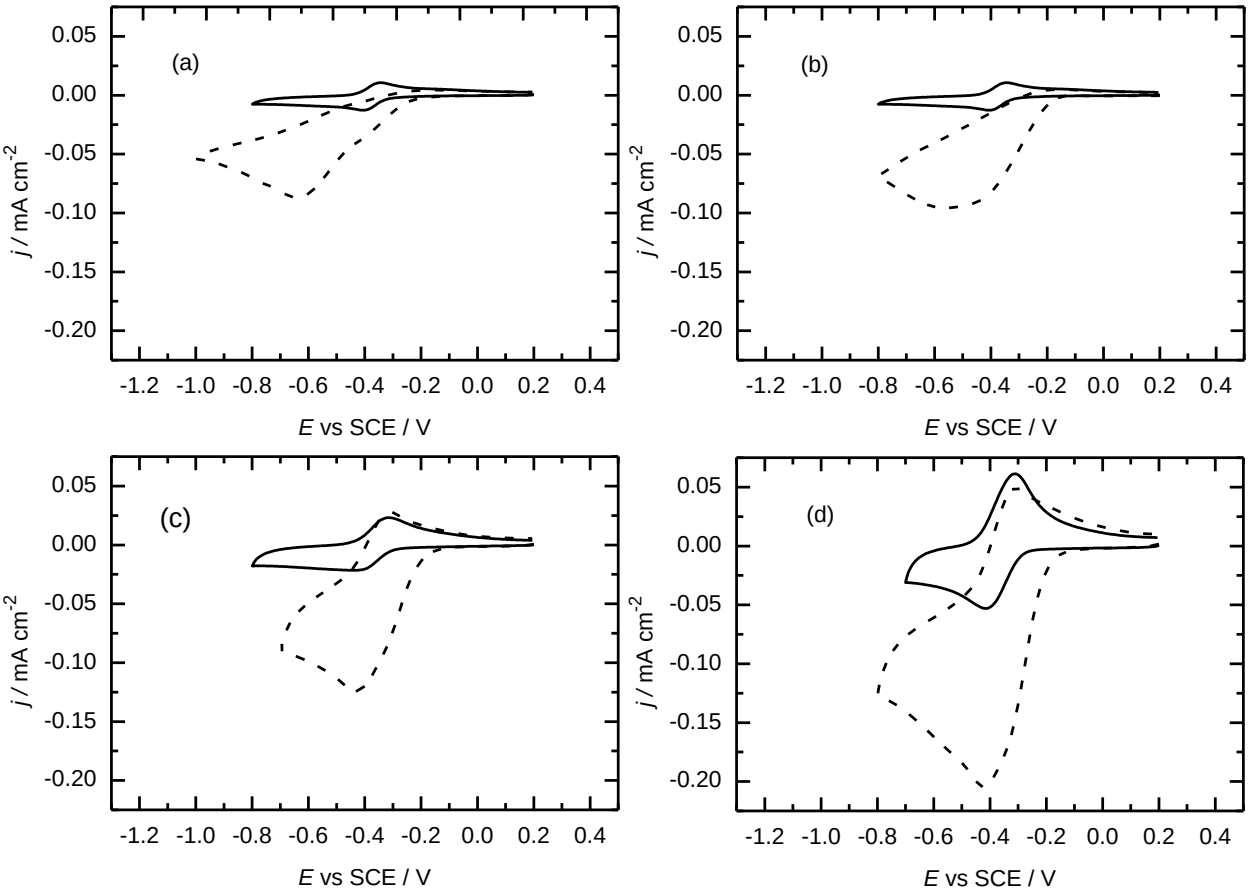

Figure 5.5. *Cyclic voltammograms recorded at 50 mV s^{-1} in 0.1 M acetate buffer, pH 5, for edge plane electrodes modified with anthraquinone for four different anthraquinone surface coverages, Γ_{AQ}, (a) 0.220, (b) 0.510, (c) 0.950, (d) 1.60 nmol cm^{-2}. Solid and dashed lines represent oxygen-free and saturated voltammograms, respectively.*

5.2.3. Oxygen Reduction Study on Unmodified and AQ-modified Carbon Nanotubes

Due to its exceptional and fascinating structural and electronic properties and mechanical strength, carbon nanotubes have attracted a great deal of interest for their nano-technological and material science applications. As we demonstrated in Chapter 3, electron kinetics at edge plane are much faster than at the basal plane and small amounts of edge defects on the basal plane make a significant difference to the electroactivity of the corresponding electrode.[12,13] As mentioned in Chapter 1, the ends of carbon nanotubes are regarded as edge sites while the walls are basal site. It is therefore worth investigating how carbon nanotubes are capable of enhancing the electrocatalytic effect for the oxygen reduction reaction. Furthermore, it was shown that the attachment of organic groups like

quinone derivatives that have catalytic effects to O_2 reduction have an advantage of reducing the large over potential. Hence, we decided to explore the oxygen reduction at chemically AQ-modified MWCNT as described in chapter 4. As given in Chapter 4, the spontaneous attachment of 4-(N-Boc-aminomethyl) benzene diazonium tetrafluoroborate salt to multi-walled carbon nanotube was achieved by mixing 0.1 g of MWCNT with 10 mM of diazonium salt containing 0.1 M TBATFB in ACN. The solution was constantly stirred for one hour at room temperature. Subsequent to the spontaneous attachment of the linker, the sample was dried in the oven. After the removal of the Boc group was carried out in 4 M of HCl in dioxane, the sample was washed with distilled water to remove acid and salt, ethanol and ACN, respectively. The coupling of AQ to MWCNT modified by the $C_6H_4CH_2NH$– linker was achieved by following solid-phase synthetic methodologies. De-protected modified MWCNT was reacted to with AQ-2-carboxylic acid in DMF in the presence of HBTU and DIEA at room temperature for sixteen hours. The sample was then thoroughly washed with water, ethanol and ACN, respectively. After the coupling of AQ to the modified MWCNT through the $C_6H_4CH_2NH$–, 10 mg of sample was placed into 5 ml of DMF and sonicated for five minutes. 2 μL of the dispersion was then deposited on the GC electrode and dried in air. The electrochemical characterization of MWCNT modified with AQ was carried out using cyclic voltammetry. Figure 5.6 shows the cyclic voltammetry (obtained after 20 cycles) at 50 mV s^{-1} in 0.1 M acetate buffer solution at pH 5 for CNT electrodes modified with an AQ probe through $C_6H_4CH_2NH$– spacer in the absence and presence of oxygen.

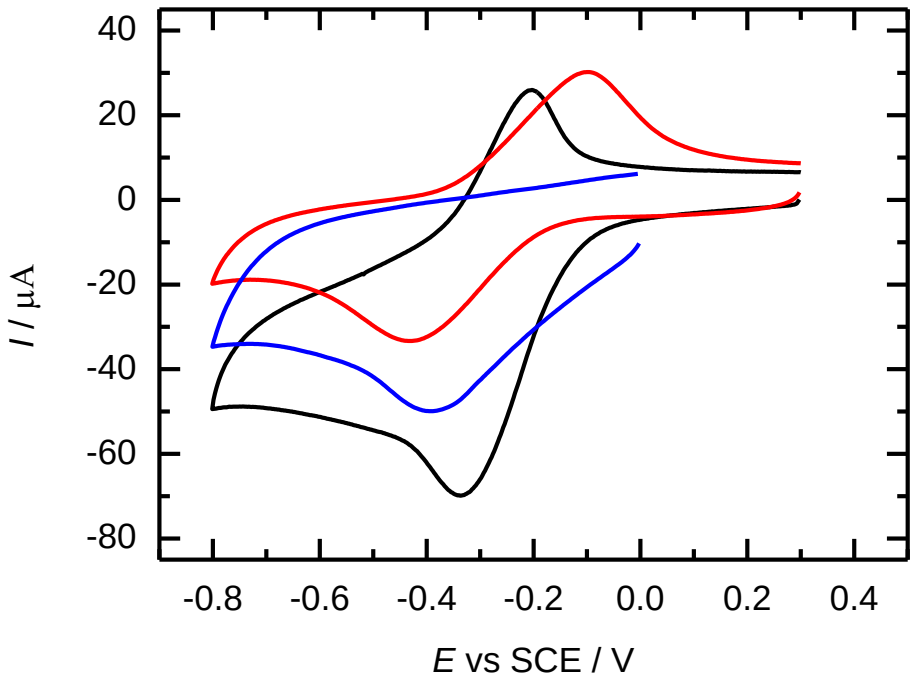

Figure 5.6. *Cyclic voltammogram of abrasively immobilised AQ-modified MWCNT through diazonium linker on GC at the scan rate of 50 mV* s^{-1} *in acetate buffer at pH 5 (red line). The blue represent the voltammogram for bare MWCNT in the presence of* O_2 *and black line is the voltammogram obtained after 20 cycles for AQ-modified MWCNT in* O_2 *free buffer solution.*

In comparison to graphite electrodes with basal and edge plane orientation or glassy carbon electrodes, bamboo multi-walled carbon nanotubes are known to have a high surface area and a high density of edge-like defects along the axis of the tube. These unique structural attributes of the MWCNT are consistent with our results as the high-density covalent attachment of AQ through $C_6H_4CH_2NH$– was accomplished. Furthermore, the oxygen reduction reaction for the AQ-modified MWCNT occurs at an over-potential of 330 mV, which is less negative by 65 mV than plain MWCNT and also AQ-modified basal plane and edge plane and GC electrodes, respectively. This can also be considered further evidence for the higher reactivity of MWCNT. Finally, the very large increase in peak current (about 35 µA) is attributed to the high surface area of MWCNT.

5.3. Oxygen Reduction Studies with the Rotating Disc Electrode

As the rate-controlling process is complicated, when cyclic voltammetry is used to study the O_2 reduction on the modified GC electrode, it might be expected that investigating the electrocatalytic activity of modified carbon electrodes towards oxygen reduction is difficult. On the other hand, in the case of the rotating disc electrode, it allows control over

mass transport so that we can support both mass transport and kinetic effects. It also has to be stressed that the contributions of mass transfer to the electron transfer kinetics might be smaller due to the fact that mass transfer at the surface is larger than charge transfer.[14] In order to determine the number of electrons transferred during O_2 reduction at anthraquinone-modified electrodes, RDE experiments were carried out at different rotation rates and at different solution pH levels. Figure 5.7 shows the RDE results for an anthraquinone-modified glassy carbon electrode at pH 7 for different rotation rates. For the bare glassy carbon electrode (dashed line), there is a wave at around -0.6 V which rises to a broad sloping plateau. This is associated with the catalytic reduction of O_2 at quinone sites on the surface.[6,11] At the anthraquinone-modified glassy carbon electrode, the oxygen reduction wave is shifted to less negative potentials and shows a peak around -0.5 V at the higher rotation rates. Similar effects were observed by Jürmann *et al.*.[11] Figure 5.8 shows the results for different solution pH levels.

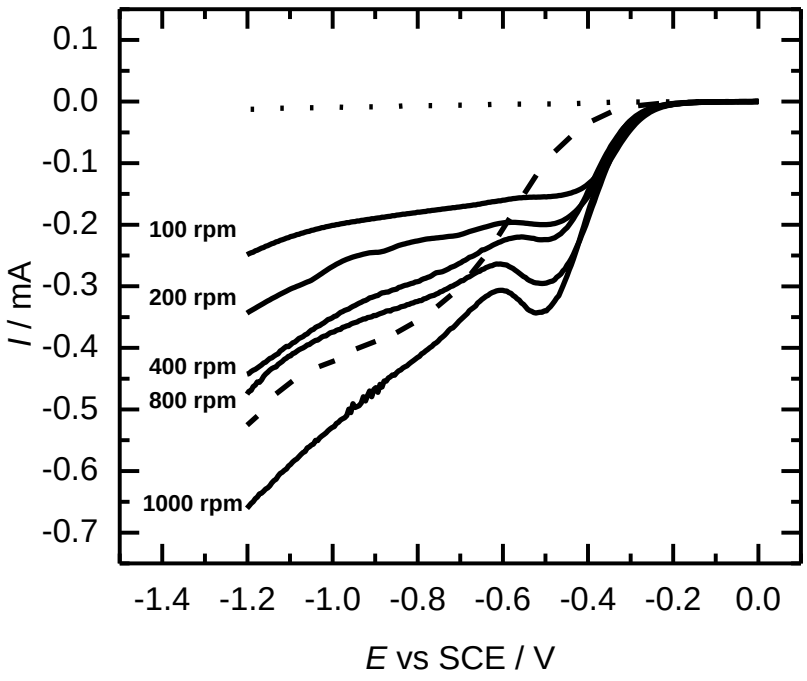

Figure 5.7. *RDE voltammograms for O_2 reduction on an AQ-modified GC electrode (0.196 cm^2) in O_2 saturated 0.1 M pH 7 phosphate buffer for pH 7 recorded at different rotation rates. The dotted and dashed curves represent voltammograms of AQ-modified RDE for pH 7 in the absence and presence of O_2 and unmodified GC electrode in oxygen saturated solution at the rotation rates of 100 and 1000 rpm, respectively*

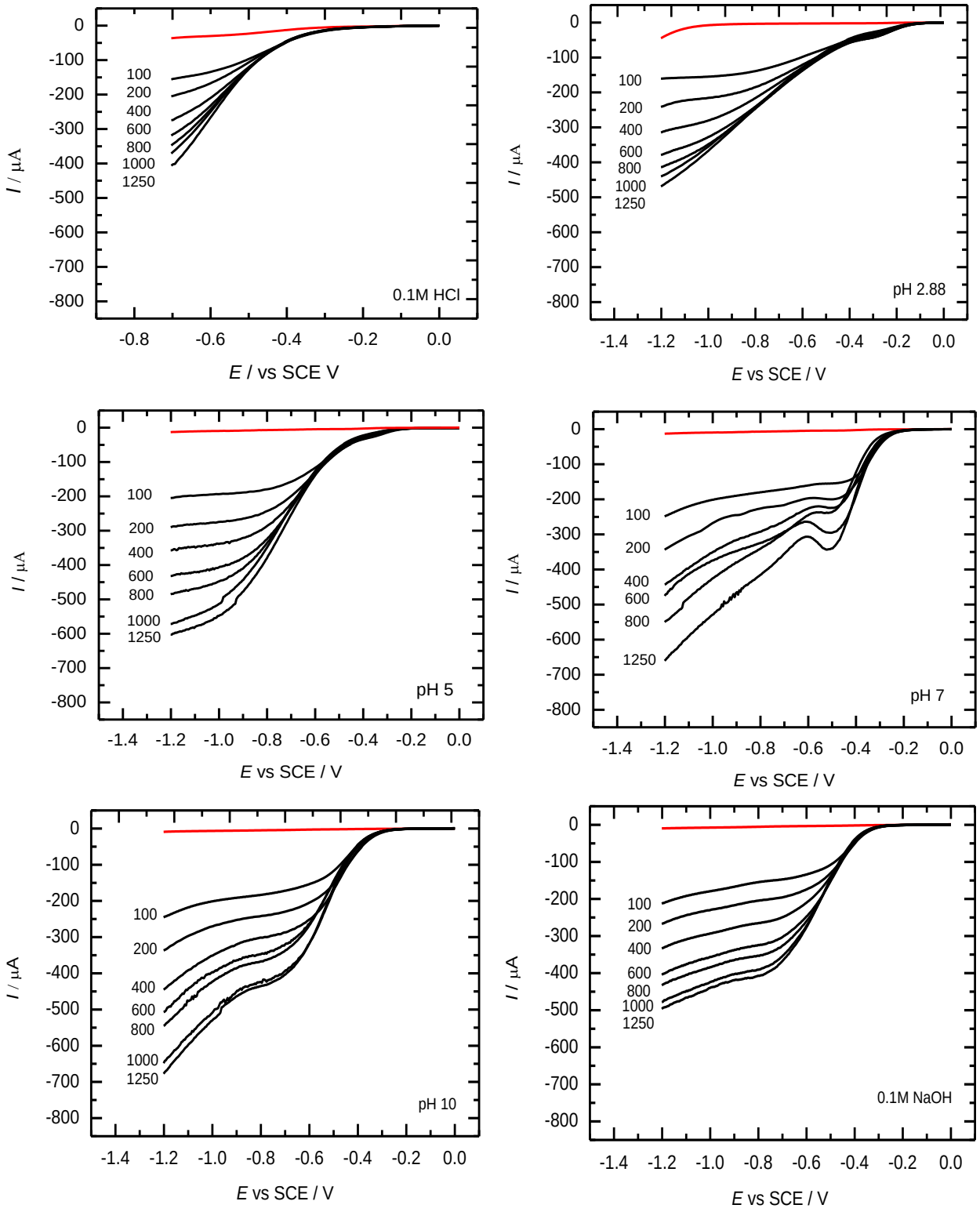

Figure 5.8. *RDE voltammograms for O_2 reduction on an AQ-modified GC electrode through EDA linker in O_2 saturated 0.1 M HCl, 0.1 M of acetate buffer for pH 2.88 and 5, 0.1 M of phosphate buffer for pH 7 and 10.20 and 0.1 M NaOH at different rotation rates. The dotted line represents the voltammogram of the AQ-modified RDE for each pH value in the absence of O_2.*

It is known that the reaction between the protonated anthrasemiquinone radical and oxygen

$$HQ^{\bullet} + O_2 \rightarrow O_2^{\bullet-} + HQ^{+} \quad (5)$$

is much slower that the reaction of the anthrasemiquinone radical anion (reaction (2) above) [6,11] and that the pK_a of the anthrasemiquinone radical is around 5.3.[15] Consequently, as seen in Figure 5.7, the catalysis of oxygen reduction by the immobilised anthraquinone is poor in acid (pH 5 and below) solution.

For the rotating disc electrode, the mass transport is calculable and reproducible. In the case where the electrode reaction is under the mixed control of mass transport and surface kinetics at the electrode, the current can be analysed using the Koutecky-Levich equation provided that the surface reaction is first-order in the reactant.[16] Given this assumption, we can calculate *n*, the number of electrons transferred for the reduction of each O_2 molecule, using the Koutecky-Levich equation[17]

$$\frac{1}{I} = \frac{1}{I_k} + \frac{1}{I_{dl}} = -\frac{1}{nFAk\,C_{O2}} - \frac{1}{0.62nFAD_{O2}^{2/3}\nu^{1/6}C_{O2}\omega^{1/2}} \quad \text{(Equation 5.1)}$$

where j_k and j_{dl} are the kinetic and diffusion limited currents, respectively; k is the rate constant for O_2 reduction, D_{O2} is the diffusion coefficient of oxygen (in acidic media D_{O2} = 1.4 x 10^{-5} cm^2 s^{-1}; for pH 7 to 13, D_{O2} = 1.9 x 10^{-5} cm^2 s^{-1} [11,18]), A is the electrode area (0.196 cm^{-2}), C_{O2} is the O_2 bulk concentration (for acidic media C_{O2} = 1.1 x 10^{-6} mol cm^{-3}; for pH 7 to 13, C_{O2} = 1.2 x 10^{-6} mol cm^{-3} [11]), ν is the kinematic viscosity of the solution (ν = 0.01 cm^2 s^{-1} [19]) and ω is the rotation speed in rad s^{-1}.

Figure 5.9 shows the Koutecky–Levich plots obtained from the RDE data for oxygen reduction on the anthraquinone-modified glassy carbon electrode. From the slope of the lines, the number of electrons transferred per O_2 molecule can be calculated. The inset shows the potential dependence of *n*. The calculated *n* values are close to 2 at all potentials except at the most cathodic values, indicating that O_2 reduction generates H_2O_2 as the final product. The intercepts decrease with increasing cathodic potential, indicating that at -0.7 to -0.9 V, the reaction is under mixed control.

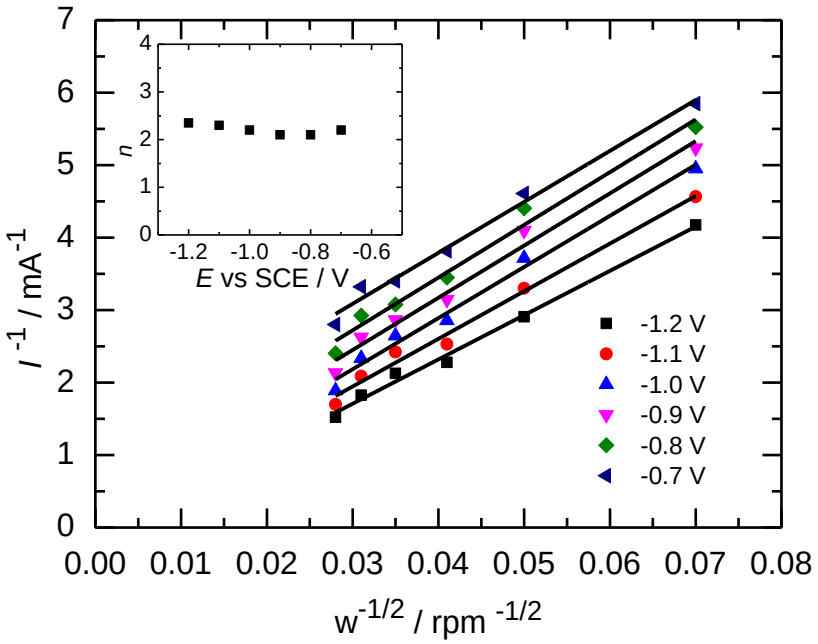

Figure 5.9. *Koutecky–Levich plots for O_2 reduction at an anthraquinone-modified glassy carbon electrode (0.196 cm^2) in oxygen saturated 0.1 M phosphate buffer pH 7 at different potentials. The inset shows potential dependence of n.*

Figure 5.10 shows Koutecky–Levich plots at different pH levels and the inset shows the derived values for *n* at the different potentials and pH values. From the data, it is apparent that the *n* values are essentially independent of the potentials and are around 2, with the values in acidic solution slightly lower than those in neutral solution.

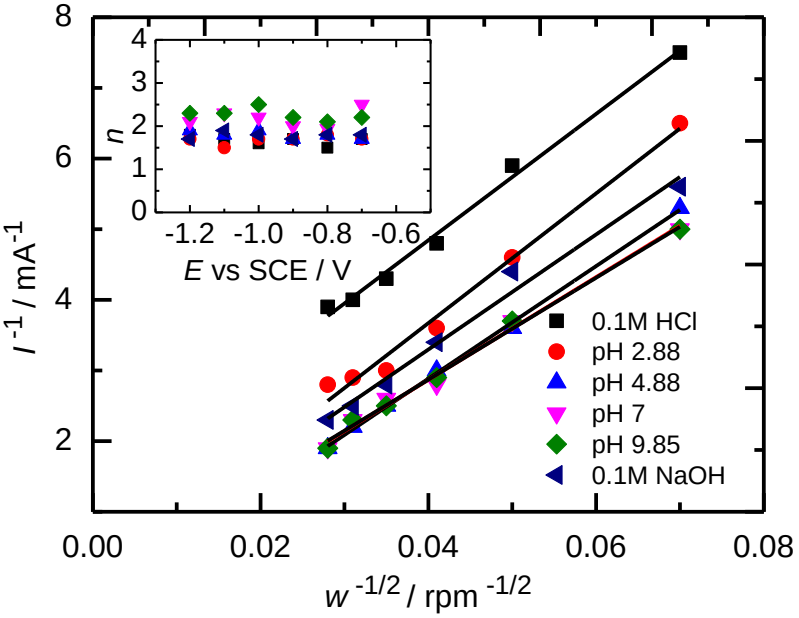

Figure 5.10. *Koutecky–Levich plots for O_2 reduction at an anthraquinone-modified glassy carbon electrode (0196 cm^2) at -0.7 V vs. SCE in the oxygen saturated solutions at different pH levels. For pH 2.88 and 5, acetate buffer solutions were used; and for pH 7 and 10 phosphate buffer solutions were used. The inset shows the potential dependence of n in each case.*

The Koutecky-Levich results in Figure 5.8 and 5.9 imply that hydrogen peroxide is the final product of oxygen reduction,[20] consistent with the work of Tammeveski, Schiffrin and colleagues.[11,18,20,21] To confirm this, we briefly studied the reduction of hydrogen peroxide on the anthraquinone-modified glassy carbon electrode. For the bare glassy carbon, there is a sluggish increase in the current at more negative potentials, whereas, for the anthraquinone-modified electrode, there is evidence for a reduction wave starting around -0.4 V. However, the plateau current for this wave is only a fraction (< 10%) of that expected for the mass transport limited reduction of hydrogen peroxide under these conditions and we attribute the current to traces of oxygen formed in the solution.

5.4. Laccase Immobilization onto Anthraquinone- and Anthracene-Modified GC Electrodes and High-throughput Screening of O_2 reduction

Laccase is a glycoprotein and an enzyme that contains different copper sites (with T1, T2, and T3 regarded as binding sites as well), which carries out a four electron reduction of dissolved molecular oxygen to water. The T1 site is capable of oxidizing the reducing substrate and transferring electrons to the T2 and T3 sites; therefore, the T1 site is known to be an enzyme site, whereas the assembly of T2 and T3 together is known to be a tri-nuclear cluster where oxygen is reduced. T1 and T2/T3 sites are attached via a histidine-cysteine bridge structure. Laccases can be abundantly found in plants, fungi and insects, and their molecular weight ranges from 55–90 kDa for fungal laccases and 110–40 kDa for enzymes from plants.[22] Substantial effort has been devoted to investigating the properties, structure and catalytic effects of laccases on oxygen reduction and for fuel cell applications. Most of the available laccases are in blue colour due to the fact that the T1 site exhibits really strong absorption at 600 nm.[23] The removal of the T1 site, which can be carried out by treatment with cyanide, significantly reduces the activity of the enzymes. Furthermore, one of the most significant features of these enzyme is that the T1 site is really abundant in terms of p electrons and, therefore, the attachment of various types of organic compounds can be achieved onto this site.[24] Another binding site of laccase is the T2 site that also has a single copper ion. However, the T3 site is bounded to the T2 copper site. Such an arrangement is called a tri-nuclear cluster, as mentioned above. Andreasson et al.[25] made an effort to shed light on how the reduction of oxygen occurs through the binding sites of laccase *Rhus vernicifera*. According to their work, the enzyme undergoes a one electron reduction reaction when an electron is transferred to the T1 site, which is immediately passed on to the T2/T3 site. An intermediate peroxide product is then generated as a consequence of the reaction

between reduced enzyme and molecular oxygen. This intermediate is bridged between the oxidized T3 and oxidized T2 sites. This intermediate product then undergoes a two electron reduction to water at tri-nuclear centres through an intermolecular electron transfer mechanism. Hence, the electrochemical reduction of dioxygen to water occurs in two steps, each one involving two electrons. The first one is recognised as the rate-determining step.

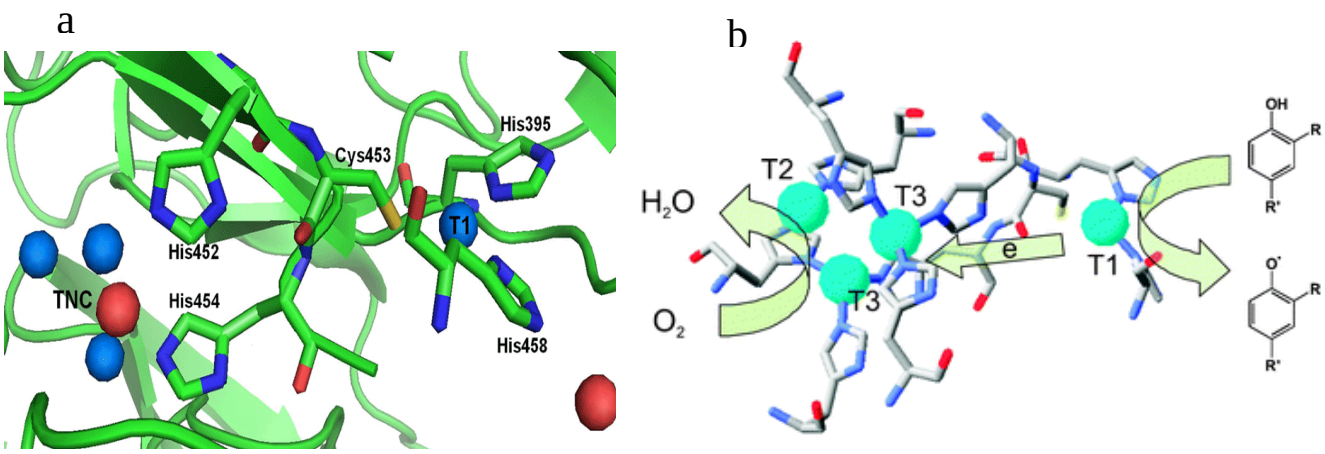

Figure 5.11. *The representation of the active sites of the Trametes hirsuta laccase. The oxygen atom is seen between the copper pair. There are also two oxygen atoms near the T1 copper site (adapted from reference [24]) b) the representation of the catalytic reaction (adapted from reference [26]).*

There is a rapidly growing interest in immobilizing laccase enzymes on conducting surfaces for their application in the field of biological biofuel cells since they can catalyse a four electron reduction of oxygen to water at high positive potentials without any unwanted side, or intermediate, products.[27-29] Hence, developing an efficient method for the robust, good electroactivity and stable attachment of laccase to electrodes is of significant interest. In such systems, the immobilized laccase carries out a direct electron transfer between the substrate and T_1 side. The most frequently employed methods for the binding of laccase as an electrocatalyst to a substrate are: i) the binding of laccase to a modified metal electrode, for instance, gold; ii) immobilising laccase with the aid of electron mediators, such as ABTS; and iii) the direct adsorption of laccase to carbon electrodes.

In this work, the electrografting of EDA and $C_6H_4CH_2NH$– linkers to GC surfaces and subsequently, the coupling of anthraquinoine (AQ) and anthracene (AC) (head groups) after the removal of the Boc group are carried out to build a platform for the further attachment of laccase, this experiment was designed to perform with three replicates for each linker and head group, which designates a library of twelve electrodes after all

functionalization and immobilization procedures are completed. We used high-throughput screening for the O_2 reduction with the aid of a multichannel potentiostat, which is capable of simultaneously running CV for the one hundred and twenty eight electrodes. After having established the homogeneous distribution of O_2 across the electrochemical cell as detailed in Chapter 2, O_2 reduction at laccase-immobilized GC electrodes was performed. The results are presented in Figure 5.12. It is difficult to distinguish a distinctive peak from the voltammogram in oxygen-free solution (Figure 5.12) because, in order to attain a sharp peak less than 2 pmol of enzyme is required based on the CV taken in the presence of O_2. It is also quite observable that the charge obtained for either the oxidation or reduction of the T_1 side of laccase is quite small. On the other hand, as seen in Figure 5.12, in an oxygen saturated solution, there is a clear increase in the peak current starting at around 0.5 V vs SCE for all twelve electrodes already, which was foreseen due to the potential of T_1[26,30] because it was experimentally verified that the electron is primarily transferred to the T1 site from the carbon electrode. Therefore, the onset in the increase in peak current can be directly attributed to the redox potential of the T1 site. The redox potential value of the T1 site is reported to be between 490 and 790 mV, which also differs with the source of the laccase. For example, the redox potential of *Rhus vernicifera* obtained from plants is about 430 mV, while *Polyporus versicolor*, which is obtained from fungi, has the potential of 780 mV vs normal hydrogen electrode.[31] The redox potential of this site can be determined by the protein redox titration method in the presence of potassium octocyanomolybdate (IV and V) mediators.[32] Furthermore, the potential of the T3 and T2 sites was found to be 480 mV and 390 mV for *R. vernicifera*. It is significant to note that the catalytic efficiency (k_{cat}/K_M) of laccases is greatly affected by the redox potential of the T1 copper site, referring to the fact that the higher redox potential of the T1 site leads to higher catalytic efficiency. As a consequence of this, there has been increasing attention to this site for biotechnological applications.[31,33]

The increase in the peak current is also evidence for O_2 reduction at all of the laccase immobilized electrodes. This indicates the successful binding of laccase to the AQ and AC modified surfaces and the direct electron transfer in oxygenated solution.[34]

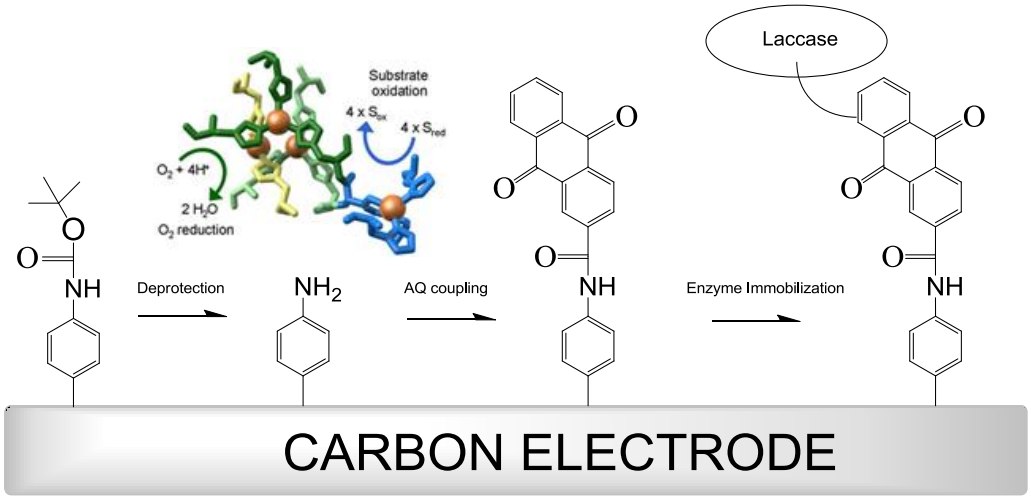

Scheme 5.1. *Representation of the immolization of laccase to a modified GC electrode with AQ through a $C_6H_4CH_2NH$– linker. Inset shows oxygen reduction mechanism on laccase enzyme.*

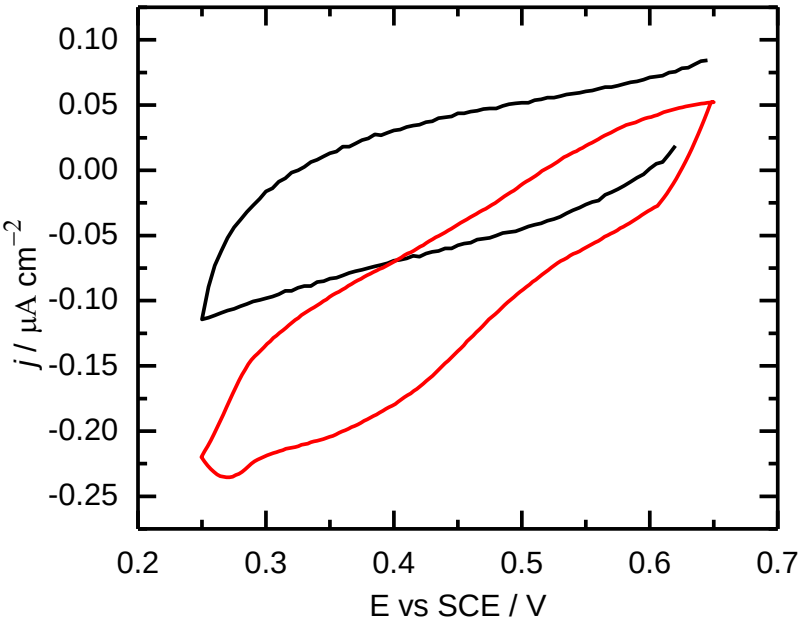

Figure 5.12. *CV recorded at the scan rate of 5 mV s-1 in oxygen saturated citrate buffer pH 5 for Laccase immobilized onto modified GC electrodes (0.071 cm2) with AC through an EDA linker. Black and red solid lines represent CV in oxygen-free and oxygenated solution, respectively.*

For some unknown reason, the CVs obtained using the multichannel potentiostat are quite noisy. Initially, we assumed that this problem stems from the reference electrode. However, when an individual experiment was carried out using the same reference electrode, the voltammogram in Figure 5.12 was obtained. We then thought that there might be interference from the other electronic devices in the vicinity of the multichannel potentiostat. All those devices were switched off during the measurement and no significant difference

was observed. When all CVs were smoothed using Origin 8 software, these voltammograms were maintained as acquired since all of the obtained CVs did not make any sense.

Control experiments were also carried out on the individual anthraquinone-modified electrodes and the electrodes treated with only the enzyme in order to determine whether the observed current in the presence of O_2 originates from immobilized an enzyme or not. Within the same potential window, and as displayed in Figure 5.14, only background currents were obtained for the two cases. The type of head group coupled to the electrode surface by EDA and $C_6H_4CH_2NH–$ linkers seems to have an impact on the O_2 reduction from the point-of-view of peak shape and the magnitude of the peak current. As clearly seen, more current and more defined voltammograms are achieved for the AQ-modified electrodes compared to the AC ones, which means that, for the AQ-terminated surfaces, direct electron transfer to the enzyme takes place more efficiently. It also has to be stressed that, when laccase is immobilized onto these head groups through a bulkier linker, $C_6H_4CH_2NH–$, the magnitude of the peak currents in oxygenated solution are consistently smaller than shorter linkers, as the only difference between these linkers is the surface coverage of AQ or other head groups. Naturally, the lower peak current for the O_2 reduction obtained for laccase immobilized by $C_6H_4CH_2NH–$ could be due to the difference in the number of head groups on the surface. However, Sosna and et al.[26] explored how variable surface coverages of anthraquinone and anthracene affects the oxygen reduction, which was carried out by changing the surface coverage of linkers with potential steps of pre-set duration. The surface coverage of head groups was found to be independent of cathodic currents. Such a finding is already anticipated due to the fact that the size of the head group is not comparable to the enzyme, so very few of them are involved in the immobilization of the enzyme. Perhaps the reason of such an outcome could be attributed to the orientation of the T1 site of laccase towards the head groups bonded to the surface through the above-mentioned linkers. It can be concluded that, as a head group, AQ and AC are able to access and remain in the T1 site of laccase and provide good stability and rigidity. They can also be regarded as p electron donors with the correct dimensions, so that they can reach close enough to the hydrophobic binding site of laccase. Therefore, the reason for the greater electrocatayltic activity for the AQ head group with respect to AC could be attributed to the fact that it is not only known to be hydrophobic but also it has the ability to interact with polar moieties in the T1 site laccase. Hence, the resulting electrode obtained subsequent to the binding of the laccase to the AQ-modified surface is inherently expected to be more stable.

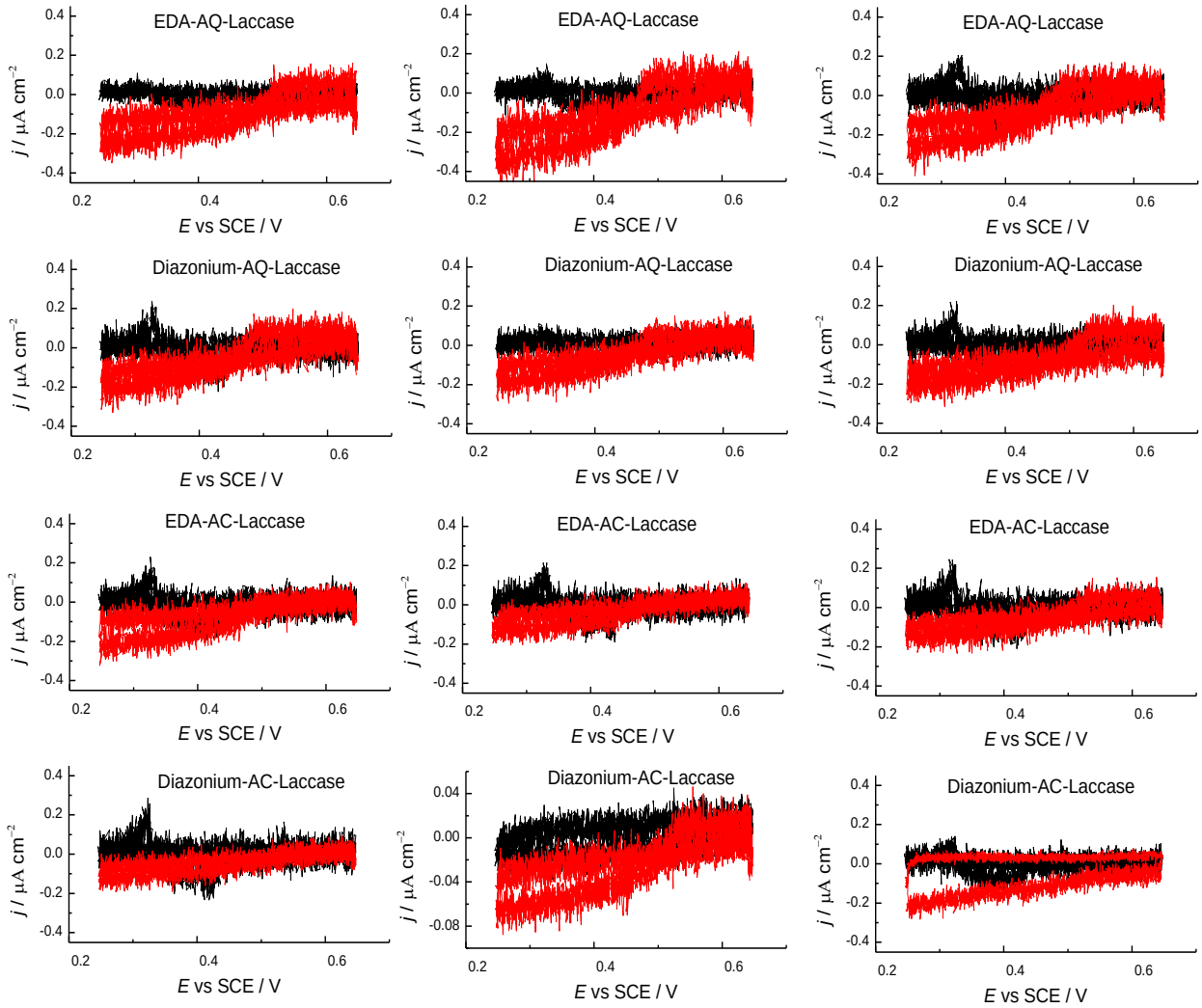

Figure 5.13. *CV performed using multichannel potentiostat at a scan rate of 5 mV s^{-1} for laccase immobilized onto modified GC electrodes (0.071 cm^2) with AQ and AC through EDA and $C_6H_4CH_2NH$– linkers. Black and red solid lines represent CVs in oxygen-free and oxygenated citrate buffer solutions at pH 5, respectively.*

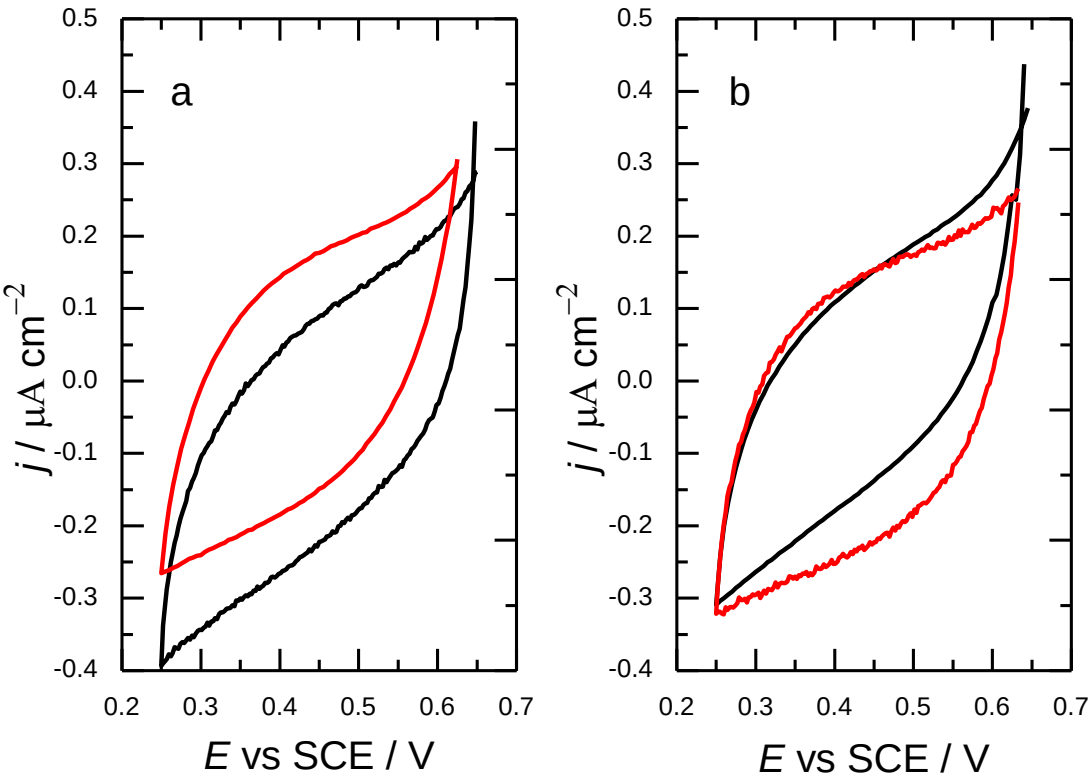

Figure 5.14 *CV recorded at the scan rate of 5 mV s^{-1} in citrate buffer at pH 5 for modified a GC electrode with AQ through an EDA linker (a) and a GC electrode (0.071 cm^2) treated with only laccase. Black and red solid lines represent CVs in oxygen-free and oxygenated solution, respectively.*

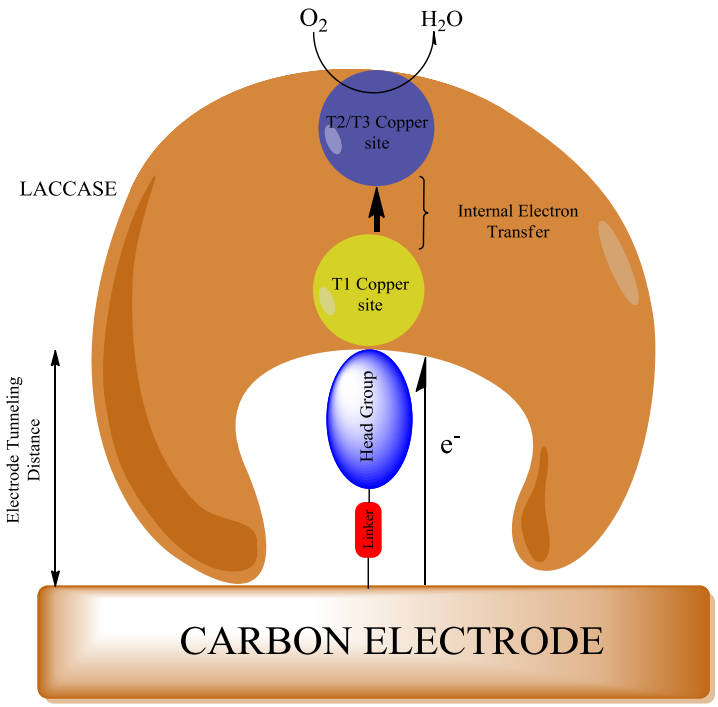

Scheme 5.2. *Proposed mechanism of direct electron transfer for laccase immobilized GC electrodes modified with AQ or AC through a EDA or $C_6H_4CH_2NH$– linkers.*

In summary, in such a system, the electrochemical reduction of oxygen reaction to water is represented in Scheme 5.2. Initially, the T1 copper site of laccase accepts the electron from the reducing substrate. This electron is then transferred to the tri-nuclear cluster of enzymes through an internal electron transfer mechanism where O_2 is reduced to water.

5.5. Conclusion

These studies show that the peak potential for O_2 reduction is more positive at glassy carbon and edge plane graphite as compared to basal plane graphite. This has been attributed to the presence of oxygen functional groups on the carbon surface that can participate in the oxygen reduction reaction. This outcome is already anticipated since edge plane graphite exhibits more reactivity towards electron transfer and adsorption than basal plane graphite,[9,35,36] as was previously explained in Chapter 3. All three anthraquinone-modified electrodes were shown to catalyse the reduction of oxygen at pH 7, with the most active surfaces being those with the largest amount of immobilised anthraquinone. The rotating disc studies show that the product of oxygen reduction was hydrogen peroxide at all pH levels, from 1 to 13.

The electron transfer properties of laccase (*ThL*) immobilized onto GC electrodes modified with AQ and AC through EDA and $C_6H_4CH_2NH$– linkers were explored by means of high-throughput screening using multichannel potentiostat for the library of twelve electrodes. All electrodes were found to exhibit electrocatalytic activity towards oxygen reduction. This indicates the successful binding of laccase to functionalized carbon surfaces and decent electrical contact between substrate and enzyme active sites because, in the case of modified electrodes with AQ and AC, oxygen reduction was not observed within the potential window that GC electrodes immobilized with laccase, thereby exhibiting a rather strong electrocatalytic activity towards dioxygen. When the surface was functionalized with AQ subsequent to electrochemical EDA coupling, the resulting electrode appeared to show the best binding of *ThL;* as a result of this, the best electrochemical activity since the largest peak current was obtained was at this GC electrode.

5.6. References

(1) K. Laszlo; A. Szucs, *Carbon* **2000**, *39*, 1945.

(2) B. Sljukic; C. E. Banks; R. G. Compton, *J. Iran. Chem. Soc.* **2005**, *2*, 1.

(3) F. Mirkhalaf; K. Tammeveski; D. J. Schiffrin, *Phys. Chem. Chem. Phys.* **2004**, *6*, 1321.

(4) D. Jeziorek; T. Ossowski; A. Liwo; D. Dyl; M. Nowacka; W. Woz´nicki *J. Chem. Soc., Perkin Trans.* **1997**, *2*, 229.

(5) Y. Okamoto, *Appl. Surf. Sci.* **2009**, *256*, 335.

(6) J.R.T.J. Wass; E. Ahlberg; I. Panasb; D. J. Schiffrin *Phys. Chem. Chem. Phys.* **2006**, *8* 4189.

(7) M. A. Ghanem; I. Kocak; A. Al-Mayouf; M. AlHoshan; P. N. Bartlett, *Electrochim. Acta* **2012**, *68*, 74.

(8) J.-M. Chrétien; M. A. Ghanem; P. N. Barlett; J. D. Kilburn, *Chem. A. Eur. J.* **2009**, *15*, 11928.

(9) M. T. McDermott; K. Kneten; R. L. McCreery, *J. Phys. Chem.* **1992**, *96*, 3124.

(10) S. Y. Yeh; C. M. Wang, *J. Electroanal. Chem.* **2006**, *592*, 131.

(11) G. Jürmann; D. J. Schiffrin; K.Tammeveski, *Electrochim. Acta* **2007**, *53*, 390.

(12) C.E. Banks; G.G. Wildgoose; C.G.R. Heald; R.G. Compton *J. Iran. Chem. Soc* **2005**, *2*, 60.

(13) Z. Gong; G. Zang; S. Wang *J. Chem.* **2013**, *2013*, 1.

(14) A. Salimi; H. Eshghi; H. Sharghi; S. M. Golabi; M. Shamsipur, *Electroanalysis* **1999**, *11*.

(15) P. S. Rao; E. Hayon, *J. Phys. Chem.* **1973**, *77* 2274.

(16) M. E. G. Lyons; C. H. Lyons; A. Michas; P. N. Bartlett, *J. Electroanal. Chem.* **1993**, *351*, 245.

(17) A. J. Bard; L. R. Faulkner, *Electrochemical Methods; Fundamentals and Applications* Wiley: New York, 2001.

(18) K.Vaik; U. Maeorg; F. C. Maschion; G. Maia; D. J. Schiffrin; K.Tammeveski, *Electrochim. Acta* **2005**, *50*, 5126.

(19) D. R. Lide, *Handbook of Chemistry and Physics*; CRC Press: Baton Rouge, 2001.

(20) K.Tammeveski; K. Kontturi; R. J. Nichols; R. J. Potter; D. J. Schiffrin, *J. Electroanal. Chem*. **2001**, *515*, 101.

(21) A. Sarapuu; K.Vaik,; D. J. Schiffrin; K. Tammeveski, *J. Electroanal. Chem*. **2003**, *541*, 23.

(22) P. N. Bartlett, *Bioelectrochemistry Fundamentals, Experimental Techniques and Applications*; John Wiley & Sons: Chichester, West Sussex, 2008.

(23) M. Antorini; I. Herpoel-Gimbert; T. Choinowski; J. C. Sigoillot; M. Asther; K. Winterhalter; K. Piontek , *Biochim. Biophys. Acta* **2002**, *1594*, 109.

(24) C. F. Blanford; R. S. Heath; F. A. Armstrong *Chem. Commun.* **2007**, 1710.

(25) L. E. Andreasson; B. Reinhammar *Biochim.Biophys. Acta* **1979**, *558*, 145.

(26) M. Sosna; J-M. Chrétien; J. D. Kilburn; P. N. Bartlett *Phys.Chem.Chem.Phys.* **2010**, *12*, 10018.

(27) A. Heller, *Anal. Bioanal. Chem*. **2006**, *385*, 469.

(28) S. C. Barton; J. Gallaway; P. Atanassov *Chem. Rev*. **2004**, *104*, 4867.

(29) R. A. Bullen; T. C. Arnot; J. B. Lakeman; F. C. Walsh, *Biosens. Bioelectron.* **2006**, *21*, 2015.

(30) B. Reinhammar, *Biochim. Biophys. Acta* **1972**, *275*, 245.

(31) S. Shleev; A. Christenson; V. Serezhenkov; D. Burbaev; A. Yaropolov; L. Gorton; T. Ruzgas, *Biochem. J.* **2005**, *385*, 745.

(32) S. Sadhasivama; S. Savitha; K. Swaminathan; F-H. Lin *Process Biochem.* **2008**, *43*, 736.

(33) S. Shleev; A. J.-Wilkolazka; A. Khalunina; O. Morozova; A. Yaropolov; T. Ruzgas; L. Gorton, *Bioelectrochemistry* **2005**, *67*, 115

(34) M. Sosna; L. Stoica; E. Wright; J. D. Kilburn; W. Schuhmann; P. N. Bartlett, *Phys.Chem.Chem.Phys.* **2012**, *14*, 11882.

(35) K. K. Cline; M. T. McDermott; R. L. McCreery, *J. Phys. Chem*. **1994**, *94*, 5314.

(36) C. C. M. Neumann; C. Batchelor-McAuley,; C. Downing; R. G. Compton, *Chem. Eur. J.* **2011**, *17*, 7320.

Chapter 6

FIRST PRINCIPLES DENSITY FUNCTIONAL THEORY: SIMULATION OF FUNCTIONALIZED GRAPHENE

6.1. Introduction

The computational assessment of conductive and semi-conductive bulk materials has been regarded as one of the most significant methods, providing valuable information regarding the interaction between a substrate and molecules. It is also quite useful for the purpose of comprehending the influence of modification on the electronic, magnetic and structural properties of the pristine substrate.[1] After the functionalization of the corresponding surface, by using DFT, we can shed light on what the most stable geometry of the functionalized substrate is, how the number of molecules attached to a substrate changes the degree of charge transfer from substrate to molecule, the binding energy of the molecule, and the electronic and magnetic properties of the substrate. DFT is also quite useful for understanding whether a reaction is predominantly driven by kinetics or thermodynamics by running minimum energy pathway calculations. If the activation energy is found to be low, this indicates that the corresponding reaction is mainly dominated by kinetics.[2,3] Furthermore, from the point-of-view of DFT, the kinetics of the desorption of molecules from a substrate can be investigated by exploring the minimum energy pathway and temperature dependent rate constant so as to acquire important information about the stability of molecules attached to the corresponding surface at different temperatures.[4] To sum up, DFT is quite beneficial as a tool for understanding experimental findings in depth.

In first principles DFT simulation calculations, HOPG electrodes with basal plane sites can be assumed to behave like a single sheet layer of graphene, which is known to be made up of sp^2 hybridized carbon atoms and to have planar morphology and aromaticity, which makes this material resistant towards functionalization. However, a source of motivation for carrying out DFT calculations on single layer graphene sheets for such systems arises from the work of Mandeltart.[5] He showed that graphene can be used instead of bilayers or multilayers of graphite if the supercell is made up of around 160 atoms. A supercell is an imaginary 3D structure where all DFT calculations are carried out on a periodic system. For such a system, we assume that all molecules or atoms are present in a box and, in this case, the calculation will be performed by considering all atoms as part of a periodic system. According to their theoretical results, if a supercell containing 72 atoms is used for the simulation, there is a 0.6 eV difference between the binding energy of the adsorption of CH_3 to single and double layers of graphene. However, in the case of a supercell made up of 160 atoms, the difference in the binding energy of the adsorption of the

CH_3 radical to single and double layers of graphene appeared to be 0.06 eV. They therefore concluded that a single layer of graphene can be used for DFT calculations if one wishes to compare the experimental reactivity of a radical on HOPG with results attained by DFT. They also confirmed that graphite can be substituted by a single layer of graphene by calculating the reaction energy for the addition of a single CH_3 group to single and double layers of graphene. It was then found that there was only a 0.1 eV difference between the two cases, which is quite low. On the basis of the corresponding DFT calculations for the addition of a CH_3 radical to single- and bi-layer graphene, it is worth noting that the number of graphene layers has an influence on the binding energy, which is in good agreement with the literature.[6,7] However, the authors concluded that the dependence of the number of layers on binding energy can be an artefact of using graphene with a supercell with few atoms. Even though the basal plane of HOPG is not going to be same as that of graphene, due to the interaction between each layer in this study, all first principle density functional theory calculations were carried out on a single layer graphene sheet with over 120 carbon atoms.

It is also well known that pristine graphene has poor solubility in water and organic solvents, and that it does not have a band gap.[3,5,8,9] Thus, performing chemical modifications on the graphene sheet is crucial as it not only improves its solubility and its chemical, magnetic, and electronic properties but also introduces new properties to graphene, thereby broadening its areas of application.[9] DFT has therefore been used in the literature for carbon nanotube, pristine graphene, and graphene with surface defects with different types of functionality in order to evaluate how the structural and electronic properties of the graphene surface are changed after functionalization. Thus, we believe that it is worth investigating the interactions between the linkers used in this work and pristine graphene using first principles DFT. From a theoretical point-of-view, for the attachment of the corresponding linkers, we mainly focused on why the edge plane is more reactive than the basal plane and why the type of linkage seems to have an effect on the surface coverage of AQ coupled to the linkers after the removal of the Boc protecting group.

6.2. Method and Computation

The geometry optimization and electronic property calculations were carried out by using the ultrasoft pseudopotentials plane-wave method, as implemented in the CASTEP[10]

code. The generalized-gradient approximation (GGA) functional (the Perdew-Burke-Ernzerhof (PBE)) was employed for the exchange correlation. Applying the GGA/PBE method in DFT calculations has the advantage of not only minimizing the overbinding effects caused by the Local Density Approximation (LDA) but also compensating for the overestimation of binding energy. Furthermore, GGA/PBE is capable of adequately calculating the density of states (DOS) as compared to experimental results . Spin polarized calculations with the plane-wave cut-off energy of 500 eV was performed for all calculations. These settings were determined by running a series of test spin polarized geometry optimizations with different values of cut-off energy, such as 100, 200, 300, 400 and 500, followed by the completion of the geometry optimization calculation for an isolated EDA linker and a single layer of graphene sheet, with one EDA linker anchored onto the graphene sheet. The binding energy for the attachment of a single EDA linker was then calculated for each energy cut-off value. It was then found that, as reported in Table 6.1, no significant difference between each cut-off energy value was observed; therefore, a 500 eV cut-off point was chosen so as to enhance the reliability and accuracy of the calculations. In this work, a spin-polarized calculation was implemented due to the fact that, in our test calculations, the binding associated with the addition of an additional EDA linker to graphene sheets obtained for spin polarized calculations is higher than that of non-spin polarized calculations by 0.4 eV. This is larger than the cut-off energy convergence tolerance. We also used an odd number of electrons on each linker used in this work. The effect of solvents was omitted for this spin-polarized geometry calculation. Throughout this work, isolated single layer of graphene sheet and amine linker and graphene anchored with each amine linker used in this work were placed in a supercell of 28.208 Å × 10 Å × 12.681 Å and DFT calculation through CASTEP code were carried out.All simulations were replicated three times to obtain fairly reproducible results. The required time for the geometry optimization calculation for the attachment of a single EDA linker to the graphene with the calibrated parameters described above lasted approximately 1.5 hours. As we attached more linkers, it reached a maximum of up to 42 hours.

Table 6.1. *Test calculation results for the effect of different energy cut-off values on the binding energy of a single attachment of an EDA linker to graphene. Spin polarized calculation was carried out with the ultra-soft pseudopotentials plane-wave method, as implemented in the CASTEP. Stable geometries are based on generalized-gradient approximation (GGA) functional with Perdew-Burke-Ernzerhof correction.*

Energy cut-off / eV	100	200	300	400	500
Binding energy / eV	0.75	0.82	0.85	1.04	1.10

A supercell of 28.208 Å × 10 Å × 12.681 Å containing a graphene sheet made up of over 120 C atoms was used. The Brillouin zone of the supercell was sampled by 1 × 1 × 1 *k*-points within the Monkhorst-Pack scheme.[11] All parameters for the calculations were chosen after the calibration of the settings (such as cut-off energy and spin-polarized calculation) was achieved. Single point energy and geometry optimization calculations were carried out for the same graphene sheet; we found that there was only a 0.2 eV difference between the single point energy of graphene and the energy obtained after the system was completely relaxed with geometry optimization. This suggests that all chosen parameters ensure a good enough convergence of total energies. As shown in Figure 6.1, in order to reduce the computational time, one methyl group of the *tert*-butyloxycarbonyl (Boc), instead of three, was used, with the solvent effect also being omitted. The binding energy (E_b) of *n*-linkers on the basal plane of a graphene sheet is defined as,

$$E_b = [nE_{linker} + E_{graphene} - E_{graphene@n\text{-}linker}] / n \qquad \text{(Equation 6.1)}$$

where E_{linker}, $E_{graphene}$, and $E_{graphene@n\text{-}linker}$ stand for the total energy of n-linkers, pristine graphene and the basal plane of graphene functionalized with n-linkers, respectively. *n* stands for the number of attached linkers on the graphene. Using this definition, a positive binding energy indicates that the linker can be stably attached on graphene.[12]

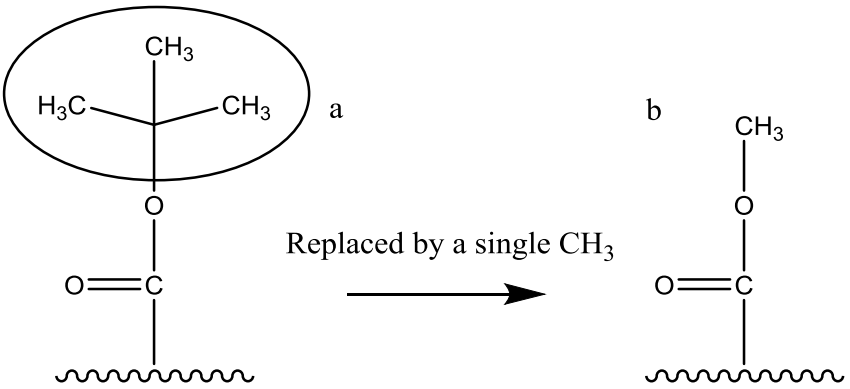

Figure 6.1. *The representation of a linker with three (a) and one (b) methyl group. Structure b is adapted for all DFT simulation for all linkers.*

6.3. Structural Properties of Mono-Functionalized Basal and Edge Planes

As observed in our experimental work, mentioned both in Chapter 3 and in published work,[13] carbon electrodes, such as glassy carbon, edge plane and basal plane, as well as multi-walled carbon nanotubes, can all be modified with either Boc-protected diamines by the electrochemical oxidation of the corresponding mono-Boc-protected diamine linker or by the electrochemical reduction of diazonium tetrafluoroborate salt. As reported in Chapter 3, however, assuming that the basal plane of HOPG is atomically flat and that the surface roughness of the edge plane of HOPG does not have any effect on the electrochemistry and electrochemical modification of HOPG electrodes, the edge plane is experimentally found to be more active towards the electrochemical attachment of all linkers used in our study, as shown by the fact that larger current densities and lower overpotentials were required on the edge plane orientation for the electrochemical grafting of Boc-protected diamine or diazonium linkers. As a consequence of these phenomena, higher anthraquinone surface coverage was obtained. Therefore, in order to shed light on why the edge plane might exhibit higher reactivity towards the electrochemically generated radical relative to the basal plane, geometry optimization was carried out by using CASTEP with the parameters that we determined in Section 6.2.

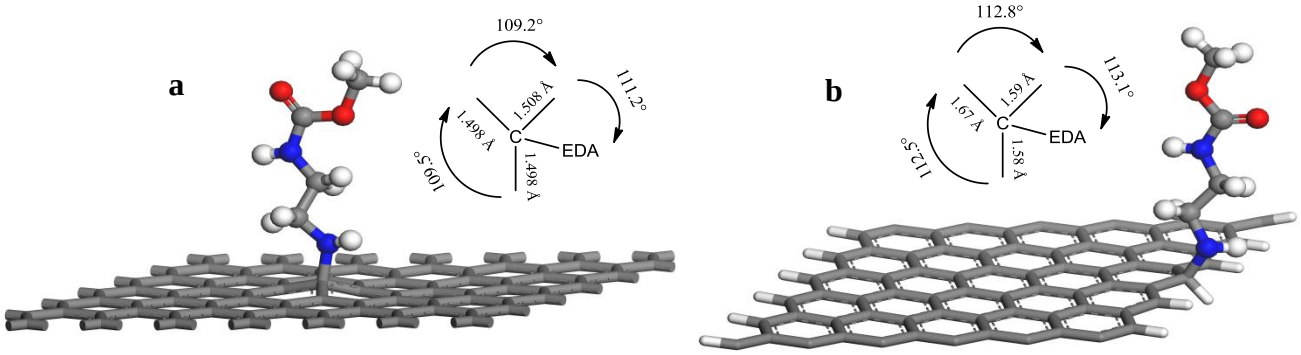

Figure 6.2. *Optimized geometry of a single EDA anchored on a pristine basal plane (a) and an edge plane (b) of a graphene sheet.*

The geometric optimization results for an EDA linker anchored onto the basal plane and edge plane electrodes obtained by the spin polarized calculation are shown in Figure 6.2. Table 6.1 summarizes C-N and C-C bond lengths, binding energies (E_b) and charge transfer (Q) from graphene to linker and from linker to graphene. The structural properties of mono-modified graphene with EDA, BDA EDDA, HDA, XDA and $–C_6H_5CH_2NH-$ linkers were also investigated. On the basis of the results presented in Figure 6.2 and Table 6.1, it can be concluded that all the linkers can be chemically immobilised to the edge and basal sites of carbon surfaces and covalently bonded with a carbon atom—namely, forming C-N and C-C bonds.

As shown in Figure 6.2, the linker pulls the C atom out a little from the surface, leading to an alteration in the geometry of the carbon surface of the edge and basal sites. The C-N and C-C bonds are almost perpendicular to the surface and, as seen in Figure 6.2, the standard C-C bond lengths of the six-membered carbon ring where the linker is anchored are increased from the 1.46 Å to 1.67, 1.59, 1.58 Å and 1.53, 1.53, 1.46 Å for edge and basal planes, respectively. Correspondingly, the bond angles are reduced from 120° to 112.5°, 112.8° and 113.1°, and to 109.5°, 109,5° and 111,2° for the edge plane and basal plane, respectively, which indicates that these C-C bond lengths and angles significantly deviate from the standard length and angle for sp^2 hybridization. On the basis of this explanation, it can be concluded that the C atom of the six-membered carbon ring where the corresponding linker is attached changes to sp^3 hybridization from sp^2 hybridization. Identical calculations were also performed for the other linkers and similar outcomes were obtained.

6.4. Energetic Properties of Mono-Functionalized Basal and Edge Planes

When the binding energy of the attachment of all linkers to the basal site and edge site of the graphene sheet are considered, it can clearly be seen that an energy level approximately thirty times larger is obtained at the edge sites compared to the basal sites. This finding is in good agreement with our experimental results where we found a higher tendency of the edge sites to take part in chemical reactions with electrochemically generated amine radicals, followed by the coupling of AQ subsequent to the de-protection of the amine group. Certainly, in this case, we have to neglect the surface roughness of the edge plane. Due to the considerably high reactivity of edges, it can be expected that edges will have an effect on the physical and chemical properties of graphene. In addition, edges are believed to consist of a random combination of zigzag and armchair structures; they also have dangling bonds and disordered structures. As a consequence of these unique structural features of edges, edge sites naturally have enhanced DOS. Edge sites therefore exhibit more chemical reactivity. [11,12] The electrochemical attachment of a linker by electrochemical oxidation or by the reduction of the corresponding linkers to the edge plane is kinetically more favourable since, experimentally, less over-potential is required at edge sites. This also suggests that the edge plane will exhibit more reactivity towards radicals. Jiang *et al.*[8] also studied the interaction between phenyl (C_6H_5) H-terminated edge and basal sites of a graphene sheet using first principles density functional theory methods implemented in the Vienna *ab initio* simulation package (VASP). They also found a higher reactivity towards the attachment of phenyl at the edge plane as compared to the basal site. However, it is commonly accepted that graphite is known to have other functional groups containing oxygen, such as carboxyl, hydroxyl and quinones, at its surface. If carboxyl or hydroxyl terminated graphene sheets were employed in such DFT calculations, we would anticipate that there would be an increase in the binding energy as a result of possible strong electrostatic interactions between the radical and these functional groups. For instance, Scipioni *et al.*[14] investigated the mechanism of adsorption of β-nicotinamide adenine dinucleotide on single-walled carbon nanotubes (SWCNT) terminated with hydrogen (-H), hydroxyl (-OH), and carboxyl (COO^-) by using a Carr Parrinello molecular dynamics (CPMD) simulation. They found that the interaction energy between NAD^+ and the edge of SWCNT terminated with OH and COO^- increased compared to the H terminated edge of SWCNT. It was also shown that the electrostatic interaction between COO^- and NAD^+ were found to be higher than that of OH. Moreover, Wood *et al.*[15] also explored methane and carbon dioxide adsorption on the edge plane of graphene

functionalized with several functional groups, such as NH_2, OH, and COOH. They demonstrated that the adsorption energy significantly increased in the case of NH_2, OH, and COOH functionalized edge planes of graphene by 7.5, 5.8, and 9.8 eV with respect to H-terminated graphene.

When the binding energy of the attachment of different linkers to the basal plane of the graphene sheet is taken into account, modification of the graphene surface by the electrochemical oxidation of EDA linkers seems to be energetically more stable with respect to the other diamine linkers. It can also be clearly observed that the binding energies of each relevant linker, calculated on the basal plane of graphene, are, in ascending order, as follows: EDA>BDA>HDA>XDA>EDDA and $-C_6H_5CH_2NH-$. This is exactly the same tendency as seen in our experimental results for the surface coverage of AQ obtained on the basal plane of HOPG for linkers. The corresponding binding energies for these amine linkers appear to be consistent with the literature.[16,17] Perhaps this could help to establish a relationship between the different types of linker and the surface coverage of linkers (the surface coverage of these linkers can also be linked to the surface coverage of AQ since we assume that an equal yield for AQ coupling is achieved in all cases after the removal of the Boc-protecting group). For instance, the binding energy of the diazonium linker is considerably lower than that of the diamine linkers, which suggests that this linker might be physically adsorbed to the carbon surface or, after being chemically bonded onto the surface, a certain amount of them can desorb. Hence, the likelihood of achieving the further modification of redox probes to this linker is not as likely as others; this, in turn, inherently leads to the low surface coverage of the corresponding electrochemically active redox molecule.

Table 6.2. *C-N or C-C bond length d between substrate and linker, binding energy E_{bind} and charge transfer. Q and Q* represent charge transfer from graphene to linker and from linker to graphene, respectively. a and b represent values obtained for a basal plane of graphene sheet and for an edge plane of graphene sheet. (E_{bind} = $[nE_{linker} + E_{graphene} - E_{graphene@linker}] / n$). Spin polarized calculation was carried out with plane-wave cut-off energy of 500 eV, as implemented in the CASTEP. DFT calculations were carried out with a plane wave basis, periodic boundary conditions, and within the generalized-gradient approximation (GGA).*

Linker	*d*(C-N) or *d*(C-C) / Å[a] (±0.02)	E_{bind} / eV[a]	*Q* (±0.01)	Q^* (±0.01)
EDA	1.509[a]	1.10[a] (±0.05)	-0.61[a]	0.170[a]
	1.485[b]	30.2[b] (±0.12)	-0.57[b]	0.000[b]
BDA	1.515[a]	0.80[b] (±0.07)	-0.60[a]	0.170[a]
	1.487[b]	29.5[b] (±0.09)	-0.57[b]	0.000[b]
HDA	1.520[a]	0.70[a] (±0.04)	-0.60[a]	0.170[a]
	1.485[b]	28.7[b] (±0.05)	-0.57[b]	0.000[b]
XDA	1.531[a]	0.40[a] (±0.04)	-0.60[a]	0.170[a]
	1.490[b]	29.0[b] (±0.09)	-0.57[b]	0.000[b]
EDDA	1.543[a]	0.57[a] (±0.08)	-0.59[a]	0.170[a]
	1.489[b]	29.6[b] (±0.15)	-0.57[b]	0.000[b]
$C_6H_5CH_2NH$	1.538[a]	0.09[a] (±0.06)	-0.01[a]	0.290[a]
	1.530[b]	30.1[b] (±0.21)	0.00[b]	-0.040[b]

Charge transfer is commonly regarded as a crucial mechanism since, subsequent to the modification of carbon structures (such as graphene and carbon nanotubes), there are significant alterations in the properties of the material.[10] Therefore, we studied the charge transfer associated with the addition of a single linker onto a graphene sheet, as summarized in Table 6.2. The charge transfer was evaluated with Mulliken population analysis[18] and was defined as being the total charge on the NH group and carbon atom of the aromatic phenyl ring where the linker is attached. A positive number is associated with charge transfer from linker to substrate, whereas a negative number refers to charge transfer from substrate to linker[19]. The Mulliken population analyses show that a fraction of electron charge is transferred from graphene to the linker. The degree of charge transfer from graphene to the corresponding linker is slightly reduced, with longer alkyl chains and larger functional groups. This trend in degree of charge transfer can be comprehended on the basis of the relative electron-withdrawing capability of the aromatic ring and the electron donating capability of the alkyl chain. It is also noteworthy that charge transfer from graphene to the -

$C_6H_5CH_2NH$- linker is 0.01, which is considerably less than for the other linkers. Furthermore, as previously explained in Chapter 1, the covalent functionalization of carbon surfaces by aryl diazonium salts occurs in two steps. Initially, electron transfer from the carbon surface to the aryl diazonium cation is converted to an aryl radical following the loss of N_2. Due to the strong electron withdrawal effect, the relatively high reactivity, and the low activation barrier for aryl diazonium salt, such a reaction is mainly driven by the kinetics rather than by the thermodynamics.[2] Therefore, the coupling of diazonium radicals to carbon surfaces takes place more readily than that of amine radicals. For the modification of the basal plane of graphene modification, it is quite apparent that, apart from the diazonium linker, there is no charge transfer from linker to graphene. On the other hand, for the functionalization of edge plane graphene, charge transfer not only takes place from substrate to linker but also from linker to graphene sheet, which is further evidence for the more facile chemical attachment of these amine radicals to edge sites as compared to basal sites, since charge transfer to the surface reduces the energy barrier for the covalent binding of these amine radicals. The accompanying charge transfer in the opposite direction (to be discussed in Section 6.6) obviously lessens the required charge transfer to adsorbate, which facilities the attachment of these linkers to edge sites on graphene. In the case of diazonium coupling, not surprisingly, the magnitude of the charge transfer from linker to substrate is larger than for the amine radicals, as was expected considering the chemical attachment of this linker to pristine graphene.

6.5. Double-Functionalized Basal and Edge Planes

Next, we studied the effect of a second linker anchored to graphene. As displayed in Figure 6.3, the attachment of the first diamine linker causes unpaired electrons on the graphene sheet. These unpaired electrons are not present on a specific carbon atom but are distributed along the entire surface. Similar spin density distributions were also observed in the literature.[1,20-22] Figure 6.3 (a) and (c) plot the spin and total electron density distribution for an EDDA linker anchored to the basal plane of graphene. It is obvious that the spin densities mainly reside on the ortho and para atoms, implying that the second linker will be preferentially attached to these carbon atoms where the spin densities are highest. Figure 6.3 (b) and (d) also demonstrate the calculated spin and total density distributions for graphene with an H-terminated zigzag edge plane modified with a single EDDA linker. It is obvious that the spin densities are evenly localized onto both edge sites. Furthermore, it is rather

noticeable that the spin densities are partially present across the basal sites of the graphene sheet. As we move towards the edge sites, not only does the fraction of spin densities increases, but also their magnitude increases; this could explain why the edge plane is more reactive towards the electrochemically formed radicals .[23,24]

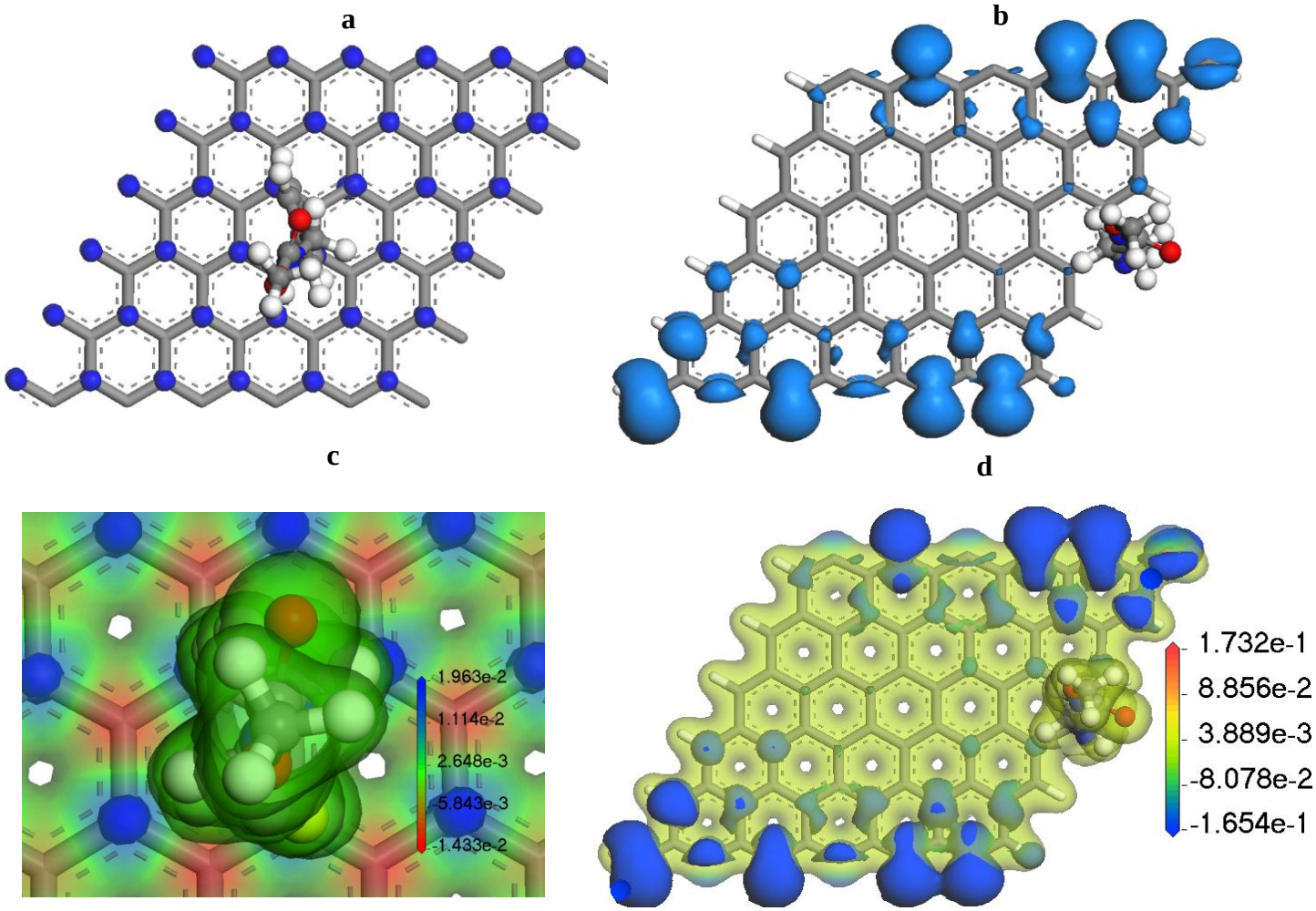

Figure 6.3. *Spin (a and b) and total (c and d) electron density representations for an EDDA linker anchored onto the basal (a and c) and edge plane (b and d) of a graphene sheet. Blue balls represent spin up and down densities. Regions coloured with red and yellow display charge accumulation and depletion, respectively.*

However, the attachment of a second linker to the ortho atoms of the aromatic rings already occupied by the first linker is unlikely when the size of the Boc protecting group is considered. The Boc Group covers 160 $Å^2$ so that, due to its steric effect, the first linker anchored is expected not to allow the next one to couple to the adjacent carbon atoms, which is 1 C-C bond away from the first anchored linker. As shown in Figure 6.4, various possible configurations were considered, and seven possible structures were computed for the addition of the second linker. Structures 1, 2, 2`, 3, 3`, 4 and 5 represent the addition of carbon atoms,

separated by 2, 3, 4, 5, and 6 C-C bonds, respectively. Structures 2` and 3` correspond to the attachment of 2 and 3 C-C bond separations where the positions are cis rather than trans to the original position. We included these in order to see what influence they had on the structural and electronic properties of the system.

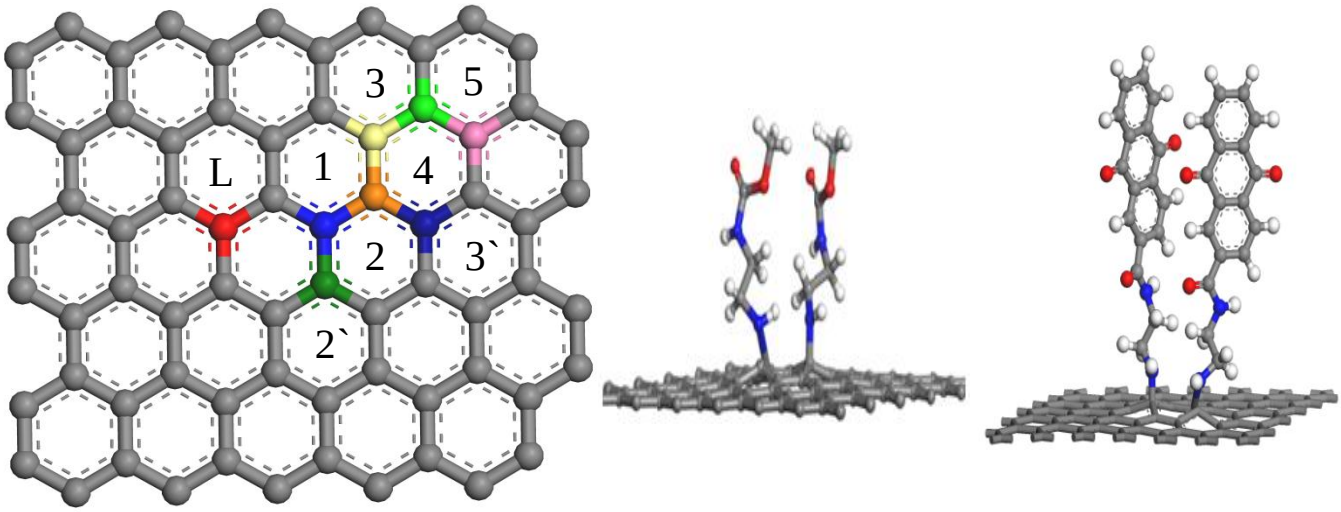

Figure 6.4. *Possible structures for the addition of a second linker to a graphene sheet. L represents the first anchored linker. Optimized geometries of a double EDA and EDA-AQ anchored onto graphene structures.*

As the values in Table 6.3 show, structures 1, 3, 4, and 5 are predicted to be the most stable ones for the EDA, BDA, HDA, EDDA, XDA and – $C_6H_5CH_2NH$- linkers, respectively. When the values of the binding energy calculated for the different positions of attachment of the second linker and AQ through the corresponding linkers to a pristine graphene sheet are examined in detail, it can be seen that, if the second linker is placed onto the para position of the aromatic ring where the first linker is attached, for all linkers, the binding energy for the attachment of the second linker was consistently found to be higher at ortho positions as compared to para positions and, not surprisingly, the meta position has the lowest binding energy for the anchored second linker. This finding is already expected due to the fact that the spin densities that emerge subsequent to the coupling of the first linker are concentrated at the ortho and para positions. Furthermore, it is noteworthy that, for the longer and bulkier diamine linkers, when two linkages are placed close to each other (for instance, in the case of structures I and II), the binding energy decreases significantly. This probably stems from steric repulsion. This can be underestimated, however, since methyl is used instead of t-butyl. On the other hand, if two longer and bulkier linkers are anchored onto the carbon atoms of the neighbouring aromatic rings, the binding energy tends to increase.

Table 6.3. *Binding energy for possible structures for the addition of a second linker and for AQ attached through linkers. Bold red and black numbers indicate the most thermodynamically stable structures for graphene anchored with single EDA linker and graphene anchored with single anthraquinone through EDA linker. Structure numbers refer to figure 6.4.*

Linker	Structure 1 E_{bind} /eV	Structure 2 E_{bind}/eV	Structure 3 E_{bind}/eV	Structure 4 E_{bind}/eV	Structure 5 E_{bind}/eV	Structure 2` E_{bind}/eV	Structure 3` E_{bind}/eV
EDA	**0.97**	0.49 (±0.01)	0.82 (±0.02)	0.64 (±0.04)	0.88 (±0.01)	0.55 (±0.01)	0.90 (±0.03)
EDA-AQ	**0.85**	0.50 (±0.04)	0.80 (±0.02)	0.52 (±0.04)	0.61 (±0.02)	0.44 (±0.04)	0.84 (±0.03)
BDA	0.50	0.31 (±0.02)	**0.90** (±0.01)	0.40 (±0.02)	0.45 (±0.01)	0.35 (±0.02)	0.82 (±0.02)
BDA-AQ	0.28	0.18 (±0.02)	**0.55** (±0.01)	0.22 (±0.03)	0.33 (±0.03)	0.28 (±0.02)	0.62 (±0.01)
HDA	0.35	0.30 (±0.05)	**0.70** (±0.04)	0.20 (±0.05)	0.30 (±0.04)	0.45 (±0.04)	0.58 (±0.04)
HDA-AQ	0.42	0.32 (±0.04)	**0.57** (±0.02)	0.22 (±0.04)	0.36 (±0.01)	0.38 (±0.05)	0.49 (±0.01)
XDA	0.25	0.40 (±0.06)	0.55 (±0.01)	0.30 (±0.02)	**0.60** (±0.04)	0.51 (±0.02)	0.47 (±0.01)
XDA-AQ	0.09	0.02 (±0.04)	0.11 (±0.06)	0.12 (±0.01)	**0.28** (±0.04)	0.08 (±0.02)	0.21 (±0.03)
EDDA	0.30	0.15 (±0.07)	0.35 (±0.04)	**0.45** (±0.01)	0.10 (±0.02)	0.24 (±0.03)	0.21 (±0.05)
EDDA-AQ	0.13	0.18 (±0.02)	0.33 (±0.03)	**0.41** (±0.01)	0.22 (±0.01)	0.31 (±0.02)	0.19 (±0.04)
$C_6H_5CH_2NH$	0.25	0.50 (±0.01)	0.30 (±0.02)	0.15 (±0.07)	**0.65** (±0.01)	0.35 (±0.04)	0.48 (±0.02)
$C_6H_5CH_2NH$ -AQ	0.54	0.32 (±0.04)	0.37 (±0.02)	0.41 (±0.05)	**0.78** (±0.01)	0.52 (±0.02)	0.55 (±0.02)

If subsequent additions were modelled in such a way that each linker group was anchored to carbon atoms by taking into account the area of the graphene surface occupied by the Boc group, then the results would be those depicted in Table 6.4. For instance, Structure 1, separated 1 C-C bond away from the first attached linker, was found to be the most thermodynamically stable configuration for the EDA linker. If the following EDA linkers are placed 1 C-C bond away from each other onto the basal plane of graphene till we reach up to a full monolayer, this leads to a surface coverage of 0.32 nmol cm^{-2}. If the same approach is pursued for the other linkers, we obtain surface coverages of 0.24, 0.24, 0.11, 0.11 and 0.14

nmol cm^{-2} for the BDA, HDA, XDA, $C_6H_5CH_2NH$ and EDDA linkers, respectively. As reported in Table 6.4, this finding is quite consistent with our experimental results obtained for the modification of a basal plane electrode with AQ through the diamine linkers.

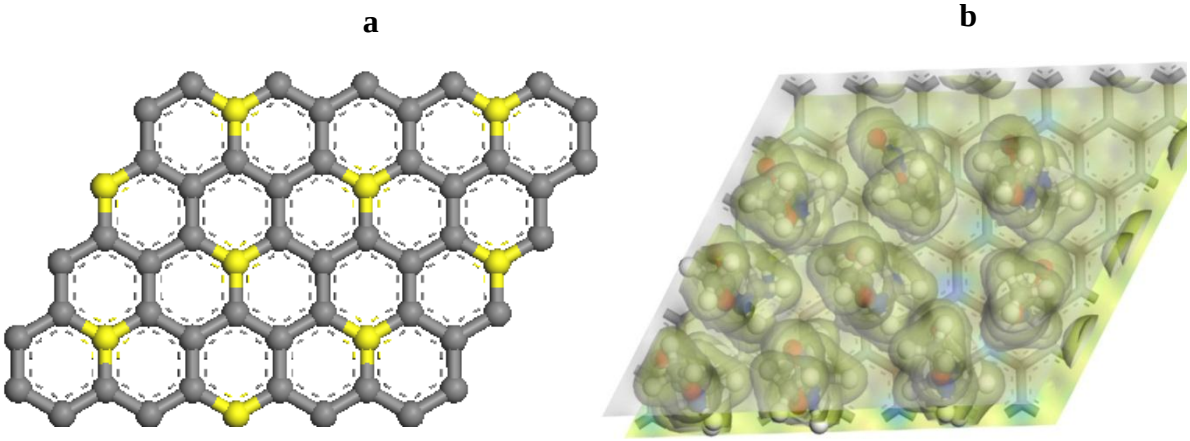

Figure 6.5. (*a) The representation of a full monolayer of BDA linker attached to the pristine graphene sheet in accordance with the largest binding energy calculated for the attachment of the second linker. Yellow balls show attachment sites. (b) displays the total electron density of a full monolayer of BDA linkers attached to graphene.*

Obviously, due to the probable surface roughness of the basal plane, it is naturally expected that experimentally obtained surface coverages of AQ are a bit larger than theoretical estimation. As seen in Figure 6.5, if BDA linkers are placed onto the pristine graphene sheet, by considering the most stable configuration for the attachment of the second linker, the pattern shown in Figure 6.5 (a) is obtained. In order to attain more reliable results, this calculation was also replicated when AQ was coupled to each linker for seven different configurations. It was found that similar tendencies were acquired for the seven possible cases, as shown in Table 6.3.

Table 6.4. *Comparison of the theoretical surface coverage of each linker and the experimental surface coverage of AQ.*

Linker	Experimental / Γ (nmol cm^{-2})	Theoretical / Γ(nmol cm^{-2})	Number of linkers anchored based on DFT calculation	Number of linkers anchored based on experiment
EDA	0.420 (±0.02)	0.32	15	19
BDA	0.350 (±0.04)	0.20	9	15
HDA	0.320 (±0.04)	0.20	9	14
XDA	0.240 (±0.02)	0.11	5	10
EDDA	0.170 (±0.01)	0.14	6	8
$C_6H_5CH_2NH$	0.145 (±0.03)	0.11	5	7

Such an alignment of the linkers across the graphene surface is referred to as low-range coupling,[2,3] which refers to the selective attachment of amine or aryl radicals to the carbon atoms of the aromatic rings, which are a certain number of C-C bonds away from the carbon atom where the related linker is attached. Since long-range coupling of molecules to the surface is based on the thermodynamics of each reaction,[2,3] the arrangement of the linkers illustrated above corresponds to the most stable structures. On the other hand, it is believed that the coupling of aryl radicals does not form such an arrangement onto the surface due to multilayer formation because of their higher reactivity. Zhu *et al.*[25] reported that Transmission Electron Microscopy (TEM) and Selected Area Electron Diffraction (SAED) prove that long-range ordering occurred for 4-nitrophenyl diazonium on graphene. However, in our case, as explained in Chapter 1, the Boc-protecting group prevents multilayer formation. We can therefore neglect the effect of multilayer formation caused by aryl radicals.

In order to understand why the attachment of the second linker to pristine graphene occurs preferentially at different positions for the different linkers, we need to determine whether the root cause of this effect is electronic, steric, or a combination of both. To do this, the surface coverage of EDA and XDA linkers on a pristine graphene layer was altered by individually adding linkers up to the highest surface coverage obtained experimentally. This was carried out by adhering them to the most thermodynamically stable structures (Structure 1 corresponds to the EDA linker and Structure 5 corresponds to the XDA linker), as reported

in Table 6.3. In Figure 6.6.a., there is a decrease in the charge transfer from graphene to linker, whereas the binding energy increases as more linkers are placed onto the graphene. This proves that the electronic effect does indeed have an influence on the subsequent additions of linkers. As shown in Figure 6.6.b., a similar calculation was also performed for the XDA linker (which is bulkier than EDA); it was found that the charge transfer from graphene to the EDA linker does not differ from the charge transfer from graphene to the XDA linker. This implies not only that the electronic effect has an impact on the modification of the basal plane of graphene but also that steric effects play quite a significant role in this system as well.[26]

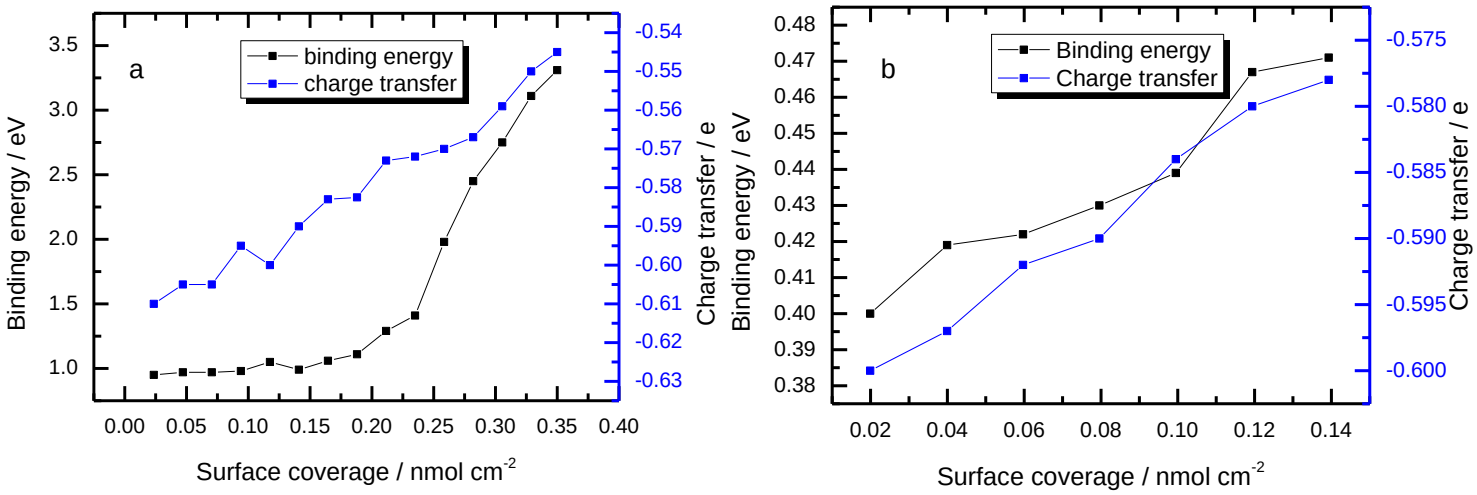

Figure 6.6. *Comparison of net charge transfer and binding energy for subsequent additions of the EDA (a) and XDA (b) linker onto a single graphene layer.*

It can be seen from Figure 6.6 that, as more linker is attached to the basal plane of graphene, the binding energy increases up to 3.5 eV for a full monolayer of EDA linker. Such a finding suggests that there is no strong repulsive intermolecular interaction amongst the linkers owing to the relatively large distance between each linker (around 2.3 Å); in such an arrangement, the EDA molecules do not repel each other strongly. In addition, each EDA and XDA linker is placed onto a graphene sheet on the basis of the most thermodynamically stable configuration (Structure I for EDA and Structure V for XDA). It is therefore expected that the covalent binding of these linkers to graphene supports the formation of such arrangements of linkers across the graphene surface. As shown in Figure 6.6 (a) and (b), the value of the charge transfer decreases as the number of attached linkers is increased, something found to be consistent with the literature.[1]

It is also notable that the binding energy does not change much at low surface coverage. This is perhaps in account of the fact that, when each linker is attached to the graphene surface, an unsymmetrical pattern is formed at lower surface coverage, which causes distortion in the geometry of the optimized graphene surface modified with EDA and XDA linkers. As more linkers are anchored to the graphene surface, it becomes more symmetrical. Furthermore, a symmetrical structure causes less distortion at the end of the geometry optimization calculation. Hence, a more stable structure is more likely to be obtained with respect to lower surface coverage at the surface. As a consequence of this enhanced stability, an increase in the binding energy at the higher surface coverage can possibly be obtained.

6.6. Electronic Properties of Modified Edge and Basal Sites

By considering HOMO and LUMO level of relevant organic substance, we can find out where attachment of chemical species to pi bonds will take place. HOMO and LUMO picture of EDDA linker (in radical form) is visualised by means of CASTEP. As seen in Figure 6.7 the HOMO is located on oxygen, carbon and nitrogen atoms, which are quite far away from nitrogen atom to be coupled to the carbon atom of aromatic ring on graphene, whereas LUMO is mostly present at N atom that is attached to the graphene during electrochemical process. In such orientation of the linker, we could therefore say that the contribution of LUMO to the attachment of this linker to graphene is incomparable to HOMO. Figure 6.9 shows the total spin polarized DOS for the functionalized graphene for EDA (a), EDDA (b), diazonium (c), and HDA (d) linkers. There is a distinctive peak around the Fermi level for spin up and spin down states. In order to detect the origin of these peaks, partial density of states (PDOS) were calculated for carbon atoms C (representing the carbon atom of the aromatic ring where the linker is attached on graphene) and C^* (the carbon atom of the aromatic ring anchored to the graphene surface for the case of diazonium coupling and the carbon atom next to the nitrogen atom in the alkyl chain of the amine linker), as well as for nitrogen (N) and oxygen (O).[27-29] As clearly seen in Figure 6.9, the peaks around the Fermi level predominantly originate from the 2p orbitals of the N or C atoms that are coupled directly to the aromatic ring of the graphene sheet. Furthermore, in the case of the attachment of the HDA linker to graphene, it is interesting to note that the C^* atom also makes a contribution to the total spin DOS of the system. This can also be verified by taking into account the spin density distribution around these N and O atoms, as seen in Figure 6.9; this

means that the spin densities around these atoms provide a certain amount of charge to the substrate. On the other hand, the contribution of the O atom is negligible with respect to the N atom. It is also noteworthy that, as the carbon atom in the chain moves away from the graphene surface, the contribution of these atoms to the total DOS lessens, as no spin density distribution is acquired onto these atoms.

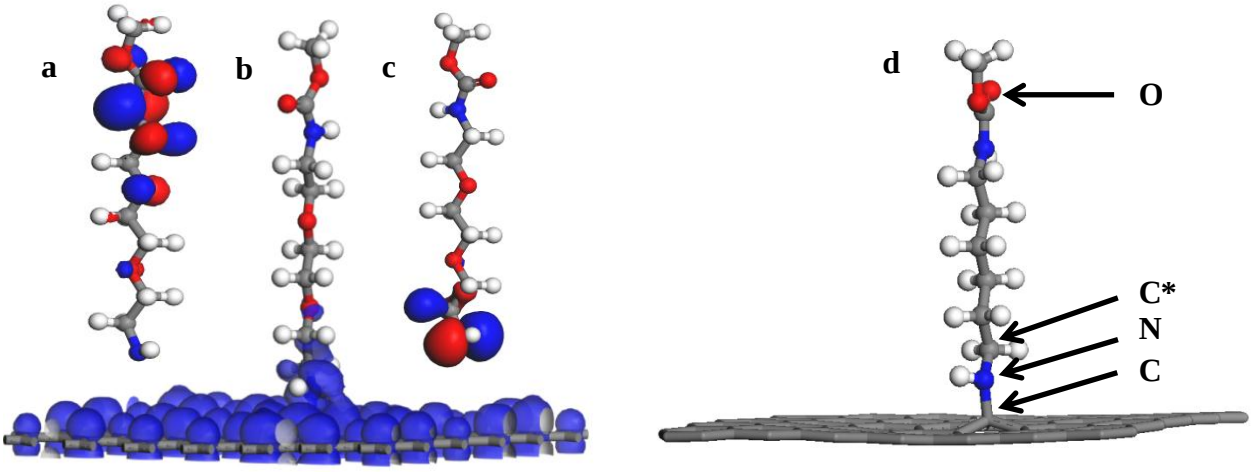

Figure 6.7. *(a) and (c) present the HOMO and LUMO of separated EDDA radicals, whereas (b) represents the spin density distribution of a single EDDA coupled onto the pristine graphene sheet. (d) represents the geometry optimized graphene functionalized with a single HDA linker. Arrows indicate the atoms upon which partial DOS was calculated in Figure 6.9.*

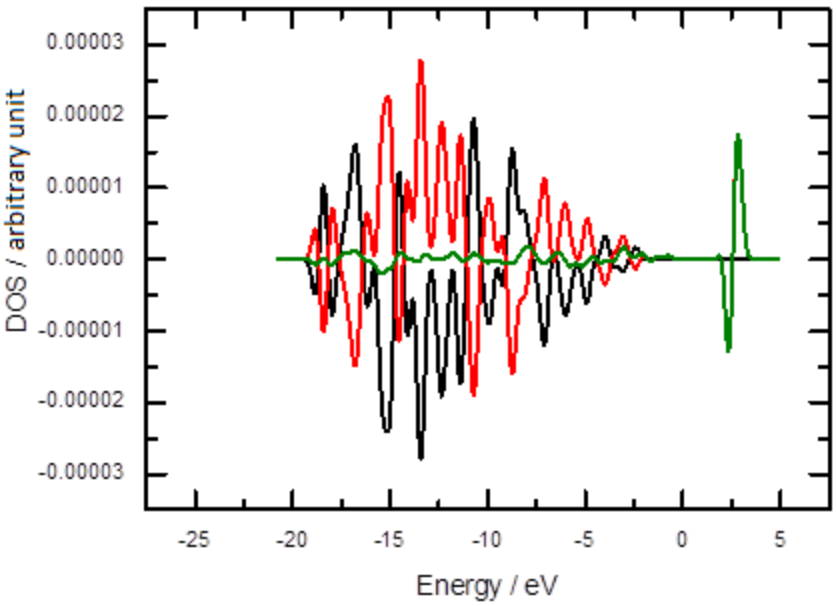

Figure 6.8. *Spin density of states for plain graphene. Black and red lines correspond to the spin densities originating from s and p orbitals, respectively. The green line represents the sum of the spin densities.*

As previously mentioned in Chapter 1 unmodified graphene exhibits a zero-gap semiconducting behaviour and its Fermi level crosses dirac point where valence and conduction bands touch each other. When we compare spin DOS of modified graphene with EDA, HDA, EDDA and diazonium linkers to unmodified graphene, it is quite noticeable the molecular level of the corresponding linkers at near the Fermi level. Undoubtedly these alterations near the Fermi level bring about a confined DOS band gap. On the basis of this outcome, it is noteworthy that semiconducting graphene without band gap has been converted into material that exhibits metallic behaviour. When graphene reacts with related amine radical, it is intrinsically expected that a charge transfer between substrate (graphene) and adsorbate (amine radical) takes place. Plotting spin DOS also permits us to work out band gap, which is described as difference between Highest Occupied Molecular Orbital (HOMO) where valance band is maximum and Lowest Unoccupied Molecular Orbital (LUMO) where conduction band is minimum. It also points out to the fact that how much energy is required to reach excited state from of relevant molecule from ground state. When a linker is attached to graphene surface, this gives rise to the sp^3 hybridization of carbon network, and a decrease in the delocalised sp^2 electrons. As a result of this, functionalization of graphene by addition of amine or aryl radicals leads to opening gap. When we take a close look at spin DOS of graphene modified with each linker, HOMO is 0.1 eV above Dirac point (Fermi level of graphene) and LUMO is 0.3 eV below Dirac point. Hence this leads to 0.4 eV band gap for modified-graphene through EDA, HDA, EDDA and diazonium linkers.

The LUMO of the EDA, EDDA and diazonium linkers on a graphene sheet are situated at around 0.3 eV, which can be related to the fact that this gives rise to a substantial amount of charge transfer from graphene to adsorbate. The HOMO of these linkers on the graphene sheet, however, is located at around -0.1 eV below the Fermi level. This also causes a very small amount of charge transfer in the opposite direction. Nevertheless, as the charge transfer through the HOMO is quite trivial compared to that which occurs via the LUMO, total charge transfer takes place towards the adsorbate.[30,31] As was mentioned previously, a charge transfer predominantly takes place from substrate to adsorbate and also from adsorbate to substrate, which is quite trivial. If the LUMO level of the electrochemically generated radical is below the Fermi energy of the graphene, then charge transfer occurs from the graphene valence band to the LUMO states of the amine radical.

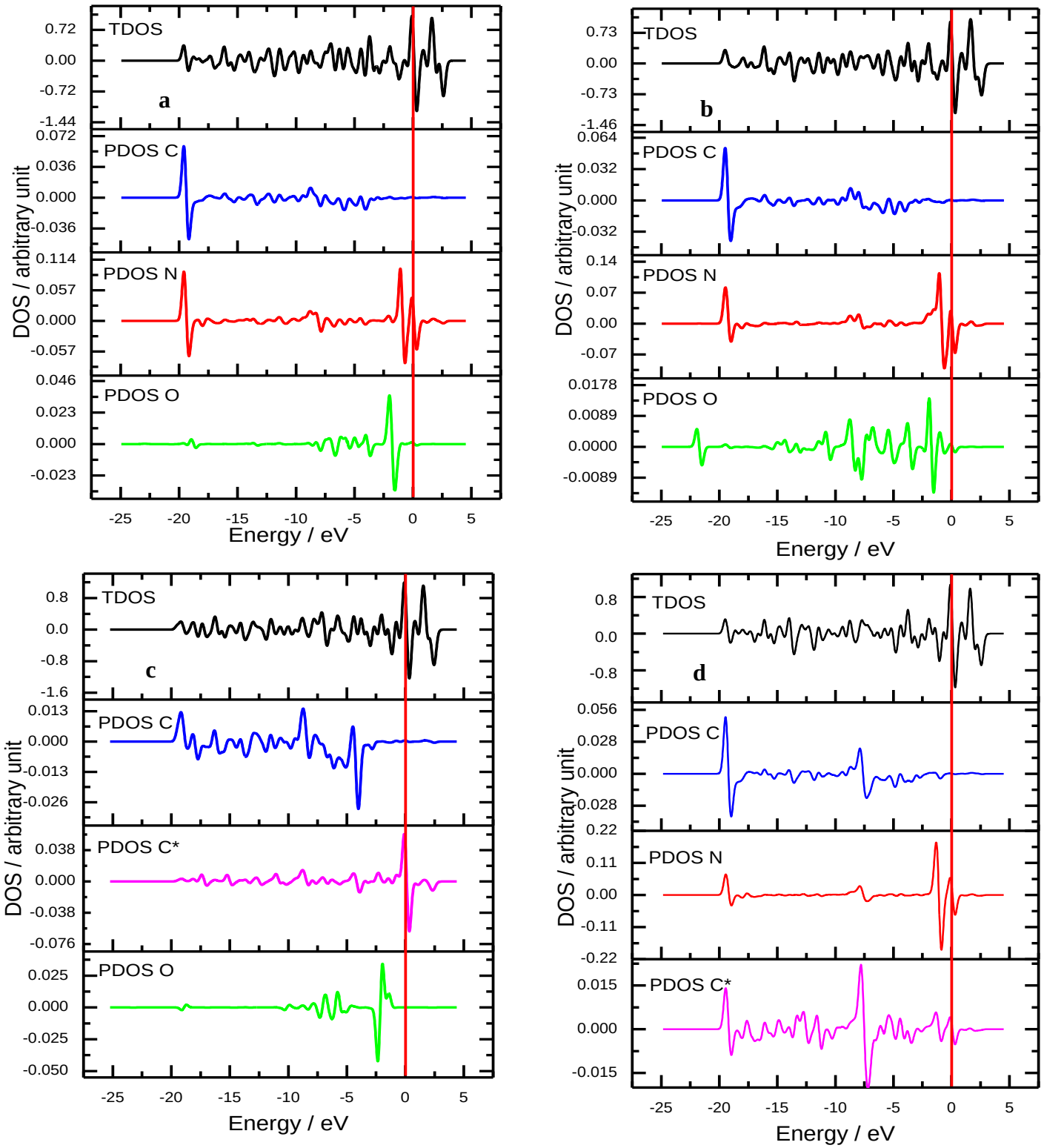

Figure 6.9. *TDOS (black line) and some PDOS for a single EDA (a), EDDA (b), diazonium (c) and HDA (d) linkers attached on the basal side of the graphene sheet. C (blue line), C* (pink line), N (red line) and O represent the carbon atom of the aromatic ring where the linker is bonded, the carbon atom that forms a chemical bond with graphene in the case of the diazonium coupling, the carbon atom next to the nitrogen atom in the alkyl chain of the amine linker, the nitrogen atom of diammine linker coupled to graphene, and the oxygen atom of the carboxyl group.*

The total spin DOS for H-terminated graphene ribbon with edge sites modified by EDA and dizonium spacers are shown in Figure 6.10. It is quite evident that the functionalization of the edge sites with these linkers enhances the conductivity of the entire system because of an immense increase in the peaks around the Fermi level.[32] Moreover, as for the functionalization of the basal plane of graphene, the Figure 6.10 a and b show that these distinctive peaks near the Fermi level are mainly contributed by N and C* atoms. However, contrary to the modification of the basal sites of graphene, in the case of the functionalization of the edge sites of graphene through EDA and diazonium spacers, from the partial DOS analysis, there are small peaks around the Fermi level originating from C atoms, which indicates that these carbon atoms also make a contribution to the electronic structure of the system. As a result of this, a certain amount of charge is transferred from adsorbate to substrate. These sharp peaks around the Fermi level also lead to a more robust binding between the linker and the edge sites of graphene.[33] This is also consistent with our previous results regarding the binding energy for each linker calculated for edge site functionalization, as relatively more energy is gained relative to the basal site of graphene.

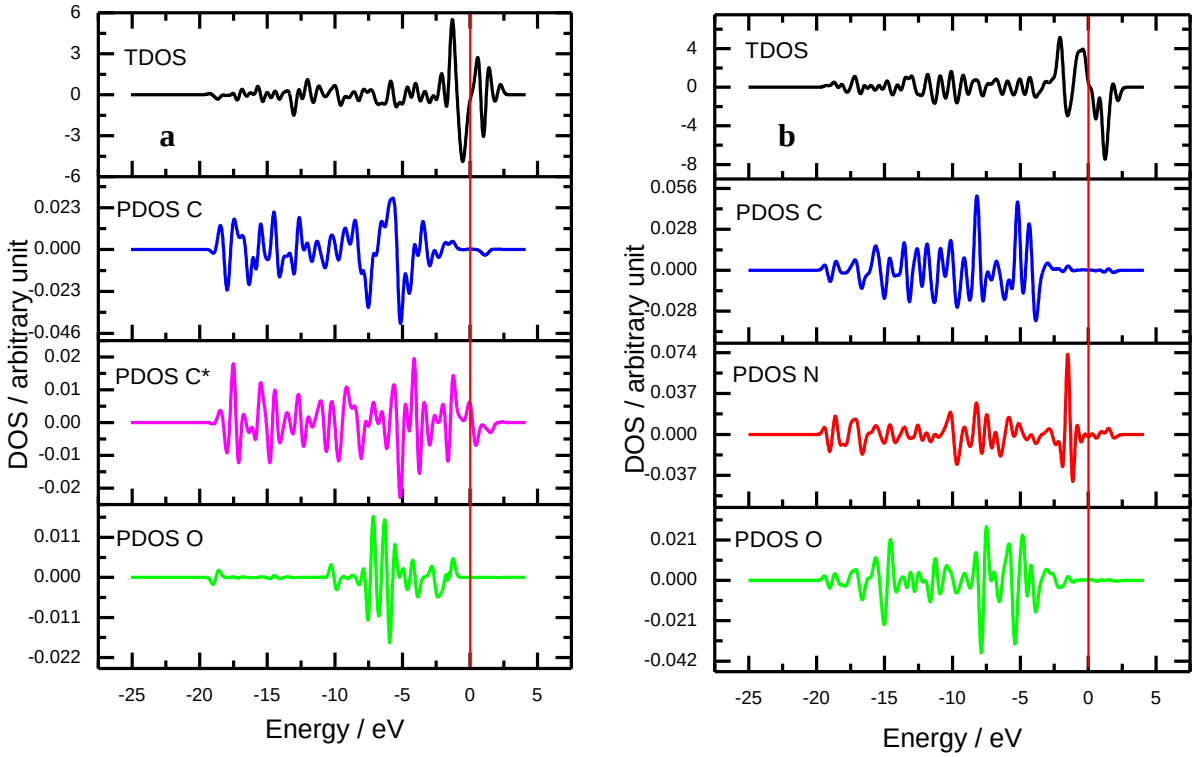

Figure 6.10. *TDOS (black line) and some PDOS for a single diazonium (a) and EDA (b) linker attached on the edge site of the graphene sheet. C (blue line), C* (pink line), N (red line) and O represent the carbon atoms of the aromatic ring where the linker is bonded, the carbon atom that forms a chemical bond with the graphene in the case of diazonium coupling, the nitrogen atom of the diamine linker coupled to graphene, and the oxygen atom of the carboxyl group.*

As shown in Figure 6.3, based on the spin density distribution at the edge site of graphene functionalized with an EDDA linker, the localization of spin densities on the H-terminated edge site and the basal site of a graphene ribbon, one can definitely expect that the band gap following the functionalization of edge and basal sites would be different. In pristine ribbons, as previously shown, C atoms distributed along the edge sites are more reactive. On the basis of this explanation, edge sites can be associated with a wider band gap compared to basal sites. As can be clearly seen in Figures 6.9 and 6.10, as a result of functionalization with the electrochemically generated EDA and diazonium linkers, the basal plane of graphene has a smaller band gap by 0.7 eV compared to the functionalized edge plane of graphene. This is in good agreement with our explanation above, as well as with the literature.[34,35]

It is also interesting to explore the effect which the number of linkers anchored onto a single layer of graphene has on the electronic properties of graphene. Figure 6.11 presents the total spin density for 3, 6, 9, and 12 EDA groups linked to a graphene sheet. It should be noticed that the electronic properties of graphene are affected by the number of linkers attached to the graphene ribbon. When an odd number of linkers are attached to the graphene, it exhibits a smaller band gap compared to when an even number of linkers are attached TO the graphene, which is in good agreement with the literature.[1]

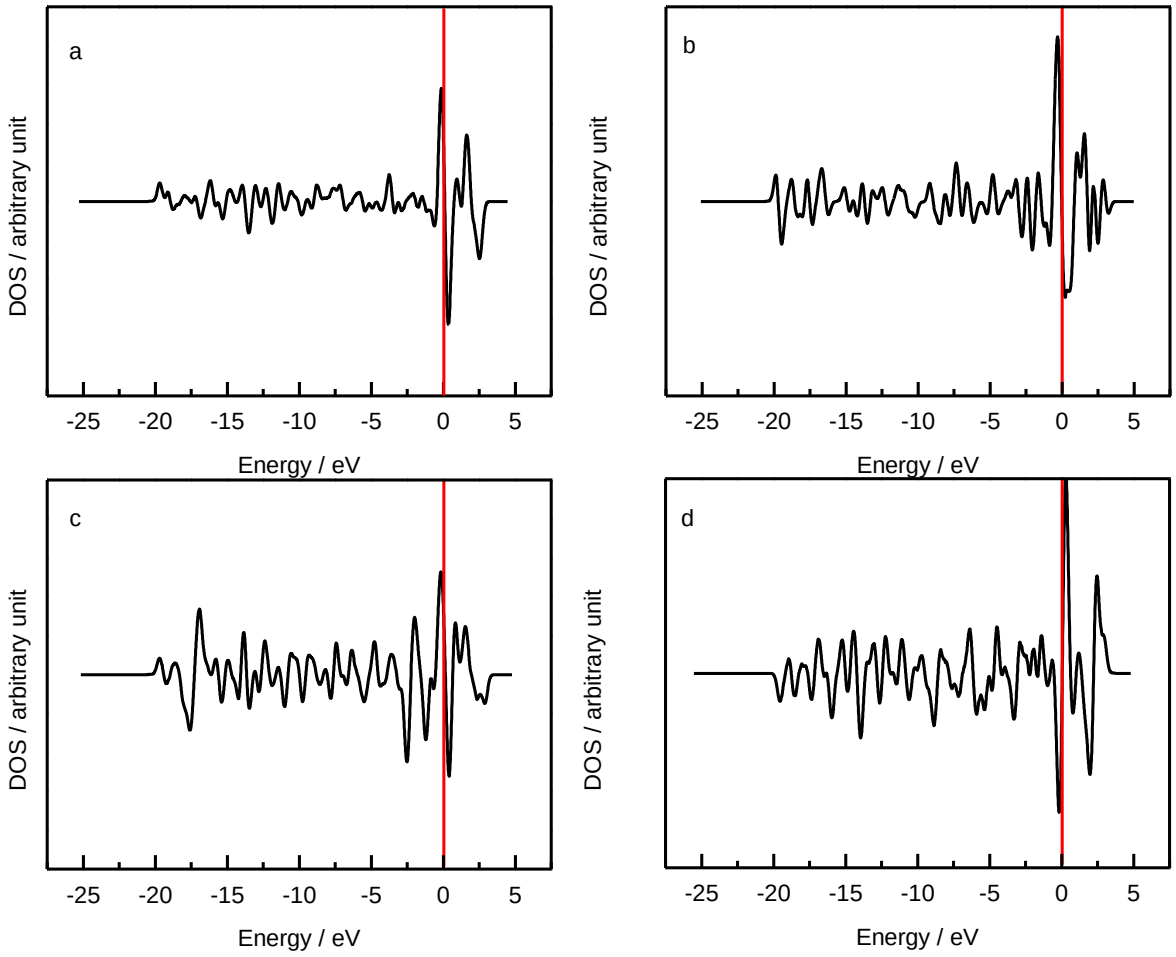

Figure 6.11. *TDOS of the 3 (0.064 nmol cm^{-2}), 6 (0.128 nmol cm^{-2}), 9 (0.192 nmol cm^{-2}) and 12 (0.256 nmol cm^{-2})-attached EDA linker to graphene sheet. The size of the graphene sheet is ~ 715 Å^2.*

6.7. Conclusion

We have investigated the functionalization of graphene by mono Boc-protected diamine and diazonium linkers using DFT. The edge plain was found to be more reactive since significantly more binding energy was gained compared to the basal plane. The interactions between the basal plane of graphene and the linker cause changes in the geometry and the electronic structures of the pristine basal plane of graphene. DFT has given us in depth insight into understanding our experimental results; it has also confirmed the experimental findings of Chapter 3 regarding the higher reactivity of edge sites towards the attaching of amine or aryl radicals in comparison to basal sites since more binding energy

was gained for the formation of the C-C or C-N bonds at the edge sites. Furthermore, as stated in Chapter 3, the type of linker seemed to have an influence on the surface coverage of AQ coupled to those linkers after the removal of the Boc protecting group. Our DFT calculations show that the binding energy for the attachment of single linkers to the basal plane of graphene exhibited exactly the same tendency as for the surface coverage of AQ for each linker. By taking the binding energy of each linker into account, it is also worth noting that the chemical bond between the amine linker and graphene is rather strong, whereas for the diazonium linker is very weak. In order to find out the most stable structures for the attachment of a second linker, seven possible scenarios were considered. By considering binding energy results obtained for the double functionalization of graphene with linkers and the size of each linker, the corresponding linker was anchored to the most thermodynamically stable carbon atom of the aromatic ring until a full monolayer was obtained. It was found that, in terms of the surface coverage of AQ, such an arrangement of linkers across the graphene surface gave rise to consistent results, as compared to the experimental results obtained for the basal plane of HOPG. By anchoring subsequent additions of EDA and XDA linkers on graphene, we attempted to understand why different types of linker are more favourably attached to the different carbon atoms of the neighbouring aromatic rings; the role of steric and electronic effects were found to be involved in this mechanism. Electronic properties of graphene also drastically changed after functionalization since the DOS of pristine graphene near the Fermi level was found to be greatly changed. This certainly led to the opening of band gaps in the graphene. The addition of an odd number of linkers to the graphene resulted in a small band gap—as compared to the addition of an even number of linkers. Therefore, the functionalized graphene surface with an odd number of linkers is expected to exhibit higher conductivity.

To sum up, the reactivity of edge sites to the coupling of any type of radical is certainly correlated with the chemical properties of carbon electrodes such as carbon nanotubes, glassy carbon, HOPG and carbon fibres, which are known to possess large proportions of edge defects. On the other hand, because of the surface heterogeneities of these carbon materials, it is really difficult to establish a relationship between the chemical reactivity of carbon materials and the theoretical evidence from the point-of-view of first principles density functional theory with spin polarized calculations[33]. This chapter has not only provided a further explanation for the experimental results but also an application for graphene in chemical sensors, biosensors and bioelectronics.

6.8. References

(1) J-X. Zhao; Y-H. Ding *J. Phys. Chem. C*, **2008**, *112*, 13141.

(2) G. L. C. Paulus; Q. H. Wang; M. S. Strano *Acc. Chem. Res.* **2013**, *46*, 160.

(3) S. Niyogi; E. Bekyarova; J. Hong; S. Khizroev; C. Berger; W. de Heer; R. C. Haddon *J. Phys. Chem. Lett*. **2011**, *2*, 2487.

(4) E. R. Margine *Nano Lett*. **2008**, *8*, 3315.

(5) L. Mandeltort; P. Choudhury; J. K. Johnson; J. T. Yates *J. Phys. Chem. C* **2012,** , *116*, 18347−18357.

(6) D. W. Boukhvalov; M. I. Katsnelson; A. I. Lichtenstein *Phys. Rev. B* **2008,**, *77*, 35427.

(7) D. W. Boukhvalov; M. I. Katsnelson *J. Phys. D: Appl. Phys.* **2010**, *43*, 175302.

(8) P. A. Denis; Iribarne, F. *Int. J. Quant. Chem*. **2010**, *110*, 1764.

(9) J. Zhao; H. Wang; B. Gao; X. Wang; Q. Cai; X. Wang *J Mol Model* **2012**, *18*, 2861.

(10) M. Segall; P. Lindan; M. Probet; C. Pickard; P. Hasnip; S. Clark; M.Payne *J. Phys. Condens. Matter* **2002**, *14*, 2717

(11) H. J. Monkhorst; J. D. Pack *Phys. Rev. B* **1976**, *13*, 5188

(12) J. Zhao; Y. Yu; Y. Bai; Lu, B.; Wang, B. *J. Mater. Chem*. **2012**, *22*.

(13) M. A. Ghanem; I. Kocak; A. Al-Mayouf; M. AlHoshan; P. N. Bartlett *Electrochim. Acta* **2012**, *68*, 74.

(14) R. Scipioni; M. Pumera; M. Boero ; Y. Miyahara; T. Ohno *J. Phys. Chem. Lett*. **2010**, *1*, 122.

(15) B. C. Wood; S. Y. Bhide; D. Dutta; V. S. Kandagal; A. Deep Pathak; S. N. Punnathanam; K. G. Ayappa; S. Narasimhan *J. Chem. Phys.* **2012**, *137*, 54702

(16) X. Wu; W. An; X. C. Zeng *J. Am. Chem. Soc.* **2006**, *128*, 12001.

(17) C. E. Junkermeier; D. Solenov; T. L. Reinecke *J. Phys. Chem. C.* **2013**, *117*, 2793.

(18) M. D. Segall; C. J. Pickard; R. Shah; M. C. Payne *Mol. Phys.* **1996**, *89*, 571.

(19) N. Al-Aqtash; I. Vasiliev *J. Phys. Chem. C.* **2011**, *115*, 18500.

(20) J. Dai; J. Yuan *J. Phys.: Condens. Matter* **2010**, *22*, 225501.

(21) K. Kusakabe; M. Maruyama *Phys. Rev. B* **2003**, *67*, 92406.

(22) P. Huang; L. Jing; H. Zhu; X. Gao *Acc. Chem. Res* **2012**, *46*, 43.

(23) K. Nakada; M. Fujita *Phys. Rev. B* **1996**, *54*, 17954.

(24) B. Huang; F. Liu; J. Wu; B-L. Gu; W.i Duan *Phys. Rev. B* **2013**, *77*, 153411.

(25) H. Zhu; P. Huang; L. Jing; T. Zuo; Y. Zhao; X. Gao *J. Mater. Chem.* **2012**, *22*, 2063.

(26) O. R. Inderwildi; D. Lebiedz; O.Deutschmann; J. Warnatz *ChemPhysChem* **2005**, *6*, 2513.

(27) Y. Zhang; C. Suc; Z. Liu; J. J. Li *Phys. Chem. B* **2006**, *110*, 22462.

(28) P. Plachinda; D. R. Evans; R. Solanki *J. Chem. Phys.* **2011**, *135*, 44103.

(29) L. Yuan; Z. Li; J. Yang; J. G. Hou *Phys. Chem. Chem. Phys.* **2012**, *14*, 8179.

(30) O. Leenaerts; B. Partoens; F. M. Peeters *Phys. Rev. B* **2008**, *77*, 125416.

(31) D.S.L. Abergel; V. Apalkov; J. Berashevich; K. Ziegler; T. Chakraborty *Advances in Physics* **2010**, *59*, 261.

(32) C. Wang; G. Zhou; H. Liu; J. Wu; Y. Qiu; B. L. Gu; W. Duan *J. Phys. Chem. B.* **2006**, *110*, 10266.

(33) D. Jiang; B. G. Sumpter; Sheng Dai *J. Chem. Phys.* **2007**, *126*,, 134701.

(34) F. Cervantes-Sodi; G. Csányi; S. Piscanec; A. C. Ferrari *Phys. Rev. B* **2008**, *77*, 165427.

(35) F. Cervantes-Sodi; G. Csányi; S. Piscanec; A. C. Ferrari *Phys. Stat. Sol.* **2008**, *245*, 2068.

Chapter 7

FUTURE SUGGESTIONS

7.1. Future Work

In Chapter 3, the modification of graphite electrodes with edge and basal sites and GC electrodes with AQ was achieved through the electrochemical oxidation of five different diamine linkers and the reduction of a $C_6H_4CH_2NH$- linker. The characterization of these AQ-modified carbon electrodes was carried out using cyclic voltammetry, and reversible behaviour, with peak potentials that alter with changing pH values consistent with the expected Nernstian value, were found. Furthermore, the electrochemical properties of anthraquinone and its derivatives in protic and aprotic solutions are quite different as two waves and one wave are observed, respectively, because hydrogen bonding stabilises the dianion form of quinone.[1,2] In our work, since we used linkers with an aromatic ring or with different lengths of alkyl chain and with flexible linkers, we could expect that local solvation around these linkers would be different in different media, which certainly affects the shape of voltammograms. Therefore, simulating and analysing the redox behaviour of AQ at different pH values by means of the "scheme of squares" (initially introduced by Jacq[3] and shown in Scheme 7.1) would be quite interesting work to carry out in order to compare the experimental and simulated voltammograms, especially as low proton concentration is known to have an effect on the voltammogram of carbon electrodes modified with AQ. Batchelor-McAuley *et al.*[4] applied the model of two proton two electron reduction to anthraquinone disulfonate (AQDS) and anthraquinone monosulfonate (AQMS) dissolved in un-buffered solution with different pH values. Moreover, for the multi-electron transfer process, Compton`s group[5,6] have devoted enormous efforts to gain insight into the dependency of the cyclic voltammogram response on the difference in the potential for the first and second electron transfers in order to simulate cyclic voltammograms using a wide range of models, such as the Marcus-Hush theory,[7-10] the Butler-Volmer model,[11,12] and the Randles–Ševcík[13] equation. It would therefore be really interesting to carry out these for the simulation of our experimental results for AQ-modified carbon electrodes. Hence, we can find out how peak shape, in terms of peak width, peak height, and peak to peak separation alters with applied potential and how electron transfer rates deviate from the theoretical ones obtained with Laviron analysis; indeed, the voltammetric peak width, height, and peak-to-peak separation is found to vary as a function of this difference in potential.

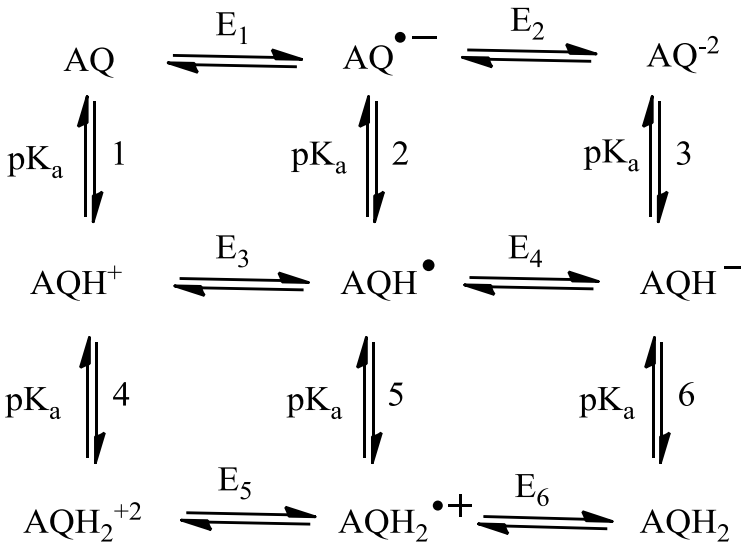

Scheme 7.1. ``*Scheme of Squares*`` *model for the reduction of anthraquinone.*

The reduction of quinone derivatives in aprotic solutions occurs by two successive one electron reduction steps generating Q^- and Q^{-2}. In the first step, two reversible cathodic waves is observed, whereas the second step is quasi-reversible.[14-17] Moreover, if the peak current for the first and second reduction waves are plotted against the square root of the scan rate, a linear relationship is attained, indicating a diffusion-controlled process.[2] Semiquinones, formed in the first step, are rapidly disprotonate, generating a quinone and its corresponding dianion (as it is short lived[18]). On the other hand, it is well known that the reduction of both oxygen and quinones greatly depends on the medium used. The solubility of oxygen in aprotic media is much higher than in aqueous solutions (for example, by a 5 factor in acetonitrile); subsequently, superoxide species are thermodynamically more stable.[19] Since a vast majority of the literature concentrates on the electrochemical reduction of quinone and oxygen using quinone derivatives, it would be worth exploring the electrochemical properties of AQ-modified graphite electrodes in non-aqueous media in the presence and absence of oxygen. The addition of a proton source into the solution also would dramatically alter the voltammetry. For instance, Hui *et al.*[20] and Lim *et al.*[21] investigated the electrochemical behaviour of vitamin K (phylloquinone) in acetonitrile in the presence of Bu_4NPF_6 as a supporting electrolyte. They found that the separation between the first and second electron transfer steps decreased as the concentration of the water in the solvent increased; and, when the concentration of the water reached up to 7 M, only one process was observed, referring to the fact that peak separation between the first and second waves diminished. Similar work can also be performed using the electrodes modified with AQ

through different types of diamine linkers. A reason for choosing different linkers bearing different atom functionalities is because they are thought to be affected by the local solvation as more proton source is added into the aprotic solvent.

The electrochemical oxidation of NADH to NAD^+ is basically an H^- transfer. (there has, however, been some discussion over whether it sequentially proceeds or whether it has a one-step mechanism). It is one of the most significant reactions due to its significant involvement as a cofactor in electron transfer in biological systems, such as enzymatic reactions.[22-24] Consequently, the construction of electrodes that are capable of oxidising NADH to NAD^+ has drawn substantial interest owing to their potential application in the fields of biosensors and biofuel cells. The electrochemical oxidation of NADH to NAD^+ at plain carbon and metal electrodes exhibits irreversible behaviour and one of the characteristic attributes of this reaction is the large activation barrier, as a result of which the corresponding anodic irreversible peak appears at high over-potential.[25-27] Furthermore, the persistent adsorption of NADH and its oxidized form, NAD^+, cause the fouling or passivation of the electrode surface and a decrease in the current. If this system is employed in biosensors, it leads to an interference that stems from the oxidation of side moieties in the sample and a lack of sensitivity, reproducibility and stability.[28,29]. In order to overcome these problems, a considerable amount of effort has been paid to find suitable mediators which are able to make the electron transfer between NADH and the substrate faster. For instance, quinone derivatives,[30] catechol,[31] ferrocene,[32] ruthenium complexes[1] have all been used to modify graphite electrodes to catalyse NADH oxidation. In Chapter 3, we have shown that the functionalization of GC and graphite electrodes with edge and basal plane orientation with dihydroxybenzene compounds through an EDA linker is successful. Ghanem *et al.*[30] have shown that di-HB modified GC electrodes have a catalytic influence on NADH oxidation as there is an increase in the peak current and a shift towards less positive values compared to bare GC electrodes. Edge sites are also more resistant to passivation compared to GC electrodes. Therefore, it would be interesting to find out how di-HB modified and unmodified graphite, GC electrodes and carbon nanotubes behave for the electrochemical oxidation of NADH. Pumera *et al.*[28] investigated the effect of different sites on graphene in NADH oxidation using a molecular dynamic simulation. When NAD^+ is oriented near the basal and H terminated edge sites that contain carboxyl and hydroxyl groups, a strong interaction is observed between NAD^+ and the carboxyl and hydroxyl groups, whereas no notable energy is gained when NAD^+ is placed close to basal sites of graphene or edge sites

of graphene only terminated with H. Similar work by the same research group[33] was also carried out for CNT, as its wall and tube ends are considered as basal and edge sites, where they utilised a similar molecular dynamics simulation and achieved similar results. Hence, the verification of the reactivity of di-HB modified edge and basal plane electrodes with respect to unmodified graphene using a molecular dynamics simulation would be a novel and interesting study as, to the best of our knowledge, there is no literature in this area.

In Chapters 3 and 5, we showed that it is possible to sequentially functionalize graphite electrodes with different redox centres, such as anthraquinone (AQ), nitrobenzene (NB) and dihydroxybenzene (di-HB), through an EDA linker. Likewise we showed that we can carry out a two electron reduction of oxygen to H_2O_2 catalysed by AQ moieties coupled with the carbon surfaces. We also showed that there was a significant change in oxygen reduction after the coupling of AQ as compared to plain carbon electrodes. It would therefore be worth investigating the effect of the alteration of the environment around AQ with electron donating and withdrawing organic functionalities on the O_2 reduction since the existence of electron withdrawing groups, such as -NO_2, -CN, and -CO_2, are anticipated to shift the peak potential of O_2 reduction towards more positive values.[34] Moreover, to the best of our knowledge, there is no literature regarding the effect of the chemical attachment of electron withdrawing and donating groups on the rate of oxygen reduction. To sum up, a comparison of the kinetics of oxygen reduction on bi-functionalized carbon electrodes with the AQ immoblised alongside either electron donating or withdrawing groups through different linkers with different lengths would be an interesting and novel study. In Chapter 5, we investigated O_2 reduction on unmodified and AQ-modified edge plane, basal plane, and GC electrodes. It was found that all these modified electrodes behave differently towards the catalysis of O_2 reduction as there was a significant difference in the peak potentials and peak currents amongst them. It is hence worth exploring modelling an O_2 reduction driven by surface bound AQ-edge plane, basal plane and GC electrodes. Li *et al.*[35] simulated the voltammetry of oxygen reduction on boron-doped diamond electrodes in a solution containing anthraquinone monosulfonate in order to verify the existence of a semiquinone intermediate product and its involvement in O_2 reduction. The simulation was carried out on the basis of reactions (1) and (2) above using the commercially available software ``DIGISIM``.

$$AQ^{\bullet -} + O_2 \rightleftharpoons AQ + O_2^{\bullet -} \quad (7.1)$$

$$AQH^{-} + O_2 \rightleftharpoons AQ + HO_2^{-} \quad (7.2)$$

Reaction 1 corresponds to a one electron reduction of oxygen to superoxide anion through a semiquinone intermediate, which is regarded as quite reactive and can be converted to molecular oxygen or hydrogen peroxide with protonation and deprotonation, respectively. Reaction 2 represents a two electron, one proton reaction of oxygen to HO_2^-. If these two reactions are used for a simulation of the voltammogram of AQ in the presence of oxygen for the carbon electrodes used in this study, we can make a comparison between theoretical and experimental outcomes.

In Chapter 4, it was demonstrated that it was possible to functionalize multi-walled carbon nanotube (MWCNT) with anthraquinone and nitrobenzene via either the electrochemical oxidation of EDA or the electrochemical reduction of $C_6H_4CH_2NH$- linkers or by the spontaneous attachment of the $C_6H_4CH_2NH$- linker. As previously mentioned, Ghanem *et al.*[30] investigated NADH oxidation on a library of twenty five GC electrodes modified with dihidroxy benzene compounds bearing different functional groups on the aromatic ring. By adopting a similar logic, it seems quite applicable to examine the electrochemical and chemical modifications of MWCNT with di-HB using solid phase synthesis methodology for NADH oxidation and to see how it differs from the di-HB modified graphite electrodes.

Recently in our research group, Pinczewska *et al.*[36] reported high-throughput screening of sixty four modified GC electrodes with ruthenium (II) and zinc (II) complexes that have the redox centre phendione by four different types of diamine linkers in order to catalyse an NADH oxidation. In Chapter 5, we also explored a four electron reduction of oxygen to water for a library of twelve GC electrodes by means of laccase immobilized on anthraquione and anthracene coupled to EDA and $C_6H_4CH_2NH$- linkers with the aid of high throughput screening. It is possible to take this idea a bit further with a wider range of species (to be chosen by considering their hydrophobic and hydrophilic properties). It was also shown in Chapter 5 that there is almost a linear relationship between oxygen concentration

and catalytic peak current. On the basis of such a finding, the kinetic parameters (k_{cat} and K_M) can be calculated using equation 7.1.

$$I_{cat} = \frac{nFA\Gamma k_{cat} c}{c + K_M} \qquad \text{Equation 7.1}$$

where n is the number of electrons transferred, F the Faraday, A the area of the electrode, Γ the enzyme coverage, and c the oxygen concentration. Once the bioelectrocatalytic current, I_{cat}, is plotted versus the oxygen concentration for different values of scan rate, it allows us to obtain $k`_{ME}$ and K_{ME} using equation 7.2 and, as a consequence of this, k_{cat} and K_M can be calculated with equations 7.3 and 7.4

$$i = nFA\frac{k`_D}{2}\left\{(K_{ME} + c) - \sqrt{(K_{ME} + c)^2 + 4k`_{ME}K_{ME}ck`_D}\right\} \qquad \text{Equation 7.2}$$

$$k_{cat} = K_{ME}k`_{ME}/\Gamma \qquad \text{Equation 7.3}$$

$$K_M = K_{ME}(1-k`_{ME}/k`_D) \qquad \text{Equation 7.4.}$$

To sum up: significant progress has been made in constructing reproducible and stable carbon electrodes functionalized with different redox centres, such as anthraquinone, nitrobenzene and dihydroybenzene, through different types of linkages. The catalytic activity of AQ-modified carbon electrodes and GC electrodes immobilized with laccase through anthraquinone and anthracene were also investigated. The first principles density functional theory simulation of carbon surfaces modified by the electro-reduction or oxidation of all linkers used in this study was also carried out on the basis of results obtained for basal plane electrodes. However, as mentioned above, there remain a great deal of ideas to be applied and works to be carried out. E.g. : a comparison of cyclic voltammograms for AQ-modified carbon electrodes with simulated ones for the purpose of finding out how the electron transfer rate constant alters with the type of carbon electrode and linker; how modified carbon electrodes with AQ by different linkers behave in the aprotic, as well as protic and aprotic, solvents; the molecular dynamic simulation of NADH oxidation on unmodified and modified surfaces with dihydroybenzene; and a high-throughput screening of a library of GC electrodes immobilised with laccase in order to catalyse an oxygen reduction.

7.2. References

(1) A. Ashnagar; J. M. Bruce; P. L. Dutton; R. C. Prince *Biochimica et Biophysica Acta* **1984**, *801*, 351.

(2) P. S. Guin; S. Das; P. C. Mandal *Int. J. Electrochem.* **2011**, *10*, 1.

(3) Jacq, J. *J. Electroanal. Chem.* **1971**, *29*, 149.

(4) C. Batchelor-McAuley; B. R. Kozub; D. Menshykau; R. G. Compton *J. Phys. Chem. C* **2011**, *115*, 714.

(5) K. R. Ward; N. S. Lawrence; R. S. Hartshorne; R. G. Compton *Phys. Chem. Chem. Phys.* **2012**, *14*, 7264.

(6) D. Menshykau; C. Batchelor-McAuley; R. G. Compton *J. Electroanal. Chem.* **2011**, *651* 118.

(7) B. R. Kozub; M. C. Henstridge; C. Batchelor-McAuley; R. G. Compton *ChemPhysChem* **2011**, *12*, 2806.

(8) M. C. Henstridge; E. Laborda; E. J. F. Dickinson; R. G. Compton *J. Electroanal. Chem.* **2012**, *664*, 73.

(9) M. C. Henstridge; C. Batchelor-McAuley ; R. Gusmão; R. G. Compton *Chem. Phys. Lett.* **2011**, *517*, 108.

(10) M. C. Henstridge; E. Laborda; R. G. Compton *J. Electroanal. Chem.* **2012**, *674*, 90.

(11) M. C. Henstridge; N. V. Rees; R. G. Compton *J. Electroanal. Chem.* **2012**, *687*, 79.

(12) E. Laborda; M. C. Henstridge; R. G. Compton; A. Molina; F. Martinez-Ortiz *J. Electroanal. Chem.* **2011**, *660*, 169.

(13) C. B.-McAuley; R.G. Compton *J. Electroanal. Chem.* **2012**, *669*, 73.

(14) N. Gupta; H. Linschitz *J. Am. Chem. Soc.* **1997**, *119*, 6384.

(15) M. Oyama; F. Marken; R. D. Webster; J. A. Cooper; R. G. Compton; S. Okazaki *J. Electroanal. Chem.* **1998**, *451*, 193.

(16) M. Shamsipur; A. Siroueinejad; B. Hemmateenejad; A. Abbaspour; H. Sharghi; K. Alizadeh; S. Arshadi *J. Electroanal. Chem.* **2007**, *600*, 345.

(17) M. W. Lehmann; D. H. Evans *J. Electroanal. Chem.* **2001**, *500*, 12.

(18) H. Lund; M. M. Baizer *Organic Electrochemistry*; Marcel Dekker: New York, 1991.

(19) R. Nissim; C. Batchelor-McAuley; Q. Li; R.G. Compton *J. Electroanal. Chem*. **2012**, *681*, 44.

(20) Y. Hui; E. L. K. Chng; C. Y. L. Chng; H. Y. Poh; R. D. Webster *J. Am. Chem. Soc*. **2009**, *131*, 1523−1534.

(21) Z. H. Lim; E. L. K. Chng; Y. Hui; R. D. Webster *J. Phys. Chem. B* **2013**, *117*, 2396−2402.

(22) L. Gorton *J. Chem. Soc*. **1986**, *82*, 1245.

(23) L. Gorton; E. Domınguez *Rev. Mol. Biotech*. **2002**, *82*, 371.

(24) Bartlett, P. N. *Bioelectrochemistry: Fundamentals, Experimental Techniques and Applications*; John Wiley & Sons: Chichester, 2008.

(25) F. Gao; Y. Yan; L. Su; L. Wang; L. Mao *Elecrochem. Commun*. **2007**, *9*, 989.

(26) B. Perez; M. del Valle; S. Alegret; A. Merkoci *Talanta* **2007**, *398*, 74.

(27) C. E. Banks; R. G. Compton *Analyst* **2005**, *130*, 1232.

(28) M. Pumera; R. Scipioni; H. Iwai; T. Ohno; Y. Miyahara; M. Boero *Chem. Eur. J*. **2009**, *15*, 10851

(29) M. Pumera *Chem. Eur. J*. **2009**, *15*, 4970.

(30) M. A. Ghanem; J.-M. Chrétien; J. D. Kilburn; P. N. Bartlett *Bioelectrochemistry* **2009**, *76*, 115.

(31) A. Maleki; D. Nematollahi; J. Clausmeyer; J. Henig; N. Plumer; W. Schuhmann *Electroanalysis* **2012**, *24*, 1932

(32) T. Matsue; M. Suda; I. Uchida; T. Kato; U. Akibi; T. Osa *J. Electroanal. Chem*. **1987**, *234*, 163.

(33) R. Scipioni; M. Pumera; M. Boero ; Y. Miyahara; T. Ohno *J. Phys. Chem. Lett*. **2010**, *1*, 122.

(34) F. Mirkhalaf; K. Tammeveski; D. J. Schiffrin *Phys. Chem. Chem. Phys*. **2004**, *6*, 1321.

(35) Q. Li; C. Batchelor-McAuley; N. S. Lawrence; R. S. Hartshorne; R. G. Compton *ChemPhysChem* **2011**, *12*, 1255.

(36) A.Pinczewska; M. Sosna; S. Bloodworth; J. D. Kilburn; P. N. Bartlett *J. Am. Chem. Soc*. **2012**, *134*, 18022.